Generation and Structural Characterisation of Transient Gaseous Species

A thesis submitted in partial fulfilment of the requirements for the degree of

Doctor of Philosophy in Chemistry

at the

University of Canterbury, Christchurch, New Zealand

Sandra Jane Atkinson

2015

Declaration

This thesis has not been previously submitted, in whole or in part, for any degree at this or any other university. The work is original and my own, carried out under the supervision of Dr Sarah Masters; where this is not so, credit has been duly given.

(Sandra Atkinson)

Acknowledgements

I would first like to thank my supervisor, Sarah Masters, for the opportunity to take on this project and the many hours of proofreading of this thesis. From the start of my PhD three years ago you have gone out of your way to teach and guide me, and we have shared the many joys and lows that are often associated with research. You have pushed me to try my best and to extend myself towards new endeavours. Without your encouragement I would not have submitted an entry for the Chemistry World Science communication competition (which I was short-listed for) or be one of the select few to attend the 63rd Lindau Nobel Laureate Meeting. For this, and many more things, I am grateful. I want you to know that I am proud to say that I did my PhD project with you.

Building a lab from the ground up during a PhD is an immense task and I could not have done it without the support of the Chemistry department technical staff. A big thanks must be extended to Wayne Mackay, Nick Oliver and Danny Leonard for all of their help. It took many laborious hours to help move and setup the GED machine and it is something that I could not have done on my own. For this I am very appreciative.

I would also like to thank my fellow physical chemistry students, in particular Andrew Wallace, Nate Gunby, Chris Burn and Marat Sibeav who have been with me for most of this PhD journey. The in-depth office discussions, weekly board games and office quote board were just part of what made for an enjoyable work environment. On numerous occasions our discussions led to solutions of the many day-to-day problems that we were trying to solve in our own work. Your support and friendship have been invaluable during my time in the department, especially during the time I was recovering from my broken foot and fretting about work.

Lastly, I would like to express my love and gratitude to my family, and to my partner Chris Bateman for being there at the end of the day with our cat Kitty. Getting through this thesis was made easier with your helpful discussions and the many hours we spent at the university in the evenings. My study and time at university was made easier knowing you were with me every step of the way.

Abstract

Gas electron diffraction (GED) is a technique that has been developed to study the molecular structure of species in the gas phase. This thesis focuses on the reconstruction of the Canterbury GED apparatus (moved from Edinburgh, UK) and the requirements for modifying the apparatus to incorporate a mass spectrometer (MS) so diffraction and MS data can be obtained within a single experiment.

The combined GED-MS system has been identified in previous work in the Masters group as a necessary development for studying the structure of short-lived species generated *in situ*. This is particularly true for the study of ketene, which as shown in this thesis, can be generated from several precursors as part of a multiple product pyrolysis system. While GED data for ketene generated from acetic anhydride has been refined, the species formed from the pyrolysis of Meldrum's acid were determined to be too difficult to deconvolute without additional experimental data from MS. A computational study of possible ketene derivatives that could be studied with a GED-MS apparatus is also presented.

Lastly, this thesis details a structural study of the gas-phase structures of tris(chloromethyl)amine and a family of substituted disilane systems which have been determined in the gas phase for the first time. A comprehensive GED, Raman spectroscopy and *ab initio* study have been undertaken for tris(chloromethyl)amine [$N(CH_2Cl)_3$] which is shown to have a different structure in the solid and gas phase. Further work in the form of a molecular dynamics investigation has been identified as necessary to describe the low amplitude motion of one of the CH_2Cl groups in the gas phase to allow for the GED refinement to be completed. The work on the substituted disilane systems $X_3SiSiXMe_2$ (X = F, Cl, Br, I) and $X_3SiSiMe_3$ (X = H, F, Cl, Br) demonstrates the effect of increased halogen substitution on the electronic effects of the disilanes, and the effect that the methyl groups have as larger halogens increase the steric bulk of the system.

Deputy Vice-Chancellor's Office
Postgraduate Office

UNIVERSITY OF CANTERBURY
Te Whare Wānanga o Waitaha
CHRISTCHURCH NEW ZEALAND

Co-Authorship Form

This form is to accompany the submission of any thesis that contains research reported in co-authored work that has been published, accepted for publication, or submitted for publication. A copy of this form should be included for each co-authored work that is included in the thesis. Completed forms should be included at the front (after the thesis abstract) of each copy of the thesis submitted for examination and library deposit.

Please indicate the chapter/section/pages of this thesis that are extracted from co-authored work and provide details of the publication or submission from the extract comes:

Chapter 6 contains work from two journal articles that have been published in Structural Chemistry.

S. J. Atkinson, H. E. Robertson, M. Hölbling, W. –W. du Mont, C. Mitrofan, K. Hassler and S. L. Masters, *Structural Chemistry*, **2013**, 24(3), 851-857.

S. L. Masters, **S. J. Atkinson**, M. Hölbling and K. Hassler, *Structural Chemistry*, **2013**, 24(4), 1201-1206.

Please detail the nature and extent (%) of contribution by the candidate:

For the publication that is second authored (related to Section 6.2 of the thesis), experimental data was collected by Dr Sarah Masters (senior PhD supervisor).The complimentary computational work, analysis of the experimental and theoretical results, and writing of the publication was conducted by the candidate.

The second publication (related to Section 6.3 of the thesis) involved a larger analysis as more experimental data had been collected. The first author publication was written by the candidate and the candidate also undertook the computational study, and analysis of the experimental and theoretical results.

For both of the journal articles, the written text, computational study and full data analysis for the results and discussion were conducted by the candidate. It is estimated that approximately 70-80% of the contribution to the publications were made by the candidate.

Certification by Co-authors:

If there is more than one co-author then a single co-author can sign on behalf of all

The undersigned certifys that:

- The above statement correctly reflects the nature and extent of the PhD candidate's contribution to this co-authored work
- In cases where the candidate was the lead author of the co-authored work he or she wrote the text

Name: Sarah Masters Signature:  Date: *25/02/2015*

Abbreviations and acronyms

BSSE	Basis Set Superposition Error
CCD	Charge-Coupled Device
CI	Chemical Ionisation
Da	Dalton
DCM	Dichloromethane
DFT	Density Functional Theory
DYNAMITE	DYNAMic Interaction of Theory and Experiment
EI	Electron Ionisation
ECP	Effective Core Potential
EXAFS	Extended X-ray Absorption Fine Structure
FC	Frozen Core
FVP	Flash Vacuum Pyrolysis
GED	Gas Electron Diffraction
GED-MS	Gas Electron Diffraction coupled with Mass Spectrometry
GGA	Generalised Gradient Approximation
HF	Hartree-Fock
k_x	Perpendicular amplitude of vibration (subscript x denotes the level of correction applied)
LCNMR	Liquid-Crystal Nuclear Magnetic Resonance
LDA	Localised Density Approximation
M06-2X	Minnesota 06-2X
MIC	Molecular Intensity Curve
MP	Møller-Plesset
MS	Mass Spectrometry
MW	Microwave
m/z	Mass-to-Charge
NSCCS	National Service for Computational Chemistry Software
NMR	Nuclear Magnetic Resonance
PES	Potential Energy Surface
QMS	Quadrupole Mass Spectrometer
r	Interatomic distance
r_a	Average interatomic distance (definition depends on method)

r_e	Equilibrium distance
r_{h1}	Interatomic distance corrected with curvilinear distance corrections
R_D	*R*-factor assuming there is no correlation in the data
R_G	*R*-factor taking into account correlation between adjacent observations in the immediately off-diagonal position of the weight matrix
RDC	Radial Distribution Curve
RMS	Root-Mean-Square
SARACEN	Structural Analysis Restrained by *ab initio* Calculations for Electron diffractioN
SEMTEX	Structural Enhancement Methodology for Theory and Experiment
TOF	Time-Of-Flight
TOF-MS	Time-Of-Flight Mass Spectrometer
u_x	Amplitude of vibration (subscript x denotes the level of correction applied)
VHT	Very-High-Temperature
VHT-GED	Very-High-Temperature nozzle coupled with Gas Electron Diffraction

Table of Contents

CHAPTER 1

Introduction

1.1 Thesis outline

This work is focussed around determining the molecular structure of gas-phase molecules by gas electron diffraction (GED), particularly for short-lived species. Part of the work undertaken for this thesis involved the reconstruction and modification of the Canterbury GED apparatus, where GED is the main technique that is used in this thesis to determine gas-phase molecular structure.

Understanding molecular structure is important for predicting and determining properties and this is especially true for intermediate species in a reaction, which are often short-lived. A recent focus on the generation and study of short-lived species *in situ* by GED has highlighted the need for mass spectrometry (MS) data to be collected simultaneously in an experiment.[1] A combined GED-MS apparatus can determine the composition of the analysed gas vapour and the relative amounts of each species, allowing this additional information to be used in a GED refinement. This is particularly important for unstable, reactive molecules (which may not be isolated after a GED experiment and analysed elsewhere) as additional experimental information may be necessary to fully determine their molecular structure.

This thesis presents several different sections of work. Following the details regarding the setup and modifications made to the Canterbury GED apparatus, the initial planning towards a GED-MS design is presented. Structural studies of ketene, an example of a short-lived species, from a variety of precursors is also given. As part of the structural study of ketene, reference has been made to the need for a GED-MS apparatus to fully refine the GED data of ketene when generated from Meldrum's acid. Lastly, two additional structural studies are also presented. Tris(chloromethyl)amine, $N(CH_2Cl)_3$, is shown to adopt different conformations between the gas and solid phases. The other study is on two complementary disilane systems, $X_3SiSiXMe_2$ (X = F, Cl, Br, I) and $X_3SiSiMe_3$ (X = H, F, Cl, Br), with a structural investigation of the effect of a series of halogen substituents, and their proximity to the methyl groups, on the overall molecular structure.

1.2 General introduction

The structure and function relationships that exist in molecules are a key aspect of chemistry. The exact atom connectivity and geometry of molecules can be used to predict and determine chemical and physical properties. These properties can, in turn, be used to design new molecules for specific applications such as synthesising medicinal compounds. Understanding molecule behaviour allows for further advances in chemistry, as more is understood about chemical reactions and properties. An example of this are anti-cancer drugs such as cis-platin,[2] where understanding how the molecule enters cells through the membrane and the mode of binding to DNA are important parts of rationalising their anti-cancer behaviour. Through this understanding, trends can be identified for similar molecules with different substituents. In many cases this results in a cheaper alternative being developed or one that works better for a specific application such as a treatment of a particular type of cancer.[3]

Molecules can exist in the gas, solution or solid phase. Chemical reactions typically take place in the solution or liquid phase. Ideally the structure would be studied in this state as the effect of intermolecular interactions, such as hydrogen bonding and dipole interactions, on the structure will be considered. However, techniques used to determine the molecular structure of liquid-phase molecules, including liquid-crystal nuclear magnetic resonance (LCNMR) and extended X-ray absorption fine structure (EXAFS), are limited for routine structure determination.[4] A closer comparison to molecular structure in the liquid state can be gained by studying structure in the gas phase rather than in the solid state. Molecules in the gas phase are free of constraints that would exist in the solid state, such as intramolecular interactions and packing forces that can distort the structure. These constraints are present in the liquid phase, but generally to a lesser extent than in the solid phase, where the relative potential energy of the molecules is much higher than the kinetic energy, resulting in the molecules being closely packed.

There are two techniques that experimental chemists can use to determine the structure of gas-phase molecules: rotational spectroscopy and gas electron diffraction (GED). Rotational spectroscopy involves determining the moments of inertia from

measured rotation constants to obtain structural information. In GED, combinations of atoms within the molecules scatter an electron beam. From the interference pattern of the scattered electrons the internuclear distances, and hence the overall three-dimensional structure, can be deduced. Both of these techniques have limitations. Rotational spectroscopy can be applied only to small molecules since only three rotational constants at most can be measured for a single isotopic species of a particular compound. Beyond this, stable isotopic molecules have to be considered, which is a problem for molecules incorporating fluorine or phosphorus due to the stability of these isotopes.[5] In this PhD research small and large molecules (greater than 10 atoms) will be considered; however, where applicable information obtained from other experiments will be utilised for completeness.

1.3 Gas Electron diffraction

1.3.1 Historical background

GED works on the principles of wave-particle duality theory; that electrons can exhibit wave properties even though they are normally considered to be particles. Studies by Louis de Broglie, in conjunction with his brother doing X-ray diffraction in 1922, led him to publish an article about black-body radiation in which photons were treated as particles (or "atoms of light").[6] After considering Thomas Young's discovery of interference phenomena in 1803, de Broglie generalised wave-particle duality in 1923. He published the famous formula linking particles (in this case electrons) to a wave[7,8] as follows:

$$\lambda = h/mv \tag{1.1}$$

where wavelength λ is related to Planck's constant h, v being the speed of the electron and m the mass of the electron. This equation ties together the wave (wavelength) and particle (momentum) properties, in particular for an electron. Taking into account de Broglie's results[7,8] and Young's double-slit experiment, it can be shown that electrons directed at multiple slits will diffract and interfere (due to the coherent nature of the scattering) to form minima and maxima as shown for a wave model (Figure 1.1).

It was observed that, when a beam of electrons is directed at a molecule, the spacing between the atoms acts as a slit resulting in diffraction of the electrons. In 1927 Germer and Davisson[9] showed that the phenomenon of electron diffraction by crystals existed (confirmed by Thomson[10]) and in 1929 Debye[11] carried out the first gas-phase X-ray diffraction experiment, followed less than a year later by the first GED by Mark and Wierl.[12]

Figure 1.1 Illustration representing maxima and minima obtained by diffraction in a double-slit experiment by **(a)** a wave model and **(b)** a particle model.

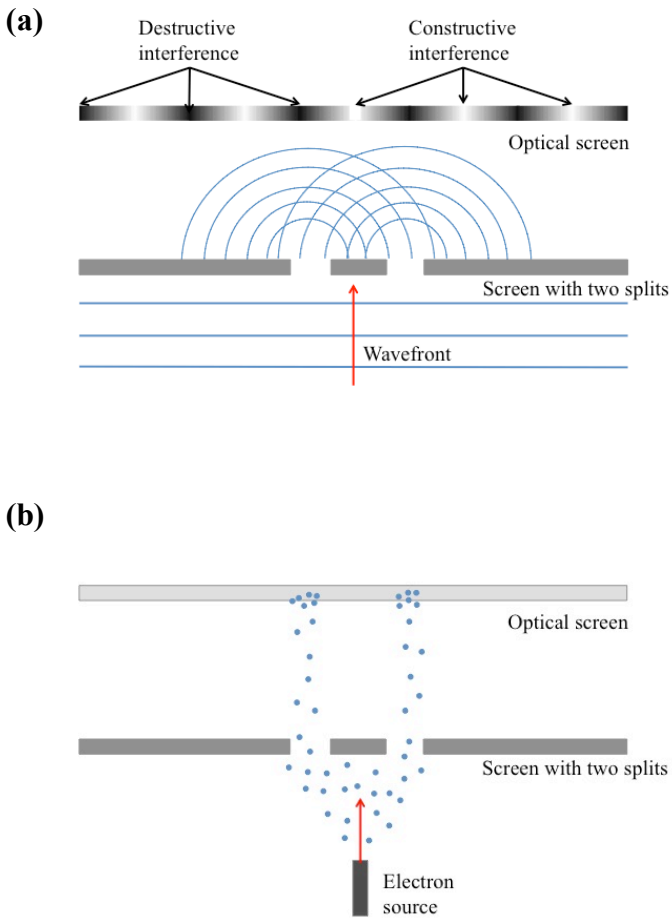

1.3.2 Gas Electron Diffraction

The general set-up for the GED apparatus to be used by the Masters research group (and previously used in Edinburgh) is shown in Figure 1.2. GED apparatus are not commercially available, so they are typically custom built. However different GED machines exploit the same underlying physical processes.

An electron beam is produced by an electron gun (with an accelerating voltage of *ca*. 40 keV) and is focussed through a series of magnetic lenses and apertures to produce a wavelength comparable to the interatomic spacing in a molecule. The gas sample is introduced to the chamber at right angles to the electron beam through a fine effusive nozzle and the resulting diffraction that occurs is recorded on a detector. The entire

system is operated under vacuum to minimise scattering of the electron beam by undesired background molecules.

Figure 1.2 Schematic representation of the components of the Canterbury GED apparatus.

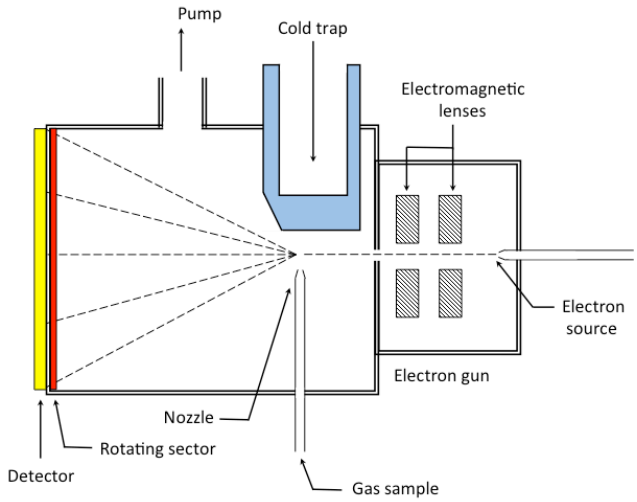

For the Masters group the scattered electrons are recorded on photographic film, although image plates or a charge-coupled device (CCD) can be used. Typically, two nozzle-to-detector distances are used to widen the angular range of the electron scattering, thus collecting more experimental data, with the overlap region ensuring consistency between the data collection. The calibration of the nozzle-to-detector distance is usually performed with benzene since its gas-phase structure is known accurately.

1.3.3 Data collection with GED

Due to the random orientation of the molecules with respect to the electron beam in the gas phase, the interference patterns are concentric rings (Figure 1.3). This is a result of maxima and minima formed by the wavefront interference, and is a measure of the intensity of the scattering. From the centre of the plate to the outside, the intensity of the scattering falls off as r^4, where r is the distance from the centre of the plate. To minimise the overall intensity in the centre from obscuring any information, a rotating sector is used to average out the intensity over the detector.[13] These sectors can come in different shapes (the one used by the Masters group is heart shaped)

with the common feature being a curved edge similar to the fourth power with an opening angle α. Similarly to the fall off in scattering intensity by the fourth power, α increases as a function of r^4 to a distance of r_0, the maximum radius of the rotating sector (see Figure 1.3). The diffraction pattern on the film is scanned using a flat-bed scanner to read the intensities over the whole plate, allowing digitisation and extraction of the data.

Figure 1.3 Example of a diffraction pattern obtained from a GED experiment (left) with the use of a rotating sector (schematically shown on the right). Rotating sector image retrieved from *Structural Methods in Molecular Inorganic Chemistry* (2013).[14]

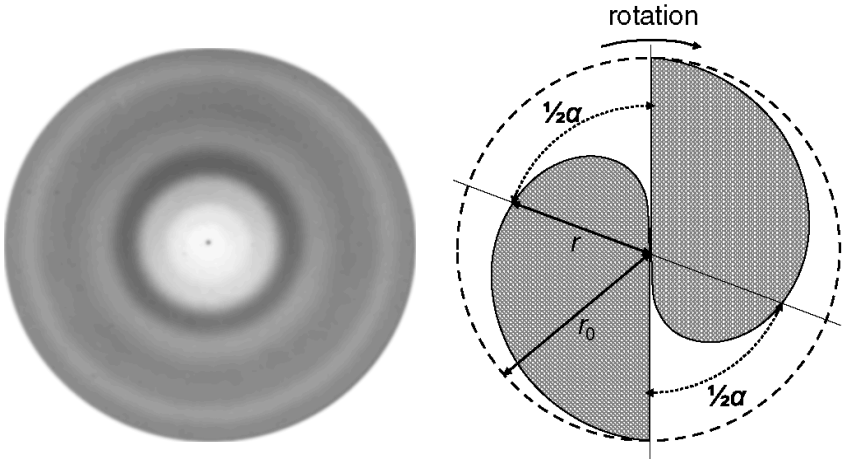

To analyse the intensities, the optical data must be first converted into the total electron scattering intensity (I_{total}) which can be expressed as:

$$I_{\text{total}} = I_{\text{atomic}} + I_{\text{molecular}} + I_{\text{background}} \quad (1.2)$$

The molecular scattering intensity must be separated from the atomic scattering, after the background scattering intensity is subtracted. This is done by subtracting tabulated atomic scattering factors for the atomic scattering.[4] The total scattering intensity can be expressed as a function of the scattering angle, θ, and then of the variable, s, given by[4]

$$s = 4\pi \sin(\theta/2)/\lambda \quad (1.3)$$

The total atomic scattering intensity for a molecule (I_{total}) is simply the sum of the contributions of the diffraction of each of the atoms (Equation 1.4) with $F_i(s)$, the atomic scattering factors, being readily calculated or obtained from published tables.[15]

$$I_{\text{atomic}}(s) = \sum_i F_i(s)^2/s^4 \tag{1.4}$$

Atomic scattering occurs via electron diffraction of single atoms so the scattering for each atom will not vary between molecules and can be subtracted from the total electron scattering intensity. The resulting molecular intensity curve (MIC) undergoes Fourier transformation to express the data in terms of its frequency components. The resulting radial distribution curve (RDC) gives the probability $P(r)$ of finding an interatomic distance r in the molecule. This probability distribution consists of Gaussian curves for each distance, superimposed to give the overall probability of an interatomic distance occurring at a particular distance (Figure 1.4).

Figure 1.4 Conversion from the MIC to RDC for a GED experiment. Note it is normal practise to refine using $s^4I_{mol}(s)$ for data from the Canterbury apparatus.

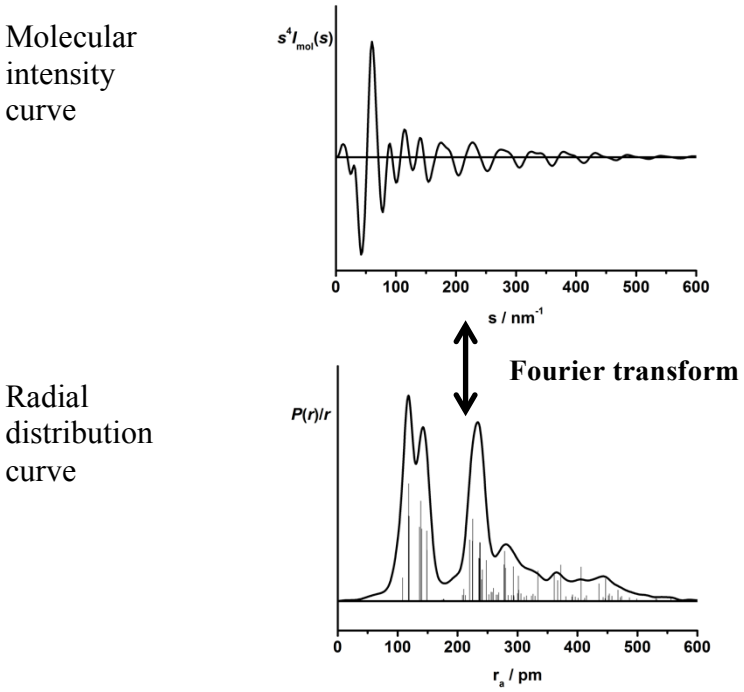

The mean vibrational amplitudes determine the width of the Gaussian curves in the RDC, with the area under each peak being given by:

$$Area \propto \frac{n_{ij} Z_i Z_j}{r_{ij}} \quad (1.5)$$

where n_{ij} is the multiplicity of r_{ij}, and Z_i and Z_j are the atomic numbers of atoms i and j. This means that similar interatomic distances will not be resolved, and a composite peak results. Also, just as with X-ray diffraction, the hydrogen atoms are not well defined by GED due to their poor scattering power. By using the known wavelength of the electrons and the distances between atoms in the molecule, the overall molecular structure can be determined by analysis of the diffraction pattern.

1.3.4 Least-squares refinement

Experimental data is analysed by a comparison of the experimental MIC to that generated from a parameterised model molecule. A Fortran model is constructed consisting of a minimum number of bond lengths, bond angles and dihedral angles to describe the geometry of the model molecule, using averages and differences where appropriate. Starting values of the parameters in the model are taken from the *ab initio* or density functional theory (DFT) calculations that provide the starting geometry for the refinement. The MIC of the model molecule is generated from scattering equations.[16]

During the least-squares refinement, the parameters of the model are allowed to change to minimise the difference between the model and experimental data. The physical reasonability of the refined values is checked throughout the refinement. The agreement between the model and experimental data is determined by the goodness-of-fit factor, *R*-factor, where a lower *R* factor denotes a better fit. Typically the R_D and R_G are the *R*-factors used in a GED refinement. R_D is the *R*-factor assuming there is no correlation in the experimental data whereas R_G takes into account correlation between adjacent observations in the immediately off-diagonal position of the weight matrix.[17,18] For a further mathematical description, refer to Reference 18. Typically correlation in experimental data is present so R_G will be larger than R_D.

Refining GED data with this least-squares refinement process requires that the content of the analysed gas vapour and approximate structure of the molecule are known. If a GED refinement suggests that there are multiple conformers present, the Boltzmann distribution can be used to determine the ratio of the conformers. The ratio of a Boltzmann distribution computed for two states is known as the Boltzmann factor. It is dependent on the energy difference between two states (Equation 1.6) where N_1 and N_2 are the number of molecules in states 1 and 2, E_1 and E_2 are the energy states 1 and 2, k is Boltzmann's constant (1.381×10^{23} J K^{-1}) and T is the temperature in Kelvin.

$$\frac{N_2}{N_1} = \exp\frac{-(E_2 - E_1)}{kT} \tag{1.6}$$

There can be limitations to fully refining GED data without the aid of additional experimental and theoretical information as discussed below.

1.3.5 Limitations of GED and solutions

GED is a very powerful technique that is used to obtain molecular structure in the gas phase. However, one method does not always provide sufficient information to determine the complete structure of a molecule – especially for more complex systems where more than one conformer may be present. There can also be a problem when there are similar internuclear distances in the molecule and overlap of peaks is observed in the RDC. When this occurs, multiple Gaussian curves overlap, rendering the individual internuclear distances difficult to distinguish (see Figure 1.4). This meant that GED was traditionally limited to small or highly symmetric molecules.

To overcome this problem, methods have been developed to analyse data obtained from several different experimental and theoretical sources. Rankin *et al.*[19-24] have developed methods to analyse data obtained by several techniques (experimental and theoretical); the Combined Analysis and SARACEN methods. The Combined Analysis method[19-21] combines data from experimental methods such as GED, rotational spectroscopy and LCNMR. The SARACEN method,[22-24] Structural Analysis Restrained by *ab initio* Calculations for Electron diffractioN, uses

experimental data in combination with data from *ab initio* or density functional theory calculations to determine the most probable structure based on experimental and theoretical data. The DYNAMITE method,[18,25] DYNAMic Interaction of Theory and Experiment, developed by the Masters research group, builds from SARACEN by dynamically linking experimental data and theoretical data within the least-squares refinement process. Thus asymmetry is allowed in ligands without the need for a large number of parameters. This technique has been further developed with the introduction of the SEMTEX method,[26] Structural Enhancement Methodology for Theory and Experiment. SEMTEX allows information from higher-level theoretical calculations to be incorporated into the refinement process without compromising computational efficiency.

Another problem to consider with GED arises from the intramolecular vibrational effects in a molecule. Since the molecule is constantly vibrating and the atoms are not stationary, the observed MIC is an average over all vibrational states. In the case of linear molecules, such as CO_2, this means that the molecule appears to be bent rather than linear as the molecule averages more of its time bent than linear (Figure 1.5). Despite this, the C=O bond length remains basically unchanged.

Figure 1.5 Vibrational states of a linear triatomic molecule

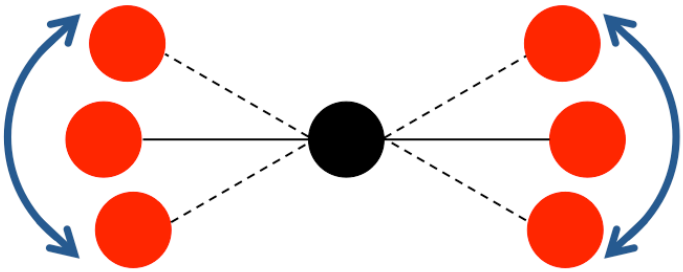

This problem is known as the shrinkage effect.[27,28] A vibrational correction is necessary in order to obtain accurate structures by GED. Corrections are obtained using the SHRINK software[29,30] and applied to each pair of atoms in the refinement. For molecules with low amplitude motions, molecular dynamics may be used to obtain the corrections instead of SHRINK to correct for the vibrational motion.[31]

1.4 Computational chemistry

1.4.1 *Ab initio* calculations

Ab initio calculations use Quantum mechanical principles to simulate the structure and electronic arrangement within molecules. This is undertaken by finding a solution to the time-independent Schrödinger equation

$$\hat{H}\Psi = E\Psi \tag{1.7}$$

where E is the total molecular energy, Ψ is the total molecular wavefunction (describing the position of nuclei and electrons) and $\hat{H}$ is the Hamiltonian operator (containing the electronic and nuclear kinetic and potential energy terms). As we can only solve the Schrödinger equation for one-electron systems, approximations to both the wavefunction and Hamiltonian operator are needed to apply it to molecular systems.

If the Hamiltonian operator of the time-independent Schrödinger equation is considered in more detail we see that there are five energy terms to account for.

$$\hat{H} = \hat{T}_e + \hat{T}_n + \hat{V}_{en} + \hat{V}_{ee} + \hat{V}_{nn} \tag{1.8}$$

Two of these are kinetic energy terms for the motion of the nuclei ($\hat{T}_n$) and the electrons ($\hat{T}_e$) and three are potential energy terms for the electron-electron repulsion ($\hat{V}_{ee}$), the nuclear-nuclear repulsion ($\hat{V}_{nn}$) and the electron-nuclear attraction ($\hat{V}_{en}$). By introducing the Born-Oppenheimer approximation that heavy nuclei are stationary in a field of light moving electrons, the nuclear energy terms can be eliminated ($\hat{T}_n$ = 0, nuclear-nuclear repulsion = constant) to leave only the electronic Hamiltonian to be considered further.

A series of one-electron Schrödinger equations can be solved with the electron repulsion term being replaced by the Hartree-Fock (HF) potential. However, this assumes that all electrons are static and that an individual electron interacts to an averaged electron density by the other electrons in the molecule. This is generally

referred to as the mean-field approximation. Whilst this approximation can account for ~99% of the energy of the system, it is not completely accurate. Electrons are able to come close together, resulting in inaccurate bond distances and energies, so therefore correcting for these small differences between the model and real case is very important.

To account for the behaviour of electrons in a system, electron correlation methods are used. Electron correlation accounts for the instantaneous interactions of pairs of electrons with opposite spin. Møller-Plesset (MP) perturbation theory adds higher excitations to the HF theory. If we divide the Hamiltonian operator into two parts, where

$$\hat{H} = \hat{H}_0 + \lambda\hat{V} \tag{1.9}$$

and $\hat{H}_0$ is solvable exactly, then $\lambda\hat{V}$ is a perturbation applied to $\hat{H}_0$. $\hat{V}$ is a small perturbation to $\hat{H}_0$ and the perturbed wavefunction and energy can be expressed as a power series in λ, where λ is an arbitrary real parameter that controls the size of the perturbation. By truncating the power series at various points we get MP2, MP3, MP4 etc.[32] The most commonly used MP2 level of theory has been utilised in this PhD thesis.

1.4.2 Density functional calculations

Other types of calculations that are utilised in this thesis include DFT methods. These are based on the electron density, rather than the wavefunction, and are favourable when studying large systems. DFT is based on the proof by Hohenberg and Kohn that there exists a one-to-one mapping between the electron density of a system and its energy.[33] The exchange-correlation functional is not known exactly and must be approximated through methods such as the Localised Density Approximation (LDA)[34] and Generalised Gradient Approximation (GGA).[35] DFT methods are generally less accurate than post-HF methods such as MP2. However, the main advantage of DFT methods lies in the speed at which large systems can be calculated. The main DFT method used in this thesis is Minnesota 06-2X (M06-

2X)[36] which consists of a set of four meta-hybrid GGA functionals. The M06-2X functional parameters are empirically fitted to suit the study of main group elements (groups 1–2, 13–18) such as those used in this project.

1.4.3 Basis sets

The total electronic wavefunction is approximated by the orbitals within a system. The orbitals of a system are described using a set of mathematical functions known as a basis set. Simplifications to the basis set are made so that the Schrödinger equation can be used to calculate it. An exact description of each electron would require a basis set of infinite size (i.e. an infinite number of functions), which is not practical. Instead, truncated basis sets are used for computational efficiency. Use of larger basis sets results in a better description of the orbitals since there are fewer restrictions on the location of each electron.

Standard basis sets use linear combinations of Gaussian functions to represent orbitals. Basis sets assign a group of basis functions to each atom in a molecule to approximate its orbitals. There are various different types of basis sets: minimal, split-valence and polarised. Minimal basis sets contain the minimum number of basis functions needed for each atom and will not be used in this PhD since larger basis sets are needed to describe the systems of interest. Split-valence basis sets are larger and have more basis functions per atom. Common split-valence basis sets, such as 3-21G[37,38] and 6-31G[39,40] have two sizes of basis function for each valence orbital. They are referred to as double-zeta and form molecular orbitals from linear combinations of two sizes of functions for each atomic orbital.

Split-valence basis sets allow orbitals to change size but not to change shape (i.e. symmetry is conserved). Polarised basis sets remove this limitation by adding orbitals with angular momentum beyond what is required for the ground state to the description of each atom. For example, 6-31G(d)[41,42] indicates a double-zeta split-valence basis set with d functions added to heavy atoms; it is also known as 6-31G*. 6-31G(d,p) (also known as 6-31G**)[41,42] adds p functions to hydrogen atoms in addition to the d functions on heavy atoms.

Diffuse functions can also be added to basis sets. Diffuse functions are large-sized versions of the s and p functions used in standard valence basis sets and allow orbitals to occupy a larger region of space. These functions are particularly important for systems where electrons are relatively far from the nucleus and include systems with lone pairs of electrons, anions, radicals and systems in excited states. The 6-31+G(d) basis set[41,42] has diffuse functions added to the heavy atoms whereas 6-311++G(d)[43,44] also has diffuse functions added to the hydrogens.

Examples of basis sets used in this work include the Pople-type split valence basis sets[37-44] and Dunnings' correlation consistent basis sets.[45,46]

1.5 Unstable and short-lived species

Recently there has been a focus on studying short-lived (transient) gas molecules in the Masters research group. Transient species are of interest since they are often the intermediate species in a reaction and by understanding their structure, the mechanism of the reaction (and other possible reactions) can be further understood. By their very nature the structure of these molecules is hard to calculate (for example due to very shallow potential energy wells) so experimental data is required to calibrate theory. However due to the nature of these molecules, multiple separate experimental techniques cannot be conducted if structural data is to be collected by GED. The species has to be generated and analysed within the electron diffraction apparatus (*in situ*), limiting the amount of experimental data that can be obtained since the species cannot be isolated and analysed elsewhere. Techniques such as Nuclear Magnetic Resonance (NMR) cannot be used due to the short lifetime of the species of interest. The timescale of a NMR experiment can span from picoseconds to days depending on the structure of the molecule under investigation.[47] This is not practical for the study of short-lived species by GED, which can fall in the femtosecond region.[48]

1.5.1 Generation of short-lived species

Whilst the study of short-lived species is often difficult, a number of techniques already exist to study such molecules.

Flash vacuum pyrolysis (FVP) and photolysis are common methods used in organic synthesis to generate short-lived species from heating (leading to decomposition)[49,50] or bond dissociation from light[51] respectively. FVP is often coupled with other techniques such as mass spectrometry (MS)[52] and matrix isolation methods[53] to further study the species once it has been trapped. However, these methods are limited to species with a sufficient lifetime, and full structure determination (from complementary techniques) may not be possible.

GED has been used to study unstable transient molecules in the past, including the indenyl radical,[54] bromoethyl radical[55] and the allyl radical,[56] but is not a routine focus of other GED research groups. The advancement of ultrafast GED, allowing

chemical processes to be studied on the femtosecond timescale,[48] has opened the avenue for studying short-lived species to other GED groups, but the equipment required is costly. Development of a new nozzle for the Canterbury GED apparatus allowed for the generation of short-lived species *in situ* on a milli to microsecond timescale, and has previously been used to collect data for ketene and the benzyl radical. However, there have been issues in refining the GED data obtained in these experiments, especially since there is no technique to confirm the pyrolysis products have been generated *in situ.*

1.5.2 Limitation of using GED to study short-lived species

Routine structure determination of short-lived species is one current research focus of the Masters group, with these species often being generated *in situ*. However, the generation of multiple molecules *in situ* can lead to issues refining the obtained GED data. GED, which routinely collects 1-dimensional data of 3-dimensional structures, is already limited to determining the structure of simple molecules. However, additional experimental and *ab initio* data can allow for the structures of more complicated systems such as $Ga(hfac)_3$ and $In(hfac)_3$ (hfac = 1,1,1,5,5,5-hexafluoropentane-2,4-dionate)[57] with more than 40 non-hydrogen atoms to be solved. A mixed vapour model contains multiple species, often with similar interatomic distances, which can lead to additional complexities in the refinement model. In such cases additional parameters are introduced to describe similar interatomic distances. Additionally, parameters are also introduced to describe the relative weighting (percentage amount) of each species for use with the GED refinement model.

Although it is already routine to use *ab initio* data with the SARACEN method[22-24] to apply restraints on computed structures, the additional experimental data available depend on the system being investigated. Often in GED rotational constants obtained from microwave (MW) spectroscopy are used in the refinement process, such as with methylphosphine, methylphosphineborane and vinylarsine.[1] However with short-lived species, collection of data such as from MW spectroscopy and NMR is limited by the short-lifetime of the species.[47] Previous work in the Masters group by Noble-Eddy[1] highlighted that the largest gain in additional data will come from the addition

of information from MS. This is particularly true as MS data can be obtained *in situ* during a GED experiment.

1.6 This work

This thesis is concerned with the developing the Canterbury GED apparatus to incorporate MS, creating a combined GED-MS system, and the structural determination of short-lived species.

The first part of this work involved the reconstruction of the Canterbury GED apparatus following its move from the University of Edinburgh (UK), and covers the modifications/repairs and calibration of the machine. Chapter 2 details the assembly and modifications made to the GED apparatus here at University of Canterbury.

This thesis commenced with the intention to have a fully working MS with the GED apparatus, but due to time and equipment constraints, the construction of the parts has not commenced whilst the planning phase is complete. Chapter 3 highlights the technical requirements for MS in a GED-MS setup and details the requirements for running GED and MS in unison during an experiment. Schematic plans are also presented for the new chamber design, which are required for a GED-MS setup.

Alongside the lab and construction work of the apparatus, studies were commenced with ketene, an example of a short-lived species of interest to the Masters group. Chapter 4 details the study of ketene from acetic anhydride and Meldrum's acid, and includes a computational study of ketene derivatives that will be explored by GED in the future.

Two additional structure determination studies are also presented. Chapter 5 considers the structure of tris(chloromethyl)amine, $N(CH_2Cl)_3$, which is shown to differ between the gas and solid phases. Chapter 6 details the study of two complementary disilane systems, $X_3SiSiXMe_2$ (X = F, Cl, Br, I) and $X_3SiSiMe_3$ (X = H, F, Cl, Br) with emphasis on the effect of the proximity of the methyl groups with respect to the halogen substituents.

Finally, Chapter 7 concludes this thesis work and comments on the next steps that will be pursued for obtaining a GED-MS setup. This chapter also considers the future direction of study for short-lived species by the Masters group and planned data

collection. Necessary upgrades to the GED refinement software, ed@ed,[18] as noted during this work are covered briefly. Lastly, planned future experimental work on $N(CH_2Cl)_3$ and its corresponding GED refinement will be covered.

1.7 References

1. R. Noble-Eddy, PhD Thesis, University of Edinburgh, Edinburgh, Scotland, **2009**.
2. Z. Liu, S. Tan, Y. Zu, Y. Fu, R. Meng and Z. Xing, *Micron*, **2010**, *41*, 833-839.
3. A. Mishra, H. Jung, J. W. Park, H. K. Kim, H. Kim, P. J. Stang and K.-W. Chi, *Organometallics*, **2012**, *31*, 3519-3526.
4. E. A. V. Ebsworth, D. W. H. Rankin and S. Cradock, *Structural Methods in Inorganic Chemistry*, Blackwell Scientific Publishing, Oxford, UK, 2nd edn., **1991**.
5. S. Cradock, P. B. Liescheski, D. W. H. Rankin and H. E. Robertson, *J. Am. Chem. Soc.*, **1988**, *110*, 2758-2763.
6. L. de Broglie, *Comptes Rendus*, **1922b**, *175*, 811-813.
7. L. de Broglie, Thèse de doctorat, Masson et Cie, Paris, **1924**.
8. L. de Broglie, *Ann. De Physique*, **1925**, *3*, 22-128.
9. C. J. Davisson and L. H. Germer, *Nature*, **1927**, *119*, 558-560.
10. G. P. Thomson and A. Reid, *Nature*, **1927**, *119*, 890-890.
11. P. Debye, L. Bewilogua and F. Ehrhardt, *Physik, Z.*, **1929**, *30*, 84-87.
12. H. Mark and R. Wierl, *Physik, Z.*, **1930**, *60*, 741-753.
13. L. O. Brockway and L. S. Bartell, *Rev. Sci. Instrum.*, **1954**, *25*, 569-575.
14. D. W. H. Rankin, N. W. Mitzel and C. A. Morrison, *Structural Methods in Molecular Inorganic Chemistry*, John Wiley & Sons, Ltd, Chichester, West Sussex, UK, **2013**.
15. A. W. Ross, M. Fink and R. Hilderbrandt, *International Tables for Crystallography*, Kluwer Academic Publishers, Dordrecht, Netherlands, **1992**, Vol. C, p. 245.
16. I. Hargittai and M. Hargittai, *Stereochemical Applications of Gas-phase Electron Diffraction*, VCH Publishers, Inc., Verlagsgesellschaft mbH, Weinheim, **1988**.
17. S. L. Masters, S. J. Atkinson, M. Hölbling and K. Hassler, *Struct. Chem.*, **2013**, *24*, 1201-1206.

18. S. L. Hinchley, H. E. Robertson, K. B. Borisenko, A. R. Turner, B. F. Johnston, D. W. H. Rankin, M. Ahmadian, J. N. Jones and A. H. Cowley, *Dalton Trans.*, **2004**, 2469-2476.
19. A. S. F. Boyd, G. S. Laurenson and D. W. H. Rankin, *J. Mol. Struct.*, **1981**, *71*, 217-226.
20. P. D. Blair, S. Cradock and D. W. H. Rankin, *J. Chem. Soc., Dalton Trans.*, **1985**, 755-759.
21. P. B. Liescheski and D. W. H. Rankin, *J. Mol. Struct.*, **1988**, *178*, 227-241.
22. A. J. Blake, P. T. Brain, H. McNab, J. Miller, C. A. Morrison, S. Parsons, D. W. H. Rankin, H. E. Robertson and B. A. Smart, *J. Phys. Chem.*, **1996**, *100*, 12280-12287.
23. P. T. Brain, C. A. Morrison, S. Parsons and D. W. H. Rankin, *J. Chem. Soc., Dalton Trans.*, **1996**, 4589-4596.
24. N. W. Mitzel and D. W. H. Rankin, *Dalton Trans.*, **2003**, 3650-3662.
25. S. L. Hinchley, M. F. Haddow and D. W. H. Rankin, *Dalton Trans.*, **2004**, 384-391.
26. G. R. Kafka, S. L. Masters and D. W. H. Rankin, *J. Phys. Chem. A*, **2007**, *111*, 5913-5920.
27. O. Bastiansen and M. Trætteberg, *Acta Crystallogr.*, **1960**, *13*, 1108-1108.
28. Y. Morino, *Acta Crystallogr.*, **1960**, *13*, 1107-1107.
29. V. A. Sipachev, *J. Mol. Struct. (Theochem)*, **1985**, *121*, 143-151.
30. V. A. Sipachev, *J. Mol. Struct.*, **2001**, *567–568*, 67-72.
31. D. A. Wann, R. J. Less, F. Rataboul, P. D. McCaffrey, A. M. Reilly, H. E. Robertson, P. D. Lickiss and D. W. H. Rankin, *Organometallics*, **2008**, *27*, 4183-4187.
32. C. Møller and M. S. Plesset, *Phys. Rev.*, **1934**, *46*, 618-622.
33. P. Hohenberg and W. Kohn, *Phys. Rev.*, **1964**, *136*, B864-B871.
34. J. P. Perdew and Y. Wang, *Phys. Rev. B*, **1992**, *45*, 13244-13249.
35. J. P. Perdew, J. A. Chevary, S. H. Vosko, K. A. Jackson, M. R. Pederson, D. J. Singh and C. Fiolhais, *Phys. Rev. B*, **1992**, *46*, 6671-6687.
36. Y. Zhao and D. G. Truhlar, *J. Phys. Chem. A*, **2006**, *110*, 5121-5129.
37. J. S. Binkley, J. A. Pople and W. J. Hehre, *J. Am. Chem. Soc.*, **1980**, *102*, 939-947.

38. M. S. Gordon, J. S. Binkley, J. A. Pople, W. J. Pietro and W. J. Hehre, *J. Am. Chem. Soc.*, **1982**, *104*, 2797-2803.
39. R. Ditchfield, W. J. Hehre and J. A. Pople, *J. Chem. Phys.*, **1971**, *54*, 720-723.
40. W. J. Hehre, R. Ditchfield and J. A. Pople, *J. Chem. Phys.*, **1972**, *56*, 2257-2261.
41. G. A. Petersson, A. Bennett, T. G. Tensfeldt, M. A. Al-Laham, W. A. Shirley and J. Mantzaris, *J. Chem. Phys.*, **1988**, *89*, 2193-2218.
42. G. A. Petersson, T. G. Tensfeldt and J. A. Montgomery Jr, *J. Chem. Phys.*, **1991**, *94*, 6091-6101.
43. A. J. H. Wachtees, *J. Chem. Phys.*, **1970**, *52*, 1033-1036.
44. P. J. Hay, *J. Chem. Phys.*, **1977**, *66*, 4377-4384.
45. T. H. Dunning Jr, *J. Chem. Phys.*, **1989**, *90*, 1007-1023.
46. R. A. Kendall, T. H. Dunning Jr and R. J. Harrison, *J. Chem. Phys.*, **1992**, *96*, 6796-6806.
47. R. G. Bryant, *J. Chem. Educ.*, **1983**, *60*, 933-935.
48. A. H. Zewail, *J. Phys. Chem.*, **1993**, *97*, 12427-12446.
49. M. Karpf, *Angew. Chem. Int. Ed.*, **1986**, *25*, 414-430.
50. H. McNab, *Aldrichimica Acta*, **2004**, *37*, 19-26.
51. C. Ornelas, J. Ruiz, J. Rodrigues and D. Astruc, *Inorg. Chem.*, **2008**, *47*, 4421-4428.
52. R. Flammang, M. Barbieux-Flammang, P. Gerbaux and C. Th. Pedersen, *J. Chem. Soc., Perkin Trans. 2*, **1997**, 1261-1264.
53. V. E. Bondybey, A. M. Smith and J. Agreiter, *Chem. Rev.*, **1996**, *96*, 2113-2134.
54. L. Schäfer, *J. Am. Chem. Soc.*, **1968**, *90*, 3919-3925.
55. T. L. Leggett, R. E. Kennerly and D. A. Kohl, *J. Chem. Phys.*, **1974**, *60*, 3264-3267.
56. E. Vajda, J. Tremmel, B. Rozsondai, I. Hargittai, A. K. Maltsev, N. D. Kagramanov and O. M. Nefedov, *J. Am. Chem. Soc.*, **1986**, *108*, 4352-4353.
57. P. T. Brain, M. Bühl, H. E. Robertson, A. D. Jackson, P. D. Lickiss, D. MacKerracher, D. W. H. Rankin, D. Shah and W. Thiel, *J. Chem. Soc., Dalton Trans.*, **1998**, 545-551.

CHAPTER 2

Reconstruction and modification of the Canterbury gas electron diffraction apparatus

2.1 Introduction

As part of the move by Dr Sarah Masters to take up an appointment at the University of Canterbury in 2011, the GED apparatus from the University of Edinburgh (UK) was deconstructed and relocated. The GED apparatus (known as the Edinburgh GED apparatus in the literature)[1] has been housed at the University of Edinburgh since 1977, and at University of Cornell (USA) prior to that.[2] Due to the relocation of the apparatus to the University of Canterbury it is now referred to as the Canterbury GED apparatus.

A significant part of my PhD has involved the reconstruction of the Canterbury GED apparatus. This was done using images taken of the GED apparatus during its deconstruction at the University of Edinburgh as a guide. The start of the reconstruction was delayed by remediation of the available lab space (which was setback due to the Canterbury earthquakes). During the reconstruction process, repairs to the apparatus have been necessary and this resulted in the need for modifications to the original apparatus design.

My involvement with the reconstruction has included the assembly and extensive testing of the apparatus under vacuum. Construction and modification of large components were made in conjunction with the University of Canterbury Chemistry workshop staff.

This chapter will cover the general construction of the Canterbury GED apparatus, with modifications to the original setup being covered in detail. The current status and future work will be highlighted. Lastly, the procedure for calibrating experiments will be described.

2.2 Reconstruction of the Canterbury GED apparatus

A major component of this thesis involved the reconstruction of the Canterbury GED apparatus, including the implementation of repairs and modifications. The overall reconstruction of the Canterbury GED apparatus has been a lengthy process, due to the time taken to remediate the current lab space, and the time required to repair/modify the existing apparatus during construction and testing. Leak testing the apparatus has not been a trivial task since this involved repetitive leak testing and retesting of the achievable vacuum, followed by repairs to the leak tester itself.

This section will cover the general setup of the Canterbury GED apparatus, highlighting modifications to the main chamber, vacuum pumps, cooling system, and electron gun. The role of the leak tester is also briefly described.

2.2.1 Main chamber attachments

The initial stages of the reconstruction of the GED apparatus involved the set up of the mounting frame to support the main chamber, electron gun, and camera. The main chamber, shown in Figure 2.1, contains two nozzle inlet ports for injecting the sample as a gas at two different nozzle-to-camera distances, and is connected to a mechanical camera and electron gun as shown. A cold trap (above the main chamber) is filled with liquid nitrogen during an experiment, minimising secondary diffraction of the sample during data collection. Oil diffusion pumps are connected to the main chamber as shown in Figure 2.2.

The mechanical camera, shown on the left in Figure 2.1, houses photographic film holders that are used to collect diffraction patterns on photographic film during an experiment. Extra plate holders have been made by the workshop (to replace the bent plate holders). The aim is to upgrade the mechanical camera to a digital detector in the future, as photographic film is no longer in production. The planned upgrade of the detector is described in Chapter 3.

Figure 2.1 Canterbury GED apparatus.

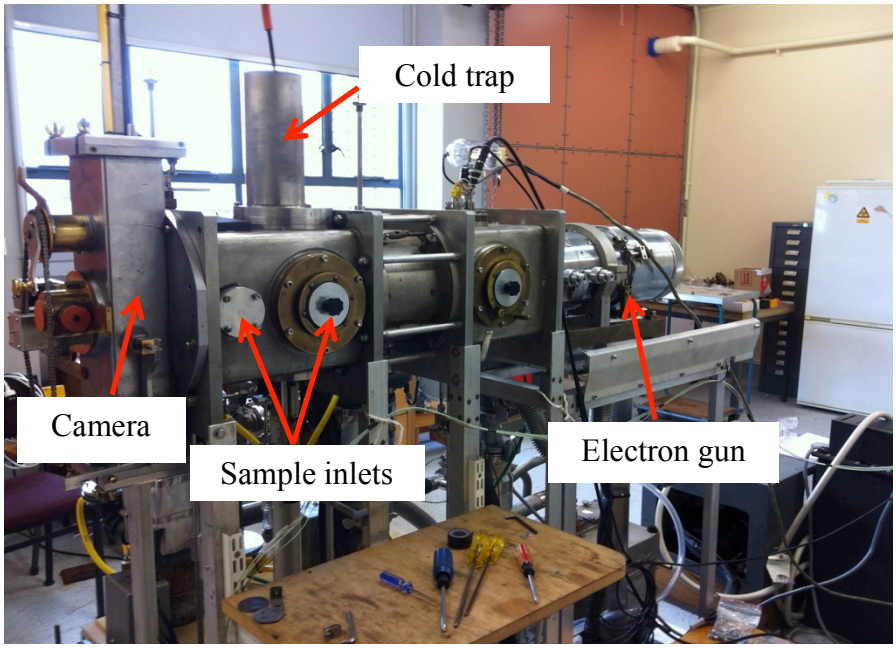

2.2.2 Vacuum pumps and cooling system

GED experiments are conducted under vacuum (10^{-6} – 10^{-7} Torr) ensuring diffraction of the electron beam occurs only at the point where it crosses the stream of gas vapour injected into the machine.[3] An operational vacuum is usually achieved with a series of diffusion pumps and/or turbomolecular pumps, run in unison with a suitable backing pump.[4]

Due to the high heat output of diffusion pump and turbomolecular pumps, external cooling is required to avoid overheating of the pumps during operation.[4,5] The vacuum system for the Canterbury GED apparatus originally consisted of two large, and one small, oil diffusion pumps (Figure 2.2), with a rotary backing pump. Cooling of the muck traps is provided by liquid nitrogen filled and there is also an external cooling water pipe around the exterior of the diffusion pumps. During initial installation, the feed pipes to the external cooling pipes (made of copper) were found to leak so these were replaced with rubber piping (Figure 2.2). The cooling water for the diffusion pumps works in conjunction with a chiller unit connected to each of the pumps.

Initial tests with these vacuum pumps resulted in an oil spill within the apparatus, with silicon oil from the smallest diffusion pump spreading into the main chamber and electron gun. Following extensive cleaning, trial repairs to the pump, and leak testing, the small diffusion pump was replaced with a small turbomolecular pump by the Chemistry workshop technical staff.

Figure 2.2 The vacuum setup of the Canterbury GED apparatus. The original three diffusion pumps are shown on the left. The smallest diffusion pump (left image as indicated) has been replaced with a small turbomolecular pump (see right image). The backing rotary pump is out of view (left of the setup as shown).

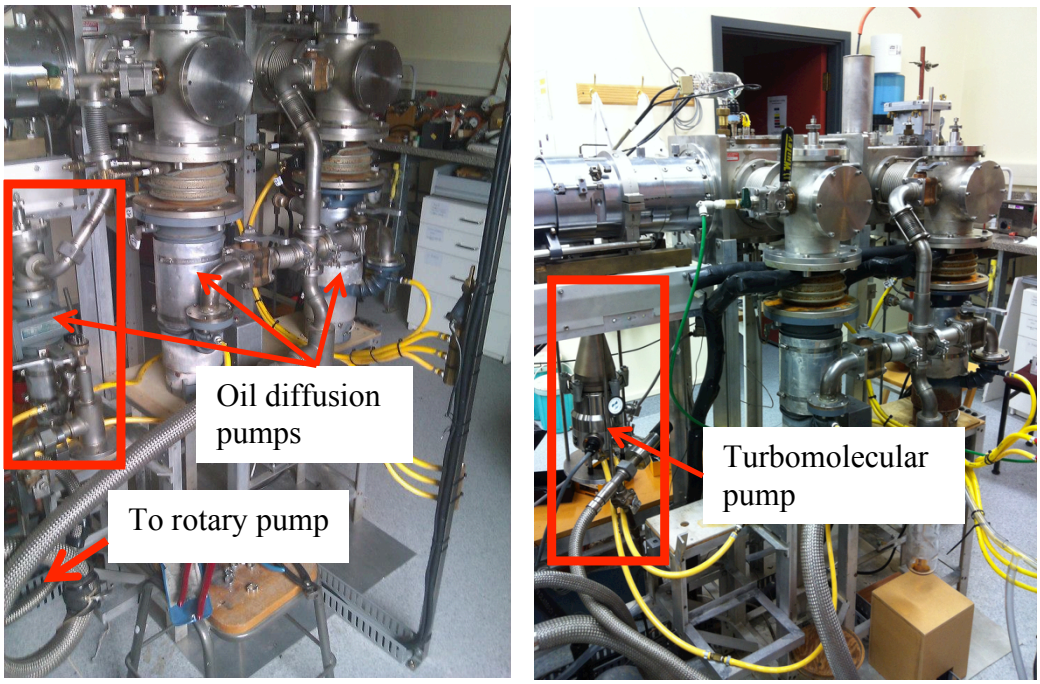

2.2.3 Electron gun

Having obtained a suitable vacuum, the electron beam needs to be aligned and focussed prior to the conduction of a GED experiment. In a GED experiment electrons are passed through an accelerating voltage of ca. 40 keV (electron wavelength ca. 6.0 pm) and are focussed through a series of lenses and apertures to provide a narrow beam. A digital camera connected to a small television set aids visualisation of the electron beam and helps to establish whether a clear path from the electron gun to the detector has been achieved.

The electron source for the Canterbury GED apparatus (Figure 2.3) has been adapted for use from a Phillips EM301 electron microscope apparatus. However since the electron microscope was designed for vertical operation, use of the electron beam in a horizontal setup (as it is for the Canterbury GED apparatus) can lead to problems with misalignment of the electron beam due to tilting of the electron gun. The construction of a sliding rack for the electron gun by the Chemistry workshop staff (see Figure 2.3) has aided the placement of the electron gun and allows for easy removal and access to the filaments.

Figure 2.3 Electron gun (attached to the main chamber) and mounted on a sliding track.

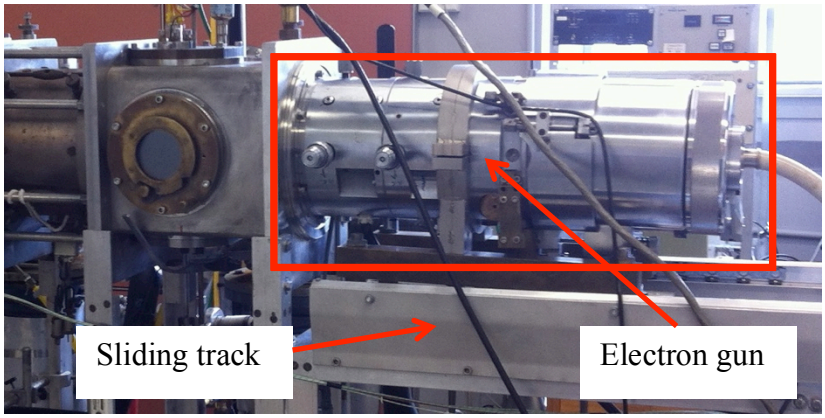

Whilst a clear path was established between the detector and electron gun using a laser, vacuum leaks were discovered when the electron gun was repositioned on the end of the main chamber (to correct for any off-tilt). Despite checking and cleaning the seals, a suitable vacuum for running the electron gun could not be re-established without extensive use of a leak tester. This meant that the vertical tilt of the electron gun, and subsequent beam alignment, could not be checked until a suitable vacuum was re-established.

2.2.4 Leak tester

Constructing or altering an apparatus that runs under high vacuum often results in vacuum leaks around the seals and valves that are so small that they cannot be detected without the use of a leak tester. During the reconstruction process of the GED apparatus, the leak tester from the Department of Physics and Astronomy

(University of Canterbury) was borrowed to aid in establishing a suitable vacuum. This leak tester works by acting as the backing pump for the apparatus, and detects leaks by indicating the presence of helium gas. Helium gas is directed at seals on the vacuum chamber externally, and is detected by the MS in the leak tester. Helium MS leak testers can typically detect leaks in the range of 10^{-2} to 10^{-8} Torr L s^{-1} so a suitable vacuum for the operation of the backing pump needs to have been established already.[4]

The leak tester was initially used whilst modifying the set up of the vacuum pumps (Section 2.1.2), after which time the electron gun and construction of the slide track were setup in position for testing. However, in the space of a few months, during which time the leak tester was not being used with the GED apparatus, the leak tester was discovered to have reached a state of disrepair and was abandoned by the Department of Physics and Astronomy. This has led to delays in getting the GED apparatus operational, as the leak tester first needs repairing. The delays and current state of the GED apparatus are described below.

2.2.5 Future work

Current efforts towards getting the Canterbury GED apparatus operational are hindered by the need for a working leak tester. This is particularly important for getting the electron gun aligned as adjustments that are made by detaching the electron gun from the main chamber can easily introduce more vacuum leaks in the apparatus. Work is underway by the Chemistry workshop staff to repair the leak tester. The rotary pump for the leak tester has already been replaced, with the oil and residue build-up from the diffusion pump and MS having been removed.

With the delay in repairs to the leak tester, the timeframe for the electron beam alignment, and experimental calibration of the GED apparatus has been set back. This has meant that the leak testing will recommence after the submission of this thesis. Future work with the Canterbury GED apparatus will involve leak testing of the GED apparatus before the electron beam alignment can continue. Following successful alignment of the electron beam (after a suitable experimental vacuum has been obtained), experimental calibration will commence.

2.3 Calibration of the GED apparatus

Following the establishment of suitable experimental conditions, calibration of the GED apparatus using benzene will be the next step. Although calibration data has not been obtained during this thesis, the methodology that will be followed for calibration of the Canterbury GED apparatus in future work will be outlined in this section.

During a GED experiment, data is collected for both a sample of interest and a calibration sample. The calibration sample will have a well-known bond length that will be used to accurately determine the nozzle-to-camera distance. Often a highly symmetrical molecule such as benzene is used,[6,7] with r_a(C–C) = 139.70 pm.[8] In the case of the Canterbury GED apparatus, benzene is collected either before or after running a sample through the apparatus to check that the nozzle-to-camera distance has not changed during the experiment.

The nozzle-to-camera distance is determined by multiplying the assumed nozzle-to-camera distance against the ratio of the refined and exact C–C distance of benzene. This can be represented as

$$\frac{r_a(\mathrm{C-C})_{\mathrm{calc}}}{r_a(\mathrm{C-C})_{\mathrm{exact}}} \times L = L_{\mathrm{exact}} \qquad (2.1)$$

where r_a is the apparent distance from the electron diffraction experiment[3] as calculated from the refinement [r_a(C–C)$_{calc}$] and from the literature [r_a(C–C)$_{exact}$], L is the assumed nozzle-to-camera distance and L_{exact} is the calculated nozzle-to-camera distance for the sample. Assumed distances of 95 mm, 210 mm and 285 mm are used during calibration for the high-temperature short, medium and long distances respectively. For the room temperature nozzle distances of 128 mm and 255 mm are used.

Following future upgrades to the GED apparatus, the nozzle-to-camera distances will change to a short and long distance upon incorporation of MS, rather than the three distances currently available. This will be discussed more in Chapter 3.

2.4 Conclusion

Following refurbishment of the available lab space, the Canterbury GED apparatus has been reassembled. Modifications to the apparatus have been made during the reconstruction process, mostly in part to repair the original vacuum pumps and cooling system. Efforts are now underway to align and focus the electron beam.

The introduction of vacuum leaks whilst adjusting the electron gun has delayed the establishment of suitable experimental conditions for the GED apparatus. The delays are also partly due to the time taken to repair the leak tester from the Department of Physics and Astronomy. Efforts are currently underway by the Chemistry workshop staff to repair the leak tester. The repairs of the leak tester have not been completed in time to include results for further leak testing of the GED apparatus and electron beam alignment in this thesis.

Future work with the GED apparatus includes the alignment of electron beam and calibration testing, once a suitable experimental vacuum has been established. The calibration method that will be used with the Canterbury GED apparatus has also been outlined.

2.5 References

1. C. M. Huntley, G. S. Laurenson and D. W. H. Rankin, *J. Chem. Soc., Dalton Trans.*, **1980**, 954-957.
2. S. H. Bauer and K. Kimura, *J. Phys. Soc. Jpn.*, **1962**, *17*, 300-305.
3. E. A. V. Ebsworth, D. W. H. Rankin and S. Cradock, *Structural Methods in Inorganic Chemistry*, Blackwell Scientific Publishing, Oxford, UK, 2nd edn., **1991**.
4. N. S. Harris, *Modern Vacuum Practice*, McGraw-Hill Companies, London, UK, **1989**.
5. A. Chambers, R. K. Fitch and B. S. Halliday, *Basic Vacuum Technology*, Taylor & Francis Group, Bristol, UK, 2nd edn., **1998**.
6. B. J. M. Bormans, G. De With and F. C. Mijlhoff, *J. Mol. Struct.*, **1977**, *42*, 121-128.
7. S. Gundersen, S. Samdal, T. G. Strand and H. V. Volden, *J. Mol. Struct.*, **2007**, *832*, 164-171.
8. G. Gundersen and D. W. H. Rankin, *Acta Chem. Scand. A*, **1983**, *37*, 865-874.

CHAPTER 3

Planning and design for a combined GED-MS apparatus

3.1 Introduction

Previous work by the Masters group[1] has focussed on developing the capability of studying the *in situ* generation of short-lived species using the Canterbury GED apparatus. However, to enable routine structure determination of short-lived species, there is a need to modify the apparatus to include MS capability.

The Canterbury GED apparatus generates short-lived species using pyrolysis methods[1] which can result in multiple species being formed in an experiment. While the composition of the gas vapour can be predicted by both *ab initio* calculations and previous experimental studies, the generation of short-lived species can result in further products being formed due to recombination[2] and/or further decomposition routes.[3] The incorporation of MS in a GED experiment not only provides additional information about the composition of the gas vapour (and relative amounts of each species), it also highlights the presence of any unexpected species. This is particularly important for future study of pyrolysis routes that are not previously detailed in the literature and those that do not cleanly form species, for example in a dissociation process, upon heating.

This chapter highlights the plans developed during this thesis for upgrades (and future upgrades) to convert the Canterbury GED apparatus to a GED-MS apparatus. The type of MS in the GED-MS apparatus design has been considered, as well as the additional requirements to perform tandem GED and MS experiments. The design presented here is discussed with comparisons to the setups used by the Girichev group (Ivanovo State University of Chemistry and Technology, Russia) and Wann group (University of York, UK). Although the implementation of all of the planned upgrades has not been achievable during the course of this thesis work, concept and schematics for the incorporation of MS with the Canterbury GED apparatus have been created and are presented here. The planned future upgrade of the mechanical camera to a CCD with the GED-MS setup will also be outlined.

The following sections present the conceptual and schematic designs for the incorporation of MS capability into the Canterbury GED apparatus. Details are presented regarding the type of ionisation method and mass analyser that is suitable

to allow simultaneous use of MS with GED in Section 3.2. For a short-term approach to a GED-MS design, Section 3.3 details the setup of an existing MS in a test rig to conduct experiments independently from GED (prior to the construction of the final GED-MS apparatus). Unfortunately the MS test rig did not work so experimental progress with the MS was halted. The last part of this chapter (Sections 3.4 – 3.6) covers the conceptual and schematic design requirements for conduction of both GED and MS techniques within a single experiment. These requirements are reflected in the concept designs to allow two nozzle-to-camera distances to be used in a GED-MS experiment. Schematic drawings are also presented giving detailed measurements of the new chamber section that is to be constructed to fit the existing framework of the GED apparatus. As a new MS could not be purchased within the timeframe of this thesis, the GED-MS designs in this chapter allow for flexibility in the required design to connect the MS unit to the GED main chamber. However, an ideal MS unit for a GED-MS design with the Canterbury GED apparatus has been highlighted as part of this planning stage.

3.2 Mass spectrometry in GED-MS

The choice of MS for a GED-MS design is strongly dictated by the samples being studied and the conditions required for a given GED-MS experiment, where the sample travels into the MS unit in the gas phase (sometimes at high temperature)[4,5] after it has diffracted the electron beam. It is possible for the sample to contain multiple molecular species therefore the chosen MS system is required to have suitable resolution for distinguishing between molecules of similar atomic mass, as well as covering a suitable range of detectable molecular masses.

MS is a technique that involves the separation of charged species by an applied magnetic field. Analysis of the charged species can be directly correlated to the species present in the original sample.[6]

Typically MS involves four stages:

(1) Ionisation of the molecule of interest after vaporisation.

(2) Separation of the charged ions by their mass-to-charge (*m/z*) ratio by a mass analyser providing an electromagnetic field.

(3) Amplification of the ion signal by a detector.

(4) Analysis of the amplified signal to obtain a mass spectrum.

Out of the four stages listed above, **(1)** and **(2)** are affected the most by a GED-MS setup and are discussed here. The type of MS that is suitable for a future GED-MS setup is also discussed.

3.2.1 Ionisation method

In a GED experiment the electron beam that is diffracted as it passes through the sample does not ionise the sample. Therefore the sample needs to be ionised separately before passing into the MS. Ionisation methods that can be used with GED are limited to those that can be applied to molecules already in the gas phase: electron ionisation (EI) and chemical ionisation (CI).

Electron ionisation

EI, also referred to as electron impact ionisation, is a harsh technique that involves bombarding the sample with electrons, producing charged species and fragmenting the molecule.[6] Reproducible fragments can be matched to databases to help

determine the overall structure of the species of interest. Ionisation occurs above the ionisation energy threshold of the sample.[7] For EI, an ionisation energy of around 70 eV (giving the electrons a wavelength that is similar to the bond length in organic molecules) so maximum energy transfer and fragmentation can occur during collisions. At energies greater than 70 eV, the probability of ionisation occurring decreases as insufficient energy is transferred in collisions with the electrons.[7] It should be noted that during a GED experiment, any ionising electron collisions occurring from the 40 keV beam can be considered negligible, i.e. such that ionisation during a GED experiment does not occur.

Chemical ionisation

CI produces ions through the collision of the sample with ions of a reagent gas such as methane, hydrogen, isobutane and ammonia.[8,9] The reagent gas is ionised preferentially to the sample (using a lower electron energy than in EI) and the resulting ionisation plasma of the reagent gas reacts with the sample to produce charged ions for analysis. Although CI is a softer technique, meaning that molecules are not as fragmented as in EI (which usually leads to simpler spectra),[8] it adds the additional complexity of introducing more gas vapours into the chamber during a GED experiment. This means that MS data cannot be collected using CI during a decomposition experiment that will produce the reagent gases as a byproduct.

Choice of ionisation method for the Canterbury GED-MS apparatus

Of the ionisation methods considered, EI was considered to be more suitable for the Canterbury GED-MS apparatus. Whilst EI can lead to greater complexity in the obtained mass spectrum, it does not limit the possible GED-MS experiments that can be investigated. The reagent gas used in CI restricts the collection of MS data to systems without the reagent gas, including those that generate it as a byproduct. Introducing more species into the main chamber also adds additional complexity, as a GED experiment will be conducted simultaneously with the MS experiment.

3.2.2 Mass analyser

There are various methods of separating the ions of different mass. Separation of the charged ions occurs within a mass analyser, such as a quadrupole mass spectrometer

(QMS), by subjecting the ions to a magnetic field, which separates the ions according to their mass-to-charge (*m/z*) ratio.[6,10] It should be noted that not all mass analysers use a magnetic field to separate the charged ions. A time-of-flight (TOF) mass analyser, for example, separates the charged ions in a field-free tube after subjecting them to an accelerating field by their flight time, as the *m/z* ratio of the charged species is related to its overall kinetic energy.[6,10]

The choice of mass analyser with a GED-MS design is dictated by the size of the MS (as it would be an additional component on the existing GED apparatus), the typical molecules used in a GED experiment, and the associated cost for purchasing a MS. Two of the features of mass analysers that are also important to consider are ion sensitivity and mass resolution. Ion sensitivity is the signal response detected normalised against the ion giving the response.[11] Mass resolution is the ability to distinguish two peaks at slightly different *m/z* ratios and is calculated in terms of the apparent width (ΔM) of the peak which appears for one type of ion (mass M), when plotted as ion current versus mass number (Equation 3.1).[10] Mass resolution is typically measured at either 5, 10 or 50 % of the total peak height.[11]

$$\text{Resolution} = \frac{M}{\Delta M} \tag{3.1}$$

Of the various mass filters that are available, a QMS and TOF mass analyser were considered for the Canterbury GED-MS design. These filters are discussed below, highlighting the achievable mass range of the analyser compared to the mass range required for future GED-MS experiments. Typically the mass range that a MS can detect is reported in daltons (Da) where 1 Da = 1.660538921(73) x 10^{-27} kg and is equivalent to 1 g mol^{-1}.[6] In this thesis, the mass range will be referred to in Da as it is cited in these units from the literature sources.

Quadrupole mass filter

A QMS works by directing an ion beam through a series of circular and hyperbolic rods, selectively filtering ions based on their *m/z* ratio.[6,10] An oscillating field is

applied between four hyperbolic rods, allowing charged ions with a particular *m/z* ratio for a given voltage to resonate and pass through the rods to a detector (Figure 3.1). The trajectory of a non-resonant ion is disrupted in the oscillating field, ejecting the ion before it reaches the detector. To build a full mass spectrum a sweeping potential voltage is usually applied so that smaller ions are detected first followed by larger ones. The continual resetting of the sweeping allows for a mass spectrum image to be built.[10]

The detectable mass range for QMS filters varies depending on the model. Typically QMS filters have low to medium resolution[11] due to an increased signal-to-noise ratio when using a sweeping voltage. However, an increased resolution of the mass analyser can be achieved by sacrificing sensitivity (ion transmission).[11] Commercial QMS filters can have mass ranges of < 100 Da to ~ 3000 Da.[11] In comparison, a TOF analyser (described below) can detect mass ranges up to several hundred, or even thousands of Da with high sensitivity and mass resolution.

Figure 3.1 Setup of a quadrupole mass analyser. An electric field is applied along the two sets of hyperbolic rods to separates ions by their charge, with a particular charge to reach the detector. A MS image is built up by sweeping the potential over a range of values.

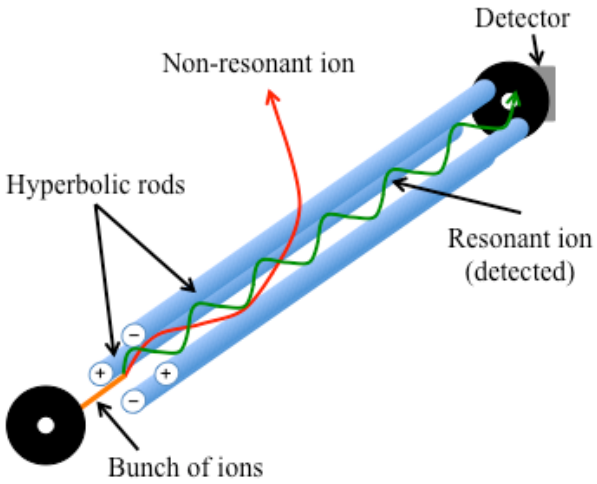

Time-of-flight mass analyser

A TOF mass analyser separates the charged ions by applying an accelerating voltage (to induce an electric field), separating the ions according to their *m/z* ratio along the

length of the TOF tube (Figure 3.2). The aim of a TOF analyser is to give all ions the same energy, so that their velocities, and hence the time taken to reach the detector, are a function of the mass/charge ratio.[6,10] As a result, lighter ions reach the detector first.

For a TOF-MS with path length l (see Figure 3.2 for reference) ions of mass m and velocity v passing through a potential V in the accelerating field, the energy of the ions, E, is given by

$$E = \frac{1}{2}mv^2 = eV \tag{3.2}$$

where e is the charge of an electron ($1.60217657 \times 10^{-19}$ coulomb). Therefore, the resulting time for the ions to reach the detector is simply[10]

$$\text{time of flight} = \frac{l}{V} = l\left[\frac{2eV}{m}\right]^{\frac{1}{2}} \tag{3.3}$$

Figure 3.2 Setup of a linear TOF-MS. The ions are accelerated before separating by their *m/z* ratios in the flight tube (**1 – 3**), with lighter ions reaching the detector first.

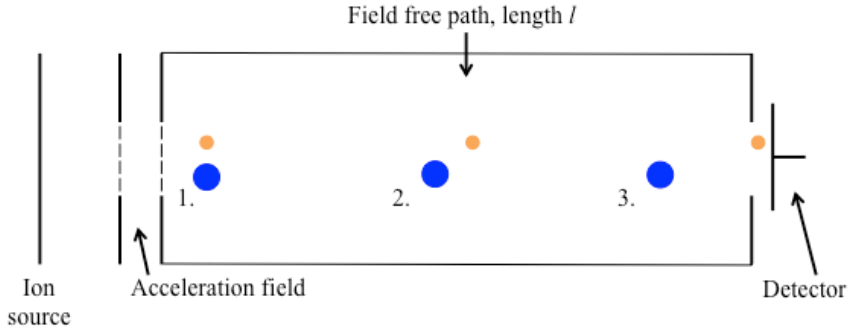

The ability of a TOF mass analyser to separate ions of similar mass has been improved by variations to a TOF analyser that include a reflectron TOF.[6] In a reflectron TOF the separated ions are reflected within an electrostatic field back towards the detector. Lighter ions penetrate further into this field before being

deflected compared to the heavier ions. This results in all of the ions reaching the detector at the same time, which is often referred to as a TOF focus. TOF mass analysers can detect upwards of 1000 – 3000 Da compared to upwards of 100,000 Da in a reflectron TOF.[11] A reflectron allows for the flight path to be double in length for half of the space required for a conventional TOF. However, for the convenience of a smaller apparatus the electronics and controls for a reflectron TOF quickly scale upwards in cost with an increase in ability to separate the ions. An increased resolution and sensitivity also scales upwards in cost with other MS filters, especially for custom designs.

Choice of mass filter for the Canterbury GED-MS apparatus

Both a QMS and TOF mass filter were proposed to be suitable for the Canterbury GED apparatus, with EI as the proposed ionisation method. While a QMS would be suitable for the current systems being studied by GED, a TOF would allow for a wider mass range of molecules to be analysed, and would provide an improvement on the resolution of a QMS. Also, if a build up of the molecular ion beam were necessary for MS analysis (due to low vapour pressure), a TOF analyser would be preferable.

3.3 Proposed MS for the Canterbury GED-MS setup

For a short-term approach to a GED-MS design, a QMS was available for use from the deconstructed molecular ion beam machine of Professor Peter Harland (University of Canterbury). However, the intention of the Canterbury GED-MS design is to incorporate a TOF for long-term use, as it would allow the study of a wider range of species. Preliminary tests with the QMS were unsuccessful as discussed below.

3.3.1 Preliminary tests with MS for GED-MS

Prior to the concept and schematic designs for the modifications to incorporate MS with the Canterbury GED apparatus, a MS test rig and vacuum setup was to be constructed. The plans to make a MS test rig occurred shortly after commencing the reconstruction and modification stage of the Canterbury GED apparatus (see Chapter 2) so it was advantageous to modify the two setups independently, prior to combining them together in the final GED-MS setup (as discussed in the later sections of this chapter). The construction of a separate MS test rig (with its own vacuum system) would allow independent experiments with the MS to be conducted before and after a GED experiment to check the purity of a sample. After establishing the combined GED-MS apparatus, a separate vacuum system for the MS would also allow the MS to be isolated from the main GED chamber (while still under vacuum) to change sample and nozzle-to-camera distance, shortening the time for an experimental vacuum to be re-established between data collection runs. Also, as gains in resolution and sensitivity with MS are ultimately linked to vacuum quality[11] it was deemed important to establish a good vacuum system for use with the MS.

As part of preliminary work towards designing the Canterbury GED-MS setup a QMS from Professor Peter Harland (University of Canterbury) was available for use. Whilst the QMS had not been used in many years, all of the electronic control units were available and it had an inbuilt EI source. The detectable mass range of up to 300 Da was also suitable for preliminary studies for simple, small molecules such as benzene and acetone.

Over the course of two years, a suitable vacuum system was constructed for the QMS using a small turbomolecular pump and rotary backing pump (Figure 3.3, left). Initial tests indicated an achievable vacuum of approximately 10^{-5} Torr, but despite this being a suitable vacuum pressure to operate the QMS with, the QMS would not turn on (presumably due to its pressure interlock). After checking the electronics of the QMS the vacuum system of the MS test rig was upgraded, changing the turbomolecular pump to a larger oil diffusion pump with a liquid nitrogen cold trap (Figure 3.3, right). Despite having achieved a better vacuum of 10^{-7} Torr compared to the initial setup (after months of leak testing with the test rig) the QMS was still not operational. Further tests at this point indicated the problem to be with the control unit used to operate the QMS.

The failure to get the QMS operational at this point led to the abandonment of experimental work with the MS test rig. Even if time (and money) were spent fixing the QMS control unit, this would not guarantee successful implementation of the QMS. Also, the intention for the GED-MS is to purchase a MS with a larger mass range (preferably a TOF). It was decided that experimental work with the MS unit would be put on hold until after the purchase of a new MS. However, the purchase of a new MS is still pending.

As a result, the following sections in this chapter present the conceptual and schematic designs for the Canterbury GED-MS apparatus. The specific requirements for MS in a GED-MS design are highlighted, while allowing for flexibility in the specific choice of MS and how it will interface the GED apparatus.

Figure 3.3 Setup of the MS test rig with **(a)** the initial setup with a turbomolecular pump and **(b)** with a larger oil diffusion pump replacing the turbomolecular pump. The quadrupole is inside the chamber as indicated. Note that the framework in **(b)** has been altered to accommodate the larger pump.

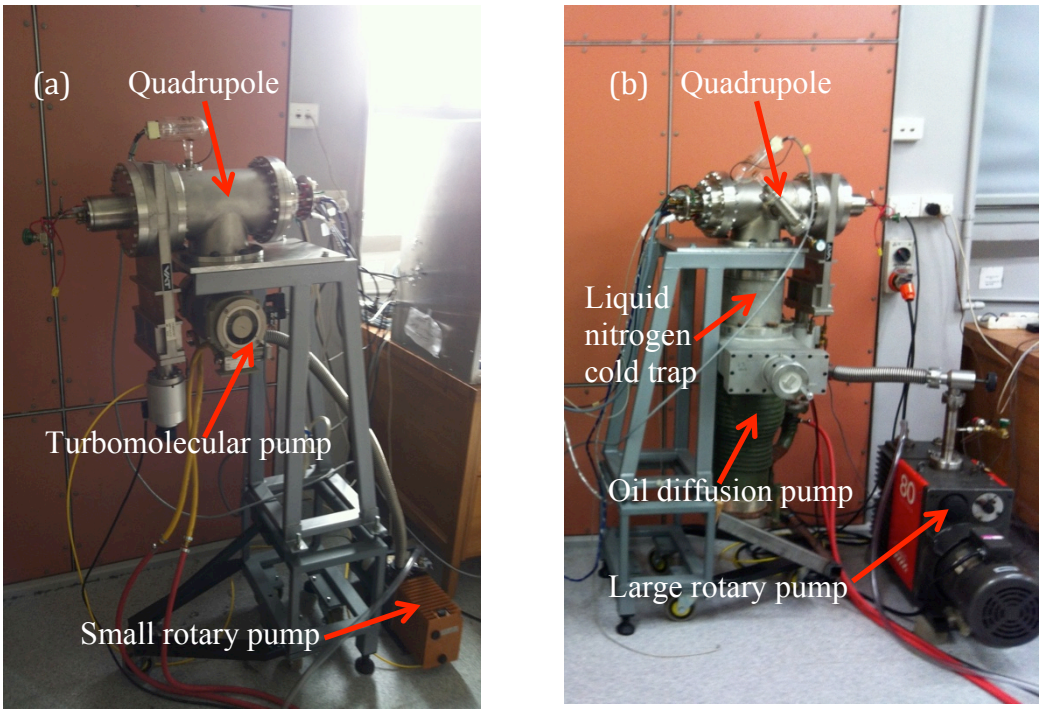

3.4 Requirements for a GED-MS design

For the incorporation of MS into a GED experiment, the sample inlet and MS unit have to be directly opposite each other. This is so when the sample is injected into the apparatus, electron diffraction occurs before the gas vapour continues to the other side of the chamber into the MS. This is illustrated in Figure 3.4.

Figure 3.4 Simplified setup of a GED-MS apparatus showing the gas vapour (blue line) interacting with the electron beam before travelling into the MS unit.

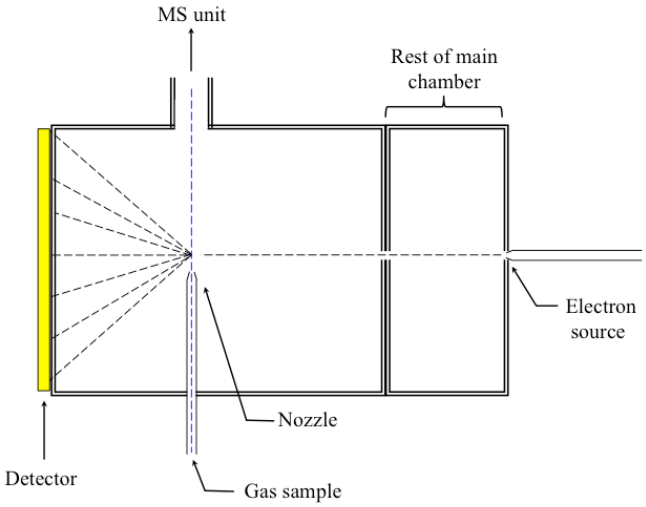

The challenge in incorporating the MS unit arises from the need to change the nozzle-to-camera distance, to allow for variable-angle data collection. In a GED experiment variable-angle data collection is necessary to obtain as much structural data as possible. A short nozzle-to-camera distance will allow wide-angle data to be collected and a longer nozzle-to-camera distance provides narrow-angle data.[6] An overlapping part of the data collection from both distances is checked to ensure the integrity of the sample between runs.

To obtain data from two different distances in a GED-MS experiment either the inlet nozzle and the MS unit, or the camera (detector), has to move. Both of these designs are currently in use by other GED groups. The choice of how to change the nozzle-to-camera distance leads to large differences in experimental design as highlighted in the next section.

3.5 Nozzle-to-camera distance design

To obtain data from two different distances in a GED-MS experiment either the inlet nozzle and the MS unit will have to move, or the camera (detector) has to move. A fixed camera is used in the GED-MS setup of the Girichev group (Ivanovo, Russia)[12] and a fixed MS position is used in the setup for the Wann group (York, UK).[13] It should be noted that GED machines are custom built so can differ widely from group to group. Both potential designs are discussed below.

3.5.1 Fixed detector, moveable inlet system (Girichev group)

The GED-MS apparatus of the Girichev group (Ivanovo, Russia) involves a monopole MS unit that moves with the inlet system in relation to a fixed image detector.[12] The nozzle-to-camera distance is changed by moving the inlet system and MS unit to one of two sets of fixed distance inlet ports (Figure 3.5).

The apparatus is vertical in its arrangement with respect to the direction of the electron beam compared to the Canterbury GED apparatus (which is horizontal). This means that the shift of the MS unit and nozzles is vertical in this apparatus (parallel to the direction of the electron beam) between the two sets of ports as shown (Figure 3.5). Since the two distances available for a GED experiment are fixed, there is minimal adjustment and alignment required. However, the main downside to this particular design is that either the whole machine has to be brought back up to atmospheric pressure to change the nozzle-to-detector distance or the MS has to be isolated under vacuum as the distance is changed. In the case of this GED-MS setup, the Girichev group bring the apparatus to atmospheric pressure between experiments to move the inlet system.

Figure 3.5 Vertical GED-MS setup of the Girichev group (Ivanovo, Russia). The setup shows the MS and nozzle in the shorter of the two available positions.

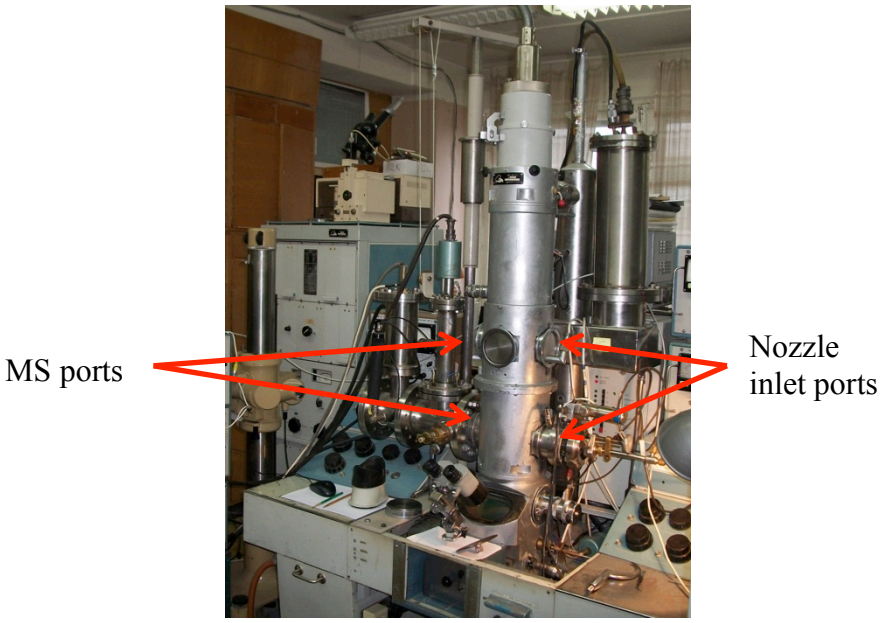

3.5.2 Fixed inlet system, moveable detector (Wann group)

The GED-MS system of the Wann group has a horizontal setup, with respect to the direction of the electron beam, similar to the Canterbury GED apparatus.[13] In this setup a QMS unit remains fixed in position while the CCD moves. The Wann group modified the CCD so that it was held within a cylindrical tube with an outer tube layer (Figure 3.6). This cylindrical tube is allowed to move within the port on the diffraction chamber while the chamber is under vacuum to alter the nozzle-to-camera distance.[13] However, this setup is not without problems. In particular, vacuum leaks around the CCD casing is an issue that is currently being addressed by the Wann group.

Figure 3.6 Front view (left) and rear view (right) of the CCD camera and vacuum casing used by the Wann group (University of York).

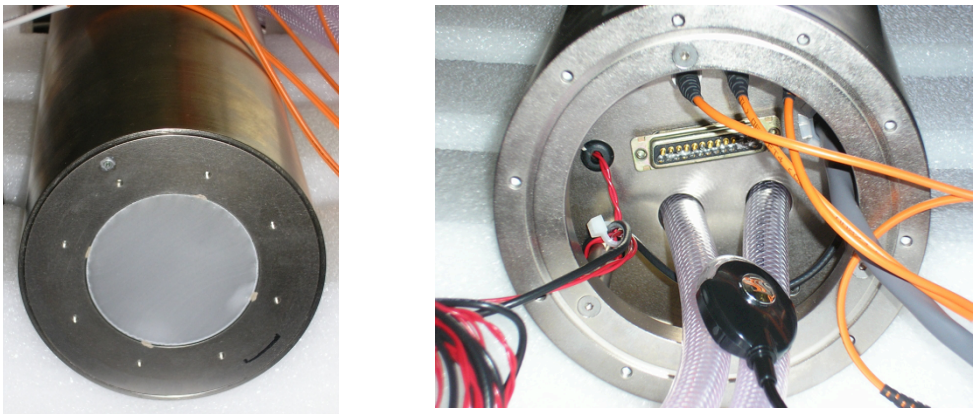

3.5.3 Nozzle-to-camera outline for Canterbury GED-MS

From consideration of the GED-MS designs from the Girichev and Wann groups, a moveable CCD with fixed inlet and MS unit was chosen for the Canterbury GED-MS design. Although both modification options are viable, a design based on that used by the York group (with a similar horizontal beam setup as the Canterbury apparatus) was determined to be the best option for the Canterbury GED-MS design. It will minimise the need to shift and readjust the position of the MS unit between experiments which will help preserve the lifetime of the MS unit, as continuously bringing the MS back to atmospheric pressure (from vacuum) will reduce its expected lifetime.[11] The downside of the design used by the Wann group is the vacuum casing for the CCD camera, which while allowing for adjustment under vacuum, is prone to generating vacuum leaks. An alternative design to change the position of the camera of the Canterbury GED-MS apparatus is given in Section 3.6. It is expected that the new design will minimise the generation of vacuum leaks compared to the Wann group's design.

3.6 Modification of the Canterbury GED apparatus

The modification of the Canterbury GED apparatus to incorporate MS capability focusses on redesigning the main chamber. As discussed in Section 3.5.3, the Canterbury GED-MS modification will involve a fixed inlet and moveable detector. The aim of this GED-MS design is to retain as much of the existing GED apparatus framework as possible. As such, the design of the GED-MS chamber is based on the existing chamber dimensions to minimise alterations to the framework and the rest of the GED apparatus.

The conceptual and schematic designs for the incorporation of MS capability into the Canterbury GED apparatus are presented. As the MS unit for the GED-MS apparatus is yet to be purchased, the schematic designs for integration of the MS to the GED chamber have not been rigorously proposed. This will allow flexibility in the schematic measurements for the interface of the MS with the chamber. An ideal MS unit for a GED-MS design with the Canterbury GED apparatus has been highlighted (Section 3.3) as part of this planning stage.

3.6.1 Outline of modification and requirements

The main chamber of the Canterbury GED apparatus is made up of three separate sections, with the section highlighted in bold in Figure 3.7 being the diffraction zone. The main chamber to be modified is connected to a camera (detector) opposite the electron beam, the sample inlet nozzle opposite one of the diffusion pumps and the cold trap opposite the room temperature nozzle inlet underneath the chamber. Schematic views of the current GED setup generated from Open Source CAD (QCAD),[14] a free online engineering software tool, are shown in Figure 3.8.

To enable the MS unit to be opposite the sample inlet the positions of the vacuum pumps around the main chamber need to be altered. This is primarily due to the position of one of the diffusion pumps occupying the proposed location of the MS unit in the original apparatus design. For this to happen a new section of the main chamber will be constructed with appropriate ports to allow the sample inlet nozzle and MS unit to align. To maintain the current experimental vacuum, both diffusion pumps on the MS side of the chamber will be moved underneath the main chamber

(replacing the room temperature nozzle since both high and room temperature experiments can be conducted using the main large nozzle port).

Figure 3.7 Highlighted section of the GED machine where the chamber will be modified (bold outline) and the section of chamber (to the right of it) to be removed to incorporate the longer GED-MS chamber design (dotted outline).

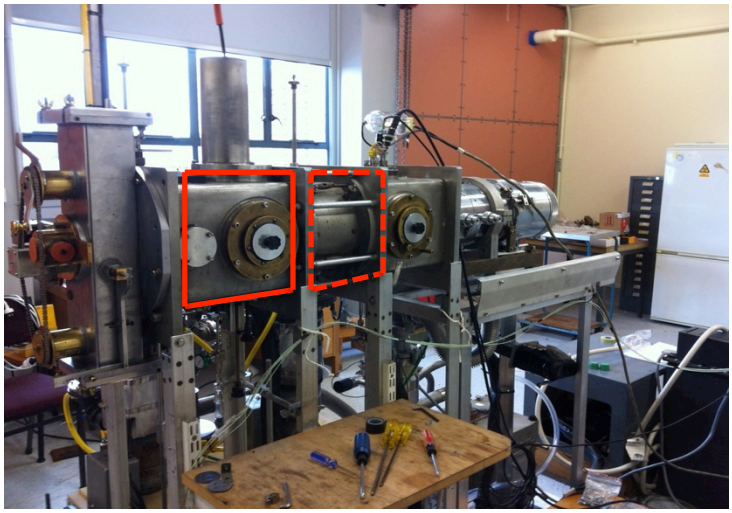

The Canterbury GED apparatus currently uses a mechanical camera with photographic film as the detector but the future aim is to have a set up with a CCD. This is a necessary upgrade as the photographic films are no longer available for purchase when the current supply runs out. Integrating a CCD will also remove the need for a rotating sector (which stops overexposure in the centre of the photographic film[6]) and will remove the problems associated with the change in measured scattered angle relative to the detector position. As such, a CCD is an integral part of the GED-MS modification to the Canterbury apparatus. The design concepts and schematics are given below in Sections 3.6.2 and 3.6.3 respectively take into account the incorporation of a CCD, while allowing the mechanical camera to be used in the interim.

Figure 3.8 Selected views of the current GED chamber design looking from the camera end **(a)** towards the electron gun showing **(b)** the port size for the current diffusion pump (left hand side), and **(c)** the inlet port sizes for the sample nozzle (right hand side). A schematic of the top side and underneath side of the diffraction chamber (showing the cold trap and room temperature inlet respectively) is not shown. Measurements were made using callipers. All dimensions are in millimetres (error ± 0.005 mm).

(a)

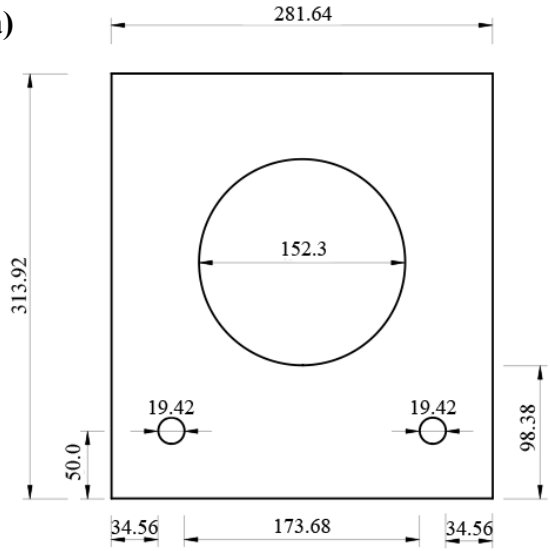

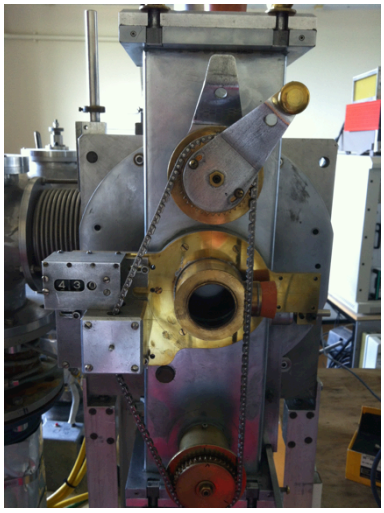

(b)

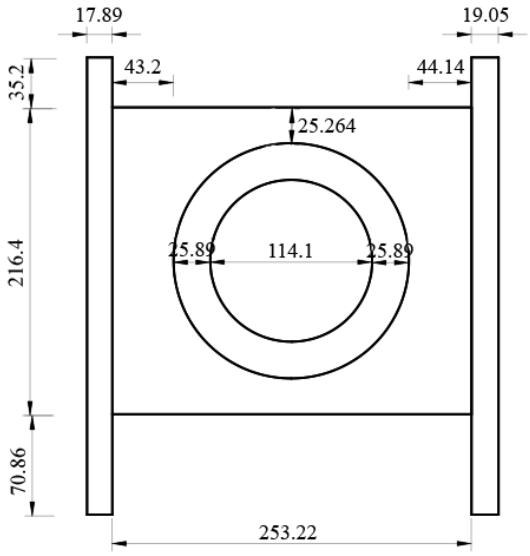

(c)

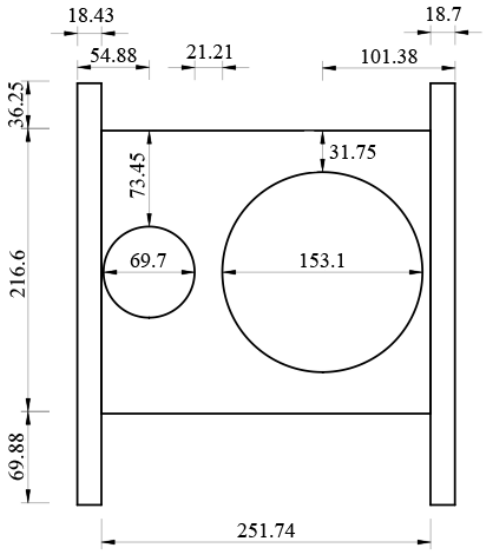

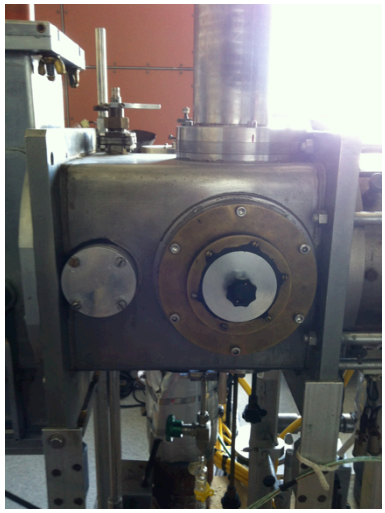

3.6.2 Design concept for the Canterbury GED-MS apparatus

As stated above, the design of the Canterbury GED-MS will be based upon that of the Wann group with a moveable CCD in relation to a fixed MS and nozzle inlet system. To allow for changes in the nozzle-to-camera distance, a spacer unit has been proposed which can be placed between the camera and main chamber, to change the nozzle-to-camera distance (Figure 3.9a and 3.9b). This will potentially be an improvement on the design used by the Wann group (Section 3.5.2) as the MS unit and main chamber can be isolated from each other to change the nozzle-to-camera distance without the issue of generating vacuum leaks around a CCD vacuum casing.

As part of this design, two inlet ports will be included so that multiple nozzle-to-camera distances can be used while the spacer unit is being constructed. Currently the very-high-temperature nozzle (VHT) (allowing sample heating of up to 1100 K)[1,15] can only be used from one distance in the chamber (the large port shown in Figure 3.8c) since the inlet ports are not the same size. The GED-MS design includes two inlet ports to incorporate the VHT nozzle at both distances. An adaptor allows for the medium temperature nozzle to be used (which is smaller in diameter than the VHT nozzle). This will mean that high temperature experiments can be conducted from each port, allowing for wide data collection.

Another advantage of having two ports for initial use during development is that it allows for the use of both the mechanical camera and photographic film until after the spacer unit has been made. Prior to the incorporation of the CCD, both ports will be used with the mechanical camera, with MS data being collected at the shortest nozzle-to-camera distance (Figure 3.10). Following the implementation of the spacer unit, the long distance port (furthest from the camera) will be no longer used, as the nozzle-to-camera distance will be completely controlled by the addition and removal of the spacer unit. This is elaborated further in Section 3.6.3 with the design requirements of the spacer unit.

Figure 3.9 Schematic top-down view of the proposed GED-MS setup **(a)** with the spacer unit and **(b)** without the added spacer unit. The second inlet port (covered with a blanking plate) will not be used once the CCD and spacer are implemented.

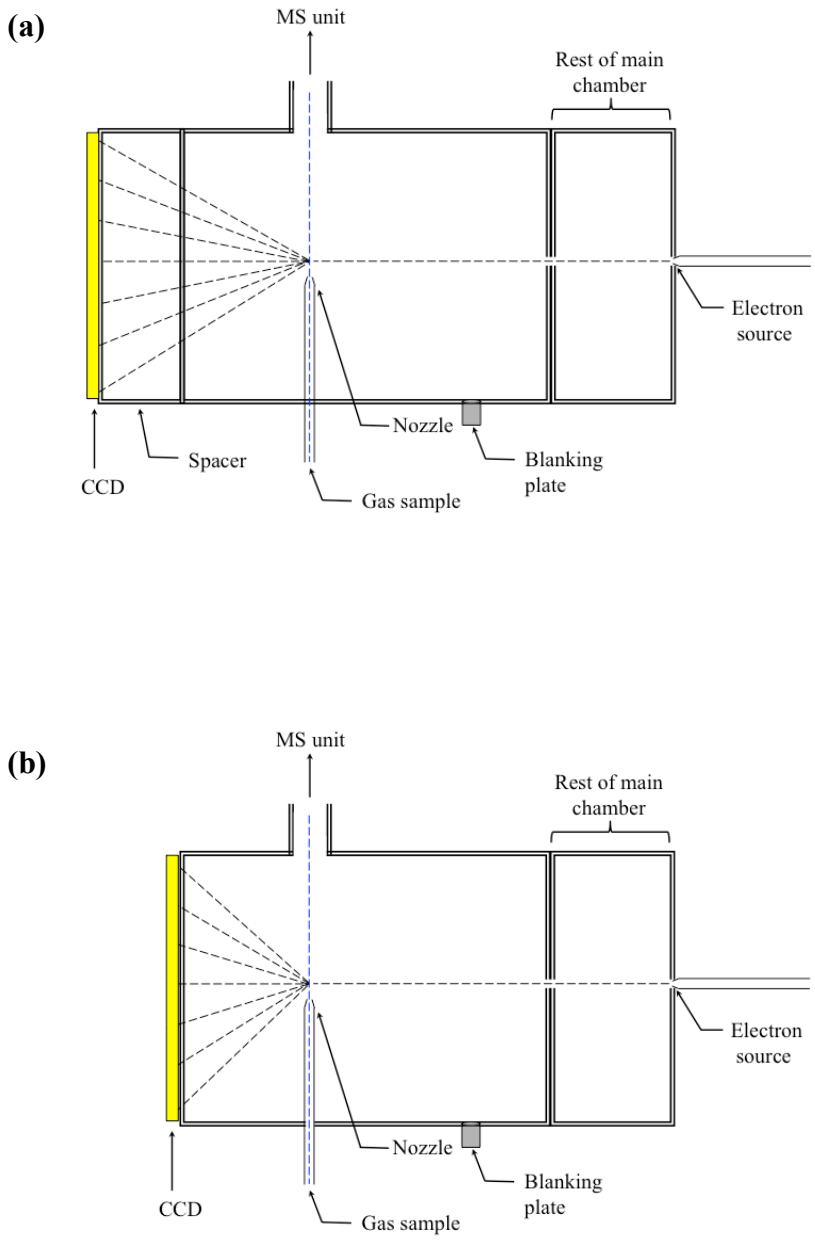

Figure 3.10 Schematic top-down view of the proposed GED-MS setup before the CCD and spacer are implemented. The position of the nozzle can change between **(a)** and **(b)**, with MS only being collected at position **(a).** This is in contrast to the final design (which will collect MS data at both distances) shown in Figure 3.8.

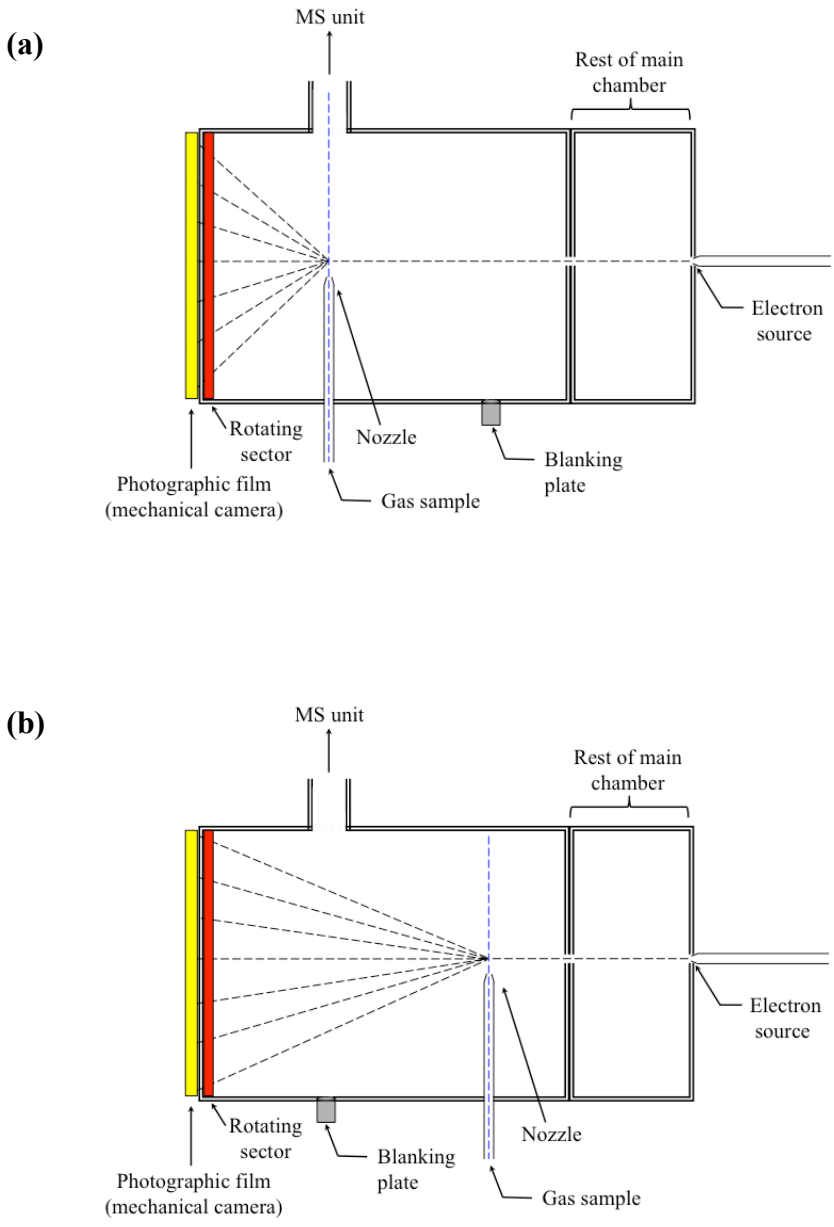

3.6.3 Schematics for the GED-MS design

The design specifics for the GED-MS chamber are highlighted below for the nozzle inlet ports and camera section of the chamber. Requirements for the side of the chamber incorporating the MS unit will be touched upon briefly. The remaining sections of the chamber involving the cold trap and repositioning of the vacuum ports is not covered, as this will allow flexibility in design during the construction process by the Chemistry technical staff, as the frame supporting the main chamber will likely be modified to allow inclusion of the pumps on the underside of the chamber.

Nozzle inlet ports

The schematics shown in Figure 3.11 highlight the planned construction of the nozzle inlet side of the GED-MS apparatus. The two large ports will allow for VHT data to be collected at both long and short distances with the mechanical camera, prior to upgrading to a CCD. From previous experiments with the Canterbury GED apparatus, the two nozzle-to-camera distances were determined to be approximately 95 mm and 285 mm. These were chosen to keep the nozzle-to-camera distances consistent with previous experiments and to accommodate two large inlet ports that can house the VHT nozzle. The required distance is measured from the centre of the inlet port to the edge of the chamber where the front edge of the CCD would align.

However, as shown in Figure 3.11, the distance for the two ports (95 mm and 285 mm), allowing for a suitable separation between the two ports, exceeds the current dimension of the diffraction chamber (approximately 300 mm as from Figure 3.8c). This means that the empty section of chamber next to the diffraction zone (Figure 3.7) will be removed to accommodate it.

Figure 3.11 Proposed schematic for the nozzle inlet side of the main chamber. The two required nozzle-to-camera distances (95 mm and 285 mm) have been indicated.

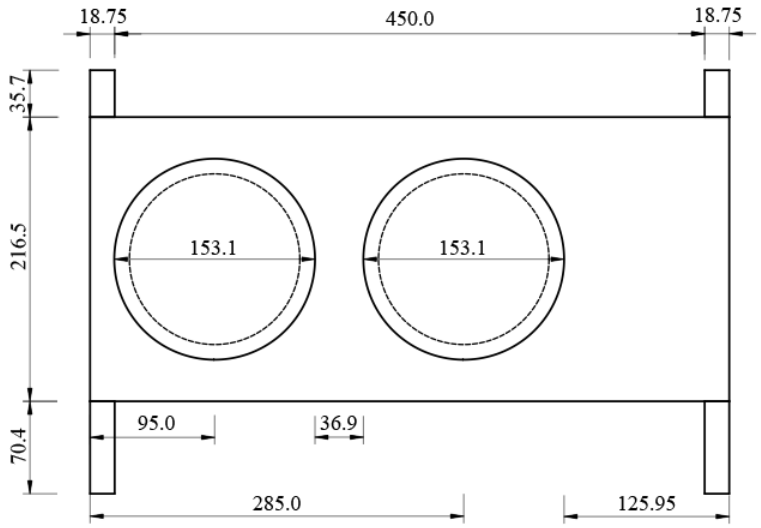

Camera port

The end of the chamber to house the CCD is to be kept the same as with the current GED chamber (Figure 3.6a) to allow for use of the mechanical camera during development of the spacer unit. As part of the planned incorporation of a CCD, an adaptor will be fitted to allow the incorporation of the CCD camera into the current camera port. This adapter has yet to be designed as it will be affected by the setup of the electronics of the CCD during preliminary testing.

MS port

The side of the chamber which will incorporate the MS unit requires a port for the MS unit to be made for it to align with the nozzle closest to the camera end (the left hand side port shown Figure 3.8). The MS unit will be placed at this port to allow for collection of data at a short nozzle-to-camera distance in the absence of the spacer unit. The width of the GED-MS chamber allows a MS to be placed within 300 mm of the inlet nozzle which, as discussed by Girichev,[12] is important to allow for laminar flow of the gas vapour into the MS chamber. Distances greater than 300 mm will mean that more gas vapour has to be produced for the sample to reach the MS, especially as resolution and ion transmission decrease with long ion paths.[11] A small port for entry of the gas vapour to the MS is preferred for differential pumping.[12]

This will be important to consider when incorporating a MS with the GED apparatus in the future.

3.7 Conclusion

Current progress towards a GED-MS apparatus has seen the identification of EI and TOF as the favoured choice of ionisation method and mass filter for the Canterbury GED-MS apparatus. A preliminary setup of an old QMS as part of the concept development was unsuccessful and experiments were put on hold until a new MS has been purchased. The requirement for performing simultaneous GED and MS experiments has led to a proposed design of a moveable CCD in relation to a fixed MS and nozzle inlet system. A new chamber for the GED-MS apparatus has yet to be constructed to allow inclusion of the MS unit (ideally a TOF) and the current vacuum pumps as the MS has yet to be purchased. Schematic designs have been presented for the new chamber while allowing flexibility in the specific choice of MS being incorporated into the new chamber, which will be mounted on the existing GED framework. Measurements and detailed schematics to allow for modification of the nozzle-to-camera distance (for wide angle data collection) have been presented.

To modify the nozzle-to-camera distance in a GED-MS experiment, a spacer unit has been proposed to work in conjunction with the CCD. The end of the chamber will be modelled using the current design to allow for the mechanical camera to be used whilst the CCD and spacer unit are developed. Two large nozzle inlet ports are included in the design to allow for collection of VHT data at short and long nozzle-to-camera distances, and for use of the mechanical camera in the interim. Following implementation of the CCD and spacer unit, only one of the nozzle inlet ports will be used, as the spacer unit will control the nozzle-to-camera distance. Plans to vary the proposed nozzle-to-camera distances (95 mm and 285 mm) and include a medium distance by construction of spacers of varying widths will be considered following the successful implementation of the GED-MS design.

3.7 References

1. R. Noble-Eddy, PhD Thesis, University of Edinburgh, Edinburgh, Scotland, **2009**.
2. F. Chick and N. T. M. Wilsmore, *J. Chem. Soc., Trans.*, **1908**, *93*, 946-950.
3. L. Khachatryan, R. Asatryan, C. McFerrin, J. Adounkpe and B. Dellinger, *J. Phys. Chem. A*, **2010**, *114*, 10110-10116.
4. J. W. Hastie, D. W. Bonnell and R. K. Schenck, *Pure Appl. Chem.*, **2000**, *72*, 2111-2126.
5. J. Drowart, C. Chatillon, J. Hastie and D. Bonnell, *Pure Appl. Chem.*, **2005**, *77*, 683-737.
6. D. W. H. Rankin, N. W. Mitzel and C. A. Morrison, *Structural Methods in Molecular Inorganic Chemistry*, John Wiley & Sons, Ltd, Chichester, West Sussex, UK, **2013**.
7. F. H. Field and J. L. Franklin, *Electron Impact Phenomena and the Properties of Gaseous Ions*, Academic Press, New York, London, Revised edn., **1970**.
8. M. S. B. Munson and F. H. Field, *J. Am. Chem. Soc.*, **1966**, *88*, 2621-2630.
9. T. Cairns and E. G. Siegmund, *Biol. Mass Spectrom.*, **1982**, *9*, 307-309.
10. P. F. Knewstubb, *Mass spectrometry & ion-molecule reactions*, Cambridge University Press, London, UK, **1969**.
11. *Atomic, Molecular and Optical Physics: Charged Particles*, Eds. F. B. Dunning and R. G. Hulet, Academic Press, Inc., San Diego, California, USA, **1995**.
12. G. V. Girichev, S. A. Shlykov and Y. F. Revichev, *Instrum. Exp. Tech. (English Transl.)*, **1986**, *29*, 939-942.
13. D. A. Wann, personal communication, **2013**.
14. Open Source CAD (QCAD), http://www.qcad.org.
15. S. L. Masters, G. V. Girichev and S. A. Shylkov, *Dalton Trans.*, **2013**, *42*, 3581-3586.

CHAPTER 4

GED investigation of the gas-phase molecular structure of ketene, and computational investigation of selected RR'C=C=O derivatives

4.1 Introduction

Previous work in the Masters group has focussed on the generation of molecules in the gas phase on the millisecond to second timescale using pyrolysis methods. In these experiments, molecules are generated using *in situ* pyrolysis techniques utilising a VHT nozzle developed by the Masters group[1,2] in conjunction with the expertise of the GED group in Ivanovo, Russia. Testing of the nozzle with antimony(III) oxide has shown the capability of the nozzle for the study of non-volatile species,[2] but not the capability of the combined VHT-GED system to generate short-lived species.

Work by Robert Noble-Eddy in the Masters group[1] focussed on the generation of ethenone (CH_2CO), the simplest example of a ketene, from three different precursors: acetic anhydride, Meldrum's acid and acetone. Ethenone ($H_2C=C=O$), referred to ketene throughout this work, was chosen as a test case, as it is an unstable molecule, dimerising rapidly to form diketene [$(CH_2CO)_2$] at room temperature.[3] Ketene itself has been studied before by GED by carefully storing a cold sample,[4,5] and can be generated from a variety of precursors. Several ketene derivatives have been studied by GED, including diketene and methyldiketene,[6] bis(trimethylgermyl)ketene,[7] bis(trifluoromethylthio)ketene[8] and, perhaps most interestingly, dichloroketene,[9] which was generated from the precursor trichloroacetyl chloride using a gas-solid reaction.

While Noble-Eddy was able to collect pyrolysis data for acetic anhydride and Meldrum's acid, there were problems regarding processing and analysing of the experimental data.[1] In particular the experimental data collected for Meldrum's acid, which pyrolyses to give carbon dioxide, ketene and acetone,[10] was thought to contain another equivalent of ketene and methane due to secondary pyrolysis of acetone.[11] This is shown to not to be the case in this chapter, as the GED data were determined to contain diketene (from the recombination of ketene to diketene).[3] The presence of diketene was not accounted for by Noble-Eddy[1] despite diketene being the same colour as the brown residue remaining after conducting the GED experiment. The analysis of the data presented in this chapter highlights the need for techniques such as GED-MS to confirm the species generated during a GED experiment.

This chapter focuses on the continuation of Noble-Eddy's work[1] on the study of the GED structure of ketene. All of the GED data processed in this chapter were collected using the Canterbury GED apparatus[2] while it was still at the University of Edinburgh. The analysis and *ab initio* studies are all my own work. Work on the gas-phase structure of acetic anhydride and its corresponding pyrolysis products is presented, with comparisons being made to other studies in the literature. In particular, the acetic anhydride data in the literature was processed using the ed@ed refinement program[12] and SARACEN method.[13-15] The data collected by Noble-Eddy[1] for Meldrum's acid and its pyrolysis products have also been reprocessed, including the description of the model for Meldrum's acid to provide an improvement in the analysis. Lastly, since the generation and study of ketene by VHT-GED allows for the study of other substituted ketenes, including asymmetrically substituted ketenes, a complementary computational study of a selection of ketene derivatives from the corresponding Meldrum's acid derivatives has been conducted and is also presented here.

4.2 Acetic anhydride

4.2.1 Introduction

Acetic anhydride has been previously studied by GED, IR spectroscopy and by *ab initio* studies,[16] revealing the gas vapour to consist of two low energy conformers. These conformers are related to each other by two large amplitude torsional motions around the central C–O–C=O dihedral angles as indicated (Figure 4.1).

Figure 4.1 Bond rotation around the C–O–C=O dihedral angles of acetic anhydride.

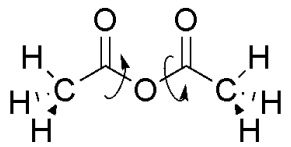

In the previous GED refinement by Wu *et al.*[16] the gas-phase structure of acetic anhydride was described by the use of a dynamic model. A dynamic model in GED aids the description of a low energy rotation in a molecule; this is typically done by implementing a potential function[17] or a series of pseudoconformers. In the case of Wu and co-workers,[16] the acetic anhydride conformers were described using a set of pseudoconformers for each of the two conformers.

However, to investigate the pyrolysis products of acetic anhydride by GED (Section 4.3) a dynamic model of acetic anhydride is too complex to incorporate into a refinement that also includes decomposition products. This section details the reanalysis of the acetic anhydride GED data obtained by Wu and co-workers[16] to test the validity of using a simpler two-conformer model to describe the gas-phase structure of acetic anhydride. As part of this work, a comparison has been conducted to show improvements on the original GED refinement of acetic anhydride by using a two-conformer model and the SARACEN method.[13-15]

4.2.2 Experimental

Theoretical methods

Geometry optimisation and frequency calculations were performed using the resources of the National Service for Computational Chemistry Software (NCSSC)[18] and the Gaussian09 program.[19] All MP2[20] methods were frozen core [MP2(fc)]. Geometry optimisations were performed on the two acetic anhydride conformers (one with C_1 symmetry and the other with C_2 symmetry) using both M06-2X[21] and MP2[20] methods.

Geometry optimisations

Two conformers of acetic anhydride were located on the potential energy surface (PES) with C_1 and C_2 symmetry. The acetic anhydride conformer geometries were optimised at the HF level with the 6-31G* basis set,[22,23] and at the M06-2X level with 6-31G*, 6-311G*,[24,25] 6-311+G*[26,27] and 6-311++G** basis sets. For comparison, the geometries were also optimised using the MP2[20] method over the same basis sets. With higher-level calculations (i.e. larger basis sets) geometry optimisations were performed using C_1 and C_2 symmetry for the two conformers.

Frequency calculations

Analytic second derivatives of the energy with respect to nuclear coordinates calculated at the M06-2X/6-311++G** level gave the force fields for the lowest energy conformers of acetic anhydride. These were used with the program SHRINK[28,29] to provide estimates of the amplitudes of vibration (u) and perpendicular distance corrections (k) for use in the GED refinement. As harmonic corrections to the amplitudes of vibration have been implemented, the refinement type is denoted r_{h1}.[30]

GED study

The GED structure of acetic anhydride was re-determined using the electron diffraction data as provided by Wu *et al.*[16] in their Supplementary Information, which used an average experimental temperature of 338.15 K. The data-reduction and least-squares-refinement processes were carried out using the ed@ed program[12] (Version 2.4) employing the scattering factors of Ross *et al.*[31] The scattering

intensities of the GED data from Wu *et al.*[16] were scaled by 50 for use with the in-house refinement program.[12] The weighting points for the off-diagonal weight matrices, electron wavelengths, correlation parameters and scale factors for the nozzle-to-camera distance are given in Appendix Table A2.1.

4.2.3 Results

Ab initio calculations

A previous *ab initio* study of acetic anhydride[16] identified two non-planar minima, labelled (*sp*, *sp*) and (*sp*, *ac*), related to each other by large amplitude torsional motions. These conformer names are based on the O=C–O–C dihedral angles. The abbreviation *sp* refers to synperiplanar (a dihedral angle of 0 ± 30°); *ac* refers to anticlinal (a dihedral angle of -90 to -150°). In this previous study, the (*sp*, *sp*) and (*sp*, *ac*) conformers were described as a series of pseudoconformers around the O=C–O–C torsion, and were grouped together to collectively describe the (*sp*, *sp*) and (*sp*, *ac*) conformers in the GED refinement.[16] This is in contrast to the work presented here, where the O=C–O–C torsions were able to alter with respect to the optimisation of the (*sp*, *sp*) and (*sp*, *ac*) conformer geometries over a range of *ab initio* calculations. The lowest energy structures of the acetic anhydride conformers [(*sp*, *sp*) and (*sp*, *ac*)] and atom numbering are presented in Figure 4.2.

Figure 4.2 The lowest energy structures of the (*sp*, *sp*) and (*sp*, *ac*) conformers of acetic anhydride with atom numbering.

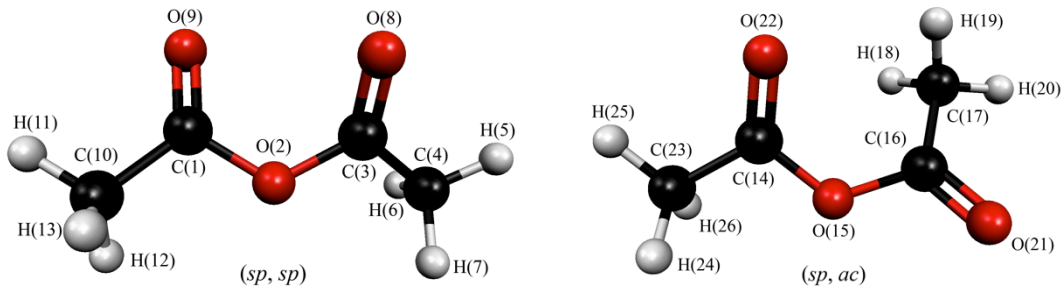

The two conformers of acetic anhydride were optimised at the HF level with the 6-31G* basis set,[22,23] and at the M06-2X[21] level with the 6-31G*, 6-311G*,[24,25] 6-311+G*[26,27] and 6-311++G** basis sets. From the *ab initio* results, (*sp*, *sp*) was determined to have C_2 geometry, whereas (*sp*, *ac*) had C_1 geometry. The results of calculations performed at the M06-2X level are presented in Appendix Table A2.2.

GED

GED refinements were re-performed for acetic anhydride, based on the *ab initio* calculations described above (optimised at the M06-2X/6-311++G** level). The gas-phase structure for acetic anhydride was re-determined by processing the raw GED data from a previous experiment,[16] using the SARACEN method.[13-15] The original investigation used a dynamic model to describe the two non-planar conformers of acetic anhydride (*sp*, *sp*) and (*sp*, *ac*) implementing eight pseudoconformers; five clustered around the (*sp*, *sp*) conformer, and three around the (*sp*, *ac*) conformer. In this present study a two-conformer model was employed, rather than a dynamic model, as a model with multiple species was to be used for the GED study of the acetic anhydride pyrolysis products (Section 4.3). This is because it would be too complicated to include a dynamic model in a refinement that also includes multiple pyrolysis products. Similar parameters were grouped together using the (*sp*, *sp*) parameter as an average, with differences applied to generate the respective values for the (*sp*, *ac*) conformer. The structure was defined in terms of 32 independent geometric parameters and 20 dependent parameters as described in Appendix 2.

Theoretical Cartesian force fields were generated for both conformers at the M06-2X/6-311++G** level and converted to a set of force fields described by sets of symmetry coordinates. Root-mean-square (RMS) amplitudes of vibration were obtained from the SHRINK program.[28,29] All independent geometric parameters were refined using a least-squares method and restraints were applied using the SARACEN method[13-15] (Table 4.1). In addition, the corresponding amplitudes of vibration were refined (see Table A2.3). The success of the refinement can be assessed numerically using the final *R* factor,[32] which was $R_G = 0.073$ ($R_D = 0.067$), and visually using the RDCs (Figure 4.3), and the MICs (Figure A2.1). The refined conformer weighting of (*sp*, *sp*) was 40.7(±9.4) %, which was comparable to the refined weighting in the original study (37±15 %).[16]

Calculations at the M06-2X level[21] showed that MP2 incorrectly predicted the (*sp, sp*) conformer as being lower in energy. In the previous GED study[16] 56.8 % was obtained as the predicted conformer weighting from the sum of the (*sp*, *sp*) pseudoconformers, compared to weighting of 28.8 % as predicted by M06-2X/6-311++G** using the Boltzmann distribution for the GED experimental conditions.

Table 4.1 Refined (r_{h1}) and calculated (r_e) geometric parameters for acetic anhydride from the SARACEN GED refinement.[a]

Parameters		GED (r_{h1})	M06-2X/ 6-311++G** (r_e)	Restraint
Independent				
p_1	*r*C–C (*sp*, *sp*)	148.5(3)	149.8	–
p_2	*r*C–C diff 1	0.1(1)	0.1	0.1(1)
p_3	*r*C–C diff 2	0.3(1)	0.3	0.3(1)
p_4	*r*C=O (*sp*, *sp*)	118.3(1)	118.7	–
p_5	*r*C=O diff 1	0.8(1)	0.8	0.8(1)
p_6	*r*C=O diff 2	0.1(1)	0.1	0.1(1)
p_7	*r*C–O (*sp*, *sp*)	138.7(2)	138.7	–
p_8	*r*C–O diff 1	2.2(1)	2.2	2.2(1)
p_9	*r*C–O diff 2	1.3(1)	1.3	1.3(1)
p_{10}	*r*C–H av	108.4(4)	108.9	108.9(6)
p_{11}	∠H(11)–C–C (*sp*, *sp*)	109.5(1)	109.5	109.5(1)
p_{12}	∠H–C–C diff 1	1.8(1)	1.8	1.8(1)
p_{13}	∠H–C–C diff 2	0.1(1)	0.1	0.1(1)
p_{14}	∠H(25)–C–H(24) (*sp*, *ac*)	110.5(1)	110.5	110.5(1)
p_{15}	∠H(20)–C–H(19) (*sp*, *ac*)	109.9(1)	109.9	109.9(1)
p_{16}	∠C–C=O (*sp*, *sp*)	126.3(5)	127.2	–
p_{17}	∠C–C=O diff 1	1.6(1)	1.6	1.6(1)
p_{18}	∠C–C=O diff 2	0.9(1)	0.9	0.9(1)
p_{19}	∠C–C–O (*sp*, *sp*)	111.2(5)	110.0	–
p_{20}	∠C–C–O diff 1	7.2(2)	7.2	7.2(2)
p_{21}	∠C–C–O diff 2	0.1(1)	0.1	0.1(1)
p_{22}	∠C–O–C (*sp*, *sp*)	120.3(1)	120.3	120.3(1)
p_{23}	∠C–O–C (*sp*, *ac*)	122.4(2)	122.5	122.5(2)
p_{24}	ϕO=C–C–H(11) (*sp*, *sp*)	5.7(20)	5.7	5.7(20)
p_{25}	ϕO=C–C–H(25) (*sp*, *ac*)	-1.1(10)	-1.0	-1.0(10)
p_{26}	ϕO=C–C–H(20) (*sp*, *ac*)	21.7(19)	21.3	21.3(20)

p_{27}	ϕO(9)=C(1)–C(10)–O(2) (*sp*, *sp*)	177.6(1)	177.6	177.6(1)
p_{28}	ϕO=C–C–O diff 1	1.4(11)	1.9	1.9(11)
p_{29}	ϕO=C–C–O diff 2	1.0(1)	1.0	1.0(1)
p_{30}	ϕC(10)–C–O–C (*sp*, *sp*)	-155.7(15)	-153.2	-153.2(20)
p_{31}	ϕC(23)–C–O–C (*sp*, *ac*)	173.5(20)	172.7	172.7(22)
p_{32}	ϕC(17)–C–O–C (*sp*, *ac*)	-41.5(15)	-38.6	-38.6(20)
Dependent				
dp_1	*r*C(14)–C(23) (*sp*, *ac*)	148.6(3)	149.9	–
dp_2	*r*C(16)–C(17) (*sp*, *ac*)	148.8(3)	150.1	–
dp_3	*r*C(14)=O(22) (*sp*, *ac*)	119.0(1)	119.5	–
dp_4	*r*C(16)=O(21) (*sp*, *ac*)	118.2(1)	118.6	–
dp_5	*r*C(14)–O(15) (*sp*, *ac*)	136.5(2)	136.5	–
dp_6	*r*C(16)–O(15) (*sp*, *ac*)	140.0(2)	140.0	–
dp_7	∠H(25)–C–C (*sp*, *ac*)	109.4(1)	109.4	–
dp_8	∠H(20)–C–C (*sp*, *ac*)	107.7(1)	107.7	–
dp_9	∠C–C=O(22) (*sp*, *ac*)	125.4(5)	126.3	–
dp_{10}	∠C–C=O(21) (*sp*, *ac*)	124.7(5)	125.6	–
dp_{11}	∠O–C=O (*sp*, *sp*)	122.5(2)	122.7	–
dp_{12}	∠O–C=O(21) (*sp*, *ac*)	116.8(2)	117.2	–
dp_{13}	∠O–C=O(22) (*sp*, *ac*)	123.3(2)	123.5	
dp_{14}	∠C(17)–C–O (*sp*, *ac*)	118.4(5)	117.2	–
dp_{15}	∠C(23)–C–O (*sp*, *ac*)	111.3(5)	110.1	–
dp_{16}	ϕO(21)=C(16)–C(17)–O(15) (*sp*, *ac*)	176.2(11)	175.7	–
dp_{17}	ϕO(22)=C(14)–C(23)–O(15) (*sp*, *ac*)	-178.6(1)	-178.6	–
dp_{18}	ϕO(8/9)=C–O–C (*sp*, *sp*)	26.6(16)	29.1	–
dp_{19}	ϕO(21)=C–O–C (*sp*, *ac*)	142.0(18)	145.3	–
dp_{20}	ϕO(22)=C–O–C (*sp*, *ac*)	-7.8(20)	-8.7	–

[a] Distances (r_{h1}) are in pm and bond angles (∠) and dihedral angles (ϕ) are in degrees.

Figure 4.3 Experimental and difference (experimental – theoretical) RDCs for acetic anhydride. Before Fourier inversion the data were multiplied by $s \cdot \exp(-0.00002s^2)/(Z_C - f_C)(Z_O - f_O)$.

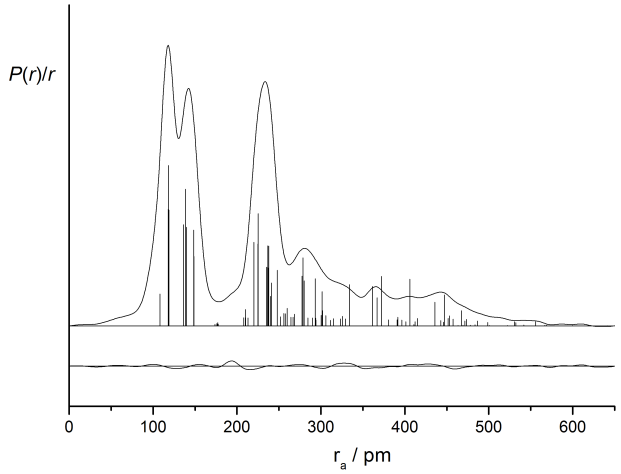

A trial refinement was conducted at the MP2/6-311++G** level and was used as the starting point for the M06-2X refinement. The energies and calculated conformer weightings at the MP2 and M06-2X level for a range of basis sets are presented in Table A2.4. The least-squares correlation matrix is given in Table A2.5 and the coordinates for the final GED structure and for the calculated structure (M06-2X/6-311++G**) are in Tables A2.6 and A2.7 respectively.

4.2.4 Discussion

The new refinement of acetic anhydride produces parameters that are, in most cases, comparable to those obtained in the previous study by Wu *et al.*[16] The bond lengths are in agreement for both studies and *ab initio* calculations obtained at the M06-2X/6-311++G** level. Errors in both studies are reported as the estimated standard deviation. The *r*C–C distance was reported in the original study to have a value of 148.9(2) pm. This is comparable to the *r*C–C distances that were individually described for the (*sp*, *sp*) and (*sp*, *ac*) conformers in this study [148.5(3) pm for (*sp*, *sp*), and 148.6(3) and 148.8(3) pm for (*sp*, *ac*)]. The *r*C–O distances for the (*sp*, *sp*) conformer were underestimated in the original study compared to the *ab initio* results [137.0(15) pm compared to 138.7 pm], with *r*C–O from this study [138.7(2) pm] in

close agreement with the M06-2X/6-311++G** value. A difference was also observed between the *ab initio* and GED values for the (*sp*, *ac*) conformer, with values for *r*C(14)–O(15) and *r*C(16)–O(15) from the original study being higher and lower than the corresponding *ab initio* values [137.0(13) pm compared to 136.5 pm, and 140.6(6) pm compared to 140.0 pm]. As before, the C–O values obtained for (*sp*, *ac*) in this study [136.5(2) pm and 140.0(2) pm] were in close agreement to the *ab initio* values.

The ∠O–C–C parameters from both studies agreed reasonably well with the *ab initio* values. This was not the case for ∠O=C–O which were wider for the (*sp*, *sp*) conformer in the original study [124.8(10)°], and overestimated for the (*sp*, *ac*) conformer [117.1(10)° and 124.2(18)°] compared to the results of this study [122.5(2)° for (*sp*, *sp*), and 116.8(2)° and 123.3(2)° for (*sp*, *ac*) respectively]. The ∠C–O–C parameters also differed between the two studies. In the previous work ∠C–O–C was reported as being 116.5(20)° and 121.0(15)° for the (*sp*, *sp*) and (*sp*, *ac*) conformers respectively which were narrower than the ∠C–O–C parameters obtained from this work [120.3(1)° for (*sp*, *sp*) and 122.4(2)° for (*sp*, *ac*)].

The differences between these angles and the *ab initio* results can be attributed to the conformational flexibility of acetic anhydride, specifically due to ϕO=C–O–C which differs significantly between the conformers. As the SARACEN method[13-15] was not used in the original study these parameters were not previously refined with high accuracy or precision. For the (*sp*, *sp*) conformer, ϕO=C–O–C agreed reasonably well with the *ab initio* calculations, but for ϕO(22)=C(14)–O(15)–C(16) and ϕO(21)=C(16)–O(15)–C(14) in (*sp*, *ac*), the previous GED study overestimated and underestimated the magnitude of the dihedral angles [-27.4(3)° and 122.0(39)°, compared to -7.8(20)° and 142.0(18)° in this study]. ϕO=C–O–C was shown to vary depending on the *ab initio* calculation used as indicated in Table A2.2. This suggested that these parameters would be poorly refined by GED data alone so in this study a restraint was applied that encompassed this range of values. The refined ϕO=C–O–C from the previous GED study[16] falls outside this range. The rest of the parameter comparisons are given in Table 4.2, with respect to the numbering scheme given in Figure 4.2.

Table 4.2 Parameter comparison for study of acetic anhydride by GED.[a]

Parameters	GED (r_{h1})	Previous GED study[13]	M06-2X/ 6-311++G** (r_e)
(*sp*, *sp*)			
C(1)–C(10)	148.5(3)	148.9(2)[b]	149.8
C(3)–C(4)	148.5(3)	–	149.8
C(1)=O(9)	118.3(1)	118.2(3)	118.7
C(3)=O(8)	118.3(1)	118.2(3)	118.7
C(1)–O(2)	138.7(2)	137.0(15)	138.7
C(3)–O(2)	138.7(2)	137.0(15)	138.7
<C–H>[c]	108.4(4)	109.9(4)	108.9
∠O(2)–C(1)=O(9)	122.5(2)	124.8(20)	122.7
∠O(2)–C(3)=O(8)	122.5(2)	124.8(20)	122.7
∠O(2)–C(1)–C(10)	111.2(5)	114.6(23)	110.0
∠O(2)–C(3)–C(4)	111.2(5)	114.6(23)	110.0
∠C(1)–O(2)–C(3)	120.3(1)	116.5(20)	120.3
ϕO(9)=C(1)–O(2)–C(3)	26.6(16)	30.9(67)	29.1
ϕO(8)=C(3)–O(2)–C(1)	26.6(16)	30.9(67)	29.1
(*sp*, *ac*)			
C(14)–C(23)	148.6(3)	148.9(2)[b]	149.9
C(16)–C(17)	148.8(3)	–	150.1
C(14)=O(22)	119.0(1)	119.4(3)	119.5
C(16)=O(21)	118.2(1)	118.2(3)	118.6
C(14)–O(15)	136.5(2)	137.0(13)	136.5
C(16)–O(15)	140.0(2)	140.6(6)	140.0
<C–H>[c]	108.4(4)	109.9(4)	108.9
∠O(15)–C(14)=O(22)	123.3(2)	124.2(18)	123.5
∠O(15)–C(16)=O(21)	116.8(2)	117.1(10)	117.2
∠O(15)–C(14)–C(23)	111.3(5)	110.9(17)	110.1
∠O(15)–C(16)–C(17)	118.4(5)	111.1(22)	117.2
∠C(14)–O(15)–C(16)	122.4(2)	121.0(15)	122.5
ϕO(21)=C(16)–O(15)–C(14)	142.0(18)	122.0(39)	145.3

ϕO(22)=C(14)–O(15)–C(16)	-7.8(20)	-27.4(53)	-8.7

[a] The distances are given in pm. Bond angles (∠) and dihedral angles (ϕ) are in °.

[b] The C–C distances were averaged over both conformers.

[c] An average C–H distance from both conformers was used.

The fact that the parameters in the original study did not describe the flexible dihedral angles overly well was reflected in the refinement of the corresponding amplitudes of vibration. This meant that the refined amplitudes for the O···O, O···C and O···C interatomic distances differed greatly from what was calculated. This is more apparent for the (*sp*, *ac*) conformer, such as for O(21)···O(22) where the calculated amplitudes were 7.8 pm (MP2/6-31G*) compared to the refined value of 14.2(24) pm.[16] Comparatively in this study the same amplitude of vibration was calculated to be 26.3 pm (M06-2X/6-311++G**) and 30.0(18) pm (GED). For these flexible dihedral angles, and their corresponding amplitudes, applying restraints with the SARACEN method[13-15] was of great benefit to the success of the refinement. A full comparison of these amplitudes against the theoretically calculated values is given in Table A2.8.

4.2.5 Conclusion

This work has demonstrated the viability of using the SARACEN method[13-15] to describe the gas-phase structures of acetic anhydride using a two-conformer model. As part of this work comparisons have been drawn between this study and the previous GED study of acetic anhydride, which used a dynamic model to describe the (*sp*, *sp*) and (*sp*, *ac*) conformers. Analysis has shown that while the previous refinement is valid, improvements to the refinement are made by implementing the SARACEN method, allowing restraints to be used to describe the varying O=C–O–C torsion angles in the molecule. This in turn allows for refinement of the amplitudes of vibration that are dependent on these torsions.

4.3 Pyrolysis of acetic anhydride

4.3.1 Introduction

Acetic anhydride, [$(CH_3CO)_2O$], is known to generate acetic acid and ethenone ($CH_2C{=}O$), the simplest example of a ketene, in good yield by FVP.[33] The pyrolysis process has not been studied by GED before in the literature. Previous studies suggest the decomposition mechanism to be an intramolecular rearrangement,[34-36] with the most obvious route involving one methyl proton moving to the central O and subsequent breaking of the C–O bond[34] as shown in Figure 4.4.

Figure 4.4 Mechanism for the pyrolysis of acetic anhydride to give acetic acid and ketene.

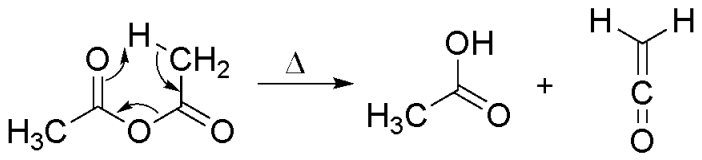

Work by Noble-Eddy in the Masters group[1] has resulted in collection of GED data for the pyrolysis of acetic anhydride, however the model descriptions reported in his thesis did not allow for the products to be treated separately in the refinement. Noble-Eddy averaged bond parameters such as C–C, C–O and C=O together, rather than refining them separately with the SARACEN method,[13-15] so the refined parameters were less accurate than what would be expected in a standard GED experiment. It was deemed necessary to repeat the data analysis along with construction of a new model for the refinement so that a more comprehensive analysis could be conducted.

The analysis of the GED structures of ketene and acetic acid, as obtained from the pyrolysis of acetic anhydride, is presented following the reconstruction of the GED model and subsequent refinement of the GED data. The experimental setup used for the pyrolysis experiment is described briefly. Selected parameters of ketene and acetic acid have been compared to previous GED[5,37] and MW[38,39] spectroscopy studies and are also presented.

4.3.2 Experimental

Synthesis

Acetic anhydride (> 99%) was obtained from Sigma Aldrich as used without further purification in the GED experiment. Acetic acid and ketene were generated by pyrolysis of acetic anhydride using the VHT nozzle system as described below.

Very-High-Temperature (VHT) nozzle system

To enable the generation of short-lived species for GED experiments, a VHT nozzle system was constructed to work with the Canterbury GED apparatus.[2] Previous work with the VHT nozzle has involved re-determination of the gas-phase structure of antimony (III) oxide.[2] The configuration of the VHT nozzle allowed for the study of relatively involatile samples, over a wider range of temperatures than are normally accessible using the Canterbury GED apparatus, by allowing a build up of vapour pressure. The setup used in the study of antimony (III) oxide is one of the four potential configurations for the VHT nozzle system.

This study is concerned with the generation of acetic acid and ketene by pyrolysis of acetic anhydride, therefore a different setup of the nozzle is required. Specific details regarding the VHT nozzle, such as the types of materials used, is covered elsewhere.[1,2] As shown in Figure 4.5, the VHT nozzle setup consists of an external sample inlet which is used to allow the sample to pass into the VHT oven in close proximity to the diffraction zone. With this design, changing the sample at the external gas inlet is simple, so benzene calibration can be obtained without removing the VHT nozzle from under vacuum. However, using an external gas inlet system is only applicable if the sample of interest has sufficient vapour pressure. Acetic anhydride has a vapour pressure of 4 Torr at 293.15 K,[40] which is sufficient for study by GED with this setup.

Figure 4.5 The VHT nozzle inlet system used in this work showing **(a)** the general set-up and **(b)** the cross-section of the path of the electron beam through the end of the nozzle. The outer inlet system cooling is not shown in **(a)**.

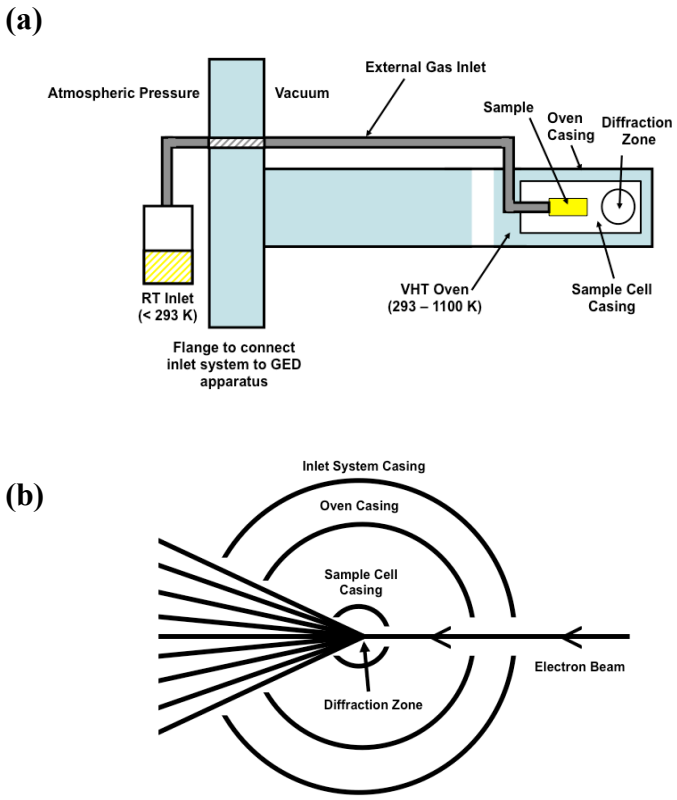

Theoretical methods

Geometry and frequency calculations were performed using the resources of the NSCCS[18] and the Gaussian09 program.[19] All MP2[20] methods were frozen core [MP2(fc)].

Geometry optimisations

Geometry optimisations were performed using C_{2v} symmetry for ketene and C_s symmetry for acetic acid at the HF level with the 6-31G* basis set,[22,23] and at the MP2 level with 6-31G*, 6-311G*,[24,25] 6-311+G*[26,27] and 6-311++G** basis sets.

Frequency calculations

Analytic second derivatives of the energy with respect to the nuclear coordinates calculated at the MP2/6-311++G** level gave the force fields for the lowest energy geometries of ketene and acetic acid. These force fields were used in the program

SHRINK[28,29] to provide estimates of the amplitudes of vibration (u) and perpendicular distance corrections (k) for use in the GED refinement.

GED (*performed by Robert Noble-Eddy, University of Edinburgh*)

Data were collected for the pyrolysis of acetic anhydride to acetic acid and ketene, using the Edinburgh GED apparatus, now located at the University of Canterbury,[2] and the VHT nozzle setup as described above. An accelerating voltage of around 40 keV was used (electron wavelength ca. 6.0 pm) with a maintained pyrolysis temperature of 823 K. Scattering intensities were recorded at a nozzle-to-plate distance of 212.2 mm on Kodak Electron Image films. An Epson Expression 1680 Pro flatbed scanner was used to convert the electron-scattering intensities to mean optical densities as a function of the scattering variable, s, using an established program.[41] The data-reduction and least-squares-refinement processes were carried out using the ed@ed program[12] (Version 2.4) employing the scattering factors of Ross *et al.*[31] The weighting points for the off-diagonal weight matrices, correlation parameters and scale factors for the nozzle-to-camera distance are given in Table A2.9, along with the electron wavelengths determined from the scattering patterns of benzene vapour.

4.3.3 Results

***Ab initio* calculations**

The gas-phase geometries of ketene (with C_{2v} symmetry) and acetic acid (with C_s symmetry) were optimised at the HF level with the 6-31G* basis set,[22,23] and at the MP2[20] level with the 6-31G*, 6-311G*,[24,25] 6-311+G*[26,27] and 6-311++G** basis sets, with the MP2 results presented in Table A2.10. The atom numbering and relative structures of ketene and acetic acid are given in Figure 4.6.

Figure 4.6 The lowest energy structures of ketene (left) and acetic acid (right) with atom numbering.

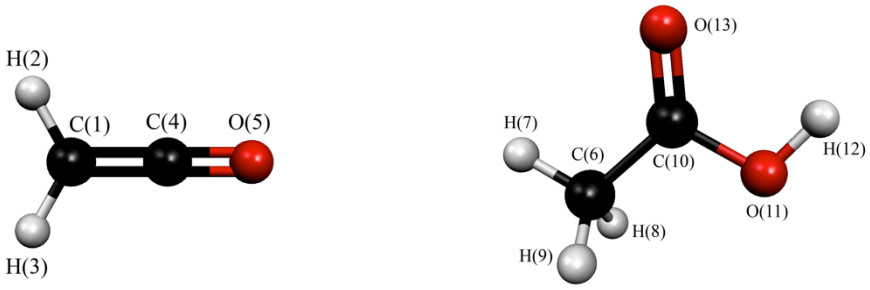

GED

GED refinements for the pyrolysis products of acetic anhydride were carried out based on *ab initio* calculations at the MP2/6-311++G** level. From the mechanism for the pyrolysis of acetic anhydride,[34-36] it is expected that ketene and acetic acid (Figure 4.6) are generated with 1:1 stoichiometry so this was fixed in the refinement. Rather than setting the amount of ketene present to be 50 %, the ratio of ketene to acetic acid was fixed at 66:33 % to reflect the ratio of the enantiomers present in the vapour. A trial refinement of the data showed that the contribution of acetic anhydride was < 2 % so only ketene and acetic acid were included in the model. The structures of ketene and acetic acid were defined in C_{2v} and C_s symmetry respectively, using 15 parameters and one dependent parameter. The 15 independent parameters comprised eight bond lengths, six bond angles and one dihedral angle. Independent parameters included *r*C=O, *r*C=C and *r*C–H for ketene (p_1, p_4 and p_7), and *r*C=O, *r*C–O, *r*C–C, *r*O–H and *r*C–H for acetic acid (p_2, p_3, p_5, p_6 and p_8). The bond angles included ∠H–C=C for ketene (p_9) and ∠H(7)–C–H(8/9), ∠C–C–H, ∠C–C=O, ∠C–C–O and ∠C–O–H for acetic acid ($p_{10} - p_{14}$). The dihedral ϕH–O–C–C for acetic acid (p_{15}) was defined, but fixed at 180° in the final refinement due to C_s symmetry. One dependent parameter, ∠H–C–H was also specified for ketene to allow comparison to previous structural studies.

The final goodness-of-fit factors, R_G and R_D, were determined to be R_G = 0.088 and R_D = 0.049. The refined GED parameters are given in Table 4.3 alongside the theoretical calculations obtained at the MP2/6-311++G** level. The refined amplitudes of vibration are given in Table A2.11. The success of the refinement is

also shown in the RDCs (Figure 4.7) and MIC (Figure A2.2). The final GED and calculated structure (MP2/6-311++G**) coordinates are also given in the Appendix (Tables A2.12 – A2.13). No significant correlation (≥ 50%) was shown between refined parameters therefore no least-squares correlation matrix is presented.

Table 4.3 Refined and calculated parameters for GED refinement of pyrolysis of acetic anhydride, $[CH_3C(=O)O]_2$, giving ketene and acetic acid.[a]

Parameters[b]		GED (r_{h1})	MP2/6-311++G** (r_e)	Restraint
Independent				
p_1	rC=O ket	115.4(3)	116.8	116.8(4)
p_2	rC=O acet	119.6(4)	121.0	121.0(5)
p_3	rC–O acet	136.5(6)	135.9	–
p_4	rC=C ket	132.3(2)	132.2	132.2(2)
p_5	rC–C acet	150.0(3)	150.4	150.4(3)
p_6	rO–H acet	96.9(3)	96.8	96.8(3)
p_7	rC–H ket	108.5(1)	108.5	108.5(1)
p_8	rC–H acet average	108.6(8)	109.1	109.1(9)
p_9	∠H–C=C ket	119.4(5)	119.1	119.1(5)
p_{10}	∠H(7)–C–H(8/9) acet	110.5(2)	110.2	–
p_{11}	∠C–C–H acet	109.5(2)	109.5	109.5(2)
p_{12}	∠C–C=O acet	126.4(6)	126.4	126.4(6)
p_{13}	∠C–C–O acet	110.4(7)	111.0	111.0(8)
p_{14}	∠C–O–H acet	105.7(27)	105.8	105.8(27)
p_{15}	ϕH–O–C–C acet	180.0[c]	180.0	–
	% Ketene	66.6[c]	66.6	–
Dependent				
dp_1	∠H–C–H ket	121.3(10)	121.8	–

[a] Distances (r_{h1}) are in pm and bond angles (∠) and dihedral angles (ϕ) are in °.

[b] ket = ketene, acet = acetic acid.

[c] This parameter was fixed.

Figure 4.7 Experimental and difference (experimental – theoretical) RDCs for the pyrolysis of acetic anhydride (giving acetic acid and ketene). Before Fourier inversion the data were multiplied by $s \cdot \exp(-0.00002s^2)/(Z_C - f_C)(Z_O - f_O)$.

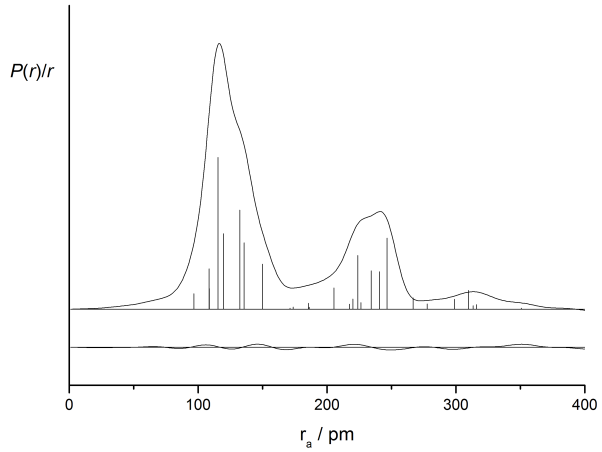

The structures of ketene and acetic acid were compared to previous GED and MW studies (Table 4.4). The theoretical *ab initio* values from MP2/6-311++G** calculations are given alongside for comparison.

Table 4.4 Selected structural parameters for the lowest energy structures of ketene and acetic acid.[a]

Parameters	GED (r_{h1})	Previous GED studies[5,37]	Previous MW studies[38,39]	MP2/6-311++G** (r_e)
Ketene				
*r*C=O	115.4(3)	116.0(20)	116.1[b]	116.8
*r*C=C	132.3(2)	130.0(20)	131.4[b]	132.2
*r*C–H	108.5(1)	107.0(20)[c]	108.3[b]	108.5
∠H–C–H	121.3(10)	117.5(125)[c]	122.4[b]	121.8
Acetic Acid				
*r*C=O	119.6(4)	121.4(3)	120.9(6)	121.0
*r*C–O	136.5(6)	136.4(3)	135.7(5)	135.9
*r*C–C	150.0(3)	152.0(5)	149.4(10)	150.4
*r*O–H	96.9(3)	97.0[c]	97.0(3)	96.8
*r*C–H av	108.6(8)	110.2(10)	110.2(12)	109.1
∠C–C=O	126.4(6)	126.6(6)	126.2(7)	126.4
∠C–C–O	110.4(7)	110.6(6)	112.0(6)	111.0
∠C–O–H	105.7(27)	107.0[c]	105.9(5)	105.8

[a] Bond distances are given in pm and bond angles (∠) in degrees.

[b] No e.s.d.'s were quoted.

[c] This parameter was assumed.

4.3.4 Discussion

From this GED study, all of the parameters agree reasonably well with the theoretical calculations (MP2/6-311++G**) except for the ketene and acetic acid C=O bond lengths (p_1 and p_2 respectively), which are somewhat shorter than may be expected. These parameter values are still considered reasonable as they fall within the range of expected values for a range of *ab initio* calculations (see Table A2.10), which were applied as restraints using the SARACEN method.[13-15]

The parameters from the MW study agree closely with the MP2/6-311++G** results (Table 4.4). The GED results from this study and previous work mostly agree with

the MW and *ab initio* results as well, although some parameters differ as described below. For ketene the C=O bond length was comparable [116.0(20) pm from previous GED compared to 115.4(3) pm in this study] but for acetic acid the C=O bond length was underestimated in this study [119.6(4) pm] when compared to prior GED results [121.4(3) pm]. However, these peaks occur in a region of considerable overlap in the RDC (Figure 4.7), when considering that the parameters for ketene and acetic acid were obtained from independent GED studies. For ketene, the ∠H–C–H value from this study, 121.3(10)°, was closer to the MW and *ab initio* values (122.4° and 121.8°) than the assumed parameter from the original GED study [117.5(125)°]. For acetic acid, the ∠C–O–H value was assumed in the previous GED study with a value of 107.0° and hence differed slightly (although still within the uncertainty) from the refined value of 105.7(27)° in this study.

When making these comparisons it is important to note that the previous studies did not apply restraints to the parameters involving hydrogen, choosing instead to assume the parameter values in the refinement. This GED study, for the pyrolysis of acetic anhydride to give ketene and acetic acid, used the SARACEN method[13-15] to apply suitable restraints to these parameters which would not normally be well refined from GED data alone. Overall, the refined parameter values from this study are in close agreement with the predicted *ab initio* values, and this work successfully demonstrates the advantages of using the SARACEN method in such refinements.

4.3.5 Conclusion

This work successfully shows the refinement of the pyrolysis products of acetic anhydride, acetic acid and ketene, from GED giving an improvement on the analysis originally conducted by Noble-Eddy.[1] The validity of the refined structures was confirmed by comparison of parameters obtained from previous GED and MW studies of acetic acid and ketene in the literature.

4.4 Meldrum's acid

4.4.1 Introduction

2,2-Dimethyl-1,3-dioxane-4,6-dione, also known as Meldrum's acid, has been the subject of previous theoretical[42] and X-ray crystallography[43] studies in the literature, although the gas-phase structure has yet to be reported.

Previous work in the Masters group[1] has involved the collection and analysis of GED data of Meldrum's acid. However limitations with the refinement model meant that it could not be applied to other Meldrum's acid derivatives, such as (but not limited to) those described in Section 4.6. The previous model also could not be easily incorporated into a multiple product refinement such as for the pyrolysis data of Meldrum's acid (Section 4.5).

This section provides a reanalysis of the GED refinement of Meldrum's acid by Noble-Eddy,[1] with construction of a model that is suitable for GED studies of other Meldrum's acid derivatives. This reanalysis improves on the description of the cyclic ring of Meldrum's acid. A comparison is also made to selected parameters from a previous X-ray study.[43] This work is also supported by complementary *ab initio* studies.

4.4.2 Experimental

A purified sample of Meldrum's acid was provided by Professor Hamish McNab (University of Edinburgh, UK).[1]

Theoretical methods

Geometry optimisations and frequency calculations were performed using the resources of the NSCCS[18] and the Gaussian09 suite of programs.[19] All MP2[20] methods were frozen core [MP2(fc)].

Geometry optimisations

The geometry of Meldrum's acid was optimised at the HF level with the 3-21G*[44-46] and 6-31G*[22,23] basis sets, and at the MP2 level with the 6-31G*, 6-311G*,[24,25] 6-

311+G*[26,27] and 6-311++G** basis sets. Across all calculations the geometry optimisations resulted in a single conformer with C_s symmetry.

Frequency calculations

Analytic second derivatives of the energy with respect to the nuclear coordinates calculated at the MP2/6-311++G** level were used to generate the force field. The force field was used in the program SHRINK[28,29] to provide estimates of the amplitudes of vibration (u) and perpendicular distance corrections (k) for use in the GED refinement.

GED (*performed by Robert Noble-Eddy, University of Edinburgh*)

Data were collected for Meldrum's acid using the Edinburgh GED apparatus (now at University of Canterbury).[2] An accelerating voltage of around 40 keV was used (electron wavelength ca. 6.0 pm) with the sample and nozzle temperatures maintained at 370 K and 402 K respectively. Scattering intensities were recorded at nozzle-to-plate distances of 189.4 mm and 253.9 mm on Kodak Image films. An Epson Expression 1680 Pro flatbed scanner was used to convert the electron-scattering intensities to mean optical densities as a function of the scattering variable, s, using an established program.[41] The data-reduction and least-squares refinement processes were carried out using the ed@ed refinement program[12] (Version 2.4) employing the scattering factors of Ross *et al*.[31] The electron wavelengths, weighting points for the off-diagonal weight matrices, correlation parameters, and scale factors for the nozzle-to-camera distances are given in Table A2.14.

4.4.3 Results

***Ab initio* calculations**

The gas-phase geometry of Meldrum's acid was optimised at the HF level with the 3-21G*[44-46] and 6-31G*[22,23] basis sets, and at the MP2[20] level with the 6-31G*, 6-311G*,[24,25] 6-311+G*[26,27] and 6-311++G** basis sets. The MP2 results are presented in Table A2.15. The geometry optimisations resulted in a single conformer adopting a boat conformation as shown in Figure 4.8. The optimised structure of Meldrum's acid was found to have C_s symmetry, with H(11) and H(16) of the methyl groups and H(17) and H(18) of the CH_2 group lying in the mirror plane of the central ring.

Figure 4.8 Optimised molecular structure of Meldrum's acid with atom numbering.

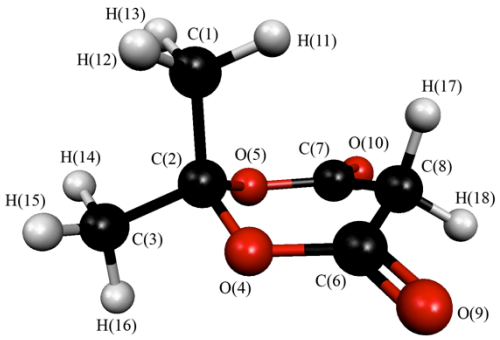

GED results

GED refinements for Meldrum's acid were carried out based on the *ab* initio calculations described above (optimised at the MP2/6-311++G** level) with C_s symmetry.

The model for Meldrum's acid was described using 26 independent parameters and five dependent parameters. The independent parameters used to describe the bond lengths included *r*C=O (p_1), *r*C–O as an average and difference (p_2, p_3), *r*C–C as an average and three differences (p_4 – p_7) and an average C–H distance (p_8). The two methyl groups were described using one α angle [∠H(16)–C–C, ∠H(11)–C–C; p_9, p_{11}] and one β angle [∠H(16)–C–H(15), ∠H(11)–C–H(12); p_{10}, p_{12}] as they were calculated as having C_s symmetry, each with one hydrogen, H(16) and H(11), in the same plane. The methyl groups were set relative to each other by ∠C(H_3)–C–C(H_3) (p_{13}) and relative to the ring with ϕO(4)–C(2)–C(1)–O(5) (p_{21}). The cyclic ring structure of Meldrum's acid was found to be symmetrical in terms of bond lengths, angles and dihedral angles. The ring was described by building one side using the ∠C(3)–C–O(4), ∠C(1)–C–O, ∠C–O–C, ∠O–C=O, ∠O–C–C (p_{14} – p_{18}) and ϕC(1)–C(2)–O(4)–C(6), ϕC(2)–O(4)–C(6)=O(9), ϕC(2)–O(4)–C(6)–C(8) and ϕO(4)–C(6)–C(8)–H(17) (p_{22} – p_{25}). The relative position of the hydrogens of the CH_2 group were described using the α angle ∠O(4)–C(6)–H(17) (p_{19}) and β angle ∠H(17)–C–H(18) (p_{20}) and were described relative to the ring using ϕC(6)–C(8)–H(17)–H(18) (p_{26}). Following this, the atoms described for one side of the ring were reflected to fully generate the ring and complete the structure. The five dependent parameters were used to obtain the absolute bond lengths for *r*C–O (dp_1, dp_2) and *r*C–C (dp_3 – dp_5).

A theoretical Cartesian force field was generated at the MP2/6-311++G** level and converted to a force field described by a set of symmetry coordinates. RMS amplitudes of vibration were obtained from the SHRINK program.[28,29] All independent geometric parameters were refined using a least-squares method and restraints were applied using the SARACEN method[13-15] (Table 4.5) based on calculations at the MP2/6-311++G** level. In addition, the corresponding amplitudes of vibration (*u*) were refined (Table A2.16). The success of the GED refinement are reflected in the final *R*-factors[32] which were $R_G = 0.080$ ($R_D = 0.042$) and in the RDC (Figure 4.9) and MIC (Figure A2.3). The least-squares correlation matrix is provided in the Appendix (Table A2.17) along with the coordinates for the final GED structure and calculated structure at the MP2/6-311++G** level (Tables A2.18 – A2.19 respectively).

Selected parameters from the GED refinement were also compared to parameters obtained from the solid-state structure[43] and *ab initio* calculations. These are presented in Table 4.6.

Table 4.5 Refined and calculated geometric parameters for Meldrum's acid (distances in pm, angles in °) from the GED study.[a]

No.	Description	GED (r_{h1})	MP2/6-311++G** (r_e)	Restraint
Independent parameters				
p_1	*r*C=O	120.1(2)	120.4	120.4(3)
p_2	*r*C–O av	139.8(1)	139.8	139.8(1)
p_3	*r*C–O diff	3.7(2)	3.6	3.6(2)
p_4	*r*C–C av	152.4(3)	151.6	–
p_5	*r*C–C diff1	0.1(1)	0.1	0.1(1)
p_6	*r*C–C diff2	0.5(1)	0.5	0.5(1)
p_7	*r*C–C diff3	0.4(1)	0.4	0.4(1)
p_8	*r*C–H av	109.3(1)	109.3	109.3(1)
p_9	∠H(16)–C–C	109.2(3)	109.2	109.2(3)
p_{10}	∠H(16)–C–H(15)	109.4(2)	109.4	109.4(2)
p_{11}	∠H(11)–C–C	112.1(2)	112.1	112.1(2)
p_{12}	∠H(11)–C–H(12)	108.5(2)	108.5	108.5(2)
p_{13}	∠C(H_3)–C–C(H_3)	113.0(2)	112.9	112.9(2)
p_{14}	∠C(3)–C–O(4)	105.5(2)	105.5	–
p_{15}	∠C(1)–C–O	110.8(2)	110.7	110.7(2)
p_{16}	∠C(2)–O(4)–C(6)	118.9(1)	118.8	118.8(1)
p_{17}	∠O(4)–C(6)=O(9)	120.3(1)	120.4	120.4(1)
p_{18}	∠O(4)–C(6)–C(8)	116.0(2)	115.8	115.8(2)
p_{19}	∠C(7)–C(8)–H(17)	108.3(3)	108.7	108.7(3)
p_{20}	∠H(17)–C(8)–H(18)	106.9(6)	106.8	106.8(6)
p_{21}	ϕO(4)–C(2)–C(1)–O(5)	124.4(4)	124.0	124.0(4)
p_{22}	ϕC(1)–C(2)–O(4)–C(6)	-77.0(6)	-75.4	-75.4(11)
p_{23}	ϕC(2)–O(4)–C(6)=O(9)	170.1(11)	169.9	169.9(12)
p_{24}	ϕC(2)–O(4)–C(6)–C(8)	-12.2(10)	-11.9	-11.9(12)
p_{25}	ϕO(4)–C(6)–C(8)–H(17)	99.9(16)	97.2	–
p_{26}	ϕC(6)–C(8)–H(17)–H(18)	116.7(2)	117.0	117.0(2)

Dependent parameters				
dp_1	rC(2)–O(4/5)	143.4(2)	143.4	–
dp_2	rC(6/7)–O(4/5)	136.1(2)	136.2	–
dp_3	rC(1)–C(2)	152.8(3)	152.1	–
dp_4	rC(2)–C(3)	151.9(3)	151.1	–
dp_5	rC(6/7)–C(8)	152.4(3)	151.5	–

[a] Figures in parentheses are the estimated standard deviations of the last digit. See text for parameter definitions.

Figure 4.9 Experimental and difference (experimental – theoretical) RDC, $P(r)/r$, for Meldrum's acid. Before Fourier inversion the data were multiplied by $s\cdot\exp(-0.00002s^2)/(Z_C - f_C)(Z_O - f_O)$.

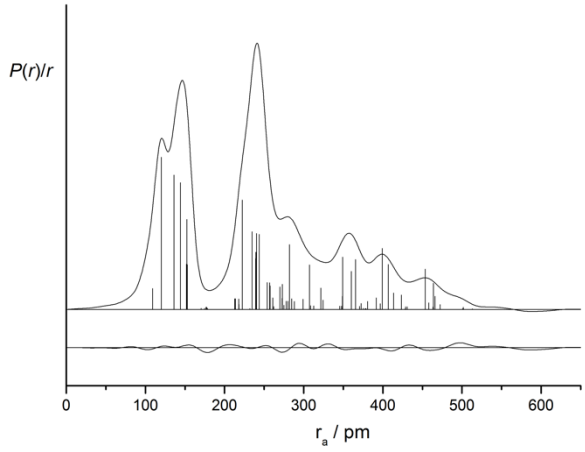

Table 4.6 Selected parameter comparison for Meldrum's acid between GED, X-ray and *ab initio* results (distances in pm, angles in °).[a]

Parameter	GED (r_{h1})	X-ray[b]	MP2/6-311++G** (r_e)
*r*C=O	120.1(2)	119.3(4)	120.4
*r*C(2)–O(4/5)	143.4(2)	144.4(4)	143.4
*r*C(6/7)–O(4/5)	136.1(2)	135.2(4)	136.2
*r*C(1)–C(2)	152.8(3)	150.4(6)	152.1
*r*C(2)–C(3)	151.9(3)	150.4(6)	151.1
*r*C(6/7)–C(8)	152.4(3)	149.4(5)	151.5
∠C(H_3)–C–C(H_3)	113.0(2)	113.7(3)[c]	112.9
∠C(2)–O(4/5)–C(6/7)	118.9(1)	120.5(3)[c]	118.8
∠O(4/5)–C(6/7)=O(9/10)	120.3(1)	119.1(3)[c]	120.4
∠C(1)–C–O	110.8(2)	110.9(3)[c]	110.7
∠C(3)–C–O	105.5(2)	105.5(3)[c]	105.5
ϕC(2)–O(4)–C(6)=O(9)	170.1(11)	–[d]	169.9
ϕC(2)–O(4)–C(6)–C(8)	-12.2(10)	–[d]	-11.9

[a] Figures in parentheses are the estimated standard deviations of the last digit. See text for parameter definitions.

[b] The crystal structure did not possess C_s symmetry so average parameters are given (see Reference 43).

[c] This error was estimated.

[d] This parameter was not reported.

4.4.4 Discussion

The GED structure of Meldrum's acid was successfully reanalysed to give a single boat conformer with C_s symmetry. All of the parameters obtained in the GED refinement agree reasonably well with the theoretical calculations. As a result of many similar internuclear distances (such is the case with a ring structure), a large number of restraints were applied using the SARACEN method,[13-15] based on the range of expected values from *ab initio* calculations (see Table A2.15).

A single boat conformation of Meldrum's acid was obtained, which is more energetically favourable than a chair conformation due to the requirement to accommodate two lactone groups (C–O–CO–C) in the ring (lactone groups are characteristically planar). The absence of significant 1,4-steric interactions also makes a boat conformation unfavourable.[42,43] This is observed in the near planarity of ϕC(2)–O(4)–C(6)=O(9) and ϕC(2)–O(4)–C(6)–C(8), with GED values of 170.1(11)° and -12.2(10)° respectively. These dihedral angles are not perfectly linear due to the tilt at either end of the ring to generate the boat shape.

This refinement provides an improvement on the work conducted by Noble-Eddy,[1] by describing the ring structure of Meldrum's acid with a range of angles, bond lengths and dihedral angles. In the original model, Noble-Eddy used two bond angles and three bond lengths, to generate the ring structure as a triangular prism, with two tilt angles at either end allowing for description of the boat conformation. While this model used far less parameters than this current work, describing the ring system this way led to ϕC(2)–O(4)–C(6)=O(9) refining to a value of 175.4(11)°, which is larger than the values obtained in this study [170.1(11)°, GED; 169.9°, MP2/6-311++G**]. A limitation of the model from the previous work[1] is the lack of adaptability of the model to describe a conformation other than a boat structure without completely rewriting the model. Derivatives of Meldrum's acid are shown to adopt chair and twist-chair conformations depending on their substituents,[42] so such a model as used in this work is especially applicable to them. This study also sets the groundwork of the model for GED studies of possible Meldrum's acid derivatives as discussed in Section 4.6.

Although the obtained boat conformation of Meldrum's acid is similar to the X-ray structure, the X-ray structure did not possess C_s symmetry.[43] Parameters have been compared in Table 4.6, with average parameters being made where necessary to allow for a general comparison. While the ring of Meldrum's acid for the X-ray structure is not symmetrical, the bond lengths are lower than the values obtained in this GED study and predicted by *ab initio* calculations, except for C(2)–O(4/5) which was reported with a value of 144.4(4) pm compared to 143.5(2) pm obtained by

GED. As a result of lengthened C(2)–O(4/5) bonds in the X-ray structure, ∠C(2)–O(4)–C(6) has increased to 120.5(3)°, with a decrease in ∠O=C–O to 119.1(3)°. The other angles of the ring are similar to those obtained in the GED study and are not shown here. This comparison, however, does not take into account distortions in the crystal structure due to intermolecular interactions. The X-ray crystallography study shows that hydrogen bonding occurs in Meldrum's acid for C–H···O, with H···O distances that are less than the sum of the van der Waals radii of oxygen and hydrogen (270 pm).[43] In the crystal structure hydrogen bonding was shown to occur for C(8)–H(17)···O(9) with an H···O distance of 243.0(30) pm but not for C(8)–H(18)···O(10) [with an H···O distance of 280.0(30) pm].[43] As hydrogen bonding plays a part in determining the molecular packing of Meldrum's acid in the crystal structure, the structural differences between the solid and gas-phase structures may be attributed to this and should not be overlooked.

4.4.5 Conclusion

The structure of Meldrum's acid obtained by GED has been reanalysed to provide a general model that can be applicable to derivatives of Meldrum's acid used in future GED studies. This work also provides an improvement on the original refinement model,[1] as it allows for a better description of parameters, particularly dihedral angles, within the ring structure.

A comparison has also been made with parameters obtained from prior X-ray studies of Meldrum's acid. While both GED and X-ray structures resulted in a single boat conformer, the X-ray structure did not have C_s symmetry so selected parameters were averaged to allow a comparison to be made. Differences between the solid and gas phase structures may be due to the intermolecular hydrogen bonding interactions that are present in the crystal structure, but absent in the gas phase.

4.5 Pyrolysis of Meldrum's acid

4.5.1 Introduction

The pyrolysis of Meldrum's acid is well known to give acetone, ketene and CO_2, via a cyclic transition state[10,47] as shown in Figure 4.10.

Figure 4.10 Mechanism for the pyrolysis of Meldrum's acid.

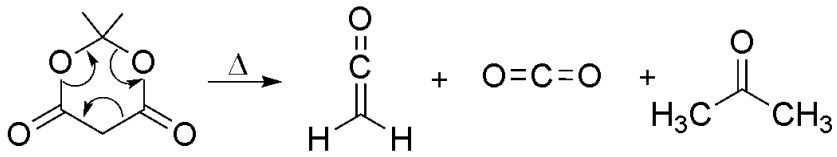

Previous work in the Masters group was directed at determining the gas-phase structure of these products following collection of pyrolysis data of Meldrum's acid by GED.[1] However, deconvolution of the data proved difficult as there appeared to be more than just Meldrum's acid, acetone, ketene and CO_2 in the GED data. Possible secondary pyrolysis (of acetone to give methane and a second equivalent of ketene)[11] was considered in the refinement, but this did not deconvolute the structures.

This section presents a reinvestigation of the refinement of pyrolysis data of Meldrum's acid which have been shown to include diketene in the GED data. While the species present have been successfully determined, limitations in the GED refinement program[12] prevent the relative percentage weighting of species present from being freely refined. This can be remedied by conducting the pyrolysis experiment with a GED-MS setup so known fixed percentage weightings can be applied and this is discussed.

4.5.2 Experimental

Synthesis

The pyrolysis of Meldrum's acid (to generate ketene, acetone and CO_2) was conducted using the VHT nozzle as described earlier in Section 4.3.2.

Theoretical methods

Geometry and frequency calculations were performed using the resources of the NSCCS[18] and the Gaussian09 suite of programs.[19] All MP2[20] methods were frozen core [MP2(fc)].

Geometry optimisations

The geometries of ketene, acetone, CO_2 and diketene were optimised at the HF level with the 3-21G*[44-46] and 6-31G*[22,23] basis sets, and at the MP2 level with the 6-31G*, 6-311G*,[24,25] 6-311+G*[26,27] and 6-311++G** basis sets.

Frequency calculations

Analytic second derivatives of the energy with respect to the nuclear coordinates were calculated at the MP2/6-311++G** level for all species. The generated force fields were used in the program SHRINK[28,29] to provide estimates of the amplitudes of vibration (*u*) and perpendicular distance corrections (*k*) for use in the GED refinement.

GED (*performed by Robert Noble-Eddy, University of Edinburgh*)

Data were collected for the pyrolysis of Meldrum's acid using the Edinburgh GED apparatus (now at University of Canterbury)[2] and the VHT nozzle setup as described earlier in the chapter. An accelerating voltage of around 40 keV was used (electron wavelength ca. 6.0 pm) with an average sample and nozzle temperature of 437.3 K respectively. Scattering intensities were recorded at a nozzle-to-plate distance of 186.32 mm on Kodak Image films. An Epson Expression 1680 Pro flatbed scanner was used to convert the electron-scattering intensities to mean optical densities as a function of the scattering variable, *s*, using an established program.[41] The data-reduction and least-squares refinement processes were carried out using the ed@ed refinement program[12] (Version 2.4) employing the scattering factors of Ross *et al.*[31] The electron wavelengths, weighting points for the off-diagonal weight matrices, correlation parameters, and scale factors for the nozzle-to-camera distances are given in Table A2.20.

4.5.3 Results

***Ab initio* calculations**

The gas-phase geometries of ketene, acetone, CO_2 and diketene were optimised at the HF level with the 3-21G*[44-46] and 6-31G*[22,23] basis sets, and at the MP2[20] level with the 6-31G*, 6-311G*,[24,25] 6-311+G*[26,27] and 6-311++G** basis sets. The MP2 results are presented in Table A2.21. Over all calculations CO_2 was linear (as expected) and ketene, acetone and diketene were shown to adopt C_{2v}, C_2 and C_s symmetry respectively. For diketene, the molecule lies on a single plane except for the two hydrogens of the CH_2 group [H(39) and H(40)] in the central four membered ring. The optimised structures of these molecules are shown in Figure 4.11.

Figure 4.11 Optimised structures of Meldrum's acid (1 - 18), CO_2 (19 – 21), acetone (22 – 31), ketene (32 – 36) and diketene (37 – 46) with atom numbering.

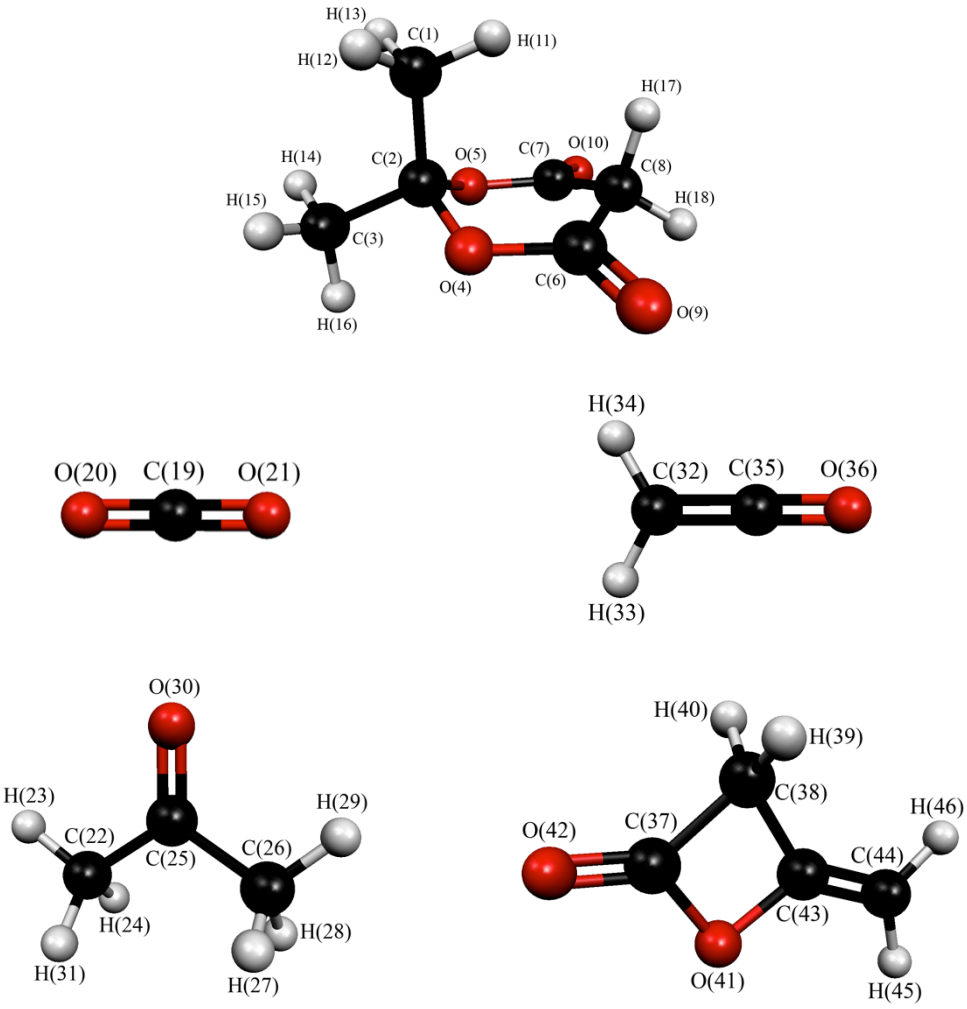

GED

GED refinements for the pyrolysis of Meldrum's acid were carried out based on the *ab* initio calculations described above (optimised at the MP2/6-311++G** level).

Prior to constructing a model and refining, the species present in the collected GED data were crudely determined using coordinates from *ab initio* calculations for Meldrum's acid, ketene, acetone, CO_2 and diketene. While this did not allow for refinement of any parameters, the fixed coordinates in the ed@ed refinement program[12] revealed that diketene and Meldrum's acid were present in the GED data, and needed to be included in a refinement model. Also, this crude refinement provided an *R*-factor of 22% with just background removal, which was much better than the *R*-factor of 28% obtained by Noble-Eddy for a full refinement of the data without including diketene in the model.[1] Tests with the coordinate model revealed that both ketene and diketene were present and that secondary pyrolysis of acetone, to give ketene and methane, did not occur. A significant amount of Meldrum's acid (such that it wasn't negligible) was also present. To refine the GED data in this work a model was constructed containing Meldrum's acid, acetone, CO_2, ketene and diketene.

The model for Meldrum's acid ($p_1 - p_8$, $p_{23} - p_{34}$, $p_{50} - p_{55}$) and ketene ($p_{13} - p_{15}$, p_{42}) were as outlined earlier in the chapter. CO_2 was described with the C=O bond length (p_9). Acetone was described with C_2 symmetry based on *ab initio* calculations at the MP2/6-311++G** level. The parameters for the bond lengths were *r*C=O, *r*C–C and the average C–H bond length ($p_{10} - p_{12}$). To describe the CH_3 groups in C_1 symmetry (reflected on a C_2 symmetry axis), and also ∠C–C=O and ∠C–C–C, six bond angles were defined ($p_{35} - p_{41}$). Lastly, as all of the atoms were not lying in the same plane, one dihedral angle ϕH(23/29)–C–C=O was defined (p_{56}). The C_s model of diketene was described using seven bond lengths ($p_{16} - p_{22}$), seven angles ($p_{43} - p_{49}$) and one dihedral angle (p_{57}). The parameters used to describe the C–O and C–C bond lengths were defined as averages and differences. An average C–H bond length was also described, with fixed differences applied to describe the hydrogens bonded to the alkene and the central ring. The one dihedral angle, ϕH(39)–C–C=O was used to describe the position of the hydrogen atoms [H(39) and H(40)] in the central ring,

that did not lie in the same plane as the rest of the molecule. In total 57 independent parameters (22 bond lengths, 27 angles and 8 dihedral angles) were used and 11 dependent parameters to describe the C–O and C–C bond lengths in Meldrum's acid, and the individual C–O, C–C and C–H bond lengths in diketene.

Theoretical Cartesian force fields were generated at the MP2/6-311++G** level and converted to force fields described by sets of symmetry coordinates. RMS amplitudes of vibration were obtained from the SHRINK program.[28,29] All independent geometric parameters were refined using a least-squares method and restraints were applied using the SARACEN method[13-15] (Table 4.7) based on calculations at the MP2/6-311++G** level. In addition, the corresponding amplitudes of vibration (u) were refined (Table A2.22).

As Meldrum's acid and diketene were both present in the GED data, the relative weighting of each species could not be determined in the refinement. This is because limitations in the ed@ed program[12] make it unable to refine groups of species together (i.e. the amount of ketene plus diketene would be relative to the amount of acetone and CO_2 present). Due to this limitation, and the unknown experimental ratios, the refinement could not be completed. Despite having obtained reasonable parameters for each species (Table 4.7) and good agreement between the RDCs (Figure 4.12) and MICs (Figure A2.4) the determined amounts of each species in the refinement were not accurate. The best R-factors that could be obtained in this study were $R_G = 0.107$ and $R_D = 0.065$. These were deemed inaccurate as the weighting of each molecule in the refinement had to be manually altered to improve the data fit. Manually altering the weighting of each molecule was deemed inaccurate as, although a low R-factor may be obtained, the weighting of each species may not correspond to the actual amount generated in the experiment. The issue with the relative species weighting was also the case for refinement of GED data collected at 556.3 K, with both Meldrum's acid and diketene present in the data (not presented here). As the GED refinement could not be completed in this study only the calculated structure coordinates at the MP2/6-311++G** level for each species is provided (Table A2.23). Several refined GED values also differed very little from their calculated restraints, suggesting that those restraints may be having a negligible effect on the refinement.

Table 4.7 Refined and calculated geometric parameters for Meldrum's acid (distances in pm, angles in °) from the GED study.[a,b]

No.	Description	GED (r_{h1})	MP2/ 6-311++G** (r_e)	Restraint
Independent parameters				
p_1	*r*C=O Meld	120.0(3)	120.4	120.4(3)
p_2	*r*C–O av Meld	139.8(1)	139.8	139.8(1)
p_3	*r*C–O diff Meld	3.5(2)	3.6	3.6(2)
p_4	*r*C–C av Meld	151.7(6)	151.6	–
p_5	*r*C–C diff1 Meld	0.1(1)	0.1	0.1(1)
p_6	*r*C–C diff2 Meld	0.5(1)	0.5	0.5(1)
p_7	*r*C–C diff3 Meld	0.4(1)	0.4	0.4(1)
p_8	*r*C–H av Meld	109.3(1)	109.3	109.3(1)
p_9	*r*C=O CO_2	117.0(1)	117.0	117.0(1)
p_{10}	*r*C=O Acet	121.9(3)	122.0	122.0(3)
p_{11}	*r*C–C Acet	151.6(2)	151.6	151.6(2)
p_{12}	*r*C–H av Acet	109.3(1)	109.3	109.3(1)
p_{13}	*r*C=O Ket	116.8(1)	116.8	116.8(1)
p_{14}	*r*C=C Ket	132.2(2)	132.2	132.2(2)
p_{15}	*r*C–H Ket	108.5(1)	108.5	108.5(1)
p_{16}	*r*C=O Dket	118.9(2)	118.9	118.9(2)
p_{17}	*r*C=C Dket	133.0(1)	133.0	133.0(1)
p_{18}	*r*C–O av Dket	140.6(2)	140.6	140.6(2)
p_{19}	*r*C–O diff Dket	0.5(2)	0.5	0.5(2)
p_{20}	*r*C–C av Dket	151.8(1)	151.8	151.8(1)
p_{21}	*r*C–C diff Dket	1.1(1)	1.1	1.1(1)
p_{22}	*r*C–H av Dket	108.7(1)	108.7	108.7(1)
p_{23}	∠H(16)–C–C Meld	109.3(3)	109.2	109.2(3)
p_{24}	∠H(16)–C–H(15) Meld	109.4(2)	109.4	109.4(2)
p_{25}	∠H(11)–C–C Meld	112.1(2)	112.1	112.1(2)
p_{26}	∠H(11)–C–H(12) Meld	108.5(2)	108.5	108.5(2)
p_{27}	∠C(H_3)–C–C(H_3) Meld	112.9(2)	112.9	112.9(2)

p_{28}	∠C(3)–C–O(4) Meld	105.5(5)	105.5	–
p_{29}	∠C(1)–C–O Meld	110.7(2)	110.7	110.7(2)
p_{30}	∠C(2)–O(4)–C(6) Meld	118.8(1)	118.8	118.8(1)
p_{31}	∠O(4)–C(6)=O(9) Meld	120.4(1)	120.4	120.4(1)
p_{32}	∠O(4)–C(6)–C(8) Meld	116.3(6)	115.8	–
p_{33}	∠C(6)–C(8)–H(17) Meld	108.7(3)	108.7	108.7(3)
p_{34}	∠H(17)–C(8)–H(18) Meld	106.8(6)	106.8	106.8(6)
p_{35}	∠H(23/29)–C–C Acet	110.1(6)	110.1	110.1(6)
p_{36}	∠H(28/31)–C–C Acet	110.5(3)	110.5	110.5(3)
p_{37}	∠H(24/27)–C–C Acet	109.2(10)	109.2	109.2(9)
p_{38}	∠H(23/29)–C–H(31/28) Acet	110.2(4)	110.2	110.2(4)
p_{39}	∠H(23/29)–C–H(24/27) Acet	109.5(1)	109.5	109.5(1)
p_{40}	∠C–C=O Acet	122.0(1)	122.0	122.0(1)
p_{41}	∠C–C–C Acet	116.1(3)	116.1	116.1(3)
p_{42}	∠H–C=C Ket	119.1(4)	119.1	119.1(4)
p_{43}	∠C=C–H(46) Dket	119.5(5)	119.5	119.5(5)
p_{44}	∠C=C–H(45) Dket	120.8(2)	120.8	120.8(2)
p_{45}	∠O–C=C Dket	126.5(3)	126.5	126.5(3)
p_{46}	∠C–O–C Dket	90.8(1)	90.8	90.8(1)
p_{47}	∠O–C=O Dket	127.5(1)	127.5	127.5(1)
p_{48}	∠O=C–C Dket	139.4(1)	139.4	139.4(1)
p_{49}	∠C–C–H Dket	114.0(2)	114.0	114.0(2)
p_{50}	ϕO(4)–C(2)–C(1)–O(5) Meld	124.0(4)	124.0	124.0(4)
p_{51}	ϕC(1)–C(2)–O(4)–C(6) Meld	-73.9(13)	-75.4	–
p_{52}	ϕC(2)–O(4)–C(6)=O(9) Meld	169.9(12)	169.9	169.9(12)
p_{53}	ϕC(2)–O(4)–C(6)–C(8) Meld	-12.7(9)	-11.9	-11.9(12)
p_{54}	ϕO(4)–C(6)–C(8)–H(17) Meld	97.2(12)	97.2	97.2(12)
p_{55}	ϕC(6)–C(8)–H(17)–H(18) Meld	116.9(2)	117.0	117.0(2)
p_{56}	ϕH(23/29)–C–C=O Acet	-8.4(45)	-8.4	-8.4(42)
p_{57}	ϕH(39)–C–C=O Dket	64.4(2)	64.4	64.4(2)

Dependent parameters				
dp_1	rC(2)–O(4/5) Meld	143.3(2)	143.4	–
dp_2	rC(6/7)–O(4/5) Meld	136.3(2)	136.2	–
dp_3	rC(1)–C(2) Meld	152.1(6)	152.1	–
dp_4	rC(2)–C(3) Meld	151.2(6)	151.1	–
dp_5	rC(6/7)–C(8) Meld	151.6(6)	151.5	–
dp_6	rC(37)–O(41) Dket	140.1(3)	140.1	–
dp_7	rC(43)–O(41) Dket	141.1(3)	141.1	–
dp_8	rC(37)–C(38) Dket	152.9(2)	152.9	–
dp_9	rC(38)–C(43) Dket	150.8(6)	150.7	–
dp_{10}	rC(38)–H(39/40) Dket	109.2(1)	109.1	–
dp_{11}	rC(44)–H(45/46) Dket	108.2(1)	108.3	–

[a] Figures in parentheses are the estimated standard deviations of the last digit. See text for parameter definitions.

[b] Meld = Meldrum's acid, Acet = acetone, Ket = ketene, Dket = diketene.

Figure 4.12 Experimental and difference (experimental – theoretical) RDC, $P(r)/r$, for the pyrolysis of Meldrum's acid. Before Fourier inversion the data were multiplied by $s\cdot\exp(-0.00002s^2)/(Z_C - f_C)(Z_O - f_O)$.

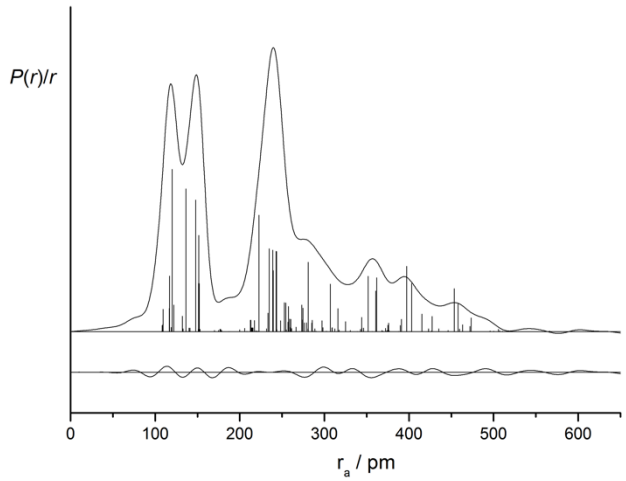

4.5.4 Discussion

The GED data for the pyrolysis of Meldrum's acid were determined to contain acetone, CO_2 and ketene with the indication that some of the ketene had recombined to form diketene. A significant amount of Meldrum's acid was still present in the data, resulting in the need to include Meldrum's acid in the refinement model. Despite the inability to completely refine the data (due to setting the conformer weightings in the refinement program) the refined parameters for the species present agreed reasonably well with the corresponding *ab initio* calculations at the MP2/6-311++G** level. As shown in Table 4.7, most of these parameters have been restrained using the SARACEN method,[13-15] which is not surprising given the degree of peak overlap in the RDC and the number of parameters containing hydrogen atoms (which are poorly defined from GED data alone).

An important part of this work was the highlighted need to know the relative amounts of each species present in the GED data. For systems that contain secondary processes (such as the recombination of ketene to form diketene) and / or significant amounts of precursor still present, knowing the relative amounts of each species present is important to include in the refinement. To refine complex conformer weightings in the GED refinement such as with this study, the ability to tie together the relative weighting of multiple species is important. The relative amounts of each species would need to be refined such that the total amount of ketene and diketene is equal to the individual amounts of acetone and CO_2 that were produced, as the amount of diketene produced is limited by how much ketene was produced during the pyrolysis.

Limitations in the ed@ed refinement program[12] prevented relative refinements of each species. Currently the amount of each species is refined individually, against fixed amounts of each species present, before refining all of the species in turn. However, even if this limitation is addressed in the refinement program it will not be easily applied to systems that are being studied for the first time. This system is a key example of what could be addressed with a GED-MS setup (see Chapter 3) as not only will it allow for using fixed species amounts in the refinement (determined from MS data), it will allow for fine tuning of the experimental conditions. This is

particularly important in this case, as even though Meldrum's acid was heated above 500 K at the nozzle tip (with an average temperature of 437.3 K in the experiment), the pyrolysis was incomplete and some ketene recombined. The use of MS would allow for fine-tuning of the experimental conditions with the VHT nozzle to obtain conditions that would provide mostly complete pyrolysis so that the precursor does not have to be included in the model.

4.5.5 Conclusion

The species present in the GED data for the pyrolysis of Meldrum's acid has been successfully determined. As well as containing ketene, acetone, and CO_2, the GED data were determined to contain diketene (from the recombination of ketene) and Meldrum's acid due to incomplete pyrolysis conditions. Despite knowing the species present, and having reasonable agreement to *ab initio* calculations with the refined parameters, limitations in the ed@ed refinement program prevented the relative amount of each species to be refined. This will be remedied by a GED-MS setup as the amount of each species present can be determined by MS and set as fixed amounts in the refinement. The use of a GED-MS setup will also allow for optimisation of the pyrolysis conditions of Meldrum's acid as refinement of this data showed that the pyrolysis was incomplete.

4.6 Computational investigation of ketene derivatives of Meldrum's acid

4.6.1 Introduction

Work in the previous sections of this chapter has focussed on determining the structure of ethenone ($CH_2C=O$), the simplest form of ketene, from acetic anhydride and Meldrum's acid. However, as highlighted in Section 4.5, if incomplete pyrolysis occurs, the amount of each species present in the GED vapour cannot be determined without the use of a GED-MS apparatus (see Chapter 3).

There are several other issues with studying ketene, particularly with an incomplete pyrolysis process or the possibility of multiple processes occurring. If the pyrolysis process is incomplete there can be difficulties in refining similar interatomic distances of the ketene and parent molecule in GED data without techniques such as the SARACEN method.[13-15] Refining GED data becomes more difficult if the species generated in the pyrolysis experiment has the potential to undergo secondary pyrolysis. Also species can dimerise (such as ketene to diketene)[3] making the determination of the relative amount of each species difficult, especially if the same ketene is produced by both pyrolysis processes (primary and secondary). Observing whether secondary pyrolysis processes are occurring is easily determined by producing substituted ketenes during the primary pyrolysis process. Derivatives of Meldrum's acid can be used to produce substituted ketenes by a similar pyrolysis process as described earlier in the chapter.

While substituted ketenes have been studied by GED before, they have often been generated and studied after isolation as a cold sample[4,5] rather than generated *in situ.* This section details the computational study of various ketene derivatives, and their corresponding parent molecules, for future pyrolysis studies using the VHT nozzle and the Canterbury GED apparatus.[1,2] With reference to the pyrolysis of Meldrum's acid (Section 4.5) the feasibility of pyrolysis studies with various ketene derivatives is shown to depend on actually conducting the experiment, rather than relying on theoretical predictions. Parameters that will be refined from GED data (in particular

the C=O and C=C distances in ketene) have been extracted from *ab initio* calculations for use in future experimental work with ketenes.

4.6.2 Experimental

Theoretical methods

Geometry optimisations and frequency calculations were performed using the resources of the NSCCS[18] and the Gaussian09 program.[19] All MP2[20] methods were frozen core [MP2(fc)].

Geometry optimisations

The geometry of the Meldrum's acid derivatives and corresponding ketene derivatives (Figure 4.13) were optimised at the HF level with the 6-31G*[22,23] basis set, and at the MP2 level with the 6-31G*, 6-311G*,[24,25] 6-311+G*[26,27] and 6-311++G** basis sets.

Figure 4.13 General pyrolysis reaction scheme for various Meldrum's acid derivatives.

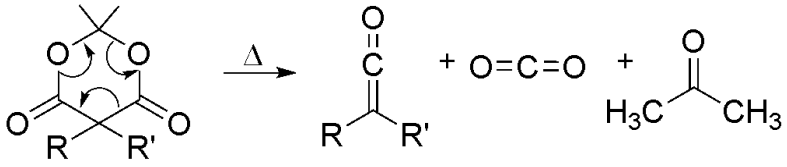

R = R' = H	**1a**	**2a**
R = H, R' = CH_3	**1b**	**2b**
R = R' = CH_3	**1c**	**2c**

Frequency calculations

Frequency calculations were conducted at the MP2/6-311++G** level for all compounds. Thermodynamic data were extracted from the Gaussian outputs using a Perl script.[48]

4.6.3 Results

Geometry optimisations

The gas-phase geometry of the parent molecules **1a – 1c** (and corresponding ketene derivatives **2a – 2c**) were optimised at the HF level with the 6-31G*[22,23] basis set, and at the MP2[20] level with the 6-31G*, 6-311G*,[24,25] 6-311+G*[26,27] and 6-311++G** basis sets. In all cases, the Meldrum's acid derivatives adopted C_s symmetry and the corresponding ketene derivatives C_{2v} symmetry, except for **2b** with C_s symmetry. The optimised structures of all compounds obtained at the MP2/6-311++G** level are given in Figure 4.14.

Figure 4.14 Optimised structures at the MP2/6-311++G** level with atom numbering.

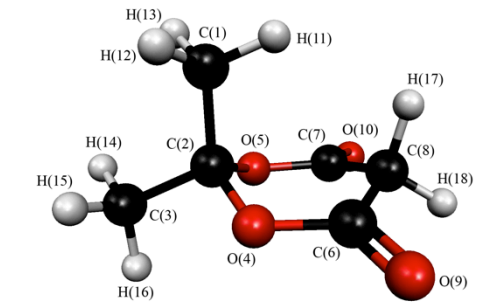

1a

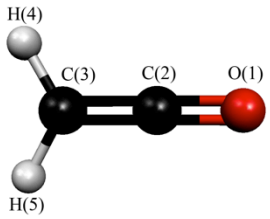

2a

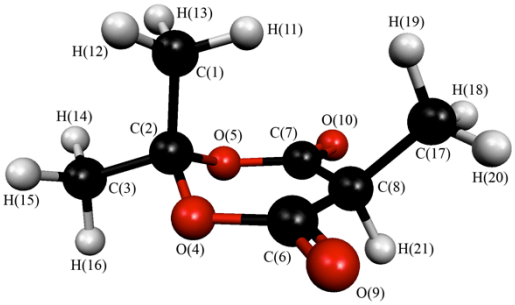

1b

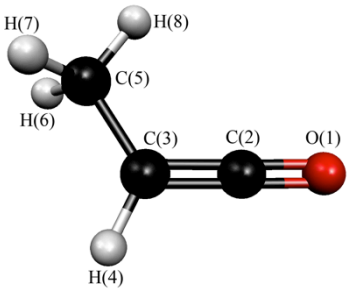

2b

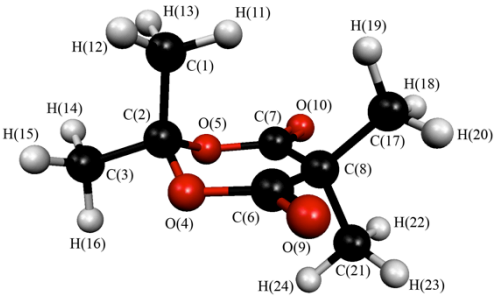

1c

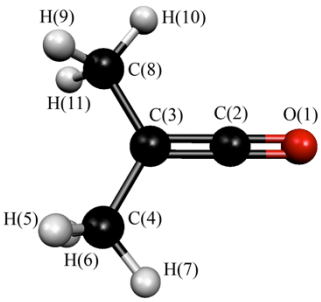

2c

Selected parameters for GED

To compare the parameters that are suitable for GED refinement, bond lengths, bond angles and dihedral angles were extracted from *ab initio* calculations at the MP2/6-311++G** level for **1a – 1c** and **2a – 2c** (Table 4.8). Geometry optimisations were performed and in each case, one conformer was located on the PES. Parameters for CO_2 and acetone (found in earlier sections of this chapter) will not be discussed here.

Table 4.8 Selected geometric parameters for **1a – 1c** and **2a – 2c** at the MP2 level with the 6-31G*, 6-311G*, 6-311+G* and 6-311++G** basis sets.[a,b]

1a	6-31G*	6-311G*	6-311+G*	6-311++G**
*r*C(6/7)=O(9/10)	121.1	120.2	120.4	120.4
*r*C(2)–O(4/5)	143.9	143.3	143.6	143.4
*r*C(6/7)–O(4/5)	136.7	136.2	136.1	136.2
*r*C(1)–C(2)	151.8	151.9	151.9	152.1
*r*C(2)–C(3)	150.9	151.0	150.9	151.1
*r*C(6/7)–C(8)	151.2	151.4	151.4	151.5
*r*C–H(11)	109.1	109.1	109.1	109.2
*r*C–H(12/13)	109.2	109.2	109.2	109.3
*r*C–H(14/15)	109.2	109.1	109.1	109.2
*r*C–H(16)	109.1	109.0	109.1	109.1
*r*C–H(17)	109.7	109.5	109.6	109.6
*r*C–H(18)	109.1	109.0	109.1	109.1
∠H(11)–C–C	111.9	112.2	112.3	112.1
∠H(16)–C–C	109.0	109.0	109.3	109.2
∠H(11)–C–H(12/13)	108.5	108.3	108.4	108.5
∠H(16)–C–H(14/15)	109.4	109.3	109.3	109.4
∠C(H_3)–C–C(H_3)	113.2	113.1	113.1	112.9
∠C(3)–C–O	105.3	105.3	105.4	105.5
∠C(1)–C–O	110.5	110.5	110.7	110.7
∠C(2)–O–C(6/7)	119.5	119.0	118.9	118.8
∠O(4/5)–C=O(9/10)	120.2	120.4	120.4	120.4
∠C(8)–C–O(4/5)	115.8	115.7	115.9	115.8

∠C–C–H(17)	108.9	108.9	108.9	108.7
∠H(17)–C(8)–H(18)	106.7	106.3	106.1	106.8
ϕO(4)–C(2)–C(1)–O(5)	124.3	124.4	124.0	124.0
ϕC(1)–C(2)–O(4)–C(6)	-79.1	-76.5	-75.6	-75.4
ϕC(2)–O–C=O	173.3	170.9	169.7	169.9
ϕC(2)–O(4)–C(6)–C(8)	-7.8	-10.8	-12.0	-11.8
ϕO(4)–C–C–H(17)	92.9	97.0	98.2	97.2
ϕC(6)–C(8)–H(17)–H(18)	117.2	116.7	116.8	117.0
1b				
*r*C(6/7)=O(9/10)	121.3	120.3	120.5	120.5
*r*C(2)–O(4/5)	143.6	143.1	143.3	143.2
*r*C(6/7)–O(4/5)	136.8	136.3	136.2	136.3
*r*C(1)–C(2)	151.7	151.8	151.9	152.1
*r*C(2)–C(3)	150.8	150.9	150.8	151.0
*r*C(6/7)–C(8)	151.7	152.0	152.0	152.1
*r*C(8)–C(17)	153.4	153.2	153.4	153.5
*r*C–H(11)	109.3	109.3	109.3	109.4
*r*C–H(12/13)	109.2	109.2	109.2	109.3
*r*C–H(14/15)	109.2	109.1	109.1	109.2
*r*C–H(16)	109.1	109.1	109.1	109.2
*r*C–H(18/20)	109.1	109.0	109.0	109.1
*r*C–H(19)	109.3	109.3	109.3	109.4
*r*C–H(21)	109.9	110.0	110.0	109.9
∠H(11)–C–C	110.7	111.1	111.4	111.1
∠H(16)–C–C	109.0	109.0	109.3	109.3
∠H(11)–C–H(12/13)	108.6	108.3	108.3	108.5
∠H(16)–C–H(14/15)	109.4	109.3	109.2	109.4
∠C(H_3)–C–C(H_3)	113.9	113.8	113.7	113.6
∠C(3)–C–O	105.7	105.8	105.9	105.9
∠C(1)–C–O	109.7	109.6	109.9	109.9
∠C(2)–O–C(6/7)	118.4	117.4	117.6	117.5
∠O(4/5)–C=O(9/10)	120.0	120.4	120.3	120.3

∠C(8)–C–O(4/5)	117.4	116.8	117.0	117.0
∠C(6/7)–C–C(17)	111.7	112.1	112.1	112.0
∠H(19)–C–C	111.4	111.3	111.5	111.2
∠H(19)–C–H(18/20)	108.6	108.4	108.4	108.5
∠H(21)–C(8)–C(17)	107.0	107.1	107.0	107.3
ϕO(4)–C(2)–C(1)–O(5)	123.5	123.5	123.1	123.1
ϕC(1)–C(2)–O(4)–C(6)	-72.7	-69.5	-69.6	-69.2
ϕC(2)–O–C=O	159.1	156.4	156.7	156.6
ϕC(2)–O(4)–C(6)–C(8)	-25.6	-28.9	-28.4	-28.5
ϕO(4)–C–C–C(17)	131.1	136.1	134.6	134.4
ϕC(6)–C(8)–C(17)–H(21)	113.6	113.1	113.3	113.3
ϕH(19)–C–C–C(6)	-66.4	-66.9	-66.7	-66.7
1c				
*r*C(6/7)=O(9/10)	121.4	120.4	120.6	120.5
*r*C(2)–O(4/5)	143.4	143.0	143.2	143.0
*r*C(6/7)–O(4/5)	136.9	136.5	136.5	136.5
*r*C(1)–C(2)	151.7	151.9	151.9	152.1
*r*C(2)–C(3)	150.8	150.9	150.8	151.0
*r*C(6/7)–C(8)	152.1	152.3	152.4	152.4
*r*C(8)–C(17)	153.3	153.0	153.2	153.3
*r*C(8)–C(21)	154.6	154.8	155.0	155.0
*r*C–H(11)	109.4	109.4	109.4	109.5
*r*C–H(12/13)	109.2	109.2	109.2	109.3
*r*C–H(14/15)	109.2	109.1	109.1	109.2
*r*C–H(16)	109.1	109.1	109.1	109.2
*r*C–H(18/20)	109.2	109.1	109.1	109.2
*r*C–H(19)	109.4	109.4	109.4	109.5
*r*C–H(22/23)	109.2	109.2	109.2	109.3
*r*C–H(24)	109.4	109.4	109.4	109.5
∠H(11)–C–C	110.6	110.9	111.2	110.9
∠H(16)–C–C	109.0	109.1	109.3	109.3
∠H(11)–C–H(12/13)	108.6	108.3	108.3	108.5

∠H(16)–C–H(14/15)	109.4	109.2	109.2	109.4
∠C(H_3)–C–C(H_3)	114.0	113.9	113.8	113.7
∠C(3)–C–O	105.9	105.9	106.0	106.1
∠C(1)–C–O	109.6	109.5	109.7	109.7
∠C(2)–O–C(6/7)	118.1	116.9	117.1	117.0
∠O(4/5)–C=O(9/10)	119.6	120.2	120.0	120.1
∠C(8)–C–O(4/5)	117.8	116.9	117.2	117.2
∠C(6/7)–C–C(17)	110.0	110.4	110.4	110.4
∠C(6/7)–C–C(21)	105.8	105.1	105.4	105.5
∠H(19)–C–C	111.7	111.6	111.8	111.7
∠H(19)–C–H(18/20)	108.4	108.3	108.3	108.5
∠H(24)–C–C	111.0	111.2	111.4	111.2
∠H(24)–C–H(22/23)	108.9	108.8	108.8	109.0
∠C(17)–C(8)–C(21)	109.4	109.7	109.5	109.3
ϕO(4)–C(2)–C(1)–O(5)	123.1	123.2	122.7	122.8
ϕC(1)–C(2)–O(4)–C(6)	-71.9	-68.5	-68.2	-68.0
ϕC(2)–O–C=O	156	152.7	152.6	153.1
ϕC(2)–O(4)–C(6)–C(8)	-30.1	-34.0	-33.9	-33.3
ϕO(4)–C–C–C(17)	133.9	140.2	139.1	137.7
ϕC(6)–C(8)–C(17)–C(21)	115.8	115.3	115.6	115.6
ϕH(19)–C–C–C(6)	-64.2	-64.7	-64.4	-64.4
ϕH(24)–C–C–C(6)	61.6	61.3	61.2	61.3
2a				
*r*C=O	118.1	116.9	116.9	116.8
*r*C=C	132.0	132.0	132.1	132.2
*r*C–H(4/5)	108.1	108.0	108.0	108.0
∠H(4/5)–C=C	119.6	119.5	119.5	119.1
∠H–C–H	120.7	121.0	121.0	121.8
ϕH–C=C=O	180.0	180.0	180.0	180.0

2b				
*r*C=O	118.4	117.2	117.3	117.2
*r*C=C	132.1	132.1	132.2	132.2
*r*C–C	150.9	151.2	151.3	151.3
*r*C–H(4)	108.4	108.4	108.5	108.4
*r*C–H(6/7)	109.4	109.3	109.3	109.4
*r*C–H(8)	109.3	109.2	109.2	109.3
∠H(4)–C=C	116.5	116.4	116.3	116.1
∠C(5)–C=C	122.7	122.7	122.6	122.5
∠C–C–H(4)	120.8	121.0	121.0	121.5
∠H(8)–C–C	111.1	111.2	111.2	111.0
∠H(8)–C–H(6/7))	107.8	107.7	107.7	107.8
ϕH(4)–C=C=O	178.7	179.9	-179.9	-178.9
ϕC(5)–C=C=O	-1.3	-0.1	0.1	1.1
ϕH(8)–C–C=C	0.1	0.1	0.1	0.1
2c				
*r*C=O	118.7	117.5	117.6	117.6
*r*C=C	132.3	132.1	132.1	132.2
*r*C(3)–C(4)	151.9	151.1	151.1	151.2
*r*C(3)–C(8)	151.9	151.1	151.1	151.1
*r*C–H(5)	109.4	109.5	109.5	109.6
*r*C–H(6)	109.3	109.5	109.5	109.6
*r*C–H(7)	109.4	109.2	109.2	109.3
*r*C–H(9)	109.4	109.5	109.5	109.6
*r*C–H(10)	109.4	109.2	109.2	109.3
*r*C–H(11)	109.3	109.5	109.5	109.6
∠C(4)–C=C	118.9	120.3	120.3	120.2
∠C(8)–C=C	118.9	120.3	120.3	120.3
∠C–C–C	122.2	119.3	119.4	119.4
∠H(7/10)–C–C	112.6	112.2	112.2	112
∠H(7/10)–C–H(5/9)	108.0	107.9	107.9	108
∠H(7/10)–C–H(6/11)	107.4	107.9	107.9	108

ϕH(7)–C–C=C	-61.2	0.1	0.1	0.3
ϕH(10)–C–C=C	61.3	-0.1	-0.1	-0.1
ϕC(4)–C=C=O	-48.6	-71.1	4.6	-59.3
ϕC(8)–C=C=O	131.4	102.9	-175.4	120.9

[a] Distances are in pm and angles are in °.

[b] Refer to Figure 4.14 for atom numbering.

Viability of using VHT nozzle

To determine the viability of using the VHT nozzle with these Meldrum's acid derivatives, the theoretical decomposition of **1a** to give **2a**, acetone and CO_2 was compared to the decomposition shown in the GED data in Section 4.5. The thermodynamic data to determine the Gibbs free energy, ΔG, at a given experimental temperature were extracted from frequency calculations at the MP2/6-311++G** level and are presented in Table 4.9.

Table 4.9 Thermodynamic output as calculated from MP2/6-311++G** frequency calculations using temperature (T), entropy (S) and enthalpy (ΔH) to find the Gibbs free energy [ΔG(T)] for the pyrolysis of Meldrum's acid.

Molecule	**T (K)**	***S* (J mol^{-1} K^{-1})**	**ΔH (kJ mol^{-1})[a]**
Meldrum's acid	437.3	462.9	52.3
	556.3	517.5	79.4
Ketene	437.3	265.3	20.1
	556.3	281.0	27.9
CO_2	437.3	229.4	15.0
	556.3	240.1	20.3
Acetone	437.3	331.2	29.1
	556.3	358.0	42.5
ΔG(437.3)[b]	-146.8		
ΔG(556.3)[b]	-189.9		

[a] $\Delta H = H(T) - H(0)$, where $H(0)$ is the zero-point energy.

[b] Units of kJ mol^{-1}.

4.6.4 Discussion

A range of Meldrum's acid derivatives (**1a – 1c**) and their corresponding ketene derivatives (**2a – 2c**) have been investigated by a range of *ab initio* calculations to determine the value of parameters that would be used in a GED refinement (Table 4.8). As indicated in Section 4.5, the pyrolysis of Meldrum's acid (**1a**) to give ketene (**2a**), acetone and CO_2, led to extensive overlap in the RDCs due to similar bond distances. The intention of these calculations was to determine if parameters between the Meldrum's acid derivative and corresponding derivative differed as the substituents changed.

For **1a – 1c**, the optimised structures have C_s symmetry, with a mirror plane through the centre of the ring. As shown in Section 4.5, **1a** was shown to adopt a boat conformation in the gas phase, and this was also shown to be the case for **1b** and **1c**. Derivatives of Meldrum's acid are shown to adopt chair and twist-chair conformations depending on their structure[42] so it was not unexpected to observe the central ring flexing to accommodate the substituents around C(8) as the substituents increased in size for **1b** and **1c**. This meant that the central ring deviated from the boat conformation required to accommodate the lactone groups (C–O–CO–C) on either side of the ring in a near planar geometry. The deviation of the central ring from the boat shape in **1a** is reflected in calculated values at the MP2/6-311++G** level of 156.6° (**1b**) and 153.1° (**1c**) for ϕC(2)–O(4)–C(6)=O(9), and -28.5° (**1b**) and -33.3° (**1c**) for ϕC(2)–O(4)–C(6)–C(8) compared to 169.9° and -11.8° for **1a**. Interestingly the substituent on C(8) which is closer to the C=O groups has an increased bond length compared to the other substituent on the same carbon. This means that for **1a** C–H(17) is longer than C–H(18) (109.6 pm compared to 109.1 pm). However, this increase in bond length is more noticeable for **1c**, with both substituents being methyl groups, giving C(8)–C(21) a calculated bond length of 155.0 pm which is much longer than the adjacent C(8)–H(17) bond length (153.3 pm) and the other C–C bonds in the rest of the molecule. It is likely that heavier substituents will cause further strain on the central ring and result in an increase in bond length, although further computational and experimental studies will be necessary to discern this. In particular, deviations in the boat geometry of the Meldrum's acid derivatives confirms the need to have a more flexible model to use

in GED refinement, as a rigid description like used previously by Noble-Eddy[1] would not be suitable for derivatives adopting a different geometry. For a full comparison of parameters for **1a – 1c** refer to Table 4.8.

For a GED refinement, the C=O, C=C and C–C bond lengths contribute most to the RDCs so differences between these parameters for **2a – 2c** were considered. Across all molecules the C=C bond length was determined to be similar (132.2 pm at MP2/6-311++G** for all **2a** – **2c**) and the C–C bond lengths were similar for **2b** and **2c** [151.3 pm in **2b,** and 151.2 pm and 151.1 pm in **2c**]. While the C=O bond length differed slightly between the ketene derivatives and lengthened with increased substitution (116.8 pm, 117.2 pm, 117.6 pm; **2a – 2c**) the bond lengths would still overlap in RDCs obtained in a GED experiment. Overall the C=O bond lengths were shorter than those obtained for the corresponding Meldrum's acid derivatives (120.5 pm, 120.5 pm, 120.4 pm; **1a – 1c**) however as they still would fall in the same region of the RDCs, the SARACEN method[13-15] would be relied upon to restrain the bond lengths for the precursor and pyrolysis products. This is particularly important if pyrolysis does not proceed fully (as shown in Section 4.5) as a heavily restrained model is affected by the accuracy of the *ab initio* calculations applied as restraints in the refinement. Ideally, a pyrolysis process studied by GED will proceed to near completion such that there is a negligible amount of precursor in the molecular beam.

To determine if a pyrolysis scheme with **1b** or **1c** were viable, thermodynamic calculations were performed for **1a**, **2a**, acetone and CO_2 at the MP2/6-311++G** level and compared to the GED results discussed in Section 4.5. Using an open source Perl script,[48] thermodynamic data were extracted from frequency calculations conducted at the MP2/6-311++G** level to determine the Gibbs free energy, ΔG, for the reaction at the given experimental temperatures (Table 4.9). Assuming that no secondary pyrolysis processes were occurring, a negative value of ΔG indicates that the reaction will proceed in the forward direction, with an equilibrium constant, K, that will favour the pyrolysis products. For both experimental temperatures (437.3 K and 556.3 K) the negative values of ΔG indicated that the reaction should have proceeded fully, with minimal precursor remaining. However, as shown in Section 4.5, this was not the case with the experimental data collection for the pyrolysis of **1a**, as a significant amount of Meldrum's acid was observed in the GED data. This

shows that despite the calculations indicating these temperatures as being suitable temperature for pyrolysis, fine-tuning of the experimental conditions will still be necessary to optimise the pyrolysis conditions for a range of systems that will be studied in the future. Along with the results in Section 4.5, this emphasises the need to use a GED-MS setup to successfully study these systems.

4.6.5 Conclusion

The optimised gas-phase structures of Meldrum's acid derivatives (**1a – 1c**) and their corresponding ketene derivatives (**2a – 2c**) have been determined from *ab initio* calculations, comparing parameters obtained for a range of basis sets.

An increase in substituent size from **1a to 1c**, resulting in a lengthened bond length to accommodate the substituent near the C=O groups. Accommodating larger substituents also led to an increase in strain on the boat geometry of the ring. With larger substituents the ring can flex to accommodate the substitutents[42] thus highlighting the need for a flexible model (with numerous dihedral angles) to describe a range of Meldrum's acid derivatives in a GED refinement.

All of the molecules **1a – 1c** and **2a – 2c** were shown to exist in areas of significant overlap in RDCs. Optimisation of pyrolysis conditions to have negligible precursor remaining would be ideal to reduce the number of restraints applied in a GED refinement. As shown by thermodynamic calculations, comparison to results in Section 4.5 indicates that optimising the pyrolysis conditions may be best done experimentally.

4.7 References

1. R. Noble-Eddy, PhD Thesis, University of Edinburgh, Edinburgh, Scotland, **2009**.
2. S. L. Masters, G. V. Girichev and S. A. Shylkov, *Dalton Trans.*, **2013**, *42*, 3581-3586.
3. F. Chick and N. T. M. Wilsmore, *J. Chem. Soc.*, **1908**, *93*, 946-950.
4. J. Y. Beach and D. P. Stevenson, *J. Chem. Phys.*, **1938**, *6*, 75-80.
5. T. T. Broun and R. L. Livingston, *J. Am. Chem. Soc.*, **1952**, *74*, 6084-6091.
6. J. Bregman and S. H. Bauer, *J. Am. Chem. Soc.*, **1955**, *77*, 1955-1965.
7. B. Rozsondai and I. Hargittai, *J. Mol. Struct.*, **1973**, *17*, 53-64.
8. M. Korn, H.-G. Mack, H.-W. Praas, C. O. Della Védova and H. Oberhammer, *J. Mol. Struct.*, **1995**, *352–353*, 145-151.
9. B. Rozsondai, J. Tremmel, I. Hargittai, V. N. Khabashesku, N. D. Kagramanov and O. M. Nefedov, *J. Am. Chem. Soc.*, **1989**, *111*, 2845-2849.
10. A. E. A. M. Gaber and H. McNab, *Synthesis*, **2001**, 2059-2074.
11. G. Froment, H. Pijcke and G. Goethals, *Chem. Eng. Sci.*, **1961**, *13*, 180-189.
12. S. L. Hinchley, H. E. Robertson, K. B. Borisenko, A. R. Turner, B. F. Johnston, D. W. H. Rankin, M. Ahmadian, J. N. Jones and A. H. Cowley, *Dalton Trans.*, **2004**, 2469-2476.
13. A. J. Blake, P. T. Brain, H. McNab, J. Miller, C. A. Morrison, S. Parsons, D. W. H. Rankin, H. E. Robertson and B. A. Smart, *J. Phys. Chem.*, **1996**, *100*, 12280-12287.
14. P. T. Brain, C. A. Morrison, S. Parsons and D. W. H. Rankin, *J. Chem. Soc., Dalton Trans.*, **1996**, 4589-4596.
15. N. W. Mitzel and D. W. H. Rankin, *Dalton Trans.*, **2003**, 3650-3662.
16. G. Wu, C. Van Alsenoy, H. J. Geise, E. Sluyts, B. J. Van Der Veken, I. F. Shishkov and L. V. Khristenko, *J. Phys. Chem. A*, **2000**, *104*, 1576-1587.
17. V. Spiridonov, N. Vogt and J. Vogt, *Struct. Chem.*, **2001**, *12*, 349-376.
18. National Service for Computational Chemistry Software (NSCCS) (http://nsccs.ac.uk).
19. M. J. Frisch, G. W. Trucks, H. B. Schlegel, G. E. Scuseria, M. A. Robb, J. R. Cheeseman, G. Scalmani, V. Barone, B. Mennucci, G. A. Petersson, H. Nakatsuji, M. Caricato, X. Li, H. P. Hratchian, A. F. Izmaylov, J. Bloino, G.

Zheng, J. L. Sonnenberg, M. Hada, M. Ehara, K. Toyota, R. Fukuda, J. Hasegawa, M. Ishida, T. Nakajima, Y. Honda, O. Kitao, H. Nakai, T. Vreven, Montgomery Jr, J. A. , J. E. Peralta, F. Ogliaro, M. Bearpark, J. J. Heyd, E. Brothers, K. N. Kudin, V. N. Staroverov, T. Keith, R. Kobayashi, J. Normand, K. Raghavachari, A. Rendell, J. C. Burant, S. S. Iyengar, J. Tomasi, M. Cossi, N. Rega, J. M. Millam, M. Klene, J. E. Knox, J. B. Cross, V. Bakken, C. Adamo, J. Jaramillo, R. Gomperts, R. E. Stratmann, O. Yazyev, A. J. Austin, R. Cammi, C. Pomelli, J. W. Ochterski, R. L. Martin, K. Morokuma, V. G. Zakrzewski, G. A. Voth, P. Salvador, J. J. Dannenberg, S. Dapprich, A. D. Daniels, O. Farkas, J. B. Foresman, J. V. Ortiz, J. Cioslowski and D. J. Fox, *Gaussian 09*, Revision D.01, Gaussian, Inc., Wallingford CT, **2013**.

20. C. Møller and M. S. Plesset, *Phys. Rev.*, **1934**, *46*, 618-622.
21. Y. Zhao and D. G. Truhlar, *J. Phys. Chem. A*, **2006**, *110*, 5121-5129.
22. G. A. Petersson, A. Bennett, T. G. Tensfeldt, M. A. Al-Laham, W. A. Shirley and J. Mantzaris, *J. Chem. Phys.*, **1988**, *89*, 2193-2218.
23. G. A. Petersson, T. G. Tensfeldt and J. A. Montgomery Jr, *J. Chem. Phys.*, **1991**, *94*, 6091-6101.
24. A. D. McLean and G. S. Chandler, *J. Chem. Phys.*, **1980**, *72*, 5639-5648.
25. K. Raghavachari, J. S. Binkley, R. Seeger and J. A. Pople, *J. Chem. Phys.*, **1980**, *72*, 650-654.
26. R. Krishnan, J. S. Binkley, R. Seeger and J. A. Pople, *J. Chem. Phys.*, **1980**, *72*, 650-654.
27. A. D. McLean and G. S. Chandler, *J. Chem. Phys.*, **1980**, *72*, 5639-5648.
28. V. A. Sipachev, *J. Mol. Struct. (Theochem)*, **1985**, *121*, 143-151.
29. V. A. Sipachev, *J. Mol. Struct.*, **2001**, *567–568*, 67-72.
30. D. A. Wann, R. J. Less, F. Rataboul, P. D. McCaffrey, A. M. Reilly, H. E. Robertson, P. D. Lickiss and D. W. H. Rankin, *Organometallics*, **2008**, *27*, 4183-4187.
31. A. W. Ross, M. Fink and R. Hilderbrandt, in *International Tables for Crystallography*, Kluwer Academic Publishers, Dordrecht, Netherlands, **1992**, Vol. C, p. 245.
32. S. L. Masters, S. J. Atkinson, M. Hölbling and K. Hassler, *Struct. Chem.*, **2013**, *24*, 1201-1206.

33. G. J. Fisher, A. F. Maclean and A. W. Schnizer, *J. Org. Chem.*, **1953**, *18*, 1055-1057.
34. P. G. Blake and H. H. Davies, *J. Chem. Soc. B*, **1971**, 1727-1728.
35. P. G. Blake and A. Speis, *J. Chem. Soc. B*, **1971**, 1877-1878.
36. I. Lee, O. J. Cha and B. S. Lee, *J. Phys. Chem.*, **1990**, *94*, 3926-3930.
37. J. L. Derissen, *J. Mol. Struct.*, **1971**, *7*, 67-80.
38. B. P. van Eijck, J. van Opheusden, M. M. M. van Schaik and E. van Zoeren, *J. Mol. Spectrosc.*, **1981**, *86*, 465-479.
39. A. P. Cox, L. F. Thomas and J. Sheridan, *Spectrochim. Acta*, **1959**, *15*, 542-543.
40. J. A. Young, *J. Chem. Educ.*, **2001**, *78*, 1176.
41. H. Fleischer, D. A. Wann, S. L. Hinchley, K. B. Borisenko, J. R. Lewis, R. J. Mawhorter, H. E. Robertson and D. W. H. Rankin, *Dalton Trans.*, **2005**, 3221-3228.
42. I. Lee, I. S. Han, C. K. Kim and H. W. Lee, *Bull. Korean Chem. Soc.*, **2003**, *24*, 1141-1149.
43. C. E. Pfluger and P. D. Boyle, *J. Chem. Soc., Perkin Trans. 2*, **1985**, 1547-1549.
44. J. S. Binkley, J. A. Pople and W. J. Hehre, *J. Am. Chem. Soc.*, **1980**, *102*, 939-947.
45. M. S. Gordon, J. S. Binkley, J. A. Pople, W. J. Pietro and W. J. Hehre, *J. Am. Chem. Soc.*, **1982**, *104*, 2797-2803.
46. W. J. Pietro, M. M. Francl, W. J. Hehre, D. J. DeFrees, J. A. Pople and J. S. Binkley, *J. Am. Chem. Soc.*, **1982**, *104*, 5039-5048.
47. C. Wentrup, G. Gross, H. M. Berstermann and P. Lorencak, *J. Org. Chem.*, **1985**, *50*, 2877-2881.
48. K. K. Irikura, THERMO.PL, National Institute of Standards and Technology, **2002**.

CHAPTER 5

Tris(chloromethyl)amine, $N(CH_2Cl)_3$: A combined GED, Raman spectroscopy and computational investigation

5.1 Introduction

Molecules that have different behaviour between the solid, liquid or gas phases, are of interest to the Masters group, particularly those that adopt different conformations or structures. Examples include *N*-methyldichloroacetamide [$MeNHC(O)CHCl_2$][1] which is shown to exhibit different conformers between the solid and gas phases and the phosphinyl radical [$\dot{P}R_2$, R = $CH(SiMe_3)_2$],[2] which undergoes bond breaking in the gas phase to relieve high steric torsion / strain. In some cases molecular behaviour can be different between all phases as observed in recent work on 1,2-bis(trifluoromethyl)-1,1,2,2-tetramethyldisilane, where more stable conformers in the solution phase (compared to the gas and solid phases) was determined to be due to interactions between the solvent and the molecule.[3]

As well as solvent interaction,[3] some molecule stability is observed to be due to hyperconjugation. Hyperconjugation is the interaction of electrons in a sigma bond with an adjacent empty (or partially filled) p- or π-orbital. An extended molecular orbital is formed by the orbital overlap, resulting in bond elongation and changes in molecular geometry.[4] This effect has been widely observed and has been used to justify the structures of trimethylamine[5] and trimethylamine derivatives.[6] In particular, perfluorotrimethylamine, $N(CF_3)_3$, is shown to have an unusual planar geometry of the amine centre[7] with C–N–C angles of 117.9(4)°.[8] The sum of the C–N–C angles are approximately 360° rather than 330° which would be expected for a pyramidal arrangement of the amine centre such as for $N(CH_3)_3$ with C-N-C angles of 110.9(4)°.[9] Resonance occurs for trimethylamine derivatives via the amine centre with the formation of a partially positive charged immonium nitrogen as shown in Figure 5.1.

Figure 5.1 Tautomeric equilibrium of tris(chloromethyl)amine (adapted from Reference 6).

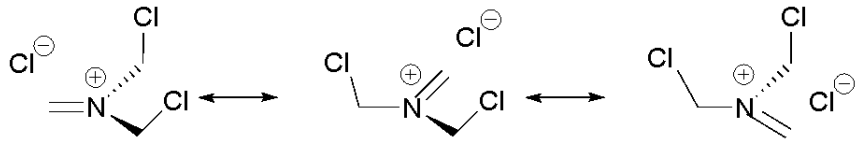

A study undertaken by Klapötke *et al*.[6] investigated the structural properties of tris(chloromethyl)amine, $N(CH_2Cl)_3$, a tertiary amine with exclusively halogenmethyl groups. A crystal structure, from X-ray diffraction, was obtained for $N(CH_2Cl)_3$, showing C_s symmetry with a near planar NC_3 unit. The three CH_2Cl groups were found to point in the same direction, away from the slight apex and lone pair of electrons on the N atom, due to steric and multiple hyperconjugative effects (Figure 5.2).[6] However, a computational investigation of tris(chloromethyl)amine was not conducted.

Figure 5.2 Molecular structure of tris(chloromethyl)amine in the solid state.

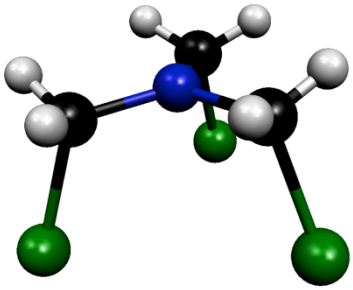

This chapter presents work done to elucidate the gas-phase structure of tris(chloromethyl)amine which is shown to have a different structure in the gas and solid phase. This is the first time the gas-phase structure has been presented. Comparisons between structural parameters obtained from the gas-phase (GED) and solid-phase (X-ray) studies have been drawn. The *ab initio* studies, conducted in parallel to this study, are presented to support the conclusions made.

5.2 Experimental

5.2.1 Synthesis

Tris(chloromethyl)amine, $N(CH_2Cl)_3$, was synthesised at a 10 times reduced scale based on a previous literature method by Fluck and Meiser.[10] The experiment was conducted under a $N_2(g)$ atmosphere to avoid decomposition due to water.[11] Due to concerns regarding the toxicity of the product, all glassware was cleaned prior to removal from the fumehood and a colleague was in attendance during the synthesis.

Hexamethylenetetramine (0.7 g; 5 mmol) and phosphorus pentachloride (4.18 g; 20 mmol) were added to 15 mL of dry dichloromethane (DCM) in a 50 mL round bottomed flask. The flask was fitted with a reflux condenser and a drying tube containing $CaCl_2(s)$ before being placed on an aluminium heat block on a stirrer hotplate. The mixture was refluxed for 20 hours at 75 °C at approximately 1.5 Torr of pressure followed by transfer to a vial under a $N_2(g)$ atmosphere. The synthesis by Fluck and Meiser[10] suggested purification of the product by resublimation or recrystalisation in DCM. Initial attempts at recrystalisation for purification led to decomposition due to water in the atmosphere. In a subsequent synthesis resublimation was used instead. Not all of the product could be retrieved from the sublimation tube before decomposition started to occur. Melting point measurements and mass spectrometry analysis could not be done due to the compound's toxicity and its ready decomposition in water (which is routinely flushed through the Chemistry department's mass spectrometer). The purity of the sample was determined by ^{1}H-NMR and ^{13}C-NMR (Appendix Figures A3.1 and A3.2), with the remaining product being sealed in a 5 mm NMR tube for analysis by Raman spectroscopy. Yield 0.5 g, 62 % (colourless crystalline solid at room temperature). ∂_H (500 MHz, $CDCl_3$) 5.13 (6H, s, $N(C\underline{H}_2Cl)_3$); ∂_C (125.6 MHz, $CDCl_3$) 65.4 (3C, t, $N(\underline{C}H_2Cl)_3$).

5.2.2 GED study

Data were collected for tris(chloromethyl)amine using the Edinburgh GED apparatus, now located at the University of Canterbury.[12] An accelerating voltage of around 40 keV was used (electron wavelength ca. 6.0 pm). Scattering intensities

were recorded at nozzle-to-plate distances of 94.29 mm and 256.16 mm on Kodak Electron Image films. The sample and nozzle temperatures were maintained at 351 K and 393 K respectively for the short camera distance and at 395 K and 413 K respectively for the long camera distance. An Epson Expression 1680 Pro flatbed scanner was used to convert the electron-scattering intensities to mean optical densities as a function of the scattering variable, *s*, using an established program.[13] The data-reduction and least-squares refinement processes were carried out using the ed@ed program[14] (Version 2.4) employing the scattering factors of Ross *et al.*[15] The weighting points for the off-diagonal weight matrices, correlation parameters and scale factors for the two nozzle-to-camera distances are given in Appendix Table A3.1, together with the electron wavelengths which were determined from the scattering patterns of benzene vapour before and after the experiment.

5.2.3 Raman spectroscopy *(with Mark Waterland and Jason Carr, Massey University)*

Raman spectra were acquired using a home-built Raman confocal microscope based on an inverted Olympus IX70 fluorescence microscope. Excitation was provided by an Ondax 785 nm fibre-coupled diode laser. Volume Bragg band-pass filters from OptiGrate Inc. were used to filter background emission from the diode laser before directing the beam into a 40 × microscope objective using a second OptiGrate band-pass filter. Rayleigh and Raman scattered light was collected in a 180° back-scattering geometry through the microscope objective. The scattered light was filtered by three sequential OptiGrate Notch filters and focussed into a 50 micron optical fibre coupled to an Acton LS 785 NIR Lens Spectrograph (Princeton Instruments) with a PIXIS 400 CCD camera for detection, controlled by Princeton LightField Software. Typical excitation power at the sample was 20 mW and integration times ranged from 1 – 5 minutes. Temperature dependent Raman spectra were acquired on a home-built temperature stage.

5.3 *Ab initio* methods

5.3.1 Theoretical methods

Geometry optimisations and frequency calculations were obtained using the resources of the NSCCS[16] and the Gaussian09 program.[17] All MP2[18] methods were frozen core [MP2(fc)].

5.3.2 Geometry optimisations

An extensive search of the PES was conducted for the gas-phase structure of $N(CH_2Cl)_3$ using the HF method and 6-31G* basis set[19,20] followed by calculations at the MP2 level[18] to locate local minima. Each CH_2Cl group was initially set at 0° relative to the lone pair of electrons on the nitrogen and rotated in turn about the molecule in 15° steps, relative to fixed positions of the other CH_2Cl groups. Using the molecular structures corresponding to the lowest single point energies of the CH_2Cl rotations, relaxed geometry optimisations were conducted at the MP2 level with the 6-31G*, 6-311G*,[21,22] 6-311+G*,[23,24] cc-pVDZ,[25] aug-cc-pVDZ,[25] cc-pVTZ[26] and aug-cc-pVTZ[26] basis sets. These calculations resulted in a minimum structure with two, almost equivalent, CH_2Cl groups pointing downwards, relative to the lone pair of electrons on the central nitrogen atom. Depending on the method and basis set used, the torsion angle of the upward pointing CH_2Cl group was observed to vary between 0° and approximately ±30°. The coordinates for each of the three conformers (**A – C**) were then optimised using the M06-2X[27] method and aug-cc-pVDZ basis set. The calculated lowest energy structures of tris(chloromethyl)amine are shown in Figure 5.3.

Figure 5.3 Lowest energy structures of tris(chloromethyl)amine with atom numbering.

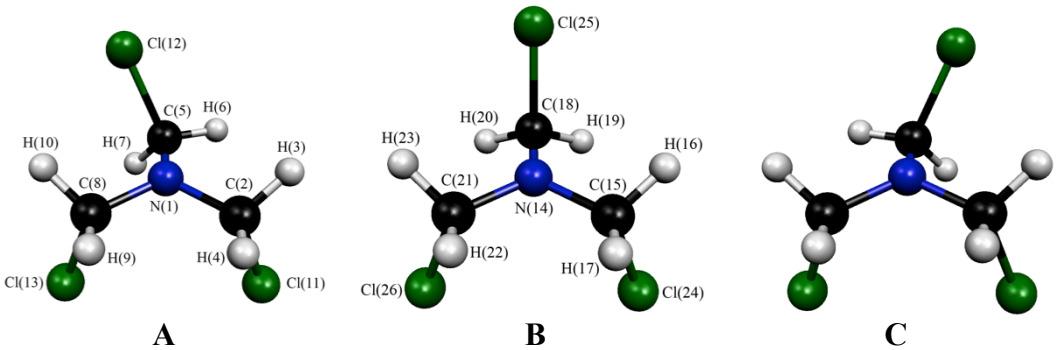

A **B** **C**

5.3.3 Frequency calculations

Analytic second derivatives of the energy with respect to nuclear coordinates calculated at the MP2/aug-cc-pVDZ level gave the force fields for the lowest energy geometries of the $N(CH_2Cl)_3$ conformers. Following a trial refinement cubic forcefields were also calculated for $N(CH_2Cl)_3$ at the M06-2X/aug-cc-pVDZ level to generate the amplitudes of vibration (u) and perpendicular corrections ($k_{a3,1}$) for use in the GED refinement by using the SHRINK program.[28,29]

5.3.4 Stabilisation interactions

An investigation was undertaken to determine if there were any stabilising interactions that would explain the difference in structure between the solid and gas phases of tris(chloromethyl)amine. A prior study of the crystal structure of $N(CH_2Cl)_3$ indicated that there were no interactions or hydrogen bonding between molecules[6] and this was confirmed with calculations at the MP2[18] and M06-2X level[27] with the aug-cc-pVDZ basis set,[25] using the counterpoise method[30,31] to account for basis set superposition error (BSSE).[30] Solid-state coordinates for a dimer and monomer unit in the crystal structure were provided by Professor Norbert Mitzel (Universität Bielefeld, Germany). While calculations were not conducted in the solid state using a periodic system, gas-phase calculations performed using the solid-state coordinates were used to calculate the relative energy differences between the solid-state and gas-phase conformers. The calculations for the solid-state structure were conducted at the MP2/aug-cc-pVDZ level and were compared to the results from the *ab initio* calculations of the gas-phase structure as described above.

5.4 Results

5.4.1 *Ab initio* calculations

An extensive PES search at the HF/6-31G* and MP2/6-31G* level was conducted to locate all local minima as described in Section 5.3.2. The coordinates from the resulting lowest single point energies were optimised with relaxed geometry optimisations conducted at the MP2 level[18] with the 6-31G*,[19,20] 6-311G*,[21,22] 6-311+G*,[23,24] cc-pVDZ,[25] aug-cc-pVDZ,[25] cc-pVTZ[26] and aug-cc-pVTZ[26] basis sets (refer to Table A3.2). Using the MP2 coordinates for each of the three possible conformers (Figure 5.3, **A** – **C**) as a starting point, the three conformers were then optimised at the M06-2X/aug-cc-pVDZ level (Table 5.1), as the optimised geometry was dependent on the starting coordinates with the M06-2X method. The calculations conducted at the M06-2X level suggested that conformers **A** and **C** were equivalent, so only **A** and **B** were considered for the GED refinement.

As the suggested conformation of $N(CH_2Cl)_3$ was different between the gas phase and the solid phase, calculations were conducted to investigate if there were any favourable interactions that were only present in the solid state. Using crystal structure coordinates as provided by Professor Norbert Mitzel (Universität Bielefeld, Germany), the crystal structure coordinates were extracted so that calculations could be performed in the gas phase. Single point energy calculations of the dimer and monomer units of the crystal structure were conducted and compared to results for the gas-phase conformers using the MP2 and M06-2X methods and the aug-cc-pVDZ basis set (Table 5.2). Whilst the crystal structure viewing program Mercury[32] showed no hydrogen bonding or other intermolecular interactions, single point energy calculations at the the MP2 and M06-2X level with the aug-cc-pVDZ basis set were conducted on both the dimer and monomer crystal structure coordinates using the counterpoise method[30,31] to account for BSSE.[30] The calculations revealed that there were no intermolecular interactions between monomer units in the crystal structure as was predicted by the Mercury program[32] (and hence are not presented). However the difference in energy between the solid state and gas-phase coordinates suggests that there is some other stabilising interaction (not necessarily due to crystal packing) that needs to be investigated further. This includes considering the dipoles

in the solid and gas-phase conformers as well as investigating the crystal structure using solid-state methods such as a periodic system.

Table 5.1 Theoretical geometrical parameters at the M06-2X/aug-cc-pVDZ level for the three conformers **A**, **B** and **C** of tris(chloromethyl)amine [$N(CH_2Cl)_3$].[a]

Parameter	**A**	**B**	**C**
*r*C(2)–Cl(11)	184.5	184.1	183.9
*r*C(5)–Cl(12)	181.4	182.7	181.4
*r*C(8)–Cl(13)	183.9	184.1	184.5
*r*N(1)–C(2)	141.1	141.1	141.4
*r*N(1)–C(5)	143.0	142.1	143.0
*r*N(1)–C(8)	141.4	141.1	141.1
*r*C(2)–H(3)	109.2	109.3	109.2
*r*C(2)–H(4)	109.1	109.1	109.1
*r*C(5)–H(6)	109.1	109.2	109.5
*r*C(5)–H(7)	109.5	109.2	109.1
*r*C(8)–H(9)	109.1	109.2	109.1
*r*C(8)–H(10)	109.2	109.3	109.2
∠N(1)–C(2)–Cl(11)	114.5	114.0	114.4
∠N(1)–C(5)–Cl(12)	111.1	111.9	111.1
∠N(1)–C(8)–Cl(13)	114.4	113.9	114.6
∠N(1)–C(2)–H(3)	110.6	110.5	109.9
∠N(1)–C(2)–H(4)	110.5	110.7	110.6
∠N(1)–C(5)–H(6)	109.9	111.1	112.2
∠N(1)–C(5)–H(7)	112.2	111.2	109.9
∠N(1)–C(8)–H(9)	110.6	110.8	110.4
∠N(1)–C(8)–H(10)	109.9	110.4	110.6
∠Cl(11)–C(2)–H(3)	104.3	104.8	104.7
∠Cl(11)–C(2)–H(4)	105.5	105.5	105.7
∠Cl(12)–C(5)–H(6)	107.0	106.0	105.8
∠Cl(12)–C(5)–H(7)	105.8	106.0	107.0
∠Cl(13)–C(8)–H(9)	105.7	105.5	105.5
∠Cl(13)–C(8)–H(10)	104.7	104.8	104.3

∠C(2)–N(1)–C(5)	117.3	118.1	116.7
∠C(2)–N(1)–C(8)	119.9	118.0	117.2
∠C(5)–N(1)–C(8)	116.7	120.6	119.9
ϕCl(11)–C(2)–N(1)–C(5)	-66.7	-72.5	-67.7
ϕCl(12)–C(5)–N(1)–C(2)	-131.3	-101.2	-76.0
ϕCl(13)–C(8)–N(1)–C(5)	67.9	72.8	66.5
Energy (Hartrees)	-1553.1935	-1553.1934	-1553.1935

[a] All distances in pm and all angles in degrees. See Figure 5.3 for atom numbering.

Table 5.2 Calculated energy differences between the gas-phase and solid phase structures of tris(chloromethyl)amine [$N(CH_2Cl)_3$].[a]

Conformer	M06-2X/ aug-cc-pVDZ	Relative energy difference (Hartrees)[b]	Relative energy difference (kJ mol^{-1})
Gas-phase			
A	-1553.1935	-	-
B	-1553.1934	0.0001	0.263
C	-1553.1935	-	-
Crystal structure[c]			
Optimised	-1553.1904	0.0031	8.139
Single-point	-1553.0491	0.1443	378.9

[a] Energies are reported in Hartrees.

[b] The energy difference was calculated relative to conformers **A** and **C**.

[c] A relaxed geometry optimisation and single point energy calculation was performed using the provided crystal structure coordinates.

5.4.2 GED

Electron diffraction refinements were carried out for tris(chloromethyl)amine based on the *ab initio* calculations described above. The *ab initio* results suggested that the two downward pointing CH_2Cl groups were somewhat equivalent, in terms of bond lengths and orientation with respect to the lone pair on the nitrogen atom. These two CH_2Cl groups were treated as equivalent in the refinement model; thus reducing the number of parameters to a manageable amount. To describe the change in torsion of the upward pointing CH_2Cl group a C_1 model was adopted. *Ab initio* calculations at the M06-2X/aug-cc-pVDZ level showed that both **A** and **B** were present in the GED data with 67 % of **A** predicted to be present in the GED data. Trial refinements conducted treating **A** and **B** separately revealed that both **A** and **B** were present in the GED data so a two-conformer model was used. The trial refinements were first conducted with harmonic corrections implemented from the MP2/aug-cc-pVDZ force fields but the amplitudes of vibration were poorly described when compared to the experimental data. Instead, cubic force fields calculated at the M06-2X/aug-cc-pVDZ level were implemented in the refinement.

The structure of tris(chloromethyl)amine in the two-conformer model was defined in terms of 21 independent parameters and six dependent parameters (Table 5.3). The 21 independent parameters comprised of five bond lengths, 10 bond angles and six dihedral angles. As the two conformers only differed in the rotation of one CH_2Cl group, the bond lengths and angles were treated as being the same across both conformers. To describe *r*C–Cl and *r*N–C of the equivalent and unique CH_2Cl groups an average and difference parameter for *r*C–Cl (p_1, p_2) and *r*N–C (p_3, p_4) was used. The *r*C–H parameter was defined as an average over both conformers (p_5). To describe ∠N–C–Cl an average and difference was used (p_6, p_7). For ∠N–C–H an average value was used (p_8), with fixed differences applied from *ab initio* calculations. For ∠C–N–C, three parameters were defined (p_{13} –p_{15}). For ∠Cl–C–H two parameters were used to describe the position of the equivalent (p_9, p_{10}) and unique (p_{11}, p_{12}) CH_2Cl groups. Lastly, to describe the torsions of the three CH_2Cl groups, three dihedral angles were used for **A** (p_{16} – p_{18}) and three for **B** (p_{19} – p_{21}). The six dependent parameters were used to obtain *r*C–Cl, *r*N–C and ∠N–C–Cl for the equivalent and unique CH_2Cl groups.

Theoretical Cartesian force fields for both conformers were generated at the M06-2X/aug-cc-pVDZ level and converted to a set of force fields described by a set of symmetry coordinates. RMS amplitudes of vibration were obtained from the SHRINK program.[28,29] All independent parameters were refined using a least-squares method and restraints were applied using the SARACEN method[33-35] (Table 5.3). The restraints were based on calculations at the M06-2X and MP2 levels. In addition the corresponding amplitudes of vibration were refined (see Table A3.3). The amplitudes of vibration were still not well described even with the cubic force field corrections. This is reflected in the RDCs (Figure 5.4) and MICs (Figure A3.3). As a result the R-factors R_G = 0.1758 (R_D = 0.1319) are significantly higher than what would be deemed suitable for a successful structure refinement. This has also resulted in an increased error for the relative conformer weighting of conformer **A** in the GED data [73.1(284) %]. The error of the conformer weighting was directly obtained from the GED refinement, although it is presumed the error would decrease slightly if a plot of R_G against the conformer weighting was used to give the 95 % confidence limit. Whilst the data have not been fully refined the least-squares correlation matrix is presented in Table A3.4 along with the GED structure coordinates and calculated coordinates at the M06-2X/aug-cc-pVDZ level in Tables A3.5 – A3.6 respectively.

Table 5.3 Refined ($r_{a3,1}$) and calculated (r_e) geometric parameters for tris(chloromethyl)amine from the SARACEN GED refinement.[a,b,c]

Parameters		GED ($r_{a3,1}$)	M06-2X/ aug-cc-pVDZ (r_e)	Restraint
Independent				
p_1	*r*C–Cl av	178.2(3)	182.8	182.8(30)
p_2	*r*C–Cl diff	2.2(10)	2.8	2.8(10)
p_3	*r*N–C av	140.4(4)	142.1	-
p_4	*r*N–C diff	-1.7(10)	-1.7	-1.7(10)
p_5	*r*C–H av	108.7(6)	109.2	109.2(1)
p_6	∠N–C–Cl av	113.8(4)	112.8	-
p_7	∠N–C–Cl diff	3.2(5)	3.3	3.3(5)
p_8	∠N–C–H av	110.2(9)	110.6	110.6(10)
p_9	∠Cl(11/13)–C(2/8)–H(3/10)	104.8(15)	104.3	104.3(15)
p_{10}	∠Cl(11/13)–C(2/8)–H(4/9)	105.8(10)	105.5	105.5(10)
p_{11}	∠Cl(12)–C(5)–H(6)	107.3(15)	107.0	107.0(15)
p_{12}	∠Cl(12)–C(5)–H(7)	106.1(10)	105.8	105.8(10)
p_{13}	∠C(5)–N(1)–C(2)	117.6(17)	117.3	117.3(30)
p_{14}	∠C(5)–N(1)–C(8)	115.2(14)	116.7	116.7(15)
p_{15}	∠C(2)–N(1)–C(8)	119.8(14)	119.9	119.9(20)
p_{16}	ϕCl(11)–C(2)–N(1)–C(5) **(A)**	-62.3(28)	-66.7	-66.7(40)
p_{17}	ϕCl(12)–C(5)–N(1)–C(2) **(A)**	-138.1(32)	-131.3	-131.3(35)
p_{18}	ϕCl(13)–C(8)–N(1)–C(5) **(A)**	59.3(43)	67.9	67.9(55)
p_{19}	ϕCl(24)–C(15)–N(14)–C(18) **(B)**	-75.5(50)	-72.5	-72.5(50)
p_{20}	ϕCl(25)–C(18)–N(14)–C(15) **(B)**	-100.5(52)	-101.2	-101.2(50)
p_{21}	ϕCl(26)–C(21)–N(14)–C(18) **(B)**	74.9(41)	72.8	72.8(40)
Dependent				
dp_1	*r*C(2/8)–Cl(11/13)	179.4(4)	184.2	-
dp_2	*r*C(5)–Cl(12)	177.1(8)	181.4	-
dp_3	*r*N(1)–C(2/8)	139.5(5)	141.3	-
dp_4	*r*N(1)–C(5)	141.2(8)	142.9	-

dp_5	∠N(1)–C(2/8)–Cl(11/13)	115.4(4)	114.4	-
dp_6	∠N(1)–C(5)–Cl(12)	112.2(5)	111.1	-

[a] Distances ($r_{a3,1}$) are in pm and bond angles (∠) and dihedral angles (ϕ) are in degrees.

[b] Difference parameters are from the equivalent CH_2Cl groups minus the unique CH_2Cl group.

[c] Dihedral angles from conformers **A** and **B** are as indicated.

Figure 5.4 Experimental and difference (experimental – theoretical) RDC, $P(r)/r$, for tris(chloromethyl)amine. Before Fourier inversion the data were multiplied by $s \cdot \exp(-0.00002s^2)/(Z_N - f_N)(Z_{Cl} - f_{Cl})$.

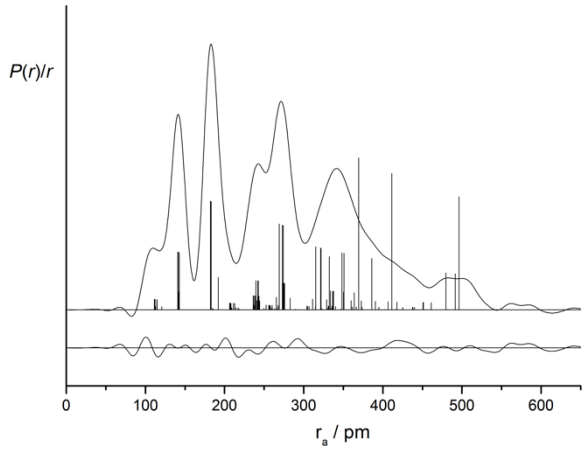

5.4.3 Raman spectroscopy

Temperature dependent Raman spectra for tris(chloromethyl)amine were collected at Massey University (Palmerston North, NZ) using the setup as described above. Noting that the reported literature melting point of tris(chloromethyl)amine is 366 K,[10] data were collected at room temperature (approximately 293 K), 333 K and 393 K to allow for comparison of the Raman spectra for the solid phase and melt. The experimental data sets were offset from each other and split into two plots with different intensity scaling to aid visualisation (Figure 5.5).

Figure 5.5 Temperature dependent Raman spectra of tris(chloromethyl)amine collected at 293 K (black), 333 K (red) and 393 K (blue).

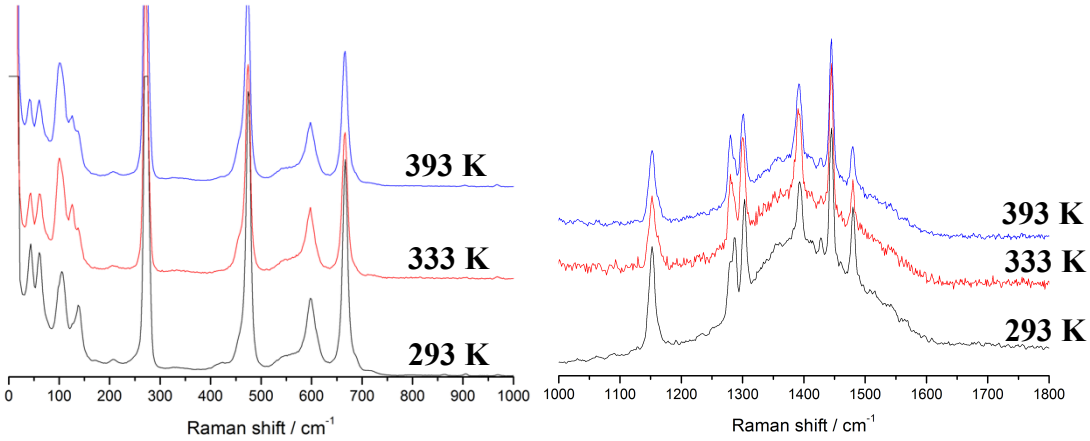

The assignment of the Raman spectra peaks were based on the calculated vibrational frequencies obtained from calculations at the M06-2X/aug-cc-pVDZ level for conformers **A**, **B** and **C**. The calculated spectra are shown in Figure 5.6, with the full table of spectra assignments being given in Appendix Table A3.7. Most of the bands were largely unchanged upon heating the sample through to its melting point. The most significant changes were seen for modes 1 – 4 (from 40 – 130 cm^{-1}) which all involve torsional motions and modes 20 and 21 (approximately 1290 cm^{-1}) which involve CH_2 wagging motion (asymmetric stretching).

Following the temperature dependent data collection, the sample of tris(chloromethyl)amine was allowed to cool. While the sample was cooling, Raman data were collected at temperatures of 363 K, 333 K and 303 K (Figure 5.7). It was

noted that sample was possibly undergoing a reversible reaction as the peak at approximately 370 cm^{-1} (Figure 5.7) was reversible with temperature. However, as $N(CH_2Cl)_3$ had become orange in colour, with the colour still lingering after cooling, this could be due to impurities present in the sample. Therefore the possibility of a reversible reaction requires further investigation.

Figure 5.6 Calculated Raman spectra for conformers **A** (black), **B** (blue) and **C** (red) of tris(chloromethyl)amine from calculations at the M06-2X/aug-cc-pVDZ level.

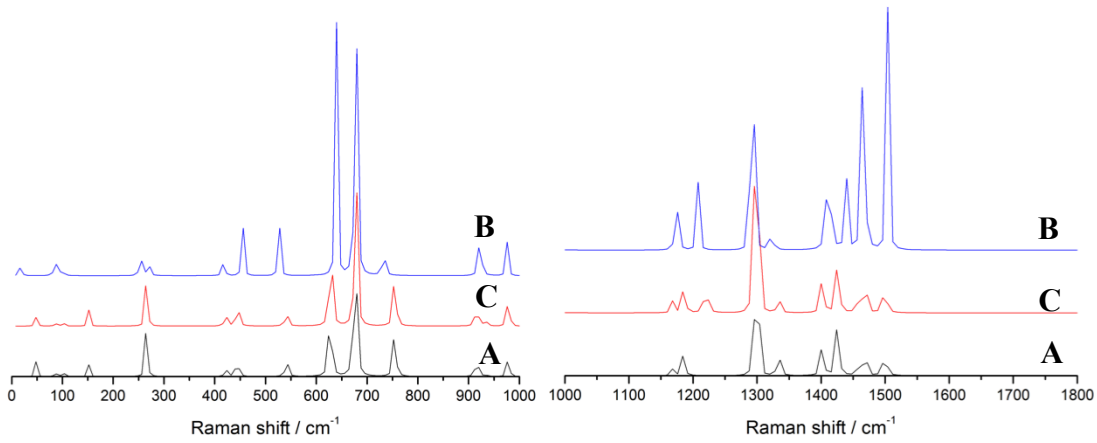

Figure 5.7 Temperature dependent Raman spectra of tris(chloromethyl)amine collected at 363 K (blue), 333 K (red) and 303 K (black) as the sample was cooling following the data collection shown in Figure 5.5.

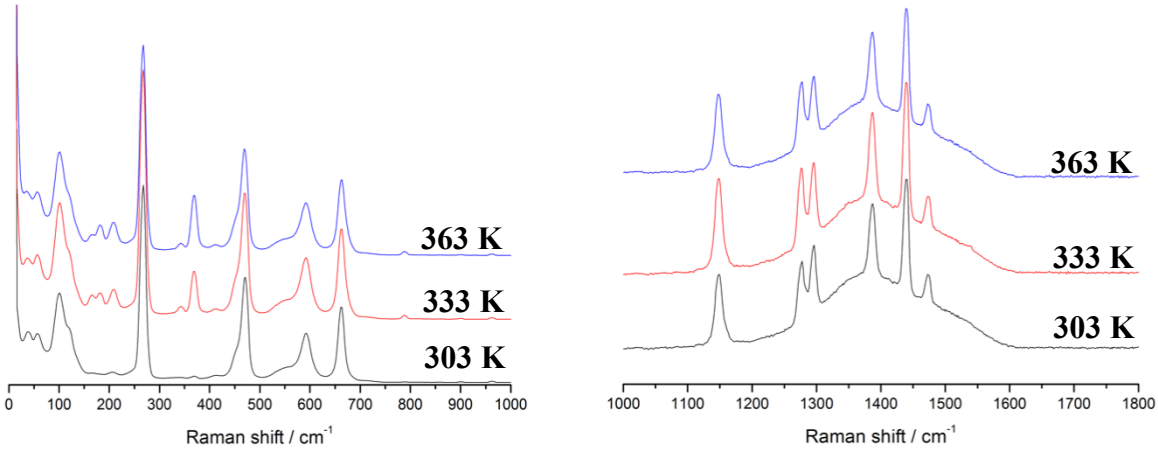

5.5 Discussion

The GED data of tris(chloromethyl)amine were determined to contain conformers **A** and **B**, with **A** being more prevalent in the data [73.1(284) %]. From *ab initio* calculations conformers **A** and **C** were considered to be equivalent enantiomers so for simplicity, **A** will be referred to here. The refined parameters for the bond lengths, angles and torsions mostly agree with the predicted *ab initio* results (Table 5.3). The C–Cl bond lengths are shorter than what was predicted by *ab initio* calculations and this can be accounted for by the *r*C–Cl average parameter having a low uncertainty [178.2(3) pm] despite a large restraint being applied [182.3(30) pm]. This suggests that the effect of the restraint in the refinement is negligible. In particular this is true for the parameters related to the different dihedral angles of **A** [-62.3(28)°, -138.1(32)° and 59.3(43)° compared to -66.7°, -131.3° and 67.9° from *ab initio* calculations] and **B** [-75.5(50)°, -100.5(52)° and 74.9(41)° compared to -72.5°, -101.2° and 72.8° from *ab initio* calculations]. However, despite successfully determining the conformers present in the GED data for tris(chloromethyl)amine, the GED data have yet to be fully refined due to issues related to the description of the amplitudes of vibration (Table A3.3).

Molecules that exhibit large amplitude motions, such as in this case, are poorly described by harmonic amplitude corrections[28] which are usually applied in a refinement (such as the r_{h1} refinements in Chapter 4). Following an initial test with harmonic amplitude corrections, cubic force fields were calculated at the M06-2X/aug-cc-pVDZ level allowing for cubic corrections to the amplitudes of vibration to be implemented in an $r_{a3,1}$ refinement[28,36] (refer to Reference 36 for more detail about the naming convention of $r_{a3,1}$). However, despite implementing better force fields in the model, the amplitudes of vibration were poorly described for the periphery atoms, in particular, the C–H bond lengths and the CH_2Cl dihedral angle of the unique CH_2Cl group. The correction to the amplitudes of vibration for the C–H bond lengths of the unique CH_2Cl group resulted in much longer C–H bond lengths than what would be expected [114.3(6) pm and 114.7(6) pm]. As the refinement cannot be fully completed without a better description of the amplitudes of vibration, especially for the motion of the CH_2Cl torsions, molecular dynamics calculations will be undertaken to implement in the refinement. This has worked well in the past

with refining GED data of molecules with low frequency torsional motions.[37] The molecular dynamics study of tris(chloromethyl)amine is currently underway.

To better understand the low frequency amplitudes in tris(chloromethyl)amine, a Raman study was undertaken with data being recorded at different temperatures. Data were collected at approximately 293 K, 333 K and 393 K (Figure 5.5) so that data for both the solid phase and melt could be collected, as the reported melting point of $N(CH_2Cl)_3$ is 366 K.[10] The experimental bands were matched to the corresponding normal modes using the calculated spectra (Figure 5.6) from frequency calculations at the M06-2X/aug-cc-pVDZ level.

Upon heating the sample through to its melting point, changes were observed in modes 1 – 4 which all involve torsional motions, and modes 20 and 21 which involve a CH_2 wagging (asymmetrical stretching) mode of vibration. As the rest of the bands were largely unchanged these bands were determined to correspond to the unique CH_2Cl group. The Raman results tie in with the results observed from GED as the description of the amplitude of the C–H bond lengths were problematic in the GED refinement, especially for the unique CH_2Cl group. Determining the main change between the solid and gas phases of tris(chloromethyl)amine as being the torsional motions also supports the gas-phase structures determined from the *ab initio* calculations.

Interestingly the main difference between the calculated Raman spectra for conformers **A** and **C** was the presence of mode 19 (1215 cm^{-1} in Figure 5.6), which was more intense in **C** and could not be seen on the same scale as the other modes in **A**. However despite being present in the calculated spectra, mode 19 was absent from the experimental data. This suggests the presence of conformer **A** rather than **C** in the GED data. Since **A** and **C** were considered equivalent from *ab initio* calculations, with essentially the same energy and parameters as expected for enantiomers, this needs further investigation.

Further investigation also needs to be undertaken to determine the reason why tris(chloromethyl)amine adopts a different conformation in the solid and gas phases. In the solid phase the CH_2Cl groups are all pointing downwards, whereas in the gas

phase one CH_2Cl group is pointing upwards, deviating from a fixed upright position due to a low frequency torsion. *Ab initio* calculations show the gas-phase conformers **A** and **B** to be lower in energy than the solid state conformer however no intermolecular interactions (such as hydrogen bonding) were deduced from *ab initio* calculations with the crystal structure coordinates. The energy difference between the solid and gas phases suggest that there is some sort of stabilisation. Further *ab initio* calculations are required to determine the reason for the difference in energy between the solid and gas phases of tris(chloromethyl)amine. This includes considering the dipoles in the solid and gas phases, and conducted calculations for the crystal structure coordinates in the solid state rather than just for the gas phase as was presented here.

5.6 Conclusions

The GED data of tris(chloromethyl)amine have been successfully determined to contain two conformers **A** and **B**, differing only in the torsion of the upward pointing CH_2Cl group. This conformation differs from that in the solid state, with all CH_2Cl groups pointing downwards.

Despite obtaining a close agreement between to the *ab initio* results for the refined independent parameters, the large amplitude motion of the upward pointing CH_2Cl group of the gas-phase conformers has led to problems in the GED refinement. In particular, the wagging motion (asymmetric stretch) of the CH_2 group on the unique CH_2Cl group is poorly described in the GED refinement with harmonic or cubic corrections to the force fields. Work is currently underway to obtain molecular dynamics data of tris(chloromethyl)amine to better describe the amplitudes of vibration in the GED refinement.

An independent Raman spectroscopy study has also been conducted on the solid and gas phases of tris(chloromethyl)amine. Upon heating, observed changes in the spectra were identified to be due to modes 1 – 4 (torsional) and modes 20 and 21 (CH_2 wagging). The change in these modes confirm the change in conformation from the solid to gas phase. The Raman data also show the change in vibration for the C–H bonds, which are currently poorly described in the GED refinement.

5.7 References

1. S. L. Hinchley, H. E. Robertson, L. J. McLachlan, C. A. Morrison, D. W. H. Rankin, S. J. Simpson and E. W. Thomas, *J. Phys. Chem A*, **2003**, *108*, 185-193.
2. S. L. Hinchley, C. A. Morrison, D. W. H. Rankin, C. L. B. Macdonald, R. J. Wiacek, A. Voigt, A. H. Cowley, M. F. Lappert, G. Gundersen, J. A. C. Clyburne and P. P. Power, *J. Am. Chem. Soc.*, **2001**, *123*, 9045-9053.
3. S. L. Masters, H. E. Robertson, D. A. Wann, M. Hölbling, K. Hassler, R. Bjornsson, S. Ó. Wallevik, and I. Arnason, *J. Phys. Chem. A.*, **2015**, *119*, 1600-1608.
4. C. L. Deasy, *Chem. Rev.*, **1945**, *36*, 145-155.
5. A. K. Chandra, S. Parveen, S. Das and T. Zeegers-Huyskens, *J. Comput. Chem.*, **2008**, *29*, 1490-1496.
6. T. M. Klapötke, B. Krumm, M. Scherr, F. Xaver Steemann, K. Banert and Y. H. Joo, *Chem. Eur. J.*, **2009**, *15*, 11341-11345.
7. R. L. Livingston and G. Vaughan, *J. Am. Chem. Soc.*, **1956**, *78*, 4866-4869.
8. H. Bürger, H. Niepel, G. Pawelke and H. Oberhammer, *J. Mol. Struct.*, **1979**, *54*, 159-174.
9. B. Beagley and A. R. Medwid, *J. Mol. Struct.*, **1977**, *38*, 229-238.
10. E. Fluck and P. Meiser, *Angew. Chem. Int. Ed.*, **1971**, *10*, 653-653.
11. T. Moeller and A. H. Westlake, *J. Inorg. Nucl. Chem.*, **1967**, *29*, 957-960.
12. S. L. Masters, G. V. Girichev and S. A. Shylkov, *Dalton Trans.*, **2013**, *42*, 3581-3586.
13. H. Fleischer, D. A. Wann, S. L. Hinchley, K. B. Borisenko, J. R. Lewis, R. J. Mawhorter, H. E. Robertson and D. W. H. Rankin, *Dalton Trans.*, **2005**, 3221-3228.
14. S. L. Hinchley, H. E. Robertson, K. B. Borisenko, A. R. Turner, B. F. Johnston, D. W. H. Rankin, M. Ahmadian, J. N. Jones and A. H. Cowley, *Dalton Trans.*, **2004**, 2469-2476.
15. A. W. Ross, M. Fink and R. Hilderbrandt, in *International Tables for Crystallography*, Kluwer Academic Publishers, Dordrecht, Netherlands, **1992**, Vol. C, p. 245.

16. National Service for Computational Chemistry Software (NSCCS) (http://nsccs.ac.uk).
17. M. J. Frisch, G. W. Trucks, H. B. Schlegel, G. E. Scuseria, M. A. Robb, J. R. Cheeseman, G. Scalmani, V. Barone, B. Mennucci, G. A. Petersson, H. Nakatsuji, M. Caricato, X. Li, H. P. Hratchian, A. F. Izmaylov, J. Bloino, G. Zheng, J. L. Sonnenberg, M. Hada, M. Ehara, K. Toyota, R. Fukuda, J. Hasegawa, M. Ishida, T. Nakajima, Y. Honda, O. Kitao, H. Nakai, T. Vreven, Montgomery Jr, J. A. , J. E. Peralta, F. Ogliaro, M. Bearpark, J. J. Heyd, E. Brothers, K. N. Kudin, V. N. Staroverov, T. Keith, R. Kobayashi, J. Normand, K. Raghavachari, A. Rendell, J. C. Burant, S. S. Iyengar, J. Tomasi, M. Cossi, N. Rega, J. M. Millam, M. Klene, J. E. Knox, J. B. Cross, V. Bakken, C. Adamo, J. Jaramillo, R. Gomperts, R. E. Stratmann, O. Yazyev, A. J. Austin, R. Cammi, C. Pomelli, J. W. Ochterski, R. L. Martin, K. Morokuma, V. G. Zakrzewski, G. A. Voth, P. Salvador, J. J. Dannenberg, S. Dapprich, A. D. Daniels, O. Farkas, J. B. Foresman, J. V. Ortiz, J. Cioslowski and D. J. Fox, *Gaussian 09*, Revision D.01, Gaussian, Inc., Wallingford CT, **2013**.
18. C. Møller and M. S. Plesset, *Phys. Rev.*, **1934**, *46*, 618-622.
19. G. A. Petersson, A. Bennett, T. G. Tensfeldt, M. A. Al-Laham, W. A. Shirley and J. Mantzaris, *J. Chem. Phys.*, **1988**, *89*, 2193-2218.
20. G. A. Petersson, T. G. Tensfeldt and J. A. Montgomery Jr, *J. Chem. Phys.*, **1991**, *94*, 6091-6101.
21. A. D. McLean and G. S. Chandler, *J. Chem. Phys.*, **1980**, *72*, 5639-5648.
22. K. Raghavachari, J. S. Binkley, R. Seeger and J. A. Pople, *J. Chem. Phys.*, **1980**, *72*, 650-654.
23. R. Krishnan, J. S. Binkley, R. Seeger and J. A. Pople, *J. Chem. Phys.*, **1980**, *72*, 650-654.
24. A. D. McLean and G. S. Chandler, *J. Chem. Phys.*, **1980**, *72*, 5639-5648.
25. T. H. Dunning Jr, *J. Chem. Phys.*, **1989**, *90*, 1007-1023.
26. R. A. Kendall, T. H. Dunning Jr and R. J. Harrison, *J. Chem. Phys.*, **1992**, *96*, 6796-6806.
27. Y. Zhao and D. G. Truhlar, *J. Phys. Chem. A*, **2006**, *110*, 5121-5129.
28. V. A. Sipachev, *J. Mol. Struct. (Theochem)*, **1985**, *121*, 143-151.
29. V. A. Sipachev, *J. Mol. Struct.*, **2001**, *567–568*, 67-72.

30. S. F. Boys and F. Bernardi, *Mol. Phys.*, **1970**, *19*, 553-566.
31. S. Simon, M. Duran and J. J. Dannenberg, *J. Chem. Phys.*, **1996**, *105*, 11024-11031.
32. P. R. Edgington, P. McCabe, C. F. Macrae, E. Pidcock, G. P. Shields, R. Taylor, M. Towler and J. Van De Streek, *J. Appl. Crystallogr.*, **2006**, *39*, 453-457.
33. A. J. Blake, P. T. Brain, H. McNab, J. Miller, C. A. Morrison, S. Parsons, D. W. H. Rankin, H. E. Robertson and B. A. Smart, *J. Phys. Chem*, **1996**, *100*, 12280-12287.
34. P. T. Brain, C. A. Morrison, S. Parsons and D. W. H. Rankin, *J. Chem. Soc., Dalton Trans.*, **1996**, 4589-4596.
35. N. W. Mitzel and D. W. H. Rankin, *Dalton Trans.*, **2003**, 3650-3662.
36. P. D. McCaffrey, R. J. Mawhorter, A. R. Turner, P. T. Brain and D. W. H. Rankin, *J. Phys. Chem A*, **2007**, *111*, 6103-6114.
37. D. A. Wann, A. V. Zakharov, A. M. Reilly, P. D. McCaffrey and D. W. H. Rankin, *J. Phys. Chem A*, **2009**, *113*, 9511-9520.

CHAPTER 6

Theoretical and experimental investigation of the gas-phase molecular structures of $X_3SiSiXMe_2$ (X = F, Cl, Br, I) and $X_3SiSiMe_3$ (X = H, F, Cl, Br)

6.1 Introduction

Previous work in the Masters group has focussed on understanding the steric bulk of substituted disilane systems in the gas phase. The study of 1,1,2,2-tetra-*tert*-butyldisilane,[1] for example, demonstrated the effect that steric bulk has on the central silicon tetrahedral angle of 109.5°, where the Si–Si–C angles were observed to increase to 117.0(5)° and 110.0(6)° to tilt the *tert*-butyl groups away from each other. Large Si–Si–C angles have been observed in other disilane systems such as 1,1,2,2-tetrakis(trimethylsilyl)disilane and 1,1,2,2-tetrakis(trimethylsilyl)dimethyldisilane,[2] 1,2-di-*tert*-butyldisilane,[3] and the tetrasilylmethane derivative $(Me_3Si)_3CSiH_3$.[4] This large deviation in Si–Si–C angle has also been observed in the solid-state for $[(Me_3Si)_3CSiH_2]_2$ which had an increase of ∠Si–Si–C to 120.05(9)°, as determined by X-ray diffraction.[4] While these studies show that the presence of bulky flexible groups can dictate changes in geometric structure to accommodate steric strain, these studies have not examined the electronic effect that substituents can have on structure – in some cases both electronic and steric effects play a part.

Substituted disilanes of the form Si_2X_6 are typically similar to substituted ethanes (which have been widely studied)[5] with properties depending on the adopted conformations around the central Si-Si bond. Substituted disilanes usually adopt a staggered conformation due to electron repulsion from bonds close together in space.[6,7] It is known that the Si-Si bond lengthens or shortens as it is rotated through 360° depending on the adopted conformation (i.e. staggered → eclipsed) and the atom (or group of atoms) in place of X.[7] The electronic effect of substituents on disilanes has been demonstrated by considering the change in Si–Si bond length compared to that in Si_2H_6.[6-9] When the hydrogen substituents are replaced with electron-withdrawing F and Cl substituents in Si_2F_6[7,8] and Si_2Cl_6,[7] the Si–Si bond is observed to shorten, whereas the Si–Si bond lengthens as the substituents are replaced with methyl groups in Si_2Me_6.[8] Previous GED studies of substituted disilanes have included 1,1,2-triiododisilane ($I_2HSiSiH_2I$),[10] 1,1,2,2-tetrachlorodisilane ($Cl_2HSiSiHCl_2$),[11] 1,2-diiododisilane (IH_2SiSiH_2I)[12] and 1,1,2,2-tetraiododisilane ($I_2HSiSiHI_2$),[12] although these studies did not look at the effect on the Si–Si bond with more than one ligand type.

This chapter details the work carried out for the refinement of the GED data for 1,1,1,2-tetrabromo-2,2-dimethyldisilane ($Br_3SiSiBrMe_2$) to determine the effect of more than one ligand type on the structural behaviour of disilanes. A computational investigation was conducted for the related halogen analogues of $X_3SiSiXMe_2$ (X = F, Cl, Br, I) to determine trends within the related halogenated disilane molecules. The study of the electronic trends of disilanes also included a GED study and complementary computational investigation of the substituted disilanes $X_3SiSiMe_3$ (X = H, F, Cl, Br), to examine the effect that the methyl groups have on the compounds. Both of these studies are covered in detail within this chapter.

6.2 $X_3SiSiXMe_2$ (X = F, Cl, Br, I)

6.2.1 Experimental

Synthesis *(with Karl Hassler, Technische Universität Graz, Austria)*

1,1,1,2-Tetrabromo-2,2-dimethyldisilane was synthesised according to the method presented by Herzog and Roewer,[13] with the purity of the sample being determined by ^{1}H and ^{29}Si NMR spectroscopy.

Theoretical methods

All geometry optimisation and frequency calculations for $F_3SiSiFMe_2$ (**1**), $Cl_3SiSiClMe_2$ (**2**), $Br_3SiSiBrMe_2$ (**3**) and $I_3SiSiIMe_2$ (**4**) were performed using the resources of the NSCCS,[14] using the Gaussian09 suite of programs.[15] All MP2[16] calculations were frozen core [MP2(fc)].

Geometry optimisations

An extensive search of the torsional potentials of $X_3SiSiXMe_2$ (X = F, Cl, Br, I) was undertaken at the HF level with the 3-21G* basis set[17-19] in order to locate all local minima. For all compounds (**1 – 4**) three equivalent minima were identified, with X–Si–Si–X torsion angles of ± 60° and 180.0° indicating staggered conformations. For X = Br three equivalent higher energy, very shallow, minima were also identified at ± 120.0° and 0.0° indicating the possibility of an eclipsed structure. These were investigated at a higher level with larger basis sets at which the eclipsed minima disappeared and only the three equivalent staggered conformers remained. Further geometry optimisations were undertaken for **1 – 4** using the HF and MP2 methods with the standard 6-31G*[20-22] basis set, and using the MP2 method with the 6-311G*[23,24] and 6-311+G* basis sets. For X = I (**4**), the SDB-aug-cc-pVTZ basis[25] was used to describe iodine above 3-21G*. The lowest energy structure of 1,1,1,2-tetrabromo-2,2-dimethyldisilane with the atom numbering scheme is shown in Figure 6.1. The structures of the related $X_3SiSiXMe_2$ (X = F, Cl, I) were similar and the same atom numbering schemes were used.

Figure 6.1 The lowest energy structure of 1,1,1,2-tetrabromo-2,2-dimethyldisilane with atom numbering.

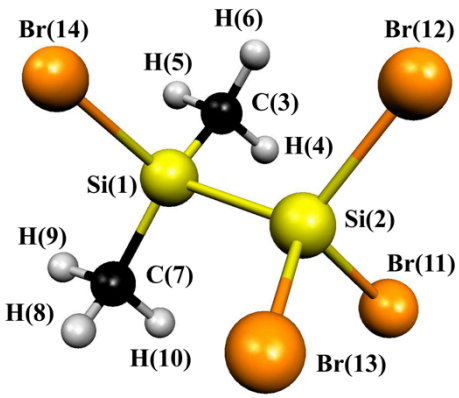

Frequency calculations

For **1 – 4**, analytic second derivatives of the energy with respect to nuclear coordinates calculated at the HF/6-31G* level (HF/6-31G*//SDB-aug-cc-pVTZ for X = I) gave the force field, which was used to provide estimates of the amplitudes of vibration (*u*) and perpendicular distance corrections for use in the GED refinement of **3**. Calculating the force field at the MP2 level of theory would make little difference to the vibrational quantities and was deemed unnecessary.

GED

Data were collected for **3** using the Edinburgh GED apparatus[26] when it was at the University of Edinburgh (it is now located at the University of Canterbury).[27] An accelerating voltage of ca. 40 keV (electron wavelength ca. 6.0 pm) was used, whilst maintaining the sample and nozzle temperatures at 394 K and 461 K respectively. Scattering intensities were recorded at nozzle-to-plate distances of 94.26 mm and 249.59 mm on Kodak Electron Image films. The electron-scattering intensities were measured using an Epson Expression 1680 Pro flatbed scanner and converted to mean optical densities as a function of the scattering variable, *s*, using an established program.[28] The data-reduction and least-squares refinement processes were carried out using the ed@ed program[29] (Version 2.4) employing the scattering factors of Ross *et al*.[30] The weighting points for the off-diagonal weight matrices, correlation parameters and scale factors for the two camera distances are given in Appendix Table A4.1, together with electron wavelengths, which were determined from the scattering patterns of benzene vapour. These were recorded immediately after the

patterns of **3** and analysed in exactly the same way, to minimise systematic errors in wavelengths and camera distances.

6.2.2 Results

Ab initio calculations

An extensive search of the torsional potentials of **3** was undertaken at the HF level with the standard 3-21G* basis set in order to locate all local minima. The investigation conducted about ϕBr–Si–Si–Me led to three equivalent minima at ± 60° and 180.0° indicating a staggered conformation (Figure 6.2). Three other small minima were observed at ± 120.0° and 0.0° but at a higher level of theory (MP2/6-311+G*) these minima were not observed.

All the potential energy scans for the other tetrahalogenated disilane analogues **1**, **2** and **4** gave only three equivalent minima at ± 60° and 180.0° similar to **3**, again implying a stable staggered conformation for each as expected. The three minima were then optimised at higher levels of theory and basis sets. For **4** there is no all-electron basis set readily available beyond 3-21G* for iodine. Therefore in all subsequent HF and MP2 calculations for **4**, the SDB-aug-cc-pVTZ effective core potential (ECP) and basis was used for iodine.[25] Whilst each calculation step is useful to show the gradual convergence towards the most accurate model of the investigated molecule (see Appendix Table A4.2), only the highest-level calculations were used for analysis of results and are presented in Table 6.1.

Figure 6.2 Potential-energy scans of ϕBr–Si–Si–Me at HF/3-21G* (black) and MP2/6-311+G* (red). Half of the scan is shown for clarity. The offset in relative energy is due to the difference in methods between HF and MP2.

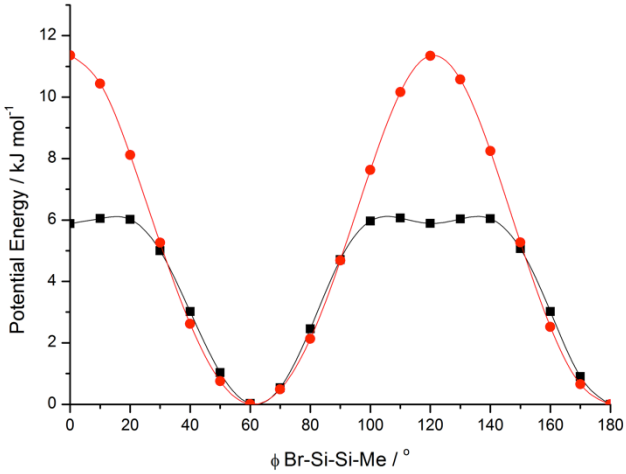

Table 6.1 Theoretical geometrical parameters at the MP2/6-311+G* level for $X_3SiSiXMe_2$ (X = F, Cl, Br, I; **1** – **4**). For X = I, the SDB-aug-cc-pVTZ basis set and ECP were used on the iodine atoms, with 6-311+G* on C, Si and H.[a]

Parameter	X = F	X = Cl	X = Br	X = I
*r*Si(1)–Si(2)	234.9	233.3	233.7	234.4
*r*Si(1)–C(3/7)	185.9	186.3	186.4	186.9
*r*Si(1)–X(14)	163.3	207.1	224.1	246.5
*r*Si(2)–X(11)	160.9	205.2	223.2	246.5
*r*Si(2)–X(12/13)	160.4	204.3	220.0	244.9
∠Si(2)–Si(1)–C(3/7)	109.8	109.5	109.4	109.7
∠Si(2)–Si(1)–X(14)	106.0	106.4	106.3	104.3
∠Si(1)–Si(2)–X(11)	110.0	108.6	107.7	107.5
∠Si(1)–Si(2)–X(12/13)	113.4	111.7	111.3	110.6
Energy (Hartrees)	-1056.5624	-2496.3927	-10947.7811	-703.1549

[a] All distances in pm and all angles in degrees. See Figure 6.1 for atom numbering.

GED

Electron diffraction refinements were carried out for **3** based on the *ab initio* calculations described above (optimised at the MP2/6-311+G* level), using a model of C_s symmetry to describe the vapour. Due to the large number of geometric parameters required to define the structure some assumptions were made in the model to reduce the number of parameters to a manageable amount.

The structure of the **3** was defined in terms of eleven independent geometric parameters, comprising four bond lengths, five bond angles, one torsion parameter, one tilt parameter, and two dependent parameters (Table 6.2). The independent parameters include the Si–Si and Si–C bond lengths (p_1 and p_3), and the average Si–Br and C–H bond lengths (p_2 and p_4), with small differences between non-equivalent bond lengths fixed at the *ab initio* values. To describe the $SiBr_3$ group the internal ∠Br–Si–Br (p_5) was used. To define the $SiBrMe_2$ group both ∠Si–Si–Br(14) (p_6) and ∠Si–Si–C (p_7) were used, as well as the Br–Si–C bond angle (p_9) to place the methyl groups relative to the lone bromine atom. The Si–C–H bond angles (p_8) were all assumed to be identical on the basis of the *ab initio* results. The remaining two independent parameters represented the H–C–Si–Si (methyl) torsion (p_{10}) and the Si–Br_3 tilt (p_{11}). For p_{11}, a positive tilt represents a tilt of the $SiBr_3$ group away from Br(14) on the $SiBrMe_2$ group. Two dependent parameters were included to obtain the values of the Si–Si–Br angles at Si(1) (dp_1 and dp_2).

A theoretical Cartesian force field was generated and converted into a force field described by symmetry coordinates. RMS amplitudes were obtained from the SHRINK program.[31,32] All independent geometric parameters were refined using a least-squares method and restraints were applied, using the SARACEN method,[33-35] to parameters that could otherwise not be refined (Table 6.2). The restraints were based on values calculated at the MP2/6-311+G* level and the uncertainties were derived from the changes in value of each parameter during the series of calculations that were performed. In addition, 10 groups of amplitudes of vibration were refined (see Appendix Table A4.3). The success of the refinement can be assessed numerically using the final *R*-factor, calculated to be $R_G = 0.065$ ($R_D = 0.036$), and by visually assessing the RDCs (Figure 6.3), and the MICs (Figure A4.1). The least-

squares correlation matrix is given in Table A4.4 and coordinates for the final GED structure and for the calculated structure (MP2/6-311+G*) are in Table A4.5 and A4.6, respectively.

Figure 6.3 Experimental and difference (experimental – theoretical) RDC, $P(r)/r$, for 1,1,1,2-tetrabromo-2,2-dimethyldisilane. Before Fourier inversion the data were multiplied by $s \cdot \exp(-0.00002s^2)/(Z_{Si} - f_{Si})(Z_{Br} - f_{Br})$.

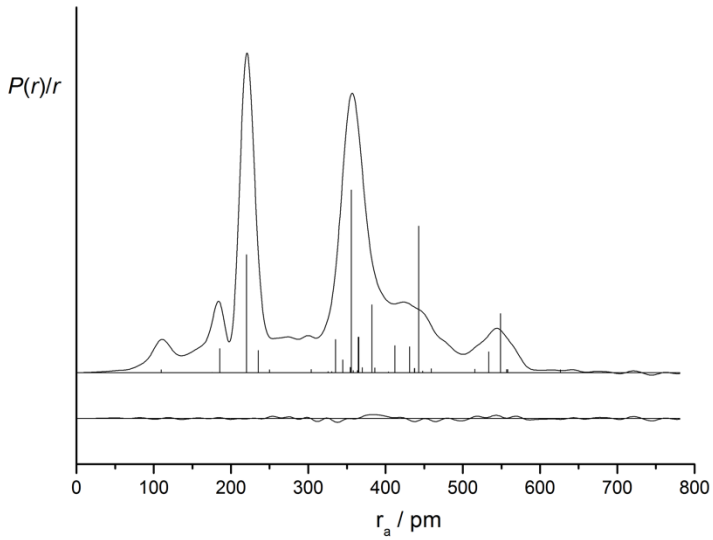

Table 6.2 Refined and calculated geometric parameters for 1,1,1,2-tetrabromo-2,2-dimethyldisilane (distances in pm, angles in °) from the GED study.[a]

No.	Description	GED (r_{h1})	MP2/6-311+G* (r_e)	Restraint
Independent parameters				
p_1	*r*Si–Si	235.6(5)	233.7	-
p_2	*r*Si–Br av	220.3(1)	222.8	-
p_3	*r*Si–C	185.4(3)	186.4	-
p_4	*r*C–H av	109.8(4)	109.4	109.4(5)
p_5	∠Br–Si–Br	107.5(1)	108.8	-
p_6	∠Si–Si–Br(14)	106.1(4)	106.3	106.3(5)
p_7	∠Si–Si–C	109.2(8)	109.4	109.4(12)
p_8	∠Si–C–H av	112.8(9)	110.9	110.9(12)
p_9	∠Br–Si–C	111.1(5)	109.0	109.0(10)
p_{10}	ϕH–C–Si–Si av	62.8(12)	62.6	62.6(15)
p_{11}	Si–Br_3 tilt	5.1(7)	2.0	2.0(13)
Dependent parameters				
dp_1	∠Si–Si–Br(11)	106.3(7)	107.7	-
dp_2	∠Si–Si–Br(12/13)	113.8(4)	111.3	-

[a] Figures in parentheses are the estimated standard deviations of the last digit. See text for parameter definitions.

6.2.3 Discussion

The GED and *ab initio* studies show that 1,1,1,2-tetrabromo-2,2-dimethyldisilane (**3**) exists as a single conformer in the gas phase, adopting a staggered conformation with ϕBr–Si–Si–Br = 180.0°. The final experimental structure proved to be in reasonable agreement with the MP2/6-311+G* *ab initio* calculations showing a variance in results of no more than 2.5 pm for bond lengths and 2.1° for the bond angles. The results obtained for the GED experiment are comparable to those obtained for Si_2Me_6.[36] The Si-Si bond length for Si_2Me_6 was 234.0(9) pm, somewhat shorter than that observed for 1,1,1,2-tetrabromo-2,2-dimethyldisilane at 235.6(5) pm. The bond angle Si–Si–C was larger for Si_2Me_6, 108.4(4)° compared to 109.2(8)° in 1,1,1,2-tetrabromo-2,2-dimethyldisilane. An experimental comparison to Si_2Br_6 could not be made as there are no GED data available. The structural trends in the series $X_3SiSiXMe_2$ (X = F, Cl, Br, I) were also investigated computationally in the absence of complete experimental data for all four molecules.

The analysis of bond lengths in molecules **1** – **4** show results concurrent with the expected behaviour for variation of the halogen types within a series (Table 6.1). Due to an increase in size of the halogen and decrease in electronegativity from F to I, the Si–X bond lengthens, whereas the Si–Si and Si–C bond lengths remains relatively unchanged by the substitution. This was also observed in DFT studies of Si_2X_6 molecules (X = F, Cl, Br and I).[7] The relative decrease in the electronegativity and increase in atomic radii of the halogens from F to I contributes to the lengthening of the Si–X bond.

The effects of substitution on the Si–Si–X bond angles will be discussed separately for the $Si(1)Me_2X$ group and the $Si(2)X_3$ group. Interestingly there is no variation of Si-Si-C angles in the $Si(1)Me_2X$ group from X = F, Cl, Br to I, with ∠Si(2)–Si(1)–C(3/7) remaining constant at ~109.5°, the accepted tetrahedral angle. The ∠Si(2)–Si(1)–X(14) remains at a value of ~106.3° for X = F, Cl and Br, only decreasing by 2° when X = I. Examination of the experimental Si–Si–X bond angles in the simple disilanes Si_2H_6 and Si_2F_6 [110.3(4)° and 110.3(2)°, respectively][37,38] reveals that, with no other substituents to exert steric influence, Si–Si–X bond angles of about 110.3° would be expected for both substituents. This can be attributed to a similar

radius of the X substituent; it is a well-known fact that F is similar in size to H.[39] Therefore, in the systems studied for this work, the methyl groups are exerting some steric influence, causing repulsion between themselves and the F substituent, thus decreasing ∠Si–Si–F to 106.0°. Sequential substitution of F by Cl and Br lengthens the Si–X bond length but results in little change to the observed ∠Si–Si–X. When X = I, there is enough steric repulsion between X and the methyl groups to further decrease ∠Si–Si–X, despite the lengthening of the Si–X bond. The overall trend in the $SiMe_2X$ group indicates that the methyl groups exert more steric influence than the halogen substituent.

In the $Si(2)X_3$ group the Si–Si–X angles are not equivalent with ∠Si(1)–Si(2)–X(11), which lies on the mirror plane of the molecule, consistently smaller than ∠Si(1)–Si(2)–X(12/13) by about 3°. This variation indicates that the SiX_3 groups are all tilted away from the lone halogen on Si(1). This could be due to the narrower ∠Si–Si–X(14) at the opposite end of the molecule as the groups at each end of the molecule are slightly tilted to accommodate each other, highlighting the flexible nature of bonding around silicon atoms.

6.2.4 Conclusion

All compounds of the $X_3SiSiXMe_2$ (X = F, Cl, Br, I) series were investigated by *ab initio* methods and were determined to exist in the staggered conformation although, for the Br analogue, there were a greater number of potentially stable eclipsed and gauche conformers. The gas-phase structure of 1,1,1,2-tetrabromo-2,2-dimethyldisilane was also successfully determined by GED to exist in a staggered conformation.

The calculated geometric parameters for each molecule were compared, while considering the accuracy of the calculations with respect to the GED results. These comparisons showed that various trends of the disilane series could be observed. In particular, the flexible nature of bonding around silicon atoms was highlighted, even in this perceived less sterically crowded system.

6.3 $X_3SiSiMe_3$ (X = H, F, Cl, Br)

6.3.1 Experimental

Synthesis ***(with Karl Hassler, Technische Universität (Graz), Austria)***

1,1,1-trimethyldisilane (**5**), 1,1,1-trifluoro-2,2,2-trimethyldisilane (**6**), 1,1,1-trichloro-2,2,2-trimethyldisilane (**7**) and 1,1,1-tribromo-2,2,2-trimethyldisilane (**8**) were synthesised as described by Zink and Hassler.[40] The purity of the samples was checked by ^{29}Si NMR and used without further purification upon arrival in Edinburgh.

Theoretical methods

Calculations were performed with the resources of the NSCCS,[14] using Gaussian 09.[15] All MP2[16] calculations were frozen core [MP2(fc)]. Geometry optimisations for **5 – 8** were performed in C_{3v} symmetry.

Geometry optimisations

An extensive potential energy scan was undertaken at the HF/6-31G*[20-22] level to confirm the minimum energy conformers for **5 – 8**. With ϕX–Si–Si–Me initially set to 180°, three equivalent minimum energy conformers were located for ϕX–Si–Si–Me at (± 60° and 180°) for **5 – 8**. For the global minimum, full optimisations were performed at the HF level using the 3-21G*[17-19] and 6-31G* basis sets, and then the level of theory was increased to MP2(fc). At this level calculations were performed using the 6-31G*, 6-311G*[23, 24] and 6-311+G* basis sets. The generic molecular structure of the $X_3SiSiMe_3$ series with common atom numbering is shown in Figure 6.4.

Figure 6.4 The lowest energy structure of $X_3SiSiMe_3$ (X = H, F, Cl, Br; **5 – 8**) showing the common atom numbering scheme.

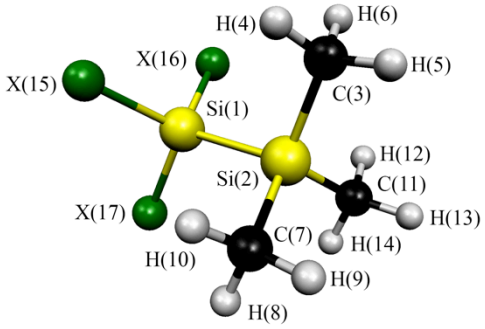

Frequency calculations

Analytic second derivatives of the energy with respect to the nuclear coordinates calculated at the HF level with the 6-31G* basis set for **5 – 8** gave force fields which were then used to provide estimates of the amplitudes of vibration (*u*) for use in the GED refinements. These force fields were also used to calculate the vibrational frequencies, which provided information about the nature of the stationary points.

GED

Data were collected for **5 – 8** using the Edinburgh GED apparatus[26] when it was at the University of Edinburgh (it is now located at the University of Canterbury).[27] An accelerating voltage of around 40 keV was used, representing an electron wavelength of approximately 6.0 pm. Scattering intensities were recorded on Kodak Electron Image films at the nozzle-to-plate distances and sample/nozzle temperatures given in Appendix Table A4.10 along with the weighting points for the off-diagonal weight matrices, correlation parameters and scale factors for both camera distances for all compounds. The electron wavelengths as determined from the scattering patterns for benzene, which were recorded immediately after the patterns for the sample compounds, are also presented (Table A4.10). The scattering intensities were measured using an Epson Expression 1680 Pro Flatbed Scanner and converted to mean optical densities as a function of the scattering variable, *s*, using an established program.[28] The data-reduction and the least-squares refinement processes were carried out using the ed@ed program[29] (Version 2.4) employing the scattering factors of Ross *et* al.[30]

6.3.2 Results

***Ab initio* calculations**

The molecular structures of a series of related molecules have been studied at the MP2/6-311+G* level. All the molecules have the general formula $X_3SiSiMe_3$ (X = H, F, Cl, Br; **5 – 8**) (Figure 6.4).

An extensive search of the PES of **5 – 8** at the HF/6-31G* and MP2/6-31G* levels was conducted to locate all local minima. The investigation about ϕX–Si–Si–Me (where X = H, F, Cl and Br) led to three equivalent minima at ± 60° and 180°, indicating a staggered conformation with C_{3v} symmetry (Figure 6.4). The barrier to internal rotation at the MP2/6-31G* level was calculated to be 4.22 kJ mol^{-1} for **5** (MP2(full)/6-31G(d), 4.39 kJ mol^{-1}),[41] 4.82 kJ mol^{-1} for **6**, 7.50 kJ mol^{-1} for **7** and 6.15 kJ mol^{-1} for **8**. The minima obtained from the potential energy scans for **5 – 8** were then optimised with larger basis sets. Although each step is useful to show the gradual convergence towards the most accurate model of the investigated molecules (refer to Appendix Table A4.11), only the highest level calculations, MP2/6-311+G*, were analysed and are presented in Table 6.3.

Table 6.3 Theoretical geometrical parameters at the MP2/6-311+G* level for $X_3SiSiMe_3$ (X = H, F, Cl, Br; **5 – 8**).[a]

Parameter	X = H	X = F	X = Cl	X = Br
*r*Si–Si	234.9	234.1	233.4	234.0
*r*Si–C	188.4	187.8	187.6	187.5
*r*Si–X	148.8	161.1	205.4	223.3
*r*C–H av	109.4	109.4	109.4	109.4
∠Si–Si–X	111.0	112.9	111.4	110.8
∠Si–Si–C	109.6	107.8	107.5	107.4
∠Si–C–H av	111.4	111.3	111.3	111.2
ϕX(15)–Si–Si–C(11)	180.0	180.0	180.0	180.0
Energy (Hartrees)	-699.1019	-996.6003	-2076.4688	-8415.0098

[a] All distances are in pm and angles in degrees. See Figure 6.4 for atom numbering.

A supplementary natural population analysis (NPA)[42-44] was conducted for a series of disilanes to evaluate the electronic effects due to the presence of the methyl and halogen groups (Table 6.4). This analysis was only conducted for the bromo-substituted disilanes $Br_3SiSiMe_3$, $Br_3SiSiBrMe_2$, $Br_3SiSiBr_2Me$ and Si_2Br_6. All calculations were performed at the MP2(fc)/6-31G* level.

Table 6.4 Natural Population Analysis (NPA) at MP2(fc)/6-31G* level for $Br_3SiSiMe_3$, $Br_3SiSiBrMe_2$, $Br_3SiSiBr_2Me$ and Si_2Br_6.

Atom	$Br_3SiSiMe_3$	$Br_3SiSiBrMe_2$	$Br_3SiSiBr_2Me$	Si_2Br_6
$Si(Br_3)$	0.89	0.89	0.89	0.90
Br [trans to unique substituent on $Si(Me_{3-n}Br_n)$]	-0.34	-0.34	-0.30	-0.30
Br	-0.34	-0.31	-0.32	-0.30
Br	-0.34	-0.31	-0.32	-0.30
$Si(Me_{3-n}Br_n)$	1.48	1.33	1.14	0.90
X [unique substituent on Si(2)]	-1.20	-0.36	-1.23	-0.30
X	-1.20	-1.21	-0.33	-0.30
X	-1.20	-1.21	-0.33	-0.30

GED

Electron diffraction refinements were carried out for **5 – 8** based on the *ab initio* calculations optimised at the MP2/6-311+G* level. A C_{3v} model was used to describe the symmetry.

All of the structures (**5 – 8**) were defined in terms of eight independent geometric parameters comprising of four bond lengths, three bond angles and one torsion angle (Table 6.5). The independent parameters include *r*Si–Si, *r*Si–C and *r*Si–H (p_1, p_2, p_4) and the bond angles ∠Si–Si–C and ∠Si–C–H (p_6 and p_7). For each investigated $X_3SiSiMe_3$ structure (X = H, F, Cl, Br; **5 – 8**) the bond length Si–X (p_3) and bond

angle Si–Si–X (p_5) were defined accordingly. The torsion angle ϕX(15)–Si–Si–C(11) (p_8) was used to define the orientation of the SiX_3 group relative to the $SiMe_3$ group. This torsion was fixed at -60° for all refinements based on the results of the *ab initio* calculations. Variation of this torsion value by ±3° did not affect the refinements or the parameters obtained from them, hence providing confidence to fix the value.

Theoretical Cartesian force fields were generated and converted into a set of force fields described by a set of symmetry coordinates and RMS amplitudes were obtained from the SHRINK program.[31,32] All independent geometric parameters were refined using a least-squares method and restraints were applied, using the SARACEN method,[33-35] to parameters that would otherwise not be refined (Table 6.5). These restraints were based on *ab initio* calculations at the MP2/6-311+G* level with the uncertainties being derived from the change in each of the parameter values during the series of calculations that were performed. In addition, groups of amplitudes of vibrations (u) for **5 – 8** were refined (see Appendix Tables A4.12 – A4.15 for details).

The success of the GED refinements for **5 – 8** are reflected in the final R-factors which were R_G = 0.088 (R_D = 0.047) for **5**, R_G = 0.049 (R_D = 0.037) for **6**, R_G = 0.062 (R_D = 0.036) for **7** and R_G = 0.055 (R_D = 0.033) for **8**.

The refinement of these structures is also observed in the RDCs (Figures 6.5a – 6.5d) and the MICs (Appendix Figures A4.2 – A4.5). The coordinates for the final GED structures and calculated structures (MP2/6-311+G*) of **5 – 8** (Appendix Tables A4.16 – A4.23) and the least-squares correlation matrices (Appendix Tables A4.24 – A4.27) are provided as supplementary material.

Table 6.5 Refined (r_{h1}) and calculated (r_e) geometric parameters for **5 – 8** from the GED study.[a]

	Description	GED(r_{h1})	MP2/6-311+G* (r_e)	Restraint
1,1,1-trimethyldisilane				
p_1	*r*Si–Si	233.5(2)	234.9	-
p_2	*r*Si–C	188.1(1)	188.4	-
p_3	*r*Si–H	150.4(4)	148.8	-
p_4	*r*C–H	108.3(2)	109.4	-
p_5	∠Si–Si–H	111.3(5)	111.0	111.0(5)
p_6	∠Si–Si–C	109.5(2)	109.6	-
p_7	∠Si–C–H av	110.8(3)	111.4	-
p_8	ϕH(15)–Si–Si–C(3)	-60.0(fixed)	-60.0	-
1,1,1-trifluoro-2,2,2-trimethyldisilane				
p_1	*r*Si–Si	233.5(2)	234.1	234.1(3)
p_2	*r*Si–C	188.0(1)	187.8	-
p_3	*r*Si–F	158.1(1)	161.1	-
p_4	*r*C–H	110.5(2)	109.4	-
p_5	∠Si–Si–F	112.0(1)	112.9	-
p_6	∠Si–Si–C	108.9(3)	107.8	-
p_7	∠Si–C–H av	111.8(4)	111.3	111.3(3)
p_8	ϕF(15)–Si–Si–C(3)	-60.0(fixed)	-60.0	-
1,1,1-trichloro-2,2,2-trimethyldisilane				
p_1	*r*Si–Si	233.4(2)	233.4	-
p_2	*r*Si–C	187.2(2)	187.6	-
p_3	*r*Si–Cl	204.8(1)	205.4	-
p_4	*r*C–H	107.7(3)	109.4	109.4(8)
p_5	∠Si–Si–Cl	111.8(1)	111.4	-
p_6	∠Si–Si–C	107.0(2)	107.5	107.5(4)
p_7	∠Si–C–H av	111.0(3)	111.3	111.3(3)
p_8	ϕCl(15)–Si–Si–C(3)	-60.0(fixed)	-60.0	-

1,1,1-tribromo-2,2,2-trimethyldisilane				
p_1	*r*Si–Si	234.8(2)	234.0	234.0(3)
p_2	*r*Si–C	189.2(1)	187.5	-
p_3	*r*Si–Br	221.2(1)	223.3	-
p_4	*r*C–H	108.8(3)	109.4	109.4(5)
p_5	∠Si–Si–Br	111.2(1)	110.8	-
p_6	∠Si–Si–C	108.8(2)	107.4	107.4(3)
p_7	∠Si–C–H av	111.1(4)	111.2	111.2(4)
p_8	ϕBr(15)–Si–Si–C(3)	-60.0(fixed)	-60.0	-

[a] Figures in parentheses are the estimated standard deviations of the last digit. See text for parameter definitions.

Figure 6.5 Experimental and difference (experimental – theoretical) RDC, $P(r)/r$, for (**a**) 1,1,1-trimethyldisilane, (**b**) 1,1,1-trifluoro-2,2,2-trimethyldisilane, (**c**) 1,1,1-trichloro-2,2,2-trimethyldisilane and (**d**) 1,1,1-tribromo-2,2,2-trimethyldisilane. Before Fourier inversion the data were multiplied by $s \cdot \exp(-0.00002s^2)/(Z_{Si} - f_{Si})(Z_X - f_X)$ where X = C, F, Cl and Br respectively.

(a)

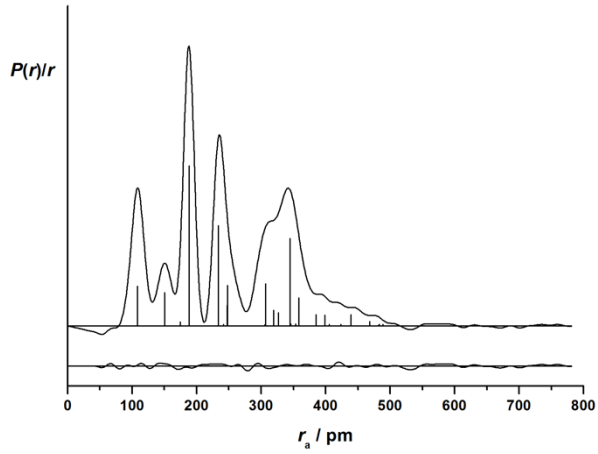

(b)

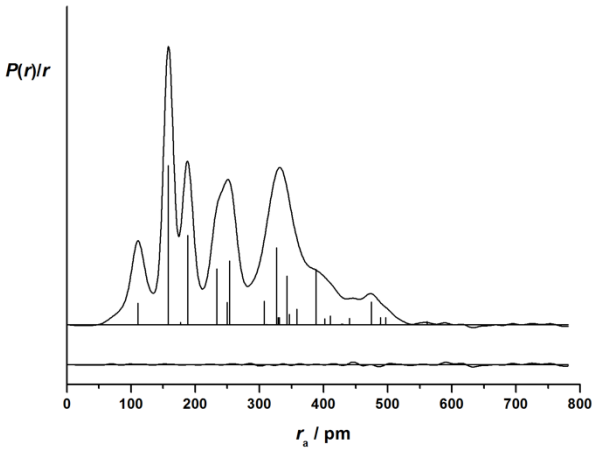

(c)

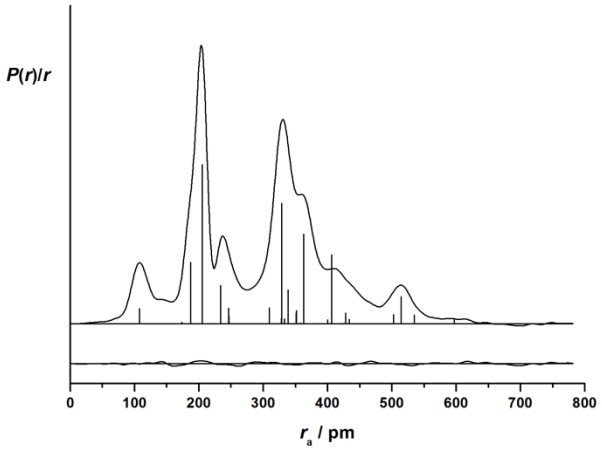
P(r)/r
0
100
200
300
400
500
600
700
800
r_a / pm

(d)

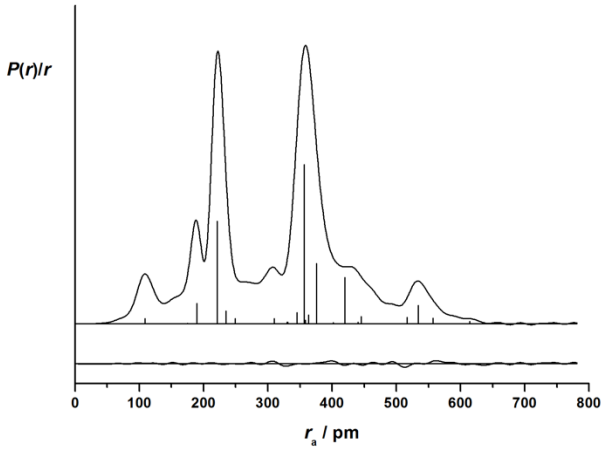
P(r)/r
0
100
200
300
400
500
600
700
800
r_a / pm

6.3.3 Discussion

The GED and *ab initio* studies show that **5 – 8** exist as single conformers in the gas phase, adopting a staggered conformation with ϕX–Si–Si–C(Me) = 180°. The final experimental structures for **5 – 8** proved to be in reasonable agreement with the respective MP2/6-311+G* *ab initio* calculations showing a variation in results of no more than 3.0 pm for bond lengths and 1.1° for the bond angles over all of the structures. The variation in the values obtained by the *ab initio* calculations in this study are comparable to results obtained from other theoretical disilane studies.[40] The structural trends in the series $X_3SiSiMe_3$ (X = H, F, Cl and Br; **5 – 8**) in this study were investigated using experimental GED data for all four molecules and are supported by complementary *ab initio* calculations.

The analysis of bond lengths in **5 – 8** shows an increase in the Si–X bond length for the investigated halogen types (Table 6.5) whilst *r*Si–C and *r*Si–Si remain relatively unchanged. This result is concurrent with the expected trends for a halogen series where the Si–X bond lengthens due to an increase in size of the halogen (and hence atomic radii) and a decrease in electronegativity. This trend has also been observed in DFT studies of Si_2X_6 molecules (X = F, Cl, Br and I)[7] and other GED studies of substituted disilanes (see Section 6.2).

For **5 – 8** the Si–C–H and Si–Si–C bond angles remained relatively unchanged for the substitution of the halogens (Table 6.5). The Si–Si–X bond angles were observed to increase from 111.3(5)° to 112.0(1)°, from **5** to **6**, before decreasing to 111.8(1)° for **7** and 111.2(1)° for **8**. This fluctuation allows for accommodation of the halogen atoms, due to increasing atomic radii and Si–X bond length, and is similar to the fluctuation observed in ∠Si–Si–X for $X_3SiSiXMe_2$ (X = F, Cl, Br and I) as described in Section 6.2. Comparing these two studies indicates that the methyl groups do play a role, but the structural trends observed are largely due to substitution of different halogen atoms. For $X_3SiSiXMe_2$, the Si–Si–X bond angle involving the halogen adjacent to the methyl groups is smaller than that for the other halogens due to the adjustment of the halogen and methyl groups to accommodate each other around the silicon atom. When comparing ∠Si–Si–X for the halogens of the SiX_3 group, similar bond angles, and fluctuations, are obtained as for the $X_3SiSiMe_3$ study. This suggests

that the methyl groups do have an effect on the angles to the halogen substituents, but this effect is greatly reduced if the methyl groups are not directly adjacent to the halogen atom(s). Otherwise it would be expected that a difference between the $X_3SiSiXMe_2$ and $X_3SiSiMe_3$ study would be observed for ∠Si–Si–X_3 since the SiX_3 group is adjacent to two different groups ($SiXMe_2$ and $SiMe_3$ respectively). These results suggest that, unless the methyl groups are on the same silicon atom as the halogens, then there will be very little steric influence on the overall structure in these non-bulky disilanes.

To consider if there were any electronic effects from the halogens and methyl groups on the overall structure, a NPA analysis was conducted (Table 6.4) at the MP2(fc)/6-31G* level. For the analysis, a series of bromo-substituted disilanes were considered ($Br_3SiSiMe_3$, $Br_3SiSiBrMe_2$, $Br_3SiSiBr_2Me$ and Si_2Br_6). For 1,1,1-tribromo-2,2,2-trimethyldisilane ($Br_3SiSiMe_3$) the charge is less than one (0.89) for the silicon of the $SiBr_3$ group as expected due to the electron-withdrawing nature of the bromine atoms. Similarly, the charge is greater than one (1.48) for the silicon of the $SiMe_3$ group due to methyl groups being electron donating.

These results were compared to the results for 1,1,1,2-tetrabromo-2,2-dimethyldisilane ($Br_3SiSiBrMe_2$) which has asymmetry introduced to the molecule. For the $SiBr_3$ group, the charge on the silicon atom did not change but for the $SiBrMe_2$ group, the charge on silicon was observed to decrease to 1.33 as a result of an electron-donating methyl group being replaced by an electron-withdrawing bromine atom. The electron-donating effect of the remaining methyl groups outweigh the withdrawing effect of the bromine atom and therefore the silicon atom remains δ^-. For 1,1,1,2,2-pentabromo-2-methyl-disilane ($Br_3SiSiBr_2Me$), as with the other structures considered thus far, the charge of the silicon atom on $SiBr_3$ is unchanged with a value of 0.89. This means that there has been no effect on the electronic arrangement of this system due to the substitution of methyl groups by bromine atoms at the other silicon atom. A reduction in charge to 1.14 is observed for the silicon atom of the $SiMeBr_2$ group and this reduction is consistent with that seen when replacing the electron-donating methyl group with an electron-withdrawing bromine atom. It is interesting to note that, in this case, the donating

effect of the methyl group still outweighs the withdrawing effect of the bromine atoms, so the silicon atom remains δ^-. Finally, for hexabromodisilane (Si_2Br_6) the charge on both silicon atoms is less than one and the charge (0.90) can be considered the same as for the other molecules in the series. It can be concluded that there is no electronic effect observed due to the substitution of the methyl groups by bromine atoms for the adjacent silicon atom. It is only when the methyl groups are fully replaced by bromine atoms that the charge observed on silicon reduces to below one for both silicon atoms.

6.3.4 Conclusion

All compounds of the investigated series $X_3SiSiMe_3$ (X = H, F, Cl and Br) were found to exist in the staggered conformation from the GED data and this was supported by *ab initio* calculations. The geometric parameters for each molecule were analysed to determine if there were any structural trends in the disilane series.

The methyl groups were determined to have a far less significant effect on ∠Si–Si–X in **5 – 8** than when they are directly adjacent to the halogen atoms, as in the $X_3SiSiXMe_2$ study (Section 6.2). In this study no significant influence was observed on the Si-Si bond length with successive substitution of halogen atoms. Therefore it can be concluded that there is no significant electronic influence of the halogen atoms on the Si-Si bond length in sterically unencumbered systems. The NBO analysis for brominated disilanes indicated a lack of contributory electronic effects by both halogen and methyl groups on the observed structural trends. However, the trends for substituted halogens down the series and the flexible nature of the silicon atoms were highlighted for systems in this and previously found systems.

6.4 References

1. S. L. Hinchley, H. E. Robertson, A. Parkin, D. W. H. Rankin, G. Tekautz and K. Hassler, *Dalton Trans.*, **2004**, 759-766.
2. J. Schwabedissen, P. D. Lane, S. L. Masters, K. Hassler and D. A. Wann, *Dalton Trans.*, **2014**, *43*, 10175-10182.
3. D. Hnyk, R. S. Fender, H. E. Robertson, D. W. H. Rankin, M. Bühl, K. Hassler and K. Schenzel, *J. Mol. Struct.*, **1995**, *346*, 215-229.
4. S. L. Masters, D. W. H. Rankin, D. B. Cordes, K. Batz, P. D. Lickiss, N. M. Boag, A. D. Redhouse and S. M. Whittaker, *Dalton Trans.*, **2010**, *39*, 9353-9360.
5. V. Pophristic and L. Goodman, *Nature*, **2001**, *411*, 565-568.
6. V. Pophristic, L. Goodman and C. T. Wu, *J. Phys. Chem. A,* **2001**, *105*, 7454-7459.
7. F. Valencia, A. H. Romero, M. Kiwi, R. Ramírez and A. Toro-Labbé, *Chem. Phys. Lett.*, **2003**, *371*, 267-275.
8. S. G. Cho, O. K. Rim and G. Park, *J. Comput. Chem.*, **1997**, *18*, 1523-1533.
9. A. H. Romero, M. Kiwi and R. Ramírez, *Phys. Status Solidi B*, **2002**, *230*, 391-395.
10. T. H. Johansen, K. Hagen, K. Hassler, G. Tekautz and R. Stølevik, *J. Mol. Struct.*, **1999**, *509*, 237-254.
11. T. H. Johansen, K. Hagen and R. Stølevik, *J. Mol. Struct.*, **1999**, *485-486*, 121-133.
12. T. H. Johansen, K. Hassler, G. Tekautz and K. Hagen, *J. Mol. Struct.*, **2001**, *598*, 171-195.
13. U. Herzog and G. Roewer, *J. Organomet. Chem.*, **1997**, *544*, 217-223.
14. National Service for Computational Chemistry Software (NSCCS) (http://nsccs.ac.uk).
15. M. J. Frisch, G. W. Trucks, H. B. Schlegel, G. E. Scuseria, M. A. Robb, J. R. Cheeseman, G. Scalmani, V. Barone, B. Mennucci, G. A. Petersson, H. Nakatsuji, M. Caricato, X. Li, H. P. Hratchian, A. F. Izmaylov, J. Bloino, G. Zheng, J. L. Sonnenberg, M. Hada, M. Ehara, K. Toyota, R. Fukuda, J. Hasegawa, M. Ishida, T. Nakajima, Y. Honda, O. Kitao, H. Nakai, T. Vreven, Montgomery Jr, J. A. , J. E. Peralta, F. Ogliaro, M. Bearpark, J. J. Heyd, E.

Brothers, K. N. Kudin, V. N. Staroverov, T. Keith, R. Kobayashi, J. Normand, K. Raghavachari, A. Rendell, J. C. Burant, S. S. Iyengar, J. Tomasi, M. Cossi, N. Rega, J. M. Millam, M. Klene, J. E. Knox, J. B. Cross, V. Bakken, C. Adamo, J. Jaramillo, R. Gomperts, R. E. Stratmann, O. Yazyev, A. J. Austin, R. Cammi, C. Pomelli, J. W. Ochterski, R. L. Martin, K. Morokuma, V. G. Zakrzewski, G. A. Voth, P. Salvador, J. J. Dannenberg, S. Dapprich, A. D. Daniels, O. Farkas, J. B. Foresman, J. V. Ortiz, J. Cioslowski and D. J. Fox, *Gaussian 09*, *Revision B.01*, Gaussian, Inc., Wallingford CT, **2010**.

16. C. Møller and M. S. Plesset, *Phys. Rev.*, **1934**, *46*, 618-622.
17. J. S. Binkley, J. A. Pople and W. J. Hehre, *J. Am. Chem. Soc.*, **1980**, *102*, 939-947.
18. M. S. Gordon, J. S. Binkley, J. A. Pople, W. J. Pietro and W. J. Hehre, *J. Am. Chem. Soc.*, **1982**, *104*, 2797-2803.
19. W. J. Pietro, M. M. Francl, W. J. Hehre, D. J. Defrees, J. A. Pople and J. S. Binkley, *J. Am. Chem. Soc.*, **1982**, *104*, 5039-5048.
20. W. J. Hehre, R. Ditchfield and J. A. Pople, *J. Chem. Phys.*, **1972**, *56*, 2257-2261.
21. P. C. Hariharan and J. A. Pople, *Theor. Chim. Acta*, **1973**, *28*, 213-222.
22. M. S. Gordon, *Chem. Phys. Lett.*, **1980**, *76*, 163-168.
23. A. D. McLean and G. S. Chandler, *J. Chem. Phys.*, **1980**, *72*, 5639-5648.
24. K. Raghavachari, J. S. Binkley, R. Seeger and J. A. Pople, *J. Chem. Phys.*, **1980**, *72*, 650-654.
25. J. M. L. Martin and A. Sundermann, *J. Chem. Phys.*, **2001**, *114*, 3408-3420.
26. C. M. Huntley, G. S. Laurenson and D. W. H. Rankin, *J. Chem. Soc., Dalton Trans.*, **1980**, 954-957.
27. S. L. Masters, G. V. Girichev and S. A. Shylkov, *Dalton Trans.*, **2013**, *42*, 3581-3586.
28. H. Fleischer, D. A. Wann, S. L. Hinchley, K. B. Borisenko, J. R. Lewis, R. J. Mawhorter, H. E. Robertson and D. W. H. Rankin, *Dalton Trans.*, **2005**, 3221-3228.
29. S. L. Hinchley, H. E. Robertson, K. B. Borisenko, A. R. Turner, B. F. Johnston, D. W. H. Rankin, M. Ahmadian, J. N. Jones and A. H. Cowley, *Dalton Trans.*, **2004**, 2469-2476.

30. A. W. Ross, M. Fink and R. Hilderbrandt, *International Tables for Crystallography*, ed. A. J. C. Wilson, Kluwer Academic Publishers, Dordrecht, Netherlands, **1992**, Vol. C, p. 245.
31. V. A. Sipachev, *J. Mol. Struct. (Theochem)*, **1985**, *121*, 143-151.
32. V. A. Sipachev, *J. Mol. Struct.*, **2001**, *567–568*, 67-72.
33. A. J. Blake, P. T. Brain, H. McNab, J. Miller, C. A. Morrison, S. Parsons, D. W. H. Rankin, H. E. Robertson and B. A. Smart, *J. Phys. Chem.*, **1996**, *100*, 12280-12287.
34. P. T. Brain, C. A. Morrison, S. Parsons and D. W. H. Rankin, *J. Chem. Soc., Dalton Trans.*, **1996**, 4589-4596.
35. N. W. Mitzel and D. W. H. Rankin, *Dalton Trans.*, **2003**, 3650-3662.
36. B. Beagley, J. J. Monaghan and T. G. Hewitt, *J. Mol. Struct.*, **1971**, *8*, 401-411.
37. B. Beagley, A. R. Conrad, J. M. Freeman, J. J. Monaghan, B. G. Norton and G. C. Holywell, *J. Mol. Struct.*, **1972**, *11*, 371-380.
38. H. Oberhammer, *J. Mol. Struct.*, **1976**, *31*, 237-245.
39. G. A. Patani and E. J. LaVoie, *Chem. Rev.*, **1996**, *96*, 3147-3176.
40. R. Zink and K. Hassler, *Spectrochim. Acta, Part A*, **1999**, *55*, 333-347.
41. T. A. Mohamed, *J. Mol. Struct. (Theochem)*, **2003**, *635*, 161-172.
42. A. E. Reed and F. Weinhold, *J. Chem. Phys.*, **1983**, *78*, 4066-4073.
43. A. E. Reed and F. Weinhold, *J. Chem. Phys.*, **1985**, *83*, 1736-1740.
44. A. E. Reed, R. B. Weinstock and F. Weinhold, *J. Chem. Phys.*, **1985**, *83*, 735-746.

CHAPTER 7

Conclusions and future work

7.1 Introduction

Determination of molecular structure continues to play a key role in our understanding of chemistry. GED is routinely used to determine the structure of small molecules in the gas phase, or those with high symmetry. The study of larger, bulky species can be conducted with the aid of *ab initio* calculations and other experimental data but can be limited by the complexity of the system, especially if large numbers of conformers are present.

This thesis presents the progress made towards the development of a GED-MS setup to allow the determination of molecular structure of short-lived species *in situ* by GED a routine method. Chapters 2 and 3 highlighted the progress towards the reconstruction of the Canterbury GED apparatus, and the planned modifications that are required to implement a GED-MS design. The study of ketene, an example of a short-lived species, was studied in Chapters 4. In particular the need for GED-MS capability was highlighted for studying ketene and other short-lived species, in order to determine the species present (in a multiple product pyrolysis system) and to optimise the methods used to generate them *in situ*. Lastly Chapters 5 and 6 involved parallel structural studies that were undertaken during this thesis. Chapter 5 involved the investigation of tris(chloromethyl)amine whose structure was determined to be different between the solid and gas phases, with investigation into this behaviour ongoing. While the study in Chapter 6 regarding related halogen-substituted disilane systems is a relatively complete set of work, this does not limit study towards other substituted disilane or halogenated systems. Extension of the further electronic and steric investigation of other halogen-substituted disilanes will not be covered here.

The conclusion and future work for each part of this thesis is presented in the following sections. In particular, focus is placed on the next stages of the Canterbury GED apparatus reconstruction and GED-MS development. Finally, the direction of research in the Masters group after establishment of a Canterbury GED-MS setup is discussed.

7.2 Canterbury GED apparatus

The first part of this thesis was concerned with the reconstruction of the Canterbury GED apparatus, as it had not been reassembled since its move to the University of Canterbury from the University of Edinburgh. Chapter 2 detailed the reconstruction of the Canterbury GED apparatus and modifications that were made to the original setup as the result of repairs and improvements.

Delays in getting the GED apparatus operational were due to the repair of the helium leak tester (acquired from the Department of Physics and Astronomy). As fine leaks were introduced to the main chamber during adjustment of the electron gun, a working leak tester was required to find them and fix the vacuum problems. Due to the significant time required for the Chemistry department technical staff to fix the leak tester, calibration of the electron gun and subsequent calibration data testing could not be conducted during this thesis.

7.2.1 Calibration and tests with the Canterbury GED apparatus

Following the successful repairs to the leak tester, the vacuum leak introduced by adjusting the position of the electron gun can be identified. Alignment of the electron gun will recommence once the leak has been identified, with the leak tester being used to locate any more introduced vacuum leaks. The process for aligning the electron beam will likely take place over several weeks as any adjustments to the filament of the electron gun will require the apparatus to be vented to atmosphere before re-establishing a suitable experimental vacuum for testing.

Initial data tests will be conducted with benzene which is often used to calibrate the nozzle-to-camera distance.[1,2] Following these tests, the Canterbury GED apparatus will be operational for data collection for other samples while the GED-MS chamber is being constructed.

7.3 Canterbury GED-MS setup

A major component of this thesis is the planned modification of the Canterbury GED apparatus to incorporate MS capability (Chapter 3). As the progress of reconstructing the GED apparatus was linked to the overall progress that can be made to a GED-MS setup during this thesis, only the conceptual design and planning has been done. In particular, the MS for the final GED-MS setup needs to be purchased and the GED-MS main chamber (to accommodate the MS setup) needs to be constructed with the help of the Chemistry department technical staff.

7.3.1 Purchasing a new MS unit

The next major step towards a GED-MS apparatus is the purchase of a suitable MS to work simultaneously with GED in an experiment. In Chapter 3 a QMS or TOF were identified as suitable MS for a GED-MS setup. However, as with most equipment purchases, an increase in cost will lead to better ion selectivity, mass resolution and a larger detectable mass range. A TOF was determined to be the preferred choice although the MS to be purchased will depend on the research funds available. The connection of the MS to the GED apparatus will depend on the specific MS being purchased and although a TOF-MS is usually quite long (about 1.5 metres), a vertical setup of the TOF tube should not be ruled out.

7.3.2 Construction of the GED-MS main chamber

Following the purchase of the MS for incorporation with GED, the main chamber for the Canterbury GED-MS apparatus can be constructed. The plan to incorporate the two nozzle-to-camera distances with the VHT nozzle has already been designed. The main chamber is designed to fit on the existing GED framework with minimal alterations. Depending on the MS purchased, the position of the two diffusion pumps on the underside of the chamber may vary, requiring the GED apparatus framework to be altered to accommodate them. The aim of the initial GED-MS setup is to allow MS data to be collected at the short nozzle-to-camera distance using photographic film as is currently done for a GED experiment. Following the construction of the spacer unit and setup of the CCD, the nozzle will be kept in a fixed position opposite

the MS, with the inclusion/removal of the spacer unit controlling the two nozzle-to-camera distances in an experiment.

7.3.3 Construction of the spacer unit

The design of the spacer unit has yet to be fully confirmed, although in this thesis it has been presumed to be a section of chamber that connects/removes from the main GED-MS chamber by a vacuum valve or seal. As the spacer unit will be constructed by the technical workshop staff to the dimensions specified (for the required experimental nozzle-to-camera distances), the design of the spacer unit seal will be dependent on the way the vacuum pumps and MS are connected to the main chamber.

Ideally, the spacer unit will be able to be removed and replaced without venting the MS unit. This would mean that the MS unit can be isolated from the main chamber, such as with a gate valve, so that continuous venting around the MS filaments can be avoided, as this will limit the lifetime of the filaments in the ion source.[3] There is allowable flexibility in the design so that the Chemistry workshop staff can choose the best way to incorporate the spacer unit as the most important part of the schematics for a GED-MS experiment is the selected nozzle-to-camera distances. The spacer unit ports for connecting to the apparatus and detector will be designed while taking the CCD into mind (see Section 7.3.4) as the detector will be upgraded at the same time the spacer unit is developed.

The spacer unit will initially be only one size, permitting two nozzle-to-camera distances of approximately 95 mm and 285 mm to be used with the GED-MS setup. This removes the option of a medium distance which can be used with the current GED setup with select nozzles (not the VHT nozzle). To allow more flexibility in the future for several nozzle-to-camera distances, differing sized spacer units may be constructed based on the required nozzle-to-camera distance.

7.3.4 Software development and incorporating a CCD with GED-MS

The next component of the final GED-MS design is the incorporation of a CCD camera to replace the current photographic film collection system. Not only is there a limited supply of photographic film remaining (it is no longer in commercial production), but changing to an electronic collection system will minimise fouling of the plates or jamming of the film plateholders in the mechanical camera during an experiment.

A CCD camera has been obtained from an old X-ray crystallography machine in the Chemistry department and will be considered in the design and construction of the spacer unit as described above. Software development for the CCD detection system will be written in conjunction with researchers at the University of York (Wann group) and will involve calibration and testing of the camera for data collection from GED and GED-MS experiments.

7.4 Study of short-lived species

Chapter 4 in this thesis involved the study of the molecular structure of ketene by GED, where FVP methods where used to generate ketene from suitable precursors. While data have been previously collected for ketene by the Masters group,[4] quality assurance of the pyrolysed data was not able to be obtained, and in particular led to problems refining the pyrolysis products of Meldrum's acid (ketene, CO_2 and acetone) when significant amounts of Meldrum's acid were still remaining such that it had to be incorporated into the refinement model. Not only was the problem in completing the refinement due to limitations in the refinement program, the amount of each species produced *in situ* (and hence the completion of the pyrolysis) could not be determined from GED alone. This has prompted the need to repeat the study of ketene using a GED-MS setup as described in Chapter 3.

7.4.1 Limitations with current ed@ed refinement program

The current study of short-lived species is limited to the refinement of systems that undergo full pyrolysis or have very little precursor remaining so that it can be

considered negligible in the refinement model. The relative amount of each product in an experiment will be directly related to the stoichiometry in the experimental process and the relative symmetry of the molecule (as GED cannot distinguish isomers). This means that to fully refine GED data from a pyrolysis experiment, the species generated cannot undergo any secondary processes otherwise the fixed amount of each species produced will not be able to be predicted from a mechanism without further experimental data collected during the GED experiment (such as MS data). This was apparent for the pyrolysis study of Meldrum's acid where significant amounts of it was still present in the vapour. While the ed@ed refinement program[5] could be improved to allow refinement of groups of molecules with relative weighting amounts, the biggest improvement will be in incorporation of fixed weightings from MS data that will be collected simultaneously in an experiment.

7.4.2 Study of short-lived species with a GED-MS setup

The incorporation of MS in a GED experiment will allow for the relative amount of species in the gas vapour to be determined. In the case of the pyrolysis of Meldrum's acid, as discussed in Chapter 4, the fit to pyrolysis data collected by Noble-Eddy[4] suggested that a large amount of Meldrum's acid was still present, even after overheating the sample. While this data has been reprocessed, the data cannot be fully refined without knowing the relative amount of each species produced, especially since that some of the ketene produced in the experiment recombined to form diketene. Not only will simultaneous collection of MS data in a GED-MS setup will allow for determining fixed ratios of each species for inclusion in the ed@ed refinement program,[5] it will allow for optimisation of the pyrolysis techniques used to generate species *in situ* for study with GED.

7.5 Further investigation of the low amplitude torsional motion of $N(CH_2Cl)_3$

As highlighted in Chapter 5, tris(chloromethyl)amine was determined to exist in different conformations in the gas and solid phases. While GED data have been collected and refined for $N(CH_2Cl)_3$, *ab initio* calculations have suggested that the

rotation of the unique upward pointing CH_2Cl group is a very low amplitude vibration (43 cm^{-1}) about the N–C bond, with the position of the group varying quite largely even with larger basis sets such as aug-cc-pVDZ and aug-cc-pVTZ.

7.5.1 Molecular dynamics investigation

As the *ab initio* calculations of tris(chloromethyl)amine suggested a different position of the unique CH_2Cl torsion depending on the basis set, a molecular dynamics approach to modelling this torsion is being considered. The molecular dynamics investigation is currently underway, with the intention to use the molecular dynamics results to better describe the amplitudes of vibration in the GED refinement.

7.6 Future work after GED-MS development

This section highlights one of future research directions of the Masters group after the GED-MS setup has been constructed and is made operational. As highlighted above, Chapter 4 in this thesis involved the study of ketene using FVP methods to generate it from suitable precursors. Not only will ketene be restudied with a GED-MS setup, the intention is to extend the study the molecular structure of other short-lived species such as the benzyl radical. This also includes studying the structure of different derivatives of short-lived species which have not been studied or generated before *in situ*. As well as refining the pyrolysis methods to generate these species *in situ*, other generation methods such as photolysis can be considered with the GED-MS setup.

7.6.1 Study of new short-lived species

Work with a GED-MS setup can be extended following this preliminary work to the study of species that have not been generated by FVP methods before. As highlighted in Chapter 4, calculations can be performed for systems to determine the likeliness of pyrolysis occurring at a given temperature. Whilst the calculations can somewhat be used to predict the conditions required to generate short-lived species *in situ*, a GED-MS setup will be able to confirm the generation of these species. A

GED-MS setup could not only lead to further investigation of substituted short-lived species and to systematic studies of structural trends in related molecules, it could offer improvements on the theoretical methods used to calculate whether pyrolysis will occur.

7.6.2 Development of photolysis methods

The generation of short-lived species will not just be limited to pyrolysis techniques. The setup of the Canterbury GED-MS apparatus will mean that the species can be generated external to the main chamber, prior to injection of the gas vapour if desired. This allows for use of other techniques, such as photolysis, to provide the energy required to drive a dissociation reaction. One of the future aims of the Masters group is to develop the capability for photolysis methods in conjunction with the current FVP methods as there will be some species that cannot be generated *in situ* by use of heat alone.

7.7 References

1. B. J. M. Bormans, G. De With and F. C. Mijlhoff, *J. Mol. Struct.*, **1977**, *42*, 121-128.
2. S. Gundersen, S. Samdal, T. G. Strand and H. V. Volden, *J. Mol. Struct*., **2007**, *832*, 164-171.
3. *Atomic, Molecular and Optical Physics: Charged Particles*, Eds. F. B. Dunning and R. G. Hulet, Academic Press, Inc., San Diego, California, USA, **1995**.
4. R. Noble-Eddy, PhD Thesis, University of Edinburgh, Edinburgh, Scotland, **2009**.
5. S. L. Hinchley, H. E. Robertson, K. B. Borisenko, A. R. Turner, B. F. Johnston, D. W. H. Rankin, M. Ahmadian, J. N. Jones and A. H. Cowley, *Dalton Trans*., **2004**, 2469-2476.

APPENDIX 1

Publications, Conferences, Achievements, Services and Funding

Appendix 1.1 – List of Publications

Do halogens and methyl substituents have electronic effects on the structures of simple disilanes? An experimental and theoretical study of the molecular structures of the series $X_3SiSiMe_3$ (X = H, F, Cl and Br).
S. J. Atkinson, H. E. Robertson, M.Hölbling, W. –W. du Mont, C. Mitrofan, K. Hassler and S. L. Masters, *Struct. Chem.*, **2013**, *24(3)*, 851-857.

Gas-phase molecular structure of 1,1,1,2-tetrabromo-2,2-dimethyldisilane: theoretical and experimental investigation of a super-halogenated disilane and computational investigation of the F, Cl and I analogues.
S. L. Masters, **S. J. Atkinson**, M. Hölbling and K. Hassler, *Struct. Chem.*, **2013**, *24(4)*, 1201-1206.

Determining the gas-phase structure of ketene and acetic acid from acetic anhydride using very-high-temperature gas electron diffraction (VHT-GED).
S. J. Atkinson, R. Noble-Eddy and S. L. Masters, Manuscript in preparation for *J. Phys. Chem. A*.

An investigation into the gas phase structure of $N(CH_2Cl)_3$: A combined GED, Raman and ab initio study.
S. J. Atkinson, S. L. Masters, H. E. Robertson, J. Carr, M. R. Waterland and N. Mitzel, Manuscript in preparation for *Inorg. Chem.*

Appendix 1.2 – Conference Contributions

University of Canterbury Postgraduate Student Showcase
University of Canterbury, New Zealand, 14 November 2012
Oral presentation: "*Generation and structural characterisation of gaseous transient species.*"

15th European Symposium on Gas-Phase Electron Diffraction
Frauenchiemsee, Germany, 23-28 June 2013
Poster presentation: "*Development of mass spectrometry capability with the Canterbury gas electron diffraction apparatus.*"

Bayer Lindau Science Dialogue as part of the 63rd Nobel Laureate Meeting
Lindau, Germany, 2 July 2013
Poster presentation: "*Enabling complete structure determination of short-lived species.*"

University of Canterbury Postgraduate Student Showcase
University of Canterbury, New Zealand, 13 November 2013
Oral presentation: "*How will mass spectrometry help to determine molecular structure in gas-phase electron diffraction?*"

New Zealand Institute of Chemistry (NZIC) Conference
Wellington, New Zealand, 1-5 December 2013
Poster presentation: "*Differences between the solid and gas phases – a puzzling problem for determining the gas phase structure of tris(chloromethyl)amine.*"

25th Austin Symposium on Molecular Structure and Dynamics in Dallas (ASMD@D)
Dallas, TX, USA, 1-4 March 2014
Oral presentation: "*A molecular muddle: the curious case of $N(CH_2Cl)_3$.*"

University of Canterbury Chemistry Postgraduate Student Showcase

University of Canterbury, New Zealand, 28 April 2014

Oral presentation: "*Generation and structural characterisation of gaseous transient species."*

Quantum and Computational Chemistry Student Conference (QUACCS)

Cass, New Zealand, 8-13 June 2014

Oral presentation: "*Generation and structural characterisation of gaseous transient species."*

Appendix 1.3 – Achievements, Professional Membership and Services

Achievements

2013	Short-listed (1 of 20 people out of ~20,000 applicants) for the international Royal Society of Chemistry (RSC) Chemistry World Science Communication competition.
2013	Selected for the 63rd Lindau Nobel Laureate Meeting (30 June – 5 July 2013) as one of 650 people (from ~20,000 applicants) from 78 different countries.
2013	One of 18 people selected to attend the Baden-Württemberg Post Conference Tour (5-11 July 2013) from attendees of the 63rd Lindau Nobel Laureate Meeting.

Professional Memberships

2009-present	New Zealand Institute of Chemistry (NZIC) student member
2010-present	Member of the University of Canterbury's Golden Key Chapter (recognises top 15% of students in their chosen field).

Voluntary Services

2014	Nitrate testing for University of Canterbury Outreach program
2014	Chemistry of Fireworks – public event run by the Canterbury branch of the NZIC
2013-2014	NZIC committee student representative and secretary
2013-2014	University of Canterbury Outreach program *Kirkwood Intermediate School (2013)* *Burnside Primary School (2014)* *St Margaret's College (2014)*
2012	NZIC Chemistry Extravaganza event (public event) University of Canterbury Postgraduate Showcase session chair.
2011-present	Student mentor at the University of Canterbury

Paid Services

2011-2014	Lab supervising/demonstrating for Chemistry undergraduate labs (CHEM111, CHEM281, CHEM382)

Appendix 1.4 – Funding received

2014	Claude McCarthy Fellowship	($3500)
2014	Evan's Fund (Hardship)	($1000)
2013	Baden-Württemberg International	(conference fee)
2013	Bayer Science and Education Foundation	(conference fee)
2013	New Zealand Institute of Chemistry Travel Grant	(conference fee)
2013	Royal Society of New Zealand Travel Grant	($1000)
2013	Canterbury Federation of Graduate Women Travel Grant	($800)
2012	Betty Wignall Scholarship/Department of Chemistry Doctoral Research Scholarship	

APPENDIX 2

GED investigation of the gas-phase molecular structure of ketene, and computational investigation of selected RR'C=C=O derivatives

Acetic anhydride

Model description for acetic anhydride

The structure of acetic anhydride was described as a two-conformer model and was defined in C_2 symmetry for the (*sp*, *sp*) conformer and in C_1 symmetry for the (*sp*, *ac*) conformer. A total of 32 independent parameters and 20 dependent parameters were used to describe the model (see Table 4.1). The atom numbering is given in Figure 4.2. The independent parameters included 10 bond lengths, 13 bond angles and nine dihedral angles. For the (*sp*, *sp*) conformer the parameters describing bond lengths included *r*C–C, *r*C=O and *r*C–O (p_1, p_4 and p_7). *r*C–H was defined as an average from both conformers (p_{10}). To describe the bond angles for the (*sp*, *sp*) conformer, ∠H(11)–C–C (p_{11}), ∠C–C=O (p_{16}), ∠C–C–O (p_{19}) and ∠C–O–C (p_{22}) were defined, with the dihedral angles being ϕO=C–C–H(11) (p_{24}), ϕO(8/9)=C–C–O (p_{27}), and ϕC(4)–C–C–O (p_{30}) .

For the (*sp*, *ac*) conformer, the C–C, C–O and C=O bond lengths were each described by two differences applied to the respective parameter value obtained for the (*sp*, *sp*) conformer. For *r*C–C these difference parameters were p_2 and p_3, and this was similarly described for *r*C–O (p_5 and p_6) and *r*C=O (p_8 and p_9). The *r*C–H parameter (p_{10}), as stated above, was the same as for (*sp*, *sp*). To describe the two methyl groups of the (*sp*, *ac*) conformer two β H–C–H angles were used (p_{14} and p_{15}) to describe the C_s and C_1 methyl groups (as determined from *ab initio* calculations) respectively, with fixed differences being applied to each of them to describe the other β angles as required. For the (*sp*, *ac*) conformer two differences were applied to ∠H(11)–C–C (p_{10}) from the (*sp*, *sp*) conformer to describe ∠H(20)–C–C and ∠H(25)–C–C (p_{12} and p_{13}). Two difference parameters relative to the (*sp*, *sp*) value was used to describe ∠C–C=O (p_{17} and p_{18}) and ∠C–C–O (p_{20} and p_{21}). A unique ∠C–O–C (p_{23}) was also defined. The remaining parameters represented ϕO=C–C–H(25) (p_{25}), ϕO=C–C–H(20) (p_{26}), two ϕO=C–C–O differences applied to ϕO(8/9)=C–C–O (*sp*, *sp*) value (p_{28} and p_{29}), ϕC(23)–C–C–O (p_{31}) and ϕC(17)–C–C–O (p_{32}) for (*sp*, *ac*).

The 20 dependent parameters were used to obtain the individual C–C, C=O and C–O bond lengths, the H–C–C, O–C=O, C–C=O and C–C–O bond angles and the O–C–C–O, O–C–O–C dihedral angles for each conformer, to allow for comparison to the previous acetic anhydride GED study.

Table A2.1 Nozzle-to-plate distances (mm), weighting functions (nm^{-1}), correlation parameters, scale factors and electron wavelengths (pm) used in the electron-diffraction study of acetic anhydride using data from the Wu *et al*. study.[a]

Nozzle-to-plate distance	200.0	350.0	600.0
Δs	2.5	2.5	2.5
s_{min}	145	75	40
sw_1	165	95	60
sw_2	270	170	110
s_{max}	315	198	128
Correlation parameter	-0.078	0.441	0.292
Scale factor[b]	2.334(87)	1.612(28)	1.178(17)
Electron wavelength	6.02	6.02	6.02

[a] *J. Phys. Chem. A*. **2000**, *104*, 1576-1587.

[b] Values in parentheses are the estimated standard deviations.

Table A2.2 Parameter values for the (*sp*, *sp*) and (*sp*, *ac*) conformers of acetic anhydride from *ab initio* calculations at the M06-2X level for a range of basis sets.[a,b]

Parameter	6-31G*	6-311G*	6-311+G*	6-311++G**
(sp, sp)				
*r*C(1)–C(10)	150.3	150.0	149.9	149.8
*r*C(3)–C(4)	150.3	150.0	149.9	149.8
*r*C(1)=O(9)	119.2	118.6	118.7	118.7
*r*C(3)=O(8)	119.2	118.6	118.7	118.7
*r*C(1)–O(2)	138.6	138.7	138.7	138.7
*r*C(3)–O(2)	138.6	138.7	138.7	138.7
*r*C–H average	109.2	109.0	109.0	109.0
∠H(11)–C–C	109.3	109.5	109.6	109.5
∠H(5)–C–C	109.3	109.5	109.6	109.5
∠H(11)–C–H(12)	110.4	110.5	110.5	110.8
∠H(11)–C–H(13)	110.2	110.0	109.9	110.2
∠H(5)–C–H(6)	110.2	110.0	109.9	110.2
∠H(5)–C–H(7)	110.4	110.5	110.5	110.8
∠C(10)–C=O	126.9	127.1	127.2	127.2
∠C(4)–C=O	126.9	127.1	127.2	127.2
∠O(9)=C–O	123.3	123.1	122.8	122.7
∠O(8)=C–O	123.3	123.1	122.8	122.7
∠C(10)–C–O	109.7	109.7	110.0	110.0
∠C(4)–C–O	109.7	109.7	110.0	110.0
∠C–O–C	120.3	120.3	120.3	120.3
ϕO(9)=C–C–H(11)	2.7	4.9	5.8	5.7
ϕO(8)=C–C–H(5)	2.7	4.9	5.8	5.7
ϕO(9)=C–C–O	177.5	177.7	177.6	177.6
ϕO(8)=C–C–O	177.5	177.7	177.6	177.6
ϕO(9)=C–O–C	26.0	27.2	29.0	29.1
ϕO(8)=C–O–C	26.0	27.2	29.0	29.1
ϕC(10)–C–O–C	-156.5	-155.0	-153.2	-153.2
ϕC(4)–C–O–C	-156.5	-155.0	-153.2	-153.2

(sp, ac)				
*r*C(14)–C(23)	150.3	150.1	149.9	149.9
*r*C(16)–C(17)	150.4	150.2	150.2	150.1
*r*C(14)=O(22)	120.0	119.4	119.5	119.5
*r*C(16)=O(21)	119.3	118.5	118.6	118.6
*r*C(14)–O(15)	136.7	136.6	136.6	136.5
*r*C(16)–O(15)	139.6	140.0	139.9	140.0
*r*C–H average	109.1	108.9	108.9	108.9
∠H(25)–C–C	109.3	109.5	109.5	109.4
∠H(20)–C–C	107.4	107.6	107.8	107.7
∠H(25)–C–H(24)	110.4	110.4	110.4	110.6
∠H(25)–C–H(26)	110.4	110.4	110.2	110.5
∠H(20)–C–H(18)	110.8	110.7	110.7	111.0
∠H(20)–C–H(19)	110.2	109.9	109.6	109.9
∠C(23)–C=O	126.1	126.2	126.4	126.3
∠C(17)–C=O	125.2	125.5	125.5	125.6
∠O(22)=C–O	124.1	124.0	123.5	123.5
∠O(21)=C–O	116.9	117.1	117.2	117.2
∠C(23)–C–O	109.8	109.8	110.1	110.1
∠C(17)–C–O	117.8	117.4	117.1	117.2
∠C–O–C	123.2	123.0	122.3	122.5
ϕO(22)=C–C–H(25)	0.3	-0.2	-1.4	-1.0
ϕO(21)=C–C–H(20)	17.0	18.1	22.0	21.3
ϕO(22)=C–C–O	-178.5	-178.6	-178.6	-178.6
ϕO(21)=C–C–O	176.1	176.0	175.8	175.7
ϕO(22)=C–O–C	-8.1	-7.7	-8.8	-8.7
ϕO(21)=C–O–C	151.2	148.6	145.0	145.3
ϕC(23)–C–O–C	173.4	173.7	172.5	172.7
ϕC(17)–C–O–C	-32.4	-35.1	-38.9	-38.6

[a] Bond lengths are in pm, bond angles (∠) and dihedral angles (ϕ) in degrees.

[b] Atom numbering is given in Figure 4.2.

Table A2.3 Refined and calculated (M06-2X/6-311++G**) amplitudes of vibration (u), associated r_a distances and corresponding correction values (k) for the r_{h1} refinement of acetic anhydride.[a,b]

	Atom pair	r_a	u_{GED}	k	$u_{calc.}$	Restraint
u_1	C(23)–H(25)	108.2(4)	7.8(Tied to u_8)	0.4	7.6	
u_2	C(10)–H(11)	108.2(4)	7.7(Tied to u_8)	0.4	7.6	
u_3	C(17)–H(20)	108.2(4)	7.8(Tied to u_8)	0.4	7.6	
u_4	C(17)–H(18)	108.2(4)	7.8(Tied to u_8)	0.4	7.6	
u_5	C(17)–H(19)	108.2(4)	7.8(Tied to u_8)	0.4	7.6	
u_6	C(4)–H(7)	108.2(4)	7.8(Tied to u_8)	0.4	7.7	
u_7	C(23)–H(24)	108.2(4)	7.9(Tied to u_8)	0.4	7.7	
u_8	C(4)–H(6)	108.2(4)	7.9(4)	0.4	7.7	7.7(8)
u_9	C(16)–O(21)	118.1(1)	3.3(Tied to u_{10})	0.1	3.6	
u_{10}	C(3)–O(8)	118.2(1)	3.3(2)	0.1	3.6	3.6(4)
u_{11}	C(14)–O(22)	119.0(1)	3.4(Tied to u_{10})	0.1	3.7	
u_{12}	C(14)–O(15)	136.3(2)	5.2(Tied to u_{13})	0.1	4.7	
u_{13}	C(1)–O(2)	138.6(2)	5.4(3)	0.1	4.9	4.9(5)
u_{14}	O(15)–C(16)	139.9(2)	5.5(Tied to u_{13})	0.2	5.0	
u_{15}	C(1)–C(10)	148.5(2)	5.0(3)	0.2	5.0	5.0(5)
u_{16}	C(14)–C(23)	148.6(3)	5.0(Tied to u_{15})	0.2	4.9	
u_{17}	C(16)–C(17)	148.8(3)	5.0(Tied to u_{15})	0.2	5.0	
u_{18}	H(18)···H(19)	173.8(8)	12.5(fixed)	-0.1	12.5	
u_{19}	H(24)···H(26)	173.8(8)	12.6(fixed)	-0.2	12.6	
u_{20}	H(12)···H(13)	175.9(6)	12.5(fixed)	-0.1	12.5	
u_{21}	H(19)···H(20)	176.4(6)	12.4(fixed)	-0.1	12.4	
u_{22}	H(11)···H(13)	175.9(6)	12.4(fixed)	-0.1	12.4	
u_{23}	H(25)···H(26)	177.0(6)	12.5(fixed)	-0.2	12.5	
u_{24}	H(11)···H(12)	175.9(6)	12.4(fixed)	-0.1	12.4	
u_{25}	H(18)···H(20)	177.7(6)	12.3(fixed)	-0.1	12.3	
u_{26}	C(16)···H(20)	208.2(4)	10.8(fixed)	-0.2	10.8	
u_{27}	C(1)···H(13)	210.2(3)	11.4(fixed)	-0.2	11.4	
u_{28}	C(14)···H(25)	210.2(4)	10.9(fixed)	-0.2	10.9	

u_{29}	C(16)···H(19)	210.0(4)	11.1(fixed)	-0.2	11.1	
u_{30}	C(1)···H(11)	210.2(3)	10.8(fixed)	-0.3	10.8	
u_{31}	C(14)···H(24)	210.3(4)	11.5(fixed)	0.0	11.5	
u_{32}	C(3)···H(7)	210.3(3)	11.2(fixed)	-0.1	11.2	
u_{33}	C(16)···H(18)	213.2(4)	10.9(fixed)	-0.1	10.9	
u_{34}	O(15)···O(21)	220.1(3)	4.4(Tied to u_{36})	0.0	5.6	
u_{35}	O(15)···O(22)	224.8(2)	4.2(Tied to u_{36})	-0.1	5.4	
u_{36}	O(2)···O(9)	225.3(2)	4.2(2)	0.0	5.4	5.4(5)
u_{37}	O(15)···C(23)	235.3(7)	6.4(Tied to u_{38})	0.0	6.5	
u_{38}	O(2)···C(4)	236.9(7)	6.6(6)	0.0	6.7	6.7(7)
u_{39}	C(17)···O(21)	236.4(4)	4.7(Tied to u_{42})	-0.4	5.9	
u_{40}	C(1)···C(3)	240.0(4)	6.7(6)	-0.3	6.8	6.8(7)
u_{41}	O(22)···C(23)	237.7(4)	4.7(Tied to u_{42})	-0.3	5.9	
u_{42}	C(4)···O(8)	237.8(4)	4.6(3)	-0.4	5.9	5.9(6)
u_{43}	C(14)···C(16)	241.4(5)	7.9(Tied to u_{40})	-0.7	8.0	
u_{44}	O(15)···C(17)	247.9(7)	6.8(Tied to u_{38})	0.0	6.9	
u_{45}	H(19)···O(22)	266.7(38)	30.9(fixed)	17.4	30.9	
u_{46}	H(20)···O(21)	252.1(9)	15.2(fixed)	1.2	15.2	
u_{47}	O(2)···H(12)	257.6(17)	19.9(fixed)	2.2	19.9	
u_{48}	O(22)···H(25)	255.8(8)	15.3(fixed)	3.2	15.3	
u_{49}	O(9)···H(11)	255.8(7)	15.0(fixed)	1.9	15.0	
u_{50}	O(15)···H(24)	259.8(12)	22.5(fixed)	2.8	22.5	
u_{51}	O(15)···H(18)	264.4(14)	17.1(fixed)	1.8	17.1	
u_{52}	O(2)···H(13)	268.5(18)	21.5(fixed)	1.1	21.5	
u_{53}	H(18)···O(22)	284.3(56)	43.6(fixed)	8.7	43.6	
u_{54}	C(16)···O(22)	277.3(6)	13.5(Tied to u_{55})	0.0	14.0	
u_{55}	C(1)···O(8)	278.4(6)	10.6(6)	1.4	11.0	11.0(10)
u_{56}	C(17)···O(22)	293.1(23)	15.9(Tied to u_{81})	8.8	16.4	
u_{57}	O(8)···O(9)	280.0(27)	19.2(18)	4.7	16.8	16.8(20)
u_{58}	C(14)···H(18)	294.0(33)	26.2(fixed)	7.5	26.2	
u_{59}	C(14)···C(17)	301.2(12)	10.2(Tied to u_{71})	4.2	10.6	
u_{60}	O(15)···H(19)	293.8(18)	18.7(fixed)	0.2	18.7	

u_{61}	H(19)···O(21)	289.9(13)	17.8(fixed)	-1.9	17.8	
u_{62}	C(14)···H(19)	311.0(31)	26.9(fixed)	7.0	26.9	
u_{63}	O(9)···H(13)	300.1(11)	19.2(fixed)	-2.6	19.2	
u_{64}	O(22)···H(26)	301.9(7)	20.9(fixed)	-3.4	20.9	
u_{65}	H(7)···O(8)	305.7(10)	16.7(fixed)	-2.7	16.7	
u_{66}	H(18)···O(21)	314.9(8)	13.0(fixed)	-2.2	13.0	
u_{67}	O(15)···H(25)	323.3(6)	10.5(fixed)	-4.1	10.5	
u_{68}	O(2)···H(11)	325.9(6)	10.5(fixed)	-3.1	10.5	
u_{69}	O(15)···H(20)	329.2(9)	11.9(fixed)	-2.7	11.9	
u_{70}	C(14)···O(21)	334.0(8)	12.4(Tied to u_{55})	-4.0	12.8	
u_{71}	C(1)···C(4)	361.2(7)	9.7(6)	-2.6	10.1	10.1(10)
u_{72}	C(16)···C(23)	366.8(6)	7.1(Tied to u_{71})	-2.0	7.4	
u_{73}	C(3)···H(13)	380.5(18)	24.4(fixed)	-0.9	24.4	
u_{74}	O(21)···O(22)	372.2(15)	30.0(Tied to u_{57})	-5.2	26.3	
u_{75}	H(20)···O(22)	396.3(22)	17.4(fixed)	4.6	17.4	
u_{76}	C(16)···H(26)	391.6(15)	20.2(fixed)	-0.3	20.2	
u_{77}	C(3)···H(12)	390.7(16)	21.0(fixed)	-3.5	21.0	
u_{78}	C(14)···H(20)	401.1(12)	13.1(fixed)	0.2	13.1	
u_{79}	H(18)···H(26)	410.6(54)	49.2(fixed)	12.4	49.2	
u_{80}	H(18)···C(23)	412.2(38)	31.2(fixed)	6.6	31.2	
u_{81}	C(4)···O(9)	405.9(13)	19.7(15)	-1.7	20.4	20.4(20)
u_{82}	O(8)···H(13)	415.0(34)	38.2(fixed)	0.7	38.2	
u_{83}	C(17)···C(23)	435.8(18)	15.4(Tied to u_{93})	1.4	15.6	
u_{84}	C(3)···H(11)	442.8(6)	12.8(fixed)	-4.8	12.8	
u_{85}	C(17)···H(26)	451.6(36)	31.4(fixed)	3.0	31.4	
u_{86}	H(19)···C(23)	453.1(34)	29.1(fixed)	2.5	29.1	
u_{87}	C(16)···H(25)	446.0(6)	12.1(fixed)	-4.9	12.1	
u_{88}	O(21)···C(23)	447.0(10)	9.9(Tied to u_{81})	-5.3	10.2	
u_{89}	O(21)···H(24)	453.2(22)	25.8(fixed)	-0.7	25.8	
u_{90}	H(7)···H(12)	463.3(52)	40.0(fixed)	2.1	40.0	
u_{91}	H(18)···H(25)	469.1(41)	37.1(fixed)	8.2	37.1	
u_{92}	O(8)···H(12)	457.4(13)	24.1(fixed)	-6.2	24.1	

u_{93}	C(4)···C(10)	467.6(16)	10.2(9)	-5.5	10.3	10.4(10)
u_{94}	C(4)···H(12)	471.5(29)	26.0(fixed)	-3.2	26.0	
u_{95}	H(5)···O(9)	473.4(13)	22.8(fixed)	-2.2	22.8	
u_{96}	H(6)···H(12)	477.9(37)	43.8(fixed)	-0.9	43.8	
u_{97}	H(19)···H(26)	483.6(45)	41.2(fixed)	-1.4	41.2	
u_{98}	C(4)···H(13)	486.7(27)	28.7(fixed)	-5.6	28.7	
u_{99}	C(17)···H(25)	498.8(16)	20.3(fixed)	2.5	20.3	
u_{100}	H(19)···H(25)	500.6(36)	34.4(fixed)	7.0	34.4	
u_{101}	H(6)···H(13)	522.1(44)	36.7(fixed)	-10.7	36.7	
u_{102}	H(20)···C(23)	532.3(20)	18.7(fixed)	-2.9	18.7	
u_{103}	H(20)···H(26)	541.7(40)	34.4(fixed)	-0.1	34.4	
u_{104}	O(21)···H(25)	530.6(10)	15.0(fixed)	-10.3	15.0	
u_{105}	H(5)···C(10)	555.8(12)	13.4(fixed)	-9.1	13.4	
u_{106}	H(7)···H(11)	566.9(28)	27.0(fixed)	-9.6	27.0	
u_{107}	H(6)···H(11)	568.8(15)	31.8(fixed)	-8.1	31.8	
u_{108}	H(20)···H(25)	599.7(19)	22.5(fixed)	-2.6	22.5	
u_{109}	H(5)···H(11)	641.8(9)	15.3(fixed)	-12.3	15.3	

[a] Distances in pm. Values in parentheses are the standard deviations in terms of the last digits. Atom numbering follows 1 – 13 for (*sp*, *sp*) and 14 – 26 for (*sp*, *ac*).

[b] Unrefined amplitudes of vibration were fixed at the values obtained using the M06-2X/6-311++G** force field.

Table A2.4 Energy comparison (Hartrees) and conformer weighting (%) calculated using the MP2 and M06-2X methods.[a]

	6-31G*	6-311G*	6-311+G*	6-311++G**
MP2				
Energy (Hartrees)				
(*sp*, *sp*)	-380.6183	-380.7839	-380.8010	-380.8440
(*sp*, *ac*)	-380.6176	-380.7828	-380.7999	-380.8429
% Conformer				
(*sp*, *sp*)	47.3	57.5	57.3	57.4
(*sp*, *ac*)	52.7	42.3	42.7	42.6
M06-2X				
Energy (Hartrees)				
(*sp*, *sp*)	-381.5666	-381.6724	-381.6810	-381.6876
(*sp*, *ac*)	-381.5673	-381.6730	-381.6813	-381.6878
% Conformer				
(*sp*, *sp*)	21.8	22.9	27.6	28.8
(*sp*, *ac*)	78.2	77.1	72.4	71.3

[a] A temperature of 338.15 K was used for all calculations.

Table A2.5 Least squares correlation matrix (× 100) for the GED refinement of acetic anhydride.[a]

	p_7	p_{19}	u_8	u_{10}	u_{13}	u_{15}	u_{42}	k_2	k_3
p_1	-54				-83	-59			
p_4			-56						
p_7					62	62			
p_{16}		-92							
u_8				52					
u_{13}						81			
u_{36}							50		
k_1								72	
k_2									-57

[a] Only elements with absolute values ≥ 50% are shown; k_1, k_2 and k_3 are scale factors.

Table A2.6 Experimental coordinates from the GED refinement of the (*sp*, *sp*) and (*sp*, *ac*) conformers of acetic anhydride.[a]

Atom	*x*	*y*	*z*
(*sp*, *sp*)			
C(1)	-120.3	69.0	0.0
O(2)	0.0	0.0	0.0
C(3)	120.3	69.0	0.0
C(4)	229.7	-13.6	-56.9
H(5)	324.4	37.0	-42.6
H(6)	212.4	-28.6	-162.8
H(7)	232.2	-109.7	-6.8
O(8)	130.9	178.0	44.6
O(9)	-130.9	178.0	-44.6
C(10)	-229.7	-13.6	56.9
H(11)	-324.4	37.0	42.6
H(12)	-232.2	-109.7	6.8
H(13)	-212.4	-28.6	162.8
(*sp*, *ac*)			
C(14)	-136.5	0.0	0.0
O(15)	0.0	0.0	0.0
C(16)	75.1	118.1	0.0
C(17)	30.3	230.5	-86.6
H(18)	-17.2	194.6	-177.2
H(19)	-42.7	289.8	-32.8
H(20)	117.2	291.0	-109.7
O(21)	173.8	118.6	64.9
O(22)	-201.8	98.6	13.6
C(23)	-190.4	-137.5	-15.6
H(24)	-150.8	-200.9	62.9
H(25)	-298.7	-134.5	-10.8
H(26)	-157.8	-178.5	-110.4

[a] Coordinates are in pm.

Table A2.7 Calculated coordinates at the M06-2X/6-311++G** level for the (*sp*, *sp*) and (*sp*, *ac*) conformers of acetic anhydride.[a]

Atom	*x*	*y*	*z*
(*sp*, *sp*)			
C(1)	0.0	120.3	-8.5
O(2)	0.0	0.0	60.5
C(3)	0.0	-120.3	-8.5
C(4)	-63.5	-227.4	75.0
H(5)	-50.2	-323.7	26.5
H(6)	-169.8	-205.1	86.0
H(7)	-19.2	-227.8	174.6
O(8)	48.5	-132.6	-116.1
O(9)	-48.5	132.6	-116.1
C(10)	63.5	227.4	75.0
H(11)	50.2	323.7	26.5
H(12)	19.2	227.8	174.6
H(13)	169.8	205.1	86.0
(*sp*, *ac*)			
C(14)	113.3	12.8	-11.3
O(15)	8.0	-70.3	14.1
C(16)	-125.1	-28.9	1.5
C(17)	-158.0	110.6	46.0
H(18)	-95.4	141.8	129.5
H(19)	-139.8	179.5	-36.5
H(20)	-263.2	112.7	73.3
O(21)	-203.4	-109.4	-36.7
O(22)	101.5	121.2	-60.2
C(23)	242.0	-53.5	27.7
H(24)	251.0	-148.6	-24.9
H(25)	325.2	11.9	2.9
H(26)	240.7	-75.0	134.6

[a] Coordinates are in pm.

Table A2.8 Comparison of refined and calculated selected RMS amplitudes, *u*, from the two GED studies of acetic anhydride.

Atom Pair	Previous GED study[a]		This Study	
	u_{GED}	$u_{calc.}$[b]	u_{GED}	$u_{calc.}$[c]
(*sp*, *sp*)				
C(1)···C(4)	16.2(24)	6.9	9.7(6)	10.1
C(1)···O(8)	12.6(25)	9.0	10.6(6)	11.0
C(3)···O(9)	17.5(25)	9.0	10.6(6)	11.0
C(3)···C(10)	14.6(23)	6.9	9.7(6)	10.1
C(4)···O(9)	16.9(23)	8.0	19.7(15)	20.4
C(4)···C(10)	9.4(75)	8.8	10.2(9)	10.3
O(8)···O(9)	16.9(25)	13.4	19.2(18)	16.8
O(8)···C(10)	6.7(23)	7.9	19.7(15)	20.4
(*sp*, *ac*)				
C(14)···C(17)	18.2(24)	7.0	10.2(Tied to C1···C4)	10.6
C(14)···O(21)	9.4(25)	9.4	12.4(Tied to C1···O8)	12.8
C(16)···O(22)	9.0(31)	6.1	13.6(Tied to C1···O8)	14.0
C(16)···C(23)	16.0(68)	8.7	7.1(Tied to C1···C4)	7.4
C(17)···O(22)	8.4(23)	7.1	15.9(Tied to C4···O9)	16.4
C(17)···C(23)	8.9(23)	8.0	15.4(Tied to C4···C10)	15.6
O(21)···O(22)	14.2(24)	7.8	30.0(Tied to O8···O9)	26.3
O(21)···C(23)	24.0(24)	13.1	9.9(Tied to C4···O9)	10.2

[a] *J. Phys. Chem. A*. **2000**, *104*, 1576-1587.

[b] Calculated from the MP2/6-31G* force field.

[c] Calculated from the M06-2X/6-311++G** force field.

Figure A2.1. Experimental and final weighted difference (experimental – theoretical) MICs from the GED study of acetic anhydride.

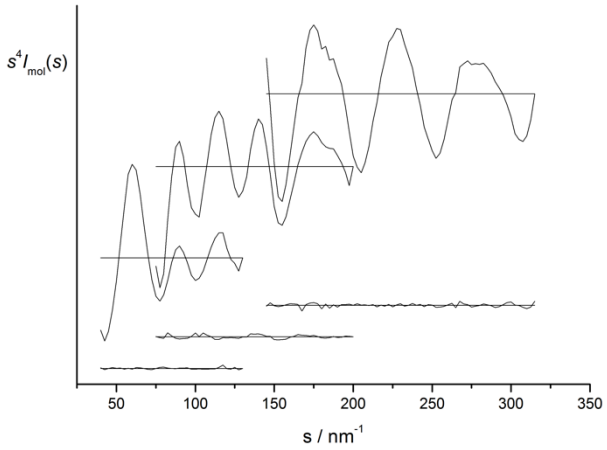

Pyrolysis of acetic anhydride

Table A2.9 Nozzle-to-plate distance (mm), weighting function (nm^{-1}), correlation parameter, scale factor and electron wavelength (pm) used in the VHT-GED study of ketene and acetic acid by the pyrolysis of acetic anhydride.

Nozzle-to-plate distance[a]	212.2
Δs	1
s_{min}	20
sw_1	40
sw_2	163
s_{max}	190
Correlation parameter	0.422
Scale factor[b]	1.207(12)
Electron wavelength	6.18

[a] Determined by reference to the scattering pattern of benzene vapour.

[b] Values in parentheses are the estimated standard deviations.

Table A2.10 Parameter values for ketene and acetic acid from *ab initio* calculations at the MP2 level for a range of basis sets.[a,b]

Parameter	6-31G*	6-311G*	6-311+G*	6-311++G**
Ketene				
*r*C=O	118.1	116.9	116.9	116.8
*r*C=C	132.0	132.0	132.1	132.2
*r*C–H	108.1	108.0	108.0	108.0
∠H–C=C	119.6	119.5	119.5	119.1
∠H–C–H	120.7	121.0	121.0	121.8
Acetic acid				
*r*C=O	121.8	121.0	121.1	121.0
*r*C–O	136.3	136.0	135.8	136.0
*r*C–C	150.2	150.3	150.1	150.4
*r*O–H	97.9	96.8	96.9	96.8
*r*C–H(7)	108.9	108.8	108.8	108.8
*r*C–H(8/9)	109.3	109.2	109.2	109.2
∠H(7)–C–H(8/9)	110.2	110.2	110.1	110.2
∠C–C–H(7)	109.3	109.5	109.5	109.5
∠C–C–H(8/9)	109.7	109.5	109.8	109.5
∠C–C=O	126.4	126.4	126.4	126.4
∠C–O–H	105.4	105.8	107.2	105.8
ϕH–O–C–C	180.0	180.0	180.0	180.0

[a] Bond parameters are in pm, bond angles (∠) and dihedral angles (ϕ) in degrees.

[b] Atom numbering is given in Figure 4.6.

Table A2.11 Refined and calculated (MP2/6-311++G**) amplitudes of vibration (u), associated r_a distances and corresponding correction values (k) for the r_{h1} refinement of ketene and acetic acid from the pyrolysis of acetic anhydride.[a,b]

	Atom pair	r_a	u_{GED}	k	$u_{calc.}$	Restraint
u_1	O(11)–H(12)	96.8(3)	6.7(7)	0.4	6.9	6.9(7)
u_2	C(1)–H(2)	108.5(1)	6.7(8)	0.4	7.5	7.5(8)
u_3	C(6)–H(7)	108.6(8)	7.1(8)	0.5	7.7	7.7(8)
u_4	C(6)–H(8)	108.6(8)	7.2(Tied to u_3)	0.5	7.8	
u_5	C(4)–O(5)	115.4(3)	3.6(4)	0.1	3.6	3.6(4)
u_6	C(10)–O(13)	119.5(4)	4.1(4)	0.1	3.9	3.9(4)
u_7	C(1)–C(4)	132.4(2)	4.7(4)	0.2	4.4	4.4(4)
u_8	C(10)–O(11)	135.7(6)	5.3(5)	0.3	5.2	5.2(5)
u_9	C(6)–C(10)	150.1(3)	5.2(6)	0.3	5.7	5.7(6)
u_{10}	H(8)···H(9)	171.2(16)	13.2(fixed)	-2.8	13.2	
u_{11}	H(7)···H(8)	173.6(14)	13.7(fixed)	-3.8	13.7	
u_{12}	C(10)···H(12)	185.6(31)	11.3(fixed)	-0.5	11.3	
u_{13}	H(2)···H(3)	186.1(9)	12.6(fixed)	-2.2	12.6	
u_{14}	H(2)···C(4)	205.2(5)	9.2(30)	-2.6	11.8	
u_{15}	H(7)···C(10)	217.4(7)	12.7(10)	5.6	13.4	13.4(10)
u_{16}	H(8)···C(10)	219.9(7)	14.7(Tied to u_{15})	8.4	15.5	
u_{17}	O(11)···O(13)	223.9(9)	5.7(7)	-0.5	6.6	6.6(7)
u_{18}	H(12)···O(13)	226.3(45)	16.2(20)	0.1	16.9	16.9(20)
u_{19}	C(6)···O(11)	234.2(11)	8.6(8)	-0.1	8.7	8.7(8)
u_{20}	C(6)···O(13)	240.6(8)	8.3(8)	-0.1	7.7	7.7(8)
u_{21}	C(1)···O(5)	246.4(3)	5.8(5)	-1.1	5.1	5.1(5)
u_{22}	H(7)···O(13)	277.7(11)	26.6(30)	23.2	25.4	25.4(30)
u_{23}	H(8)···O(11)	266.7(14)	50.5(Tied to u_{27})	16.4	49.6	
u_{24}	H(8)···O(13)	299.0(10)	44.4(Tied to u_{22})	-4.7	42.4	
u_{25}	H(2)···O(5)	309.6(7)	17.1(18)	-4.8	15.3	15.3(20)
u_{26}	C(6)···H(12)	313.4(21)	10.9(fixed)	-3.3	10.9	
u_{27}	H(7)···O(11)	315.9(12)	13.6(10)	-10.9	13.3	13.3(10)
u_{28}	H(8)···H(12)	350.8(17)	34.7(fixed)	6.5	34.7	

u_{29}	H(7)···H(12)	389.8(29)	16.0(fixed)	-7.0	16.0

[a] Distances in pm. Values in parentheses are the standard deviations in terms of the last digits. Atom numbering follows 1 – 5 for ketene and 6 – 13 for acetic acid.
[b] Unrefined amplitudes of vibration were fixed at the values obtained using the MP2/6-311++G** force field.

Table A2.12 Experimental GED coordinates for ketene and acetic acid from the refinement from the pyrolysis of acetic anhydride. [a]

Atom	*x*	*y*	*z*
Ketene			
C(1)	0.0	0.0	0.0
H(2)	-53.2	94.6	0.0
H(3)	-53.2	-94.6	0.0
C(4)	132.3	0.0	0.0
O(5)	247.7	0.0	0.0
Acetic Acid			
C(6)	-187.9	-140.6	0.0
H(7)	-296.4	-138.9	0.0
H(8)	-150.7	-193.1	-87.5
H(9)	-150.7	-193.1	87.5
C(10)	-135.6	0.0	0.0
O(11)	0.0	0.0	0.0
H(12)	26.2	93.2	0.0
O(13)	-201.0	100.0	0.0

[a] Coordinates are in pm.

Table A2.13 Calculated coordinates at the MP2/6-311++G** level for ketene and acetic acid from the refinement from the pyrolysis of acetic anhydride. [a]

Atom	*x*	*y*	*z*
Ketene			
C(1)	0.0	0.0	0.0
H(2)	-52.8	94.8	0.0
H(3)	-52.8	-94.8	0.0
C(4)	132.2	0.0	0.0
O(5)	249.0	0.0	0.0
Acetic Acid			
C(6)	-189.8	-140.4	0.0
H(7)	-298.3	-137.6	0.0
H(8)	-153.7	-193.1	-87.7
H(9)	-153.7	-193.1	87.7
C(10)	-135.9	0.0	0.0
O(11)	0.0	0.0	0.0
H(12)	26.4	93.1	0.0
O(13)	-201.1	101.9	0.0

[a] Coordinates are in pm.

Figure A2.2 Experimental and final weighted difference (experimental – theoretical) MIC for ketene and acetic acid from the GED study of the pyrolysis of acetic anhydride.

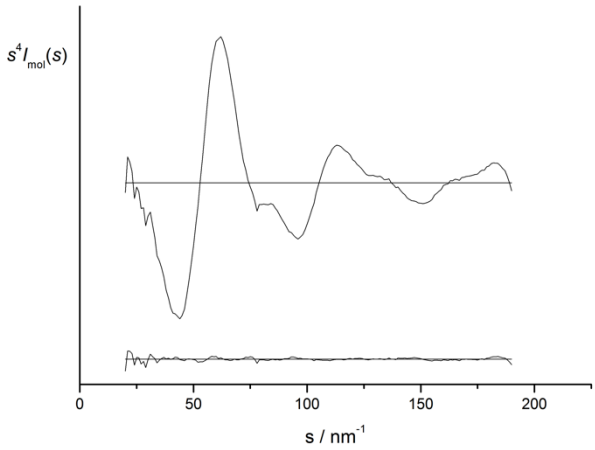

Meldrum's acid

Table A2.14 Nozzle-to-plate distance (mm), weighting function (nm^{-1}), correlation parameter, scale factor and electron wavelength (pm) used in the GED study of Meldrum's acid.

Nozzle-to-plate distance[a]	189.3	253.9
Δs	2	1
s_{min}	40	20
sw_1	60	40
sw_2	172	112
s_{max}	200	130
Correlation parameter	0.477	0.490
Scale factor[b]	0.621(7)	0.524(7)
Electron wavelength	6.18	6.18

[a] Determined by reference to the scattering pattern of benzene vapour.

[b] Values in parentheses are the estimated standard deviations.

Table A2.15 Parameter values for Meldrum's acid from *ab initio* calculations at the MP2 level for a range of basis sets.[a,b]

Parameter	6-31G*	6-311G*	6-311+G*	6-311++G**
*r*C(6)=O(9)	121.1	120.2	120.4	120.4
*r*C(7)=O(10)	121.1	120.2	120.4	120.4
*r*C(2)–O(4)	143.9	143.3	143.6	143.4
*r*C(2)–O(5)	143.9	143.3	143.6	143.4
*r*C(6)–O(4)	136.7	136.2	136.1	136.2
*r*C(7)–O(5)	136.7	136.2	136.1	136.2
*r*C(1)–C(2)	151.8	151.9	151.9	152.1
*r*C(2)–C(3)	150.9	151.0	150.9	151.1
*r*C(6)–C(8)	151.2	151.4	151.4	151.5
*r*C(7)–C(8)	151.2	151.4	151.4	151.5
*r*C–H average	109.2	109.2	109.2	109.3
∠H(11)–C–C	111.9	112.2	112.3	112.1
∠H(16)–C–C	109.0	109.0	109.3	109.2
∠H(11)–C–H(12)	108.5	108.3	108.4	108.5
∠H(11)–C–H(13)	108.5	108.3	108.4	108.5
∠H(16)–C–H(14)	109.4	109.3	109.3	109.4
∠H(16)–C–H(15)	109.4	109.3	109.3	109.4
∠C(H_3)–C–C(H_3)	113.2	113.1	113.1	112.9
∠C(3)–C–O	105.3	105.3	105.4	105.5
∠C(1)–C–O	110.5	110.5	110.7	110.7
∠C(2)–O–C(6)	119.5	119.0	118.9	118.8
∠C(2)–O–C(7)	119.5	119.0	118.9	118.8
∠O(4)–C=O(9)	120.2	120.4	120.4	120.4
∠O(5)–C=O(10)	120.2	120.4	120.4	120.4
∠C(8)–C–O(4)	115.8	115.7	115.9	115.8
∠C(8)–C–O(5)	115.8	115.7	115.9	115.8
∠C–C–H(17)	108.9	108.9	108.9	108.7
∠H(17)–C(8)–H(18)	106.7	106.3	106.1	106.8
ϕO(4)–C(2)–C(1)–O(5)	124.3	124.4	124.0	124.0

ϕC(1)–C(2)–O(4)–C(6)	-79.1	-76.5	-75.6	-75.4
ϕC(2)–O–C=O	173.3	170.9	169.7	169.9
ϕC(2)–O(4)–C(6)–C(8)	-7.8	-10.8	-12.0	-11.8
ϕO(4)–C–C–H(17)	92.9	97.0	98.2	97.2
ϕC(6)–C(8)–H(17)–H(18)	117.2	116.7	116.8	117.0

[a] Bond lengths are in pm, bond angles (∠) and dihedral angle (ϕ) in degrees.

[b] See Figure 4.8 for atom numbering.

Table A2.16 Refined and calculated (MP2/6-311++G**) amplitudes of vibration (u), associated r_a distances and corresponding correction values (k) for the r_{h1} refinement of Meldrum's acid.[a,b]

	Atom pair	r_a	u_{GED}	k	$u_{calc.}$	Restraint
u_1	C(8)–H(18)	109.1(1)	8.3(Tied to u_5)	0.4	7.6	
u_2	C(3)–H(16)	109.1(1)	8.3(Tied to u_5)	0.4	7.6	
u_3	C(1)–H(11)	109.1(1)	8.3(Tied to u_5)	0.4	7.6	
u_4	C(3)–H(14)	109.1(1)	8.3(Tied to u_5)	0.4	7.6	
u_5	C(1)–H(12)	109.1(1)	8.3(7)	0.4	7.6	7.6(8)
u_6	C(8)–H(17)	109.0(1)	8.4(Tied to u_5)	0.4	7.6	
u_7	C(7)–O(10)	120.1(2)	3.6(4)	0.1	3.7	3.7(4)
u_8	O(4)–C(6)	136.1(2)	4.5(Tied to u_9)	0.1	4.8	
u_9	C(2)–O(5)	144.1(6)	4.9(4)	0.3	5.1	5.1(5)
u_{10}	C(2)–C(3)	151.9(3)	4.1(Tied to u_{12})	0.2	5.0	
u_{11}	C(7)–C(8)	152.3(3)	4.2(Tied to u_{12})	0.0	5.1	
u_{12}	C(1)–C(2)	152.8(3)	4.2(5)	0.1	5.1	5.1(5)
u_{13}	H(17)···H(18)	174.8(7)	12.5(fixed)	0.1	12.5	
u_{14}	H(11)···H(13)	176.5(3)	12.3(fixed)	-0.1	12.3	
u_{15}	H(14)···H(16)	177.5(3)	12.3(fixed)	0.0	12.3	
u_{16}	H(12)···H(13)	170.3(10)	12.3(fixed)	-0.1	12.3	
u_{17}	H(14)···H(15)	178.5(11)	12.3(fixed)	0.0	12.3	
u_{18}	C(7)···H(18)	213.3(5)	10.9(fixed)	0.1	10.9	
u_{19}	C(7)···H(17)	212.8(5)	11.2(fixed)	-0.3	11.2	
u_{20}	C(2)···H(16)	213.6(5)	10.7(fixed)	-0.2	10.7	
u_{21}	C(2)···H(15)	213.6(5)	10.8(fixed)	-0.2	10.8	
u_{22}	C(2)···H(12)	218.0(4)	10.9(fixed)	-0.2	10.9	
u_{23}	C(2)···H(11)	218.1(4)	10.7(fixed)	-0.2	10.7	
u_{24}	H(11)···H(17)	232.0(41)	29.8(fixed)	7.2	29.8	
u_{25}	O(4)···O(9)	222.5(3)	4.9(9)	0.2	5.3	5.4(5)
u_{26}	C(3)···O(4)	234.8(4)	7.7(7)	0.4	6.9	6.9(7)
u_{27}	O(4)···O(5)	239.2(8)	6.5(6)	-0.4	6.4	6.4(6)
u_{28}	C(8)···O(10)	240.4(4)	6.2(6)	-0.2	6.1	6.1(6)

u_{29}	C(2)···C(6)	239.6(2)	6.7(6)	-0.9	6.5	6.5(6)
u_{30}	C(1)···O(4)	243.7(4)	6.7(7)	0.0	7.2	7.2(7)
u_{31}	O(5)···C(8)	243.8(4)	5.9(6)	-0.8	6.2	6.2(6)
u_{32}	C(1)···C(3)	254.0(6)	6.8(7)	0.2	7.4	7.4(7)
u_{33}	C(6)···C(7)	257.1(6)	6.8(7)	-1.2	7.2	7.2(7)
u_{34}	H(12)···H(15)	262.0(9)	25.2(fixed)	4.2	25.2	
u_{35}	O(5)···H(16)	257.5(17)	17.4(fixed)	0.6	17.4	
u_{36}	O(4)···H(15)	257.6(9)	18.4(fixed)	0.7	18.4	
u_{37}	O(9)···H(18)	261.1(7)	14.3(fixed)	1.6	14.3	
u_{38}	O(5)···H(13)	269.9(18)	18.0(fixed)	0.5	18.0	
u_{39}	C(8)···H(11)	274.9(24)	20.5(fixed)	2.6	20.5	
u_{40}	C(2)···C(8)	272.9(6)	8.2(7)	-0.5	7.3	
u_{41}	O(5)···H(11)	272.7(19)	17.6(fixed)	0.0	17.6	
u_{42}	C(3)···H(12)	280.0(7)	17.8(fixed)	0.5	17.8	
u_{43}	C(1)···H(15)	277.6(7)	17.2(fixed)	0.5	17.2	
u_{44}	O(5)···C(6)	282.0(5)	9.1(7)	-1.4	7.8	7.8(8)
u_{45}	C(7)···H(11)	288.0(22)	25.5(fixed)	0.1	25.5	
u_{46}	O(9)···H(17)	284.7(11)	16.4(fixed)	-1.1	16.4	
u_{47}	O(5)···H(17)	299.0(14)	18.8(fixed)	-1.1	18.8	
u_{48}	C(1)···H(17)	308.7(35)	27.2(fixed)	0.9	27.2	
u_{49}	C(1)···C(7)	307.1(14)	12.2(13)	-1.7	15.0	15.0(20)
u_{50}	C(2)···H(17)	312.7(22)	22.7(fixed)	-0.4	22.7	
u_{51}	C(1)···C(8)	321.5(17)	12.5(10)	-0.9	13.1	13.1(10)
u_{52}	O(5)···H(18)	324.3(8)	12.4(fixed)	-2.6	12.4	
u_{53}	C(6)···H(12)	348.9(12)	26.1(fixed)	-2.1	26.1	
u_{54}	C(1)···H(16)	345.6(6)	10.4(fixed)	-1.6	10.4	
u_{55}	C(3)···H(11)	347.6(6)	10.3(fixed)	-1.6	10.3	
u_{56}	C(2)···O(10)	349.0(6)	8.4(6)	-1.8	7.2	7.2(7)
u_{57}	C(3)···C(6)	360.0(4)	8.6(8)	-1.2	7.6	7.6(8)
u_{58}	C(6)···O(10)	365.5(7)	10.3(8)	-2.1	9.4	9.5(9)
u_{59}	H(13)···H(17)	378.6(35)	33.0(fixed)	-0.9	33.0	
u_{60}	H(11)···H(18)	378.7(28)	22.4(fixed)	0.8	22.4	

u_{61}	C(2)···H(18)	370.5(7)	11.0(fixed)	-2.6	11.0	
u_{62}	C(6)···H(16)	372.6(9)	18.9(fixed)	-0.6	18.9	
u_{63}	H(12)···H(16)	377.7(7)	18.2(fixed)	-1.9	18.2	
u_{64}	H(11)···H(14)	375.4(7)	18.0(fixed)	-2.0	18.0	
u_{65}	O(9)···H(11)	380.5(13)	34.5(fixed)	-1.6	34.5	
u_{66}	C(8)···H(12)	396.5(20)	21.4(fixed)	-2.6	21.4	
u_{67}	C(6)···H(15)	391.6(9)	18.2(fixed)	-1.3	18.2	
u_{68}	O(4)···O(10)	399.1(6)	10.5(6)	-2.6	9.6	9.6(10)
u_{69}	C(1)···O(9)	406.8(10)	20.5(17)	-3.2	21.8	21.8(20)
u_{70}	C(3)···C(8)	413.5(7)	7.9(7)	-1.1	7.4	7.4(7)
u_{71}	O(10)···H(13)	423.4(23)	35.2(fixed)	-3.2	35.2	
u_{72}	C(1)···H(18)	428.8(17)	15.1(fixed)	-2.8	15.1	
u_{73}	H(11)···H(16)	428.0(7)	14.0(fixed)	-2.8	14.0	
u_{74}	C(8)···H(16)	430.8(12)	16.2(fixed)	-0.8	16.2	
u_{75}	C(3)···O(9)	453.4(4)	11.9(7)	-2.2	9.5	9.5(9)
u_{76}	O(10)···H(16)	458.1(20)	24.3(fixed)	-1.3	24.3	
u_{77}	C(3)···H(17)	463.4(21)	22.4(fixed)	-1.3	22.4	
u_{78}	O(9)···O(10)	464.0(12)	16.8(10)	-3.3	14.0	14.0(10)
u_{79}	O(10)···H(14)	465.7(16)	21.6(fixed)	-1.7	21.6	
u_{80}	C(8)···H(15)	472.4(9)	14.5(fixed)	-2.1	14.5	
u_{81}	H(13)···H(18)	500.8(17)	23.5(fixed)	-4.7	23.5	
u_{82}	H(16)···H(17)	500.7(17)	23.6(fixed)	-2.4	23.6	
u_{83}	C(3)···H(18)	501.5(13)	13.0(fixed)	-3.4	13.0	
u_{84}	H(16)···H(18)	502.2(23)	22.1(fixed)	-2.7	22.1	
u_{85}	H(15)···H(17)	513.2(25)	26.4(fixed)	-1.8	26.4	
u_{86}	H(14)···H(18)	561.7(14)	18.3(fixed)	-4.6	18.3	

[a] Distances in pm. Values in parentheses are the standard deviations in terms of the last digits.

[b] Unrefined amplitudes of vibration were fixed at the values obtained using the MP2/6-311++G** force field.

Table A2.17 Least squares correlation matrix (× 100) for the GED refinement of Meldrum's acid.[a]

	p_{25}	p_{26}
p_{24}	-81	
p_{25}		-54

[a] Only elements with absolute values ≥ 50% are shown.

Table A2.18 Experimental coordinates for the GED refinement of Meldrum's acid.[a]

Atom	*x*	*y*	*z*
C(1)	-322.7	2.3	1.3
C(2)	-240.3	131.0	-0.3
C(3)	-326.1	256.3	-0.1
O(4)	-161.5	139.5	-119.9
O(5)	-161.5	139.5	119.9
C(6)	-48.2	64.7	-129.3
C(7)	-48.2	64.7	129.3
C(8)	0.0	0.0	0.0
O(9)	10.0	55.8	-233.9
O(10)	10.0	55.8	233.9
H(11)	-259.7	-86.9	1.1
H(12)	-391.5	-3.6	-83.5
H(13)	-389.6	-2.6	87.7
H(14)	-387.6	257.7	90.3
H(15)	-389.5	256.7	-89.1
H(16)	-261.3	344.3	-1.3
H(17)	-31.7	-104.6	0.0
H(18)	109.3	0.0	0.0

[a] Coordinates are in pm.

Table A2.19 Calculated coordinates at the MP2/6-311++G** level for Meldrum's acid. [a]

Atom	*x*	*y*	*z*
C(1)	112.9	171.8	0.0
C(2)	-25.8	109.5	0.0
C(3)	-136.5	212.3	0.0
O(4)	-46.3	31.2	118.5
O(5)	46.3	31.2	-118.5
C(6)	13.9	-90.6	128.0
C(7)	13.9	-90.6	-128.0
C(8)	74.8	-144.2	0.0
O(9)	13.9	-150.6	232.3
O(10)	13.9	-150.6	-232.3
H(11)	191.9	96.3	0.0
H(12)	124.3	233.9	89.2
H(13)	124.3	233.9	-89.2
H(14)	-128.4	274.7	-89.3
H(15)	-128.4	274.7	89.3
H(16)	-232.9	161.3	0.0
H(17)	182.0	-121.5	0.0
H(18)	65.7	-252.9	0.0

[a] Coordinates are in pm.

Figure A2.3 Experimental and final weighted difference (experimental – theoretical) MICs from the GED study of Meldrum's acid.

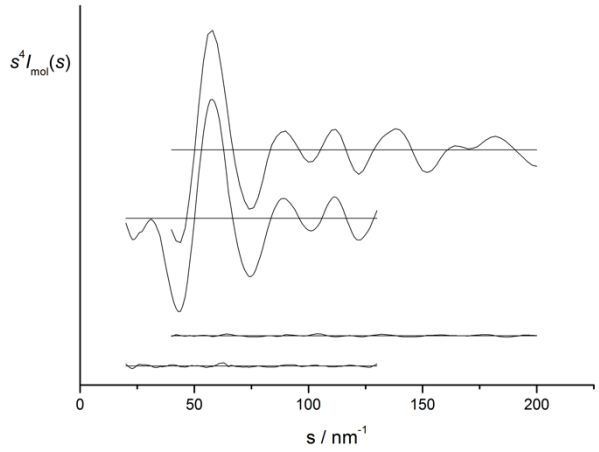

Pyrolysis of Meldrum's acid

Table A2.20 Nozzle-to-plate distance (mm), weighting function (nm^{-1}), correlation parameter, scale factor and electron wavelength (pm) used in the VHT-GED study of Meldrum's acid, CO_2, acetone, ketene and diketene by the pyrolysis of Meldrum's acid.

Nozzle-to-plate distance[a]	186.3
Δs	2
s_{min}	44
sw_1	64
sw_2	190
s_{max}	220
Correlation parameter	0.472
Scale factor[b]	1.891(33)
Electron wavelength	6.18

[a] Determined by reference to the scattering pattern of benzene vapour.

[b] Values in parentheses are the estimated standard deviations.

Table A2.21 Parameter values for Meldrum's acid, CO_2, acetone, ketene and diketene from *ab initio* calculations at the MP2 level for a range of basis sets.[a,b]

Parameter	6-31G*	6-311G*	6-311+G*	6-311++G**
Meldrum's acid				
*r*C(6)=O(9)	121.1	120.2	120.4	120.4
*r*C(7)=O(10)	121.1	120.2	120.4	120.4
*r*C(2)–O(4)	143.9	143.3	143.6	143.4
*r*C(2)–O(5)	143.9	143.3	143.6	143.4
*r*C(6)–O(4)	136.7	136.2	136.1	136.2
*r*C(7)–O(5)	136.7	136.2	136.1	136.2
*r*C(1)–C(2)	151.8	151.9	151.9	152.1
*r*C(2)–C(3)	150.9	151.0	150.9	151.1
*r*C(6)–C(8)	151.2	151.4	151.4	151.5
*r*C(7)–C(8)	151.2	151.4	151.4	151.5
*r*C–H average	109.2	109.2	109.2	109.3
∠H(11)–C–C	111.9	112.2	112.3	112.1
∠H(16)–C–C	109.0	109.0	109.3	109.2
∠H(11)–C–H(12)	108.5	108.3	108.4	108.5
∠H(11)–C–H(13)	108.5	108.3	108.4	108.5
∠H(16)–C–H(14)	109.4	109.3	109.3	109.4
∠H(16)–C–H(15)	109.4	109.3	109.3	109.4
∠C(H_3)–C–C(H_3)	113.2	113.1	113.1	112.9
∠C(3)–C–O	105.3	105.3	105.4	105.5
∠C(1)–C–O	110.5	110.5	110.7	110.7
∠C(2)–O–C(6)	119.5	119.0	118.9	118.8
∠C(2)–O–C(7)	119.5	119.0	118.9	118.8
∠O(4)–C=O(9)	120.2	120.4	120.4	120.4
∠O(5)–C=O(10)	120.2	120.4	120.4	120.4
∠C(8)–C–O(4)	115.8	115.7	115.9	115.8
∠C(8)–C–O(5)	115.8	115.7	115.9	115.8
∠C–C–H(17)	108.9	108.9	108.9	108.7
∠H(17)–C(8)–H(18)	106.7	106.3	106.1	106.8

ϕO(4)–C(2)–C(1)–O(5)	124.3	124.4	124.0	124.0
ϕC(1)–C(2)–O(4)–C(6)	-79.1	-76.5	-75.6	-75.4
ϕC(2)–O–C=O	173.3	170.9	169.7	169.9
ϕC(2)–O(4)–C(6)–C(8)	-7.8	-10.8	-12.0	-11.8
ϕO(4)–C–C–H(17)	92.9	97.0	98.2	97.2
ϕC(6)–C(8)–H(17)–H(18)	117.2	116.7	116.8	117.0
CO_2				
*r*C=O	118.0	116.9	117.0	117.0
Acetone				
*r*C=O	122.8	121.8	122.1	122.0
*r*C–C	151.3	151.6	151.5	151.6
*r*C–H average	109.3	109.2	109.3	109.3
∠H(23/29)–C–C	109.4	109.5	110.0	110.1
∠H(24/27)–C–C	110.3	110.1	109.7	109.2
∠H(28/31)–C–C	110.3	110.8	110.7	110.5
∠H(23/29)–C–H(28/31)	109.8	109.9	110.0	110.2
∠H(23/29)–C–H(24/27)	109.8	109.4	109.3	109.5
∠C–C=O	121.7	121.9	121.8	122.0
∠C–C–C	116.5	116.3	116.3	116.1
ϕH(23/29)–C–C=O	-2.8	-4.2	-6.7	-8.4
Ketene				
*r*C=O	118.1	116.9	116.9	116.8
*r*C=C	132.0	132.0	132.1	132.2
*r*C–H(33/34)	108.1	108.0	108.0	108.0
∠H(33/34)–C=C	119.6	119.5	119.5	119.1
∠H(33)–C–H(34)	120.7	121.0	121.0	121.8
ϕO=C=C–H(33/34)	180.0	180.0	180.0	180.0
Diketene				
*r*C=O	119.9	118.8	119.0	118.9
*r*C=C	132.7	132.8	132.9	133.0
*r*C(37)–O(41)	140.4	140.1	140.0	140.1
*r*C(43)–O(41)	141.9	140.8	141.2	141.1

*r*C(37)–C(38)	152.6	152.9	152.8	152.9
*r*C(38)–C(43)	150.3	150.6	150.6	150.7
*r*C(38)–H(39)	109.3	109.1	109.2	109.1
*r*C(38)–H(40)	109.3	109.1	109.2	109.1
*r*C(44)–H(45)	108.3	108.3	108.3	108.3
*r*C(44)–H(46)	108.3	108.2	108.2	108.2
*r*C–H average	108.8	108.7	108.7	108.7
∠C=C–H(45)	121.0	120.7	120.9	120.8
∠C=C–H(16)	120.0	120.0	119.8	119.5
∠O–C=C	126.3	126.7	126.4	126.5
∠C–O–C	90.5	90.7	90.8	90.8
∠O–C=O	127.6	127.5	127.5	127.5
∠O=C–C	139.2	139.4	139.4	139.4
∠C(37)–C–H	114.3	114.2	114.1	114.0
ϕH(39)–C–C=O	64.0	64.3	64.2	64.4

[a] Distances are in pm and angles and dihedral angles are in °.

[b] Atom numbering follows 1 – 18 for Meldrum's acid, 19 – 21 for CO_2, 22 – 31 for acetone, 32 – 36 for ketene and 43 – 46 for diketene. See Figure 4.11.

Table A2.22 Refined and calculated (MP2/6-311++G**) amplitudes of vibration (u), associated r_a distances and corresponding correction values (k) for the r_{h1} refinement of Meldrum's acid, CO_2, acetone, ketene and diketene from the pyrolysis of Meldrum's acid.[a,b]

	Atom pair	r_a	u_{GED}	k	$u_{calc.}$	Restraint
u_1	C(32)–H(33)	108.3(1)	7.4(8)	0.3	7.4	7.4(7)
u_2	C(44)–H(46)	108.0(1)	7.4(Tied to u_6)	0.3	7.5	
u_3	C(44)–H(45)	108.0(1)	7.5(Tied to u_6)	0.3	7.5	
u_4	C(22)–H(23)	109.2(1)	7.5(9)	0.4	7.7	7.7(8)
u_5	C(8)–H(18)	109.3(1)	6.7(Tied to u_8)	0.4	7.6	
u_6	C(38)–H(40)	109.1(1)	7.6(9)	0.4	7.6	7.6(8)
u_7	C(3)–H(16)	109.3(1)	6.7(Tied to u_8)	0.4	7.6	
u_8	C(1)–H(11)	109.3(1)	6.7(8)	0.4	7.6	7.6(8)
u_9	C(3)–H(14)	109.3(1)	6.7(Tied to u_8)	0.4	7.6	
u_{10}	C(1)–H(12)	109.3(1)	6.7(Tied to u_8)	0.4	7.6	
u_{11}	C(26)–H(28)	109.2(1)	7.4(Tied to u_4)	0.4	7.6	
u_{12}	C(26)–H(27)	109.2(1)	7.4(Tied to u_4)	0.4	7.7	
u_{13}	C(8)–H(17)	109.3(1)	6.8(Tied to u_8)	0.4	7.6	
u_{14}	C(35)–O(36)	116.8(1)	3.5(3)	0.1	3.5	3.5(3)
u_{15}	C(19)–O(20)	117.0(1)	3.4(3)	0.1	3.5	3.5(3)
u_{16}	C(37)–O(42)	118.9(2)	3.6(4)	0.1	3.7	3.7(4)
u_{17}	C(7)–O(10)	120.0(3)	3.5(4)	0.1	3.7	3.7(4)
u_{18}	C(25)–O(30)	121.9(3)	3.8(4)	0.1	3.8	3.8(4)
u_{19}	C(32)–C(35)	132.2(2)	4.1(4)	0.1	4.1	4.1(4)
u_{20}	C(43)–C(44)	133.0(1)	4.1(4)	0.1	4.1	4.1(4)
u_{21}	O(4)–C(6)	136.3(2)	4.7(Tied to u_{24})	0.1	4.8	
u_{22}	C(37)–O(41)	139.9(3)	5.2(5)	0.0	5.2	5.2(5)
u_{23}	O(41)–C(43)	141.1(3)	5.0(Tied to u_{22})	0.2	5.0	
u_{24}	C(2)–O(5)	147.8(11)	5.1(5)	0.3	5.2	5.2(5)
u_{25}	C(38)–C(43)	150.9(6)	5.0(Tied to u_{30})	0.3	5.0	
u_{26}	C(2)–C(3)	151.3(6)	4.3(Tied to u_{29})	0.2	5.0	
u_{27}	C(7)–C(8)	151.5(5)	4.4(Tied to u_{29})	0.0	5.2	

u_{28}	C(25)–C(26)	151.6(2)	5.1(5)	0.2	5.2	5.2(5)
u_{29}	C(1)–C(2)	152.2(6)	4.4(5)	0.2	5.2	5.2(5)
u_{30}	C(37)–C(38)	152.9(2)	5.3(5)	0.2	5.3	5.3(5)
u_{31}	H(17)···H(18)	174.7(8)	12.5(fixed)	0.1	12.5	
u_{32}	H(27)···H(28)	174.8(15)	12.5(fixed)	-0.4	12.5	
u_{33}	H(11)···H(13)	176.5(3)	12.3(fixed)	-0.1	12.3	
u_{34}	H(14)···H(16)	177.5(3)	12.3(fixed)	0.0	12.3	
u_{35}	H(12)···H(13)	170.2(10)	12.4(fixed)	-0.1	12.4	
u_{36}	H(23)···H(24)	177.1(2)	12.8(fixed)	-0.5	12.8	
u_{37}	H(14)···H(15)	178.5(12)	12.3(fixed)	0.0	12.3	
u_{38}	H(28)···H(29)	177.9(5)	12.4(fixed)	-0.5	12.4	
u_{39}	H(39)···H(40)	179.1(5)	12.3(fixed)	0.0	12.3	
u_{40}	H(45)···H(46)	185.4(6)	11.9(fixed)	-0.9	11.9	
u_{41}	H(33)···H(34)	187.5(8)	12.0(fixed)	-1.4	12.0	
u_{42}	C(37)···C(43)	200.0(4)	5.1(5)	-0.1	5.1	5.1(5)
u_{43}	H(33)···C(35)	205.7(5)	10.5(fixed)	-1.6	10.5	
u_{44}	C(43)···H(46)	207.8(6)	10.1(fixed)	-0.5	10.1	
u_{45}	C(43)···H(45)	209.0(3)	10.1(fixed)	-0.6	10.1	
u_{46}	C(38)···O(41)	212.5(4)	5.1(5)	-0.3	5.1	5.1(5)
u_{47}	C(7)···H(18)	212.8(7)	11.0(fixed)	0.1	11.0	
u_{48}	C(7)···H(17)	212.5(7)	11.4(fixed)	-0.3	11.4	
u_{49}	C(2)···H(16)	213.0(6)	10.9(fixed)	-0.2	10.9	
u_{50}	C(2)···H(15)	213.1(6)	11.0(fixed)	-0.2	11.0	
u_{51}	H(24)···C(25)	213.9(13)	12.6(fixed)	0.6	12.6	
u_{52}	C(2)···H(12)	217.4(6)	11.1(fixed)	-0.2	11.1	
u_{53}	H(23)···C(25)	214.8(8)	11.4(fixed)	0.2	11.4	
u_{54}	C(25)···H(28)	215.7(5)	11.9(fixed)	0.7	11.9	
u_{55}	C(2)···H(11)	217.5(6)	10.9(fixed)	-0.2	10.9	
u_{56}	H(11)···H(17)	219.1(51)	31.9(fixed)	8.1	31.9	
u_{57}	C(37)···H(40)	220.2(3)	11.7(fixed)	-0.3	11.7	
u_{58}	H(40)···C(43)	221.3(6)	11.2(fixed)	-0.2	11.2	
u_{59}	O(4)···O(9)	222.7(3)	5.3(6)	0.3	5.5	5.5(6)

u_{60}	O(41)···O(42)	231.8(4)	5.9(6)	-0.5	5.9	5.9(6)
u_{61}	O(20)···O(21)	233.4(2)	4.1(4)	-0.5	4.1	4.1(4)
u_{62}	C(3)···O(4)	234.8(5)	7.3(7)	0.5	7.3	7.3(7)
u_{63}	O(4)···O(5)	238.9(14)	6.7(7)	-0.4	6.7	6.7(7)
u_{64}	C(22)···O(30)	239.4(4)	6.4(6)	-0.1	6.4	6.4(6)
u_{65}	C(8)···O(10)	239.1(10)	6.4(6)	-0.2	6.3	6.3(6)
u_{66}	C(2)···C(6)	239.5(2)	6.8(7)	-1.1	6.8	6.8(7)
u_{67}	C(1)···O(4)	242.8(6)	7.5(8)	0.0	7.5	7.5(8)
u_{68}	O(5)···C(8)	243.5(7)	6.5(6)	-1.0	6.5	6.5(6)
u_{69}	O(41)···C(44)	243.9(5)	6.6(8)	-0.7	6.6	6.6(7)
u_{70}	C(32)···O(36)	248.2(2)	4.6(5)	-0.7	4.6	4.6(5)
u_{71}	C(1)···C(3)	252.7(10)	7.5(9)	0.2	7.7	7.7(8)
u_{72}	H(29)···O(30)	259.1(14)	18.0(fixed)	6.4	18.0	
u_{73}	C(38)···O(42)	255.0(3)	6.3(6)	0.0	6.3	6.3(6)
u_{74}	C(6)···C(7)	254.5(10)	7.4(9)	-1.5	7.6	7.6(8)
u_{75}	H(12)···H(15)	261.1(12)	26.5(fixed)	4.8	26.5	
u_{76}	O(5)···H(16)	260.5(34)	18.3(fixed)	0.7	18.3	
u_{77}	C(22)···C(26)	256.9(6)	7.7(9)	0.0	7.7	7.7(8)
u_{78}	O(4)···H(15)	257.6(10)	19.4(fixed)	0.9	19.4	
u_{79}	O(9)···H(18)	259.0(12)	14.8(fixed)	2.0	14.8	
u_{80}	H(27)···H(31)	290.0(29)	41.5(fixed)	29.9	41.5	
u_{81}	C(38)···C(44)	266.5(7)	6.8(8)	0.0	6.8	6.8(7)
u_{82}	O(5)···H(13)	274.6(29)	19.0(fixed)	0.6	19.0	
u_{83}	C(8)···H(11)	266.6(38)	21.8(fixed)	2.9	21.8	
u_{84}	C(2)···C(8)	273.4(12)	8.1(8)	-0.7	7.6	7.6(8)
u_{85}	O(41)···H(45)	270.8(7)	16.1(fixed)	-1.3	16.1	
u_{86}	O(5)···H(11)	273.7(35)	18.6(fixed)	0.0	18.6	
u_{87}	C(3)···H(12)	278.9(10)	18.7(fixed)	0.7	18.7	
u_{88}	C(22)···H(28)	280.4(32)	27.0(fixed)	5.9	27.0	
u_{89}	C(1)···H(15)	276.4(10)	18.0(fixed)	0.7	18.0	
u_{90}	O(5)···C(6)	280.7(6)	9.4(8)	-1.7	8.3	8.3(8)
u_{91}	C(7)···H(11)	285.0(45)	27.3(fixed)	0.2	27.3	

u_{92}	O(9)···H(17)	285.6(18)	17.3(fixed)	-1.1	17.3	
u_{93}	H(24)···C(26)	288.6(38)	29.8(fixed)	3.0	29.8	
u_{94}	H(39)···O(41)	286.9(4)	13.9(fixed)	-1.5	13.9	
u_{95}	H(28)···H(31)	281.5(119)	73.4(fixed)	3.1	73.4	
u_{96}	O(5)···H(17)	297.0(15)	19.9(fixed)	-1.4	19.9	
u_{97}	C(1)···H(17)	298.2(41)	29.1(fixed)	1.0	29.1	
u_{98}	C(38)···H(46)	301.1(12)	16.0(fixed)	0.4	16.0	
u_{99}	H(40)···O(42)	302.4(4)	14.3(fixed)	-0.2	14.3	
u_{100}	H(24)···O(30)	298.3(30)	28.6(fixed)	-3.8	28.6	
u_{101}	C(1)···C(7)	306.8(28)	13.7(18)	-2.0	16.2	16.2(20)
u_{102}	C(2)···H(17)	309.1(27)	24.2(fixed)	-0.5	24.2	
u_{103}	O(30)···H(31)	308.8(21)	23.0(fixed)	-5.2	23.0	
u_{104}	H(34)···O(36)	312.4(6)	12.8(fixed)	-3.4	12.8	
u_{105}	H(39)···C(44)	316.9(9)	14.8(fixed)	-0.1	14.8	
u_{106}	C(1)···C(8)	316.0(26)	13.9(11)	-1.0	14.1	14.1(10)
u_{107}	O(42)···C(43)	317.3(4)	5.4(5)	-1.0	5.4	5.4(5)
u_{108}	O(5)···H(18)	324.8(8)	12.9(fixed)	-3.0	12.9	
u_{109}	C(37)···C(44)	330.5(4)	5.8(6)	-1.6	5.8	5.9(6)
u_{110}	H(40)···H(46)	332.2(14)	23.2(fixed)	1.1	23.2	
u_{111}	H(24)···H(27)	314.4(105)	68.2(fixed)	-9.0	68.2	
u_{112}	O(41)···H(46)	338.8(6)	9.8(fixed)	-1.7	9.8	
u_{113}	C(6)···H(12)	343.9(19)	28.0(fixed)	-2.4	28.0	
u_{114}	C(1)···H(16)	344.2(10)	10.6(fixed)	-1.7	10.6	
u_{115}	C(3)···H(11)	346.3(10)	10.6(fixed)	-1.8	10.6	
u_{116}	C(22)···H(29)	342.6(9)	12.6(fixed)	-6.4	12.6	
u_{117}	C(2)···O(10)	351.7(9)	8.8(8)	-2.1	7.6	7.6(8)
u_{118}	C(38)···H(45)	356.5(6)	10.3(fixed)	-1.5	10.3	
u_{119}	C(3)···C(6)	360.5(6)	9.0(8)	-1.4	8.1	8.1(8)
u_{120}	C(6)···O(10)	361.6(12)	11.9(10)	-2.5	10.2	10.2(10)
u_{121}	H(13)···H(17)	368.0(42)	35.3(fixed)	-1.2	35.3	
u_{122}	H(11)···H(18)	368.9(41)	23.7(fixed)	1.0	23.7	
u_{123}	C(2)···H(18)	372.2(9)	11.4(fixed)	-2.9	11.4	

u_{124} C(6)···H(16)	375.0(13)	19.9(fixed)	-0.6	19.9	
u_{125} H(12)···H(16)	376.3(10)	18.9(fixed)	-2.1	18.9	
u_{126} H(11)···H(14)	374.0(10)	18.7(fixed)	-2.2	18.7	
u_{127} H(23)···H(28)	369.9(15)	23.1(fixed)	-9.2	23.1	
u_{128} H(24)···H(29)	372.9(14)	26.2(fixed)	-6.1	26.2	
u_{129} O(9)···H(11)	375.7(18)	37.2(fixed)	-1.9	37.2	
u_{130} C(37)···H(45)	387.4(6)	13.9(fixed)	-3.1	13.9	
u_{131} C(8)···H(12)	389.7(31)	22.9(fixed)	-3.0	22.9	
u_{132} C(6)···H(15)	391.0(11)	19.2(fixed)	-1.4	19.2	
u_{133} O(4)···O(10)	397.1(9)	10.0(8)	-3.1	10.4	10.4(10)
u_{134} C(37)···H(46)	401.7(8)	12.3(fixed)	-2.0	12.3	
u_{135} C(1)···O(9)	403.1(14)	21.9(20)	-3.7	23.7	23.7(20)
u_{136} H(40)···H(45)	410.8(8)	16.7(fixed)	-1.9	16.7	
u_{137} C(3)···C(8)	415.2(13)	8.0(8)	-1.3	7.8	7.8(8)
u_{138} O(10)···H(13)	427.2(37)	38.1(fixed)	-3.7	38.1	
u_{139} C(1)···H(18)	423.0(26)	16.0(fixed)	-3.2	16.0	
u_{140} H(23)···H(29)	422.6(16)	15.1(fixed)	-6.3	15.1	
u_{141} H(11)···H(16)	426.6(11)	14.2(fixed)	-3.1	14.2	
u_{142} C(8)···H(16)	435.2(22)	16.9(fixed)	-0.9	16.9	
u_{143} O(42)···C(44)	446.1(4)	6.2(6)	-3.2	6.2	6.2(6)
u_{144} C(3)···O(9)	453.6(6)	11.8(9)	-2.5	10.2	10.2(10)
u_{145} O(10)···H(16)	463.2(42)	26.0(fixed)	-1.5	26.0	
u_{146} C(3)···H(17)	459.6(26)	23.9(fixed)	-1.6	23.9	
u_{147} O(9)···O(10)	458.1(17)	18.1(20)	-3.8	15.2	15.2(20)
u_{148} O(10)···H(14)	473.3(28)	23.1(fixed)	-1.9	23.1	
u_{149} C(8)···H(15)	472.1(12)	15.1(fixed)	-2.4	15.1	
u_{150} H(13)···H(18)	495.9(25)	25.1(fixed)	-5.3	25.1	
u_{151} O(42)···H(45)	495.1(7)	15.3(fixed)	-5.1	15.3	
u_{152} H(16)···H(17)	500.2(26)	24.9(fixed)	-2.7	24.9	
u_{153} C(3)···H(18)	505.9(14)	13.5(fixed)	-3.8	13.5	
u_{154} H(16)···H(18)	510.7(28)	23.2(fixed)	-3.0	23.2	
u_{155} H(15)···H(17)	507.3(27)	28.0(fixed)	-2.0	28.0	

u_{156} O(42)···H(46)	518.9(8)	12.6(fixed)	-3.8	12.6
u_{157} H(14)···H(18)	566.0(16)	19.1(fixed)	-5.2	19.1

[a] Distances in pm. Values in parentheses are the standard deviations in terms of the last digits. Atom numbering follows 1 – 18 for Meldrum's acid, 19 – 21 for CO_2, 22 – 31 for acetone, 32 – 36 for ketene and 43 – 46 for diketene.

[b] Unrefined amplitudes of vibration were fixed at the values obtained using the MP2/6-311++G** force field.

Table A2.23 Calculated coordinates at the MP2/6-311++G** level for Meldrum's acid, CO_2, acetone, ketene and diketene. [a]

Atom	*x*	*y*	*z*
Meldrum's acid			
C(1)	112.9	171.8	0.0
C(2)	-25.8	109.5	0.0
C(3)	-136.5	212.3	0.0
O(4)	-46.3	31.2	118.5
O(5)	46.3	31.2	-118.5
C(6)	13.9	-90.6	128.0
C(7)	13.9	-90.6	-128.0
C(8)	74.8	-144.2	0.0
O(9)	13.9	-150.6	232.3
O(10)	13.9	-150.6	-232.3
H(11)	191.9	96.3	0.0
H(12)	124.3	233.9	89.2
H(13)	124.3	233.9	-89.2
H(14)	-128.4	274.7	-89.3
H(15)	-128.4	274.7	89.3
H(16)	-232.9	161.3	0.0
H(17)	182.0	-121.5	0.0
H(18)	65.7	-252.9	0.0
CO_2			
C(19)	0.0	0.0	0.0
O(20)	0.0	0.0	117.0
O(21)	0.0	0.0	-117.0
Acetone			
C(22)	0.0	128.6	-61.7
H(23)	-15.0	214.0	4.4
H(24)	96.0	138.8	-113.4
C(25)	0.0	0.0	18.5
C(26)	0.0	-128.6	-61.7

H(27)	-96.0	-138.8	-113.4
H(28)	78.1	-125.8	-138.3
H(29)	15.0	-214.0	4.4
O(30)	0.0	0.0	140.5
H(31)	-78.1	125.8	-138.3
Ketene			
C(32)	0.0	0.0	-121.8
H(33)	0.0	94.3	-174.4
H(34)	0.0	-94.3	-174.4
C(35)	0.0	0.0	10.4
H(36)	0.0	0.0	127.2
Diketene			
C(37)	-105.0	-0.5	0.0
C(38)	-5.4	115.5	0.0
H(39)	-9.2	177.3	89.9
H(40)	-9.2	177.3	-89.9
O(41)	-3.9	-97.4	0.0
O(42)	-222.6	-18.5	0.0
C(43)	95.1	3.2	0.0
C(44)	226.8	-15.3	0.0
H(45)	268.7	-115.1	0.0
H(46)	292.6	70.6	0.0

[a] Coordinates are in pm.

Figure A2.4 Experimental and final weighted difference (experimental – theoretical) MIC for Meldrum's acid, CO_2, acetone, ketene and diketene from the GED study of the pyrolysis of Meldrum's acid.

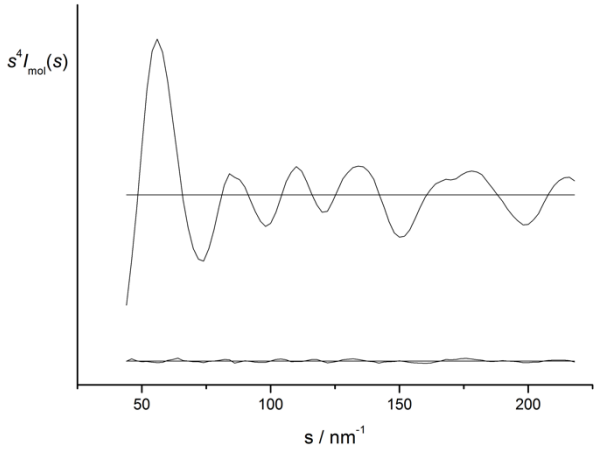

APPENDIX 3

Tris(chloromethyl)amine, $N(CH_2Cl)_3$: A combined GED, Raman spectroscopy and computational investigation

Table A3.1 Nozzle-to-plate distances (mm), weighting functions (nm^{-1}), correlation parameters, scale factors and electron wavelengths (pm) used in the electron-diffraction study of tris(chloromethyl)amine.

Nozzle-plate distance[a]	256.89	94.29
Δs	2	4
s_{min}	30	92
sw_1	50	112
sw_2	94	248
s_{max}	110	288
Correlation parameter	0.458	0.403
Scale factor[b]	3.040(129)	3.409(271)
Electron wavelength	6.02	6.02

[a] Determined by reference to the scattering pattern of benzene vapour.

[b] Values in parentheses are the estimated standard deviations.

Table A3.2 Theoretical geometrical parameters at the MP2 level with the 6-31G*, 6-311G*, 6-311+G*, cc-pVDZ, aug-cc-pVDZ, cc-pVTZ and aug-cc-pVTZ basis sets for tris(chloromethyl)amine.[a,b]

Parameter	6-31G*	6-311G*	6-311+G*	cc-pVDZ	aug-cc-pVDZ	cc-pVTZ	aug-cc-pVTZ
*r*C(2)–Cl(11)	182.2	182.3	182.4	183.1	185.0	182.3	182.4
*r*C(5)–Cl(12)	180.7	179.9	180.7	181.5	180.8	179.2	178.9
*r*C(8)–Cl(13)	182.3	182.5	182.4	183.1	184.4	182.8	183.0
*r*N(1)–C(2)	141.6	141.8	141.4	141.8	142.1	141.5	141.7
*r*N(1)–C(5)	142.6	143.3	142.5	143.0	144.4	142.3	143.6
*r*N(1)–C(8)	141.5	141.6	141.4	141.8	142.4	141.1	141.3
*r*C(2)–H(3)	109.0	108.8	108.9	109.9	109.7	108.5	108.5
*r*C(2)–H(4)	108.9	108.8	108.8	109.8	109.6	108.4	108.5
*r*C(5)–H(6)	109.0	109.1	108.9	109.9	109.7	108.8	109.0
*r*C(5)–H(7)	109.0	108.8	108.9	109.9	110.0	108.5	108.6
*r*C(8)–H(9)	108.9	108.8	108.8	109.8	109.6	108.5	108.5
*r*C(8)–H(10)	109.0	108.9	108.9	109.9	109.6	108.5	108.6
∠N(1)–C(2)–Cl(11)	115.2	115.5	114.8	115.2	115.3	115.1	114.9
∠N(1)–C(5)–Cl(12)	112.3	111.4	111.9	112.2	110.8	111.2	110.9
∠N(1)–C(8)–Cl(13)	115.3	115.5	114.8	115.2	115.1	115.5	115.2

∠N(1)–C(2)–H(3)	109.7	109.3	109.9	109.9	110.2	109.7	109.8
∠N(1)–C(2)–H(4)	109.9	109.8	110.1	110.1	110.2	110.0	110.1
∠N(1)–C(5)–H(6)	110.9	112.1	111.0	110.9	109.3	112.4	112.4
∠N(1)–C(5)–H(7)	110.7	109.6	111.0	111.0	112.5	109.2	109.2
∠N(1)–C(8)–H(9)	109.9	109.6	110.1	110.1	110.1	110.0	110.1
∠N(1)–C(8)–H(10)	109.8	109.8	109.9	109.9	109.8	110.2	110.3
∠Cl(11)–C(2)–H(3)	105.5	105.4	105.4	105.2	104.2	104.9	104.8
∠Cl(11)–C(2)–H(4)	106.3	106.2	106.1	106.0	105.5	106.0	106.0
∠Cl(12)–C(5)–H(6)	106.7	106.4	106.7	106.7	107.3	106.3	106.3
∠Cl(12)–C(5)–H(7)	106.8	107.4	106.7	106.6	106.2	107.5	107.6
∠Cl(13)–C(8)–H(9)	106.2	106.1	106.1	106.0	105.8	105.7	105.6
∠Cl(13)–C(8)–H(10)	105.5	105.2	105.4	105.2	104.5	104.6	104.4
∠C(2)–N(1)–C(5)	117.8	116.5	117.8	117.6	115.3	116.2	116.0
∠C(2)–N(1)–C(8)	120.7	119.6	120.6	120.4	116.0	119.1	115.3
∠C(5)–N(1)–C(8)	118.0	116.9	117.8	117.6	118.8	116.1	118.7
ϕCl(11)–C(2)–N(1)–C(5)	-71.6	-68.1	-71.9	-70.1	-61.9	-64.4	-62.5
ϕCl(12)–C(5)–N(1)–C(2)	-98.0	-79.6	-101.0	-102.8	-144.7	-71.5	-68.9
ϕCl(13)–C(8)–N(1)–C(5)	71.5	65.8	72.0	70.2	62.6	64.1	65.5

Energy (Hartrees)	-1550.9255	-1551.0915	-1551.1089	-1551.0561	-1551.1411	-1551.4456	-1551.4794

[a] The distances are given in pm. Bond angles and dihedral angles are in °.

[b] Refer to Figure 5.3 in the main text for atom numbering.

Table A3.3 Refined and calculated (M06-2X/aug-cc-pVDZ) amplitudes of vibration (u), associated r_a distances and corresponding correction values (k) for the $r_{a3,1}$ refinement of tris(chloromethyl)amine.[a,b]

	Atom pair	r_a	u_{GED}	k	$u_{calc.}$	Restraint
u_1	N(1)–C(2)	141.3(5)	4.9(Tied to u_3)	1.8	4.8	
u_2	N(1)–C(5)	142.7(8)	5.1(Tied to u_3)	1.5	4.9	
u_3	N(1)–C(8)	141.0(5)	5.0(4)	1.4	4.8	4.8(5)
u_4	C(2)–H(3)	111.3(6)	8.4(Tied to u_8)	2.6	7.5	
u_5	C(2)–H(4)	111.5(6)	8.4(Tied to u_8)	2.9	7.5	
u_6	C(2)–Cl(11)	182.3(4)	6.0(Tied to u_9)	3.0	6.2	
u_7	C(5)–H(6)	114.3(6)	8.4(Tied to u_8)	5.6	7.5	
u_8	C(5)–H(7)	114.7(6)	8.4(7)	6.0	7.6	7.6(8)
u_9	C(5)–Cl(12)	183.1(8)	5.6(4)	6.0	5.8	5.8(6)
u_{10}	C(8)–H(9)	112.3(6)	8.4(Tied to u_8)	3.6	7.6	
u_{11}	C(8)–H(10)	112.1(6)	8.4(Tied to u_8)	3.4	7.6	
u_{12}	C(8)–Cl(13)	182.4(4)	5.9(Tied to u_9)	3.0	6.1	
u_{13}	N(1)···H(3)	207.0(13)	10.1(fixed)	3.3	10.1	
u_{14}	N(1)···H(4)	208.1(13)	10.1(fixed)	4.0	10.1	
u_{15}	N(1)···H(6)	212.8(14)	10.2(fixed)	4.5	10.2	
u_{16}	N(1)···H(7)	211.2(14)	10.3(fixed)	5.8	10.3	
u_{17}	N(1)···H(9)	206.5(13)	10.1(fixed)	2.8	10.1	
u_{18}	N(1)···H(10)	207.7(13)	10.2(fixed)	3.6	10.2	
u_{19}	N(1)···Cl(11)	274.0(6)	8.5(Tied to u_{20})	3.6	7.4	
u_{20}	N(1)···Cl(12)	269.1(10)	8.2(4)	4.1	7.2	7.2(7)
u_{21}	N(1)···Cl(13)	273.1(6)	8.4(Tied to u_{20})	2.7	7.3	
u_{22}	C(2)···C(5)	242.0(22)	7.7(Tied to u_{25})	1.8	7.0	
u_{23}	C(2)···H(6)	255.9(38)	14.8(fixed)	5.5	14.8	
u_{24}	C(2)···H(7)	303.8(37)	20.1(fixed)	2.4	20.1	
u_{25}	C(2)···C(8)	242.6(19)	7.3(5)	1.1	6.6	6.6(7)
u_{26}	C(2)···H(9)	252.4(40)	15.4(fixed)	0.3	15.4	
u_{27}	C(2)···H(10)	330.9(22)	10.3(fixed)	3.5	10.3	
u_{28}	C(2)···Cl(12)	385.9(22)	18.3(16)	2.7	15.5	15.5(20)
u_{29}	C(2)···Cl(13)	350.8(32)	16.9(Tied to u_{28})	0.7	14.3	

u_{30}	H(3)···H(4)	182.4(33)	12.2(fixed)	3.4	12.2
u_{31}	H(3)···C(5)	267.5(49)	15.2(fixed)	2.9	15.2
u_{32}	H(3)···H(6)	241.4(85)	23.7(fixed)	5.0	23.7
u_{33}	H(3)···H(7)	350.0(64)	22.6(fixed)	2.9	22.6
u_{34}	H(3)···C(8)	331.6(22)	10.2(fixed)	3.0	10.2
u_{35}	H(3)···H(9)	346.9(47)	16.9(fixed)	1.9	16.9
u_{36}	H(3)···H(10)	402.3(31)	14.6(fixed)	5.6	14.6
u_{37}	H(3)···Cl(11)	236.2(22)	11.2(fixed)	4.0	11.2
u_{38}	H(3)···Cl(12)	390.5(50)	32.7(fixed)	2.6	32.7
u_{39}	H(3)···Cl(13)	450.7(21)	14.2(fixed)	2.1	14.2
u_{40}	H(4)···C(5)	335.7(18)	10.1(fixed)	3.6	10.1
u_{41}	H(4)···H(6)	362.7(39)	16.2(fixed)	6.8	16.2
u_{42}	H(4)···H(7)	393.1(33)	19.5(fixed)	4.1	19.5
u_{43}	H(4)···C(8)	257.1(43)	14.8(fixed)	2.1	14.8
u_{44}	H(4)···H(9)	218.3(71)	21.8(fixed)	0.8	21.8
u_{45}	H(4)···H(10)	346.4(46)	17.1(fixed)	3.9	17.1
u_{46}	H(4)···Cl(11)	237.3(15)	11.3(fixed)	3.7	11.3
u_{47}	H(4)···Cl(12)	461.0(24)	20.9(fixed)	3.3	20.9
u_{48}	H(4)···Cl(13)	372.9(84)	26.9(fixed)	0.2	26.9
u_{49}	C(5)···C(8)	239.7(19)	7.4(Tied to u_{25})	2.6	6.8
u_{50}	C(5)···H(9)	333.6(16)	10.2(fixed)	3.8	10.2
u_{51}	C(5)···H(10)	268.9(48)	16.5(fixed)	4.5	16.5
u_{52}	C(5)···Cl(11)	321.9(27)	21.6(Tied to u_{28})	1.7	18.3
u_{53}	C(5)···Cl(13)	315.0(48)	19.4(Tied to u_{28})	2.0	16.4
u_{54}	H(6)···H(7)	185.7(33)	12.3(fixed)	8.9	12.3
u_{55}	H(6)···C(8)	335.7(18)	10.4(fixed)	5.1	10.4
u_{56}	H(6)···H(9)	416.3(25)	13.7(fixed)	5.8	13.7
u_{57}	H(6)···H(10)	374.3(46)	16.9(fixed)	6.4	16.9
u_{58}	H(6)···Cl(11)	311.0(55)	27.0(fixed)	5.0	27.0
u_{59}	H(6)···Cl(12)	243.5(23)	11.2(fixed)	9.8	11.2
u_{60}	H(6)···Cl(13)	406.5(63)	19.9(fixed)	4.2	19.9
u_{61}	H(7)···C(8)	260.2(45)	17.7(fixed)	5.7	17.7
u_{62}	H(7)···H(9)	361.4(47)	17.6(fixed)	6.3	17.6

u_{63}	H(7)···H(10)	289.7(78)	34.0(fixed)	4.4	34.0	
u_{64}	H(7)···Cl(11)	328.8(63)	43.1(fixed)	-3.2	43.1	
u_{65}	H(7)···Cl(12)	241.9(16)	11.1(fixed)	9.9	11.1	
u_{66}	H(7)···Cl(13)	265.3(84)	26.8(fixed)	4.4	26.8	
u_{67}	C(8)···Cl(11)	348.2(35)	15.1(Tied to u_{28})	1.7	12.8	
u_{68}	C(8)···Cl(12)	321.3(44)	23.3(Tied to u_{28})	2.6	19.8	
u_{69}	H(9)···H(10)	184.4(33)	12.3(fixed)	5.3	12.3	
u_{70}	H(9)···Cl(11)	359.9(86)	26.5(fixed)	-0.7	26.5	
u_{71}	H(9)···Cl(12)	417.8(55)	18.8(fixed)	4.1	18.8	
u_{72}	H(9)···Cl(13)	237.3(22)	11.2(fixed)	5.1	11.2	
u_{73}	H(10)···Cl(11)	451.2(24)	13.6(fixed)	3.8	13.6	
u_{74}	H(10)···Cl(12)	282.8(83)	30.7(fixed)	3.4	30.7	
u_{75}	H(10)···Cl(13)	238.8(15)	11.1(fixed)	5.1	11.1	
u_{76}	Cl(11)···Cl(12)	496.2(23)	19.0(14)	2.2	16.1	16.1(20)
u_{77}	Cl(11)···Cl(13)	369.4(51)	26.4(Tied to u_{76})	0.0	22.4	
u_{78}	Cl(12)···Cl(13)	411.4(67)	46.4(Tied to u_{76})	-1.6	39.3	
u_{79}	N(14)–C(15)	141.9(5)	4.9(Tied to u_3)	2.4	4.7	
u_{80}	N(14)–C(18)	142.9(8)	5.0(Tied to u_3)	1.7	4.8	
u_{81}	N(14)–C(21)	141.9(5)	4.9(Tied to u_3)	2.4	4.7	
u_{82}	C(15)–H(16)	112.3(6)	8.4(Tied to u_8)	3.6	7.6	
u_{83}	C(15)–H(17)	111.8(6)	8.4(Tied to u_8)	3.1	7.6	
u_{84}	C(15)–Cl(24)	182.9(4)	5.8(Tied to u_9)	3.5	6.0	
u_{85}	C(18)–H(19)	120.6(6)	8.4(Tied to u_8)	11.9	7.6	
u_{86}	C(18)–H(20)	120.5(6)	8.4(Tied to u_8)	11.8	7.6	
u_{87}	C(18)–Cl(25)	192.1(8)	5.6(Tied to u_9)	14.9	5.7	
u_{88}	C(21)–H(22)	112.6(6)	8.4(Tied to u_8)	3.9	7.5	
u_{89}	C(21)–H(23)	112.8(6)	8.4(Tied to u_8)	4.2	7.6	
u_{90}	C(21)–Cl(26)	182.5(4)	5.7(Tied to u_9)	3.2	5.9	
u_{91}	N(14)···H(16)	207.9(13)	10.2(fixed)	4.2	10.2	
u_{92}	N(14)···H(17)	208.4(13)	10.1(fixed)	4.3	10.1	
u_{93}	N(14)···H(19)	217.0(14)	10.3(fixed)	8.7	10.3	
u_{94}	N(14)···H(20)	214.2(14)	10.4(fixed)	8.9	10.4	
u_{95}	N(14)···H(22)	208.0(13)	10.2(fixed)	4.3	10.2	

u_{96}	N(14)···H(23)	209.1(13)	10.2(fixed)	5.0	10.2
u_{97}	N(14)···Cl(24)	275.7(6)	8.4(Tied to u_{20})	5.3	7.3
u_{98}	N(14)···Cl(25)	273.5(10)	8.5(Tied to u_{20})	8.5	7.4
u_{99}	N(14)···Cl(26)	274.9(6)	8.4(Tied to u_{20})	4.5	7.3
u_{100}	C(15)···C(18)	241.9(22)	7.8(Tied to u_{25})	1.7	7.1
u_{101}	C(15)···H(19)	260.3(43)	17.8(fixed)	9.0	17.8
u_{102}	C(15)···H(20)	329.6(29)	16.2(fixed)	6.3	16.2
u_{103}	C(15)···C(21)	244.4(19)	7.2(Tied to u_{25})	3.0	6.6
u_{104}	C(15)···H(22)	263.2(46)	15.3(fixed)	3.4	15.3
u_{105}	C(15)···H(23)	337.1(19)	10.4(fixed)	5.9	10.4
u_{106}	C(15)···Cl(25)	350.3(56)	40.9(Tied to u_{28})	-1.9	34.7
u_{107}	C(15)···Cl(26)	337.4(46)	16.9(Tied to u_{28})	2.7	14.3
u_{108}	H(16)···H(17)	184.2(33)	12.3(fixed)	5.1	12.3
u_{109}	H(16)···C(18)	258.2(50)	16.8(fixed)	2.1	16.8
u_{110}	H(16)···H(19)	250.1(105)	33.1(fixed)	6.8	33.1
u_{111}	H(16)···H(20)	363.6(53)	18.9(fixed)	5.3	18.9
u_{112}	H(16)···C(21)	336.6(18)	10.4(fixed)	5.4	10.4
u_{113}	H(16)···H(22)	361.4(48)	17.2(fixed)	5.8	17.2
u_{114}	H(16)···H(23)	413.8(29)	14.9(fixed)	8.5	14.9
u_{115}	H(16)···Cl(24)	236.8(22)	11.2(fixed)	4.5	11.2
u_{116}	H(16)···Cl(25)	314.7(99)	62.7(fixed)	-12.3	62.7
u_{117}	H(16)···Cl(26)	437.5(42)	14.2(fixed)	4.6	14.2
u_{118}	H(17)···C(18)	334.6(20)	10.2(fixed)	3.8	10.2
u_{119}	H(17)···H(19)	366.7(43)	18.5(fixed)	9.2	18.5
u_{120}	H(17)···H(20)	414.4(28)	16.3(fixed)	7.9	16.3
u_{121}	H(17)···C(21)	266.0(49)	15.2(fixed)	3.9	15.2
u_{122}	H(17)···H(22)	237.2(81)	22.0(fixed)	4.2	22.0
u_{123}	H(17)···H(23)	362.2(49)	17.4(fixed)	6.5	17.4
u_{124}	H(17)···Cl(24)	237.6(15)	11.2(fixed)	3.9	11.2
u_{125}	H(17)···Cl(25)	425.0(62)	31.8(fixed)	0.3	31.8
u_{126}	H(17)···Cl(26)	366.1(100)	27.8(fixed)	1.3	27.8
u_{127}	C(18)···C(21)	240.7(19)	7.8(Tied to u_{25})	3.7	7.2
u_{128}	C(18)···H(22)	334.2(18)	10.2(fixed)	5.4	10.2

u_{129}	C(18)···H(23)	259.5(42)	16.8(fixed)	5.9	16.8
u_{130}	C(18)···Cl(24)	336.5(58)	19.9(Tied to u_{28})	3.0	16.9
u_{131}	C(18)···Cl(26)	333.6(50)	20.5(Tied to u_{28})	4.5	17.4
u_{132}	H(19)···H(20)	196.9(33)	12.3(fixed)	20.1	12.3
u_{133}	H(19)···C(21)	322.8(37)	15.5(fixed)	5.5	15.5
u_{134}	H(19)···H(22)	411.8(32)	15.8(fixed)	7.2	15.8
u_{135}	H(19)···H(23)	359.4(55)	18.7(fixed)	7.1	18.7
u_{136}	H(19)···Cl(24)	304.9(104)	34.7(fixed)	6.1	34.7
u_{137}	H(19)···Cl(25)	258.0(23)	11.2(fixed)	24.2	11.2
u_{138}	H(19)···Cl(26)	373.4(89)	39.1(fixed)	0.1	39.1
u_{139}	H(20)···C(21)	249.7(36)	17.9(fixed)	10.5	17.9
u_{140}	H(20)···H(22)	356.5(38)	18.7(fixed)	10.9	18.7
u_{141}	H(20)···H(23)	231.7(90)	34.2(fixed)	6.6	34.2
u_{142}	H(20)···Cl(24)	394.9(77)	40.9(fixed)	4.7	40.9
u_{143}	H(20)···Cl(25)	256.5(16)	11.2(fixed)	24.4	11.2
u_{144}	H(20)···Cl(26)	306.5(93)	35.6(fixed)	12.1	35.6
u_{145}	C(21)···Cl(24)	337.5(52)	16.3(Tied to u_{28})	4.0	13.8
u_{146}	C(21)···Cl(25)	363.8(54)	41.3(Tied to u_{28})	5.6	35.1
u_{147}	H(22)···H(23)	185.2(33)	12.3(fixed)	6.1	12.3
u_{148}	H(22)···Cl(24)	361.1(106)	27.4(fixed)	2.3	27.4
u_{149}	H(22)···Cl(25)	437.9(58)	31.4(fixed)	6.4	31.4
u_{150}	H(22)···Cl(26)	236.6(22)	11.2(fixed)	4.3	11.2
u_{151}	H(23)···Cl(24)	439.9(42)	14.0(fixed)	6.5	14.0
u_{152}	H(23)···Cl(25)	340.0(100)	62.7(fixed)	1.5	62.7
u_{153}	H(23)···Cl(26)	239.2(15)	11.2(fixed)	5.5	11.2
u_{154}	Cl(24)···Cl(25)	479.7(85)	46.6(Tied to u_{76})	-3.3	39.4
u_{155}	Cl(24)···Cl(26)	332.1(97)	28.1(Tied to u_{76})	3.1	23.8
u_{156}	Cl(25)···Cl(26)	491.4(69)	49.8(Tied to u_{76})	3.9	42.2

[a] Distances in pm. Values in parentheses are the standard deviations in terms of the last digits. See Figure 5.3 in the main text for atom numbering.

[b] Unrefined amplitudes of vibration were fixed at the values obtained using the M06-2X/aug-cc-pVDZ force field.

Table A3.4 Least squares correlation matrix (× 100) for the GED refinement of tris(chloromethyl)amine.[a]

	p_2	p_4	p_{15}	p_{16}	k_2
p_1	-62				
p_3		-50			
p_{13}			-61	57	
k_1					-62

[a] Only elements with absolute values ≥ 50% are shown; k_1 and k_2 are scale factors.

Table A3.5 Experimental GED coordinates from the refinement of tris(chloromethyl)amine. [a,b]

Atom	*x*	*y*	*z*
N(1)	0.0	0.0	0.0
C(2)	-64.6	0.0	123.7
H(3)	-30.6	84.6	182.7
H(4)	-172.3	3.4	109.4
C(5)	141.2	0.0	0.0
H(6)	182.4	29.5	96.1
H(7)	178.1	-99.1	-25.1
C(8)	-59.4	-63.2	-109.3
H(9)	-167.5	-62.0	-98.0
H(10)	-29.4	-141.0	-201.5
Cl(11)	-33.5	-143.4	226.8
Cl(12)	208.1	109.6	-122.1
Cl(13)	-17.4	-236.3	-130.3
N(14)	0.0	0.0	0.0
C(15)	-64.6	0.0	123.7
H(16)	-14.8	69.3	191.0
H(17)	-169.2	26.6	111.0
C(18)	141.2	0.0	0.0
H(19)	182.5	-35.2	94.2
H(20)	178.1	-63.2	-80.4
C(21)	-59.4	-63.2	-109.3
H(22)	-165.2	-38.6	-112.7
H(23)	-9.6	-33.4	-201.1
Cl(24)	-64.3	-156.8	210.7
Cl(25)	208.1	161.3	-29.9
Cl(26)	-54	-242.5	-106.8

[a] Coordinates are given in pm.

[b] Atom numbering follows 1 – 13 for conformer **A** and 14 – 26 for conformer **B**. Refer to Figure 5.3 in the main text.

Table A3.6 Calculated coordinates for tris(chloromethyl)amine at the M06-2X/aug-cc-pVDZ. [a,b]

Atom	*x*	*y*	*z*
N(1)	-15.8	-31.6	60.8
C(2)	-95.7	-112.5	91.1
H(3)	-66.3	-217.5	97.8
H(4)	-143.4	-78.7	183.2
C(5)	96.4	-70.3	-50.8
H(6)	70.7	-171.7	-81.9
H(7)	87.0	-0.7	-134.8
C(8)	13.9	106.1	93.0
H(9)	-40.0	122.9	186.3
H(10)	116.0	144.4	98.6
Cl(11)	-228.7	-110.6	-36.8
Cl(12)	272.5	-71.3	-7.1
Cl(13)	-69.0	212.3	-32.2
N(14)	24.6	-1.0	47.9
C(15)	-36.2	-122.6	85.6
H(16)	37.5	-203.2	87.4
H(17)	86.2	-112.6	182.1
C(18)	114.1	-2.3	-62.4
H(19)	101.3	-92.7	-122.5
H(20)	101.7	86.7	-124.5
C(21)	-32.2	122.4	85.7
H(22)	-82.0	114.1	182.5
H(23)	44.1	200.6	87.1
Cl(24)	-166.1	-180.6	-31.3
Cl(25)	288.6	-2.1	-8.4
Cl(26)	-160.8	184.2	-30.7

[a] Coordinates are given in pm.

[b] Atom numbering follows 1 – 13 for conformer **A** and 14 – 26 for conformer **B**. Refer to Figure 5.3 in the main text.

Table A3.7 Calculated and experimental Raman frequencies for tris(chloromethyl)amine.[a]

Mode	Calculated frequencies (cm^{-1}) from M06-2X/aug-cc-pVDZ calculations			Experimental frequencies (cm^{-1})
	A	**B**	**C**	
1	40.4	9.9	41.2	43
2	77.7	77.6	77.9	60
3	93.4	84.1	93.5	98
4	144.2	92.2	144.2	130
5	257.4	246.2	257.6	271
6	258.9	261.8	259.6	271
7	414.7	410.9	414.3	453
8	436.9	447.8	437.7	474
9	534.3	519.9	534.1	540
10	620.7	632.5	621.9	595
11	670.1	671.2	671.1	666
12	748.0	726.2	748.1	-
13	910.1	916.6	909.8	905
14	926.7	920.0	926.7	-
15	969.3	968.4	968.9	968
16	975.7	970.6	976.0	968
17	1163.9	1166.8	1163.6	1152
18	1179.9	1171.4	1180.5	1165
19	1214.4	1202.1	1214.6	-
20	1289.3	1282.5	1289.4	1280
21	1298.5	1290.4	1298.9	1282
22	1328.2	1317.6	1328.4	1299
23	1396.9	1406.4	1396.9	1390
24	1420.8	1433.8	1421.0	1390
25	1455.4	1460.4	1455.3	1445
26	1465.6	1462.7	1465.6	1445
27	1494.6	1498.8	1494.4	1480
28	3125.9	3135.7	3125.8	-

29	3135.3	3136.7	3135.5	-
30	3144.0	3142.6	3143.8	-
31	3211.1	3212.4	3210.9	-
32	3213.6	3216.1	3213.3	-
33	3222.7	3217.3	3222.5	-

[a] Raw experimental and calculated data available upon request.

Figure A3.1 ^{1}H-NMR (500 MHz, $CDCl_3$) spectrum of tris(chloromethyl)amine.

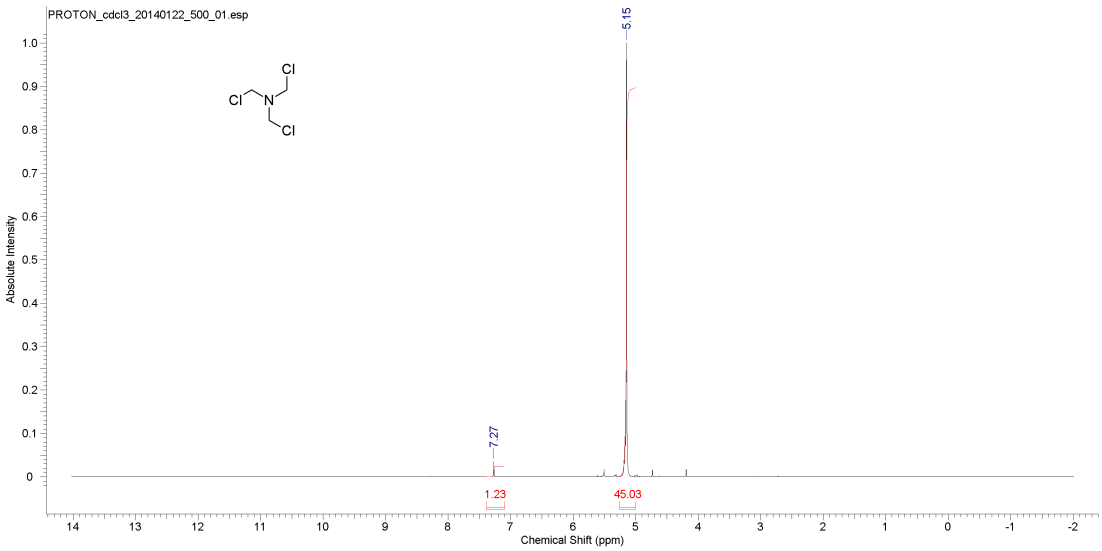

Figure A3.2 ^{13}C-NMR (125.6 MHz, $CDCl_3$) spectrum of tris(chloromethyl)amine.

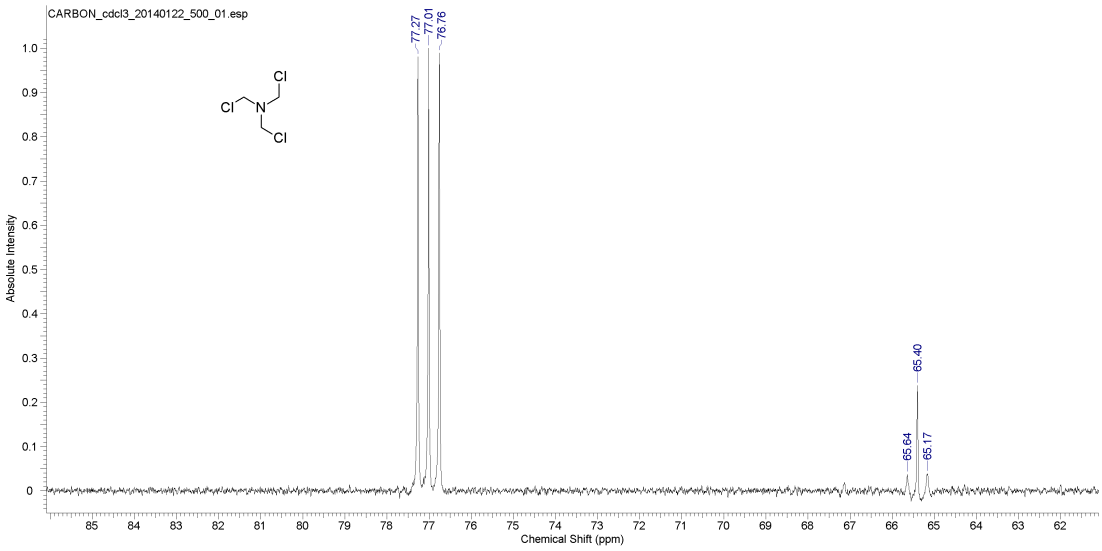

Figure A3.3 Experimental and final weighted difference (experimental – theoretical) MICs for tris(chloromethyl)amine.

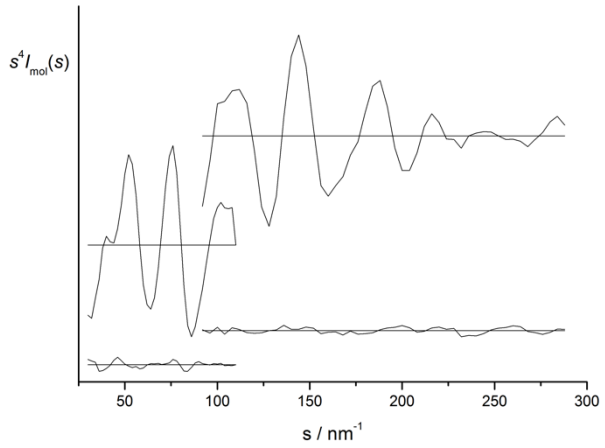

APPENDIX 4

Theoretical and experimental investigation of the gas-phase molecular structures of $X_3SiSiXMe_2$ (X = F, Cl, Br, I) and $X_3SiSiMe_3$ (X = H, F, Cl, Br)

Table A4.1 Nozzle-to-plate distances (mm), weighting functions (nm^{-1}), correlation parameters, scale factors and electron wavelengths (pm) used in the electron-diffraction study of 1,1,1,2-tetrabromo-2,2-dimethyldisilane.

Nozzle-plate distance[a]	249.59	94.26
Δs	1	2
s_{min}	20	80
sw_1	40	100
sw_2	120	258
s_{max}	140	300
Correlation parameter	0.480	0.207
Scale factor[b]	0.910(6)	0.876(14)
Electron wavelength	6.18	6.18

[a] Determined by reference to the scattering pattern of benzene vapour.

[b] Values in parentheses are the estimated standard deviations.

Table A4.2 Theoretical geometrical parameters at the HF level with the 3-21G* and 6-31G* basis sets, and at the MP2 level with the 6-31G*, 6-311G* and 6-311+G* basis sets for **1** – **4**.[a,b]

Parameter	HF/3-21G*	HF/6-31G*	MP2/6-31G*	MP2/6-311G*	MP2/6-311+G*
$F_3SiSiFMe_2$					
*r*Si(1)–Si(2)	229.8	233.6	232.7	233.9	234.9
*r*Si(1)–C(3/7)	186.2	187.4	186.7	185.9	185.9
*r*Si(1)–X(14)	160.3	160.6	163.3	162.9	163.3
*r*Si(2)–X(11)	157.9	158.2	160.9	160.3	160.9
*r*Si(2)–X(12/13)	157.8	157.9	160.6	160.0	160.4
∠Si(2)–Si(1)–C(3/7)	109.7	110.5	110.0	109.9	109.8
∠Si(2)–Si(1)–X(14)	107.2	106.3	106.8	106.6	106.0
∠Si(1)–Si(2)–X(11)	110.2	110.4	109.3	109.8	110.0
∠Si(1)–Si(2)–X(12/13)	113.7	113.1	113.1	113.2	113.4
Energy (Hartrees)	-10497785	-1055.1196	-1056.2306	-1056.5393	-1056.5624
$Cl_3SiSiClMe_2$					
*r*Si(1)–Si(2)	233.3	235.6	233.5	233.3	233.3
*r*Si(1)–C(3/7)	187.0	187.7	187.1	186.2	186.3
*r*Si(1)–X(14)	206.8	208.0	207.3	207.0	207.1

*r*Si(2)–X(11)	205.0	206.2	205.9	205.2	205.2
*r*Si(2)–X(12/13)	204.0	205.3	205.0	204.3	204.3
∠Si(2)–Si(1)–C(3/7)	109.4	109.8	109.7	109.5	109.5
∠Si(2)–Si(1)–X(14)	106.4	106.5	106.2	106.5	106.4
∠Si(1)–Si(2)–X(11)	108.7	109.1	108.8	108.8	108.6
∠Si(1)–Si(2)–X(12/13)	111.9	112.1	111.6	111.7	111.7
Energy (Hartrees)	-2483.6530	-2495.2321	-2496.1689	-2496.3751	-2496.3927
$Br_3SiSiBrMe_2$					
*r*Si(1)–Si(2)	230.9	234.0	232.1	233.6	233.7
*r*Si(1)–C(3/7)	187.0	187.6	187.1	186.4	186.4
*r*Si(1)–X(14)	220.7	222.9	223.0	224.0	224.1
*r*Si(2)–X(11)	219.9	222.2	222.8	223.2	223.2
*r*Si(2)–X(12/13)	218.5	220.6	221.1	222.0	220.0
∠Si(2)–Si(1)–C(3/7)	108.6	108.9	108.3	109.5	109.4
∠Si(2)–Si(1)–X(14)	106.7	106.8	106.4	106.6	106.3
∠Si(1)–Si(2)–X(11)	105.8	106.4	105.6	107.5	107.7
∠Si(1)–Si(2)–X(12/13)	111.6	112.2	112.1	111.3	111.3
Energy (Hartrees)	-10895.1417	-10936.8917	-10937.7654	-10947.7709	-10947.7811

$I_3SiSiIMe_2$					
*r*Si(1)–Si(2)	233.7	237.3	234.5	234.4	234.4
*r*Si(1)–C(3/7)	187.4	188.2	187.6	186.9	186.9
*r*Si(1)–X(14)	247.9	248.5	246.8	246.5	246.5
*r*Si(2)–X(11)	247.7	248.3	246.7	246.5	246.5
*r*Si(2)–X(12/13)	246.1	246.7	245.1	244.9	244.9
∠Si(2)–Si(1)–C(3/7)	109.2	109.8	109.7	109.7	109.7
∠Si(2)–Si(1)–X(14)	107.1	107.2	104.6	104.3	104.3
∠Si(1)–Si(2)–X(11)	106.3	107.4	107.5	107.5	107.5
∠Si(1)–Si(2)–X(12/13)	111.1	111.6	110.7	110.6	110.6
Energy (Hartrees)	-28205.6296	-702.0173	-703.0732	-703.1527	-703.1549

[a] All distances in pm and all angles in degrees. See Figure 6.1 in the main text for atom numbering.

[b] For $I_3SiSiIMe_2$, calculations beyond HF/3-21G* utilised the SDB-aug-cc-pVTZ ECP and basis for iodine.

Table A4.3 Refined and calculated (HF/6-31G*) amplitudes of vibration (u), associated r_a distances and corresponding correction values (k) for the r_{h1} refinement of 1,1,1,2-tetrabromo-2,2-dimethyldisilane.[a,b]

	Atom pair	r_a	u_{GED}	k	$u_{calc.}$	Restraint
u_1	C(3)–H(6)	109.6	6.8(8)	0.2	7.5	
u_2	C(3)–H(5)	109.6	6.8(Tied to u_1)	0.2	7.5	
u_3	C(3)–H(4)	109.6	6.8(Tied to u_1)	0.2	7.5	
u_4	H(5)···H(6)	175.4	12.0(fixed)	0.9	12.0	
u_5	H(4)···H(5)	175.4	12.1(fixed)	0.9	12.1	
u_6	H(4)···H(6)	175.5	12.1(fixed)	1.0	12.1	
u_7	Si(1)–C(3)	185.3	4.3(3)	0.0	5.2	5.2(5)
u_8	Si(2)–Br(12)	220.2	5.5(1)	0.0	5.0	
u_9	Si(2)–Br(11)	220.2	5.4(Tied to u_8)	0.0	4.9	
u_{10}	Si(1)–Br(14)	220.2	5.5(Tied to u_8)	-0.0	5.0	
u_{11}	Si(1)–Si(2)	235.5	6.3(4)	0.0	5.6	5.6(6)
u_{12}	Si(1)···H(4)	249.9	11.9(fixed)	0.9	11.9	
u_{13}	Si(1)···H(5)	249.7	11.7(fixed)	0.7	11.7	
u_{14}	Si(1)···H(6)	249.8	11.7(fixed)	0.9	11.7	
u_{15}	C(3)···C(7)	303.9	10.5(fixed)	0.6	10.5	
u_{16}	H(4)···H(10)	306.2	33.7(fixed)	-0.6	33.7	
u_{17}	H(5)···H(9)	316.4	33.2(fixed)	-0.8	33.2	
u_{18}	C(3)···H(10)	325.8	23.2(fixed)	1.3	23.2	
u_{19}	C(3)···H(9)	330.4	22.7(fixed)	1.1	22.7	
u_{20}	C(3)···Br(14)	335.3	12.6(17)	0.6	10.4	
u_{21}	Si(2)···C(3)	344.6	10.9(fixed)	0.4	10.9	
u_{22}	H(6)···Br(14)	354.4	24.4(fixed)	1.3	24.4	
u_{23}	H(5)···Br(14)	355.2	23.4(fixed)	1.1	23.4	
u_{24}	Si(2)···H(6)	358.2	24.4(fixed)	1.0	24.4	
u_{25}	Si(2)···H(4)	363.5	24.0(fixed)	1.0	24.0	
u_{26}	Br(11)···Br(12)	355.6	11.4(2)	0.5	10.1	
u_{27}	Br(12)···Br(13)	355.6	11.5(Tied to u_{26})	0.5	10.2	
u_{28}	H(4)···Br(11)	369.8	33.3(fixed)	8.7	33.3	
u_{29}	H(4)···H(9)	361.8	36.0(fixed)	4.5	36.0	

u_{30}	Si(1)···Br(11)	365.2	12.6(12)	0.6	10.5	
u_{31}	Si(2)···Br(14)	364.7	12.6(Tied to u_{30})	0.7	10.5	
u_{32}	H(6)···Br(12)	386.2	35.0(fixed)	9.3	35.0	
u_{33}	Si(1)···Br(12)	382.2	14.2(Tied to u_{30})	0.6	11.8	
u_{34}	C(3)···H(8)	403.8	11.9(fixed)	3.3	11.9	
u_{35}	C(3)···Br(11)	412.1	24.2(28)	4.7	26.3	
u_{36}	C(3)···Br(12)	431.1	25.9(Tied to u_{35})	5.4	28.1	
u_{37}	H(4)···Br(14)	437.4	11.8(fixed)	3.5	11.8	
u_{38}	H(4)···H(8)	430.6	23.0(fixed)	4.4	23.0	
u_{39}	H(5)···H(8)	436.3	22.7(fixed)	4.3	22.7	
u_{40}	Br(12)···Br(14)	442.8	37.3(21)	5.7	28.6	28.6(30)
u_{41}	Si(2)···H(5)	448.1	12.3(fixed)	3.3	12.3	
u_{42}	H(6)···Br(11)	437.6	43.7(fixed)	4.4	43.7	
u_{43}	H(4)···Br(12)	459.2	46.2(fixed)	5.4	46.2	
u_{44}	H(6)···H(8)	494.5	14.6(fixed)	5.4	14.6	
u_{45}	H(5)···Br(11)	515.6	26.7(fixed)	6.7	26.7	
u_{46}	H(5)···Br(12)	533.5	28.0(fixed)	7.4	28.0	
u_{47}	C(3)···Br(13)	533.4	22.3(fixed)	-4.7	22.3	
u_{48}	Br(11)···Br(14)	548.8	17.3(6)	-5.3	21.0	21.0(20)
u_{49}	H(4)···Br(13)	558.1	42.6(fixed)	-4.8	42.6	
u_{50}	H(6)···Br(13)	556.7	44.4(fixed)	-4.2	44.4	
u_{51}	H(5)···Br(13)	626.3	24.6(fixed)	0.9	24.6	

[a] Distances in pm. Values in parentheses are the standard deviations in terms of the last digits. See Figure 6.1 in the main text for atom numbering.

[b] Unrefined amplitudes of vibration were fixed at the values obtained using the HF/6-31G* force field.

Table A4.4 Least squares correlation matrix (× 100) for the GED refinement of 1,1,1,2-tetrabromo-2,2-dimethyldisilane.[a]

	p_9	u_{11}	u_{26}	u_{30}	u_{35}	u_{40}	k_2
p_1							51
p_5				77			
p_7	-62					59	
p_{11}				-65	-66		
u_8		62					79
u_{20}			56				
u_{30}					66		

[a] Only elements with absolute values ≥ 50% are shown; k_2 is a scale factor.

Table A4.5 Experimental GED coordinates from the refinement of 1,1,1,2-tetrabromo-2,2-dimethyldisilane. [a]

Atom	*x*	*y*	*z*
Si(1)	235.6	0.0	0.0
Si(2)	0.0	0.0	0.0
C(3)	296.7	-87.1	151.9
H(4)	267.1	-192.8	155.2
H(5)	406.2	-86.3	160.3
H(6)	259.0	-42.3	244.8
C(7)	296.7	-87.1	-151.9
H(8)	259.0	-42.3	-244.8
H(9)	406.2	-86.3	-160.3
H(10)	267.1	-192.8	-155.2
Br(11)	-61.8	-211.5	0.0
Br(12)	-88.9	95.2	177.7
Br(13)	-88.9	95.2	-177.7
Br(14)	296.6	211.7	0.0

[a] Coordinates are given in pm.

Table A4.6 Calculated coordinates at the MP2/6-311+G* level for 1,1,1,2-tetrafluoro-2,2-dimethyldisilane. [a]

Atom	*x*	*y*	*z*
Si(1)	-47.8	107.6	0.0
Si(2)	42.8	-109.1	0.0
C(3)	1.8	196.6	155.5
H(4)	110.5	207.1	162.1
H(5)	-41.5	297.1	157.9
H(6)	-32.2	143.6	244.9
C(7)	1.8	196.6	-155.5
H(8)	-32.2	143.6	-244.9
H(9)	-41.4	297.1	-157.9
H(10)	110.5	207.1	-162.1
F(11)	203.6	-101.5	0.0
F(12)	1.8	-195.4	-128.9
F(13)	1.8	-195.4	128.9
F(14)	-210.0	88.6	0.0

[a] Coordinates are given in pm.

Table A4.7 Calculated coordinates at the MP2/6-311+G* level for 1,1,1,2-tetrachloro-2,2-dimethyldisilane. [a]

Atom	*x*	*y*	*z*
Si(1)	-139.5	45.8	-0.0
Si(2)	88.2	-4.9	0.0
C(3)	-182.3	138.8	155.6
H(4)	-128.6	234.1	160.2
H(5)	-289.5	160.7	158.8
H(6)	-157.4	81.4	245.2
C(7)	-182.3	138.8	-155.6
H(8)	-157.4	81.4	-245.2
H(9)	-289.5	160.7	-158.8
H(10)	-128.6	234.1	-160.2
Cl(11)	194.5	170.6	-0.0
Cl(12)	141.9	-111.5	-165.8
Cl(13)	141.9	-111.5	165.8
Cl(14)	-239.7	-135.4	0.0

[a] Coordinates are given in pm.

Table A4.8 Calculated coordinates at the MP2/6-311+G* level for 1,1,1,2-tetrabromo-2,2-dimethyldisilane. [a]

Atom	*x*	*y*	*z*
Si(1)	-135.6	113.6	0.0
Si(2)	66.2	-4.3	0.0
C(3)	-148.0	215.2	155.8
H(4)	-68.0	289.8	159.9
H(5)	-243.7	268.2	159.0
H(6)	-141.3	153.0	245.3
C(7)	-148.0	215.2	-155.8
H(8)	-141.3	152.9	-245.3
H(9)	-243.7	268.2	-159.0
H(10)	-68.0	289.8	-159.9
Br(11)	232.1	144.9	0.0
Br(12)	85.4	-131.3	181.0
Br(13)	85.4	-131.3	-181.0
Br(14)	-298.5	-40.4	0.0

[a] Coordinates are given in pm.

Table A4.9 Calculated coordinates at the MP2/6-311+G* level for 1,1,1,2-tetraiodo-2,2-dimethyldisilane. [a,b]

Atom	*x*	*y*	*z*
Si(1)	-115.5	0.0	156.9
Si(2)	59.7	0.0	1.1
C(3)	-109.2	-156.6	258.7
H(4)	-16.8	-160.5	317.4
H(5)	-194.1	-160.2	327.9
H(6)	-113.5	-245.4	195.2
C(7)	-109.2	156.6	258.7
H(8)	-113.5	245.4	195.2
H(9)	-194.1	160.2	327.9
H(10)	-16.8	160.5	317.4
I(11)	271.3	0.0	127.6
I(12)	50.1	-200.5	-139.2
I(13)	50.1	200.5	-139.2
I(14)	-319.8	0.0	18.9

[a] The SDB-aug-cc-pVTZ basis set and ECP were used on the iodine atoms, with 6-311+G* on C, Si and H.

[b] Coordinates are given in pm.

Figure A4.1 Experimental and final weighted difference (experimental – theoretical) MICs for 1,1,1,2-tetrabromo-2,2-dimethyldisilane.

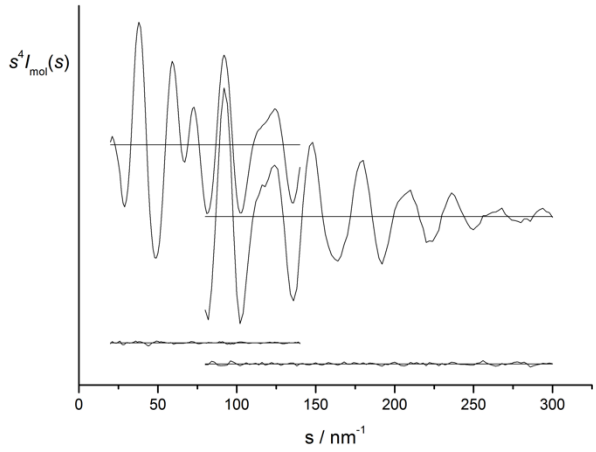

Table A4.10 Nozzle-to-plate distances (mm), weighting points (nm^{-1}), correlation parameters, scale factors, electron wavelengths (pm) and sample and nozzle temperatures (K) used in the electron diffraction study of $X_3SiSiMe_3$ (X = H, F, Cl, Br; **1 – 4**).[a,b]

	X = H		X = F		X = Cl		X = Br	
Nozzle-plate distance[a]	282.69	130.69	278.13	128.41	292.17	131.10	262.34	97.43
Δs	1	2	1	2	1	2	1	2
s_{min}	26	60	24	70	20	80	20	60
sw_1	40	80	40	90	40	100	40	80
sw_2	112	258	103	258	112	276	120	240
s_{max}	130	300	120	300	130	290	140	250
Correlation parameter	0.4949	0.3735	0.3864	0.0835	0.4933	0.3368	0.4418	0.0933
Scale factor[b]	0.684(9)	0.537(7)	0.459(4)	0.555(5)	0.775(5)	0.829(18)	0.857(8)	0.850(11)
Electron wavelength	6.18	6.18	6.18	6.18	6.13	6.13	6.13	6.13
Sample temperature	243	247	276	275	293	298	323	325
Nozzle temperature	243	293	293	275	293	293	350	351

[a] Determined by reference to the scattering pattern of benzene vapour.

[b] Values in parentheses are the estimated standard deviations.

Table A4.11 Geometric structures of $X_3SiSiMe_3$ (X = H, F, Cl, Br; **1 – 4**) at the HF level using the 3-21G* and 6-31G* basis sets, and at the MP2 level using the 6-31G* and 6-311G* basis sets.[a]

Parameter	HF/3-21G*	HF/6-31G*	MP2/6-31G*	MP2/6-311G*
$H_3SiSiMe_3$				
*r*Si–Si	234.9	236.3	234.9	234.9
*r*Si–C	189.2	189.8	189.2	188.5
*r*Si–H	148.2	148.2	149.1	148.8
*r*C–H_{av}	108.8	108.7	109.4	109.4
∠Si–Si–H	111.3	111.3	111.3	111.1
∠Si–Si–C	109.3	109.6	109.6	109.6
∠Si–C–H_{av}	111.2	111.3	111.2	111.3
ϕH(15)–Si–Si–C(11)	180.0	180.0	180.0	180.0
Energy (Hartrees)	-694.9408	-698.4430	-699.0009	-699.0983
$F_3SiSiMe_3$				
*r*Si–Si	230.4	233.9	232.4	233.3
*r*Si–C	188.4	189.2	188.5	187.8
*r*Si–F	158.1	158.4	161.0	160.6
*r*C–H_{av}	108.8	108.7	109.4	109.4
∠Si–Si–F	113.1	112.7	112.4	112.6
∠Si–Si–C	108.2	108.4	108.4	108.3
∠Si–C–H_{av}	111.2	111.3	111.1	111.2
ϕF(15)–Si–Si–C(11)	180.0	180.0	180.0	180.0
Energy (Hartrees)	-990.2005	-995.2391	-996.3123	-996.5815
$Cl_3SiSiMe_3$				
*r*Si–Si	233.8	236.1	233.6	233.4
*r*Si–C	188.3	188.9	188.4	187.6
*r*Si–Cl	205.2	206.4	206.1	205.5
*r*C–H_{av}	108.8	108.7	109.4	109.4
∠Si–Si–Cl	111.6	111.8	111.4	111.5
∠Si–Si–C	107.3	107.7	107.7	107.6
∠Si–C–H_{av}	111.2	111.2	111.0	111.1

ϕCl(15)–Si–Si–C(11)	180.0	180.0	180.0	180.0
Energy (Hartrees)	-2065.6038	-2075.3198	-2076.2620	-2076.4543
$Br_3SiSiMe_3$				
*r*Si–Si	231.8	234.9	232.7	233.9
*r*Si–C	188.3	188.9	188.3	187.6
*r*Si–Br	219.8	222.0	222.5	223.3
*r*C–H_{av}	108.8	108.6	109.4	109.4
∠Si–Si–Br	110.4	111.2	110.9	110.8
∠Si–Si–C	107.0	107.1	106.5	107.5
∠Si–C–H_{av}	111.1	111.2	110.9	111.1
ϕBr(15)–Si–Si–C(11)	180.0	180.0	180.0	180.0
Energy (Hartrees)	-8374.2192	-8406.5636	-8407.4586	-8415.0008

[a] All distances in pm and all angles in degrees. See Figure 6.4 in the main text for atom numbering.

Table A4.12 Refined and calculated (HF/6-31G*) amplitudes of vibration (u), associated r_a distances and corresponding correction values (k) for the r_{h1} refinement of 1,1,1-trimethyldisilane.[a,b]

	Atom pair	r_a	u_{GED}	k	$u_{calc.}$	Restraint
u_1	C(3)–H(4)	108.4(2)	6.0(2)	0.4	7.5	7.5(7)
u_2	C(3)–H(5)	108.3(2)	6.0(Tied to u_1)	0.4	7.5	
u_3	Si(1)–H(17)	150.4(4)	6.4(4)	0.3	8.6	8.6(8)
u_4	H(4)···H(5)	174.4(5)	12.1(fixed)	-0.2	12.1	
u_5	H(4)···H(6)	174.4(5)	12.0(fixed)	-0.2	12.0	
u_6	Si(2)–C(3)	188.1(1)	4.8(1)	0.1	5.1	
u_7	Si(1)–Si(2)	233.4(2)	5.8(2)	0.1	5.3	
u_8	H(17)···H(16)	241.5(10)	14.4(fixed)	-0.3	14.4	
u_9	Si(2)···H(5)	247.5(4)	10.6(5)	-0.3	11.7	
u_{10}	Si(2)···H(4)	247.5(4)	10.5(Tied to u_9)	-0.3	11.6	
u_{11}	C(3)···C(7)	306.5(3)	10.3(4)	-0.2	9.6	
u_{12}	H(5)···H(9)	305.3(12)	30.9(fixed)	-3.1	30.9	
u_{13}	H(4)···H(10)	305.4(9)	31.6(fixed)	-3.0	31.6	
u_{14}	H(17)···Si(2)	319.5(9)	14.3(fixed)	-0.3	14.3	
u_{15}	C(3)···H(9)	326.6(7)	21.2(18)	0.3	21.2	21.2(20)
u_{16}	C(3)···H(10)	326.6(4)	21.7(Tied to u_{15})	0.2	21.7	
u_{17}	Si(1)···C(3)	344.5(4)	12.3(2)	-0.4	11.3	
u_{18}	H(4)···H(9)	353.5(7)	33.7(fixed)	-0.9	33.7	
u_{19}	H(17)···H(8)	345.8(14)	40.3(fixed)	-5.8	40.3	
u_{20}	Si(1)···H(4)	358.2(7)	23.4(fixed)	0.3	23.4	
u_{21}	H(17)···C(7)	385.2(12)	29.8(fixed)	0.9	29.8	
u_{22}	C(3)···H(8)	398.7(3)	11.5(fixed)	-2.6	11.5	
u_{23}	H(17)···H(10)	405.8(11)	43.9(fixed)	-1.1	43.9	
u_{24}	H(4)···H(13)	423.3(8)	21.6(fixed)	-2.7	21.6	
u_{25}	H(4)···H(8)	423.3(6)	21.9(fixed)	-2.8	21.9	
u_{26}	Si(1)···H(5)	439.4(4)	12.4(fixed)	-3.0	12.4	
u_{27}	H(17)···C(3)	468.3(7)	13.3(fixed)	-4.5	13.3	
u_{28}	H(17)···H(9)	483.3(12)	29.1(fixed)	-2.6	29.1	
u_{29}	H(4)···H(14)	482.1(6)	14.3(fixed)	-4.5	14.3	

u_{30}	H(17)···H(4)	488.7(8)	24.3(fixed)	-5.1	24.3
u_{31}	H(17)···H(5)	552.8(8)	16.2(fixed)	-6.4	16.2

[a] Distances are in pm. Estimated standard deviations, obtained in the least-squares refinement, are given in parentheses.

[b] Unrefined amplitudes of vibration were fixed at the values obtained using the HF/6-31G* force field.

Table A4.13 Refined and calculated (HF/6-31G*) amplitudes of vibration (u), associated r_a distances and corresponding correction values (k) for the r_{h1} refinement of 1,1,1-trifluoro-2,2,2-trimethyldisilane.[a,b]

	Atom pair	r_a	u_{GED}	k	$u_{calc.}$	Restraint
u_1	C(3)–H(4)	110.6(2)	5.3(2)	0.4	7.5	
u_2	C(3)–H(5)	110.6(2)	5.3(Tied to u_1)	0.4	7.5	
u_3	Si(1)–F(15)	158.1(1)	3.4(1)	0.1	3.9	3.9(3)
u_4	H(4)···H(5)	176.8(6)	12.1(fixed)	-0.1	12.1	
u_5	H(4)···H(6)	176.8(6)	12.0(fixed)	-0.1	12.0	
u_6	Si(2)–C(3)	187.9(1)	4.6(1)	0.1	5.1	
u_7	Si(1)–Si(2)	233.4(2)	6.5(2)	0.1	5.2	
u_8	Si(2)···H(5)	250.0(6)	11.7(fixed)	-0.3	11.7	
u_9	Si(2)···H(4)	250.0(6)	11.6(fixed)	-0.3	11.6	
u_{10}	F(15)···F(16)	253.5(2)	7.4(2)	-0.2	7.1	
u_{11}	C(3)···C(7)	307.4(5)	11.6(7)	-0.2	10.0	10.0(9)
u_{12}	H(4)···H(10)	308.0(14)	32.9(fixed)	-3.6	32.9	
u_{13}	H(5)···H(9)	311.2(20)	32.3(fixed)	-3.2	32.3	
u_{14}	Si(2)···F(15)	326.7(2)	10.5(4)	-0.3	10.4	
u_{15}	C(3)···H(10)	329.4(8)	22.5(fixed)	0.4	22.5	
u_{16}	C(3)···H(9)	330.6(11)	22.1(fixed)	0.3	22.1	
u_{17}	Si(1)···C(3)	343.1(5)	10.7(5)	-0.4	11.7	
u_{18}	Si(1)···H(4)	358.4(8)	24.6(fixed)	0.4	24.6	
u_{19}	H(4)···F(15)	346.7(11)	41.9(fixed)	-6.6	41.9	
u_{20}	H(4)···H(9)	358.5(12)	35.5(fixed)	-0.9	35.5	
u_{21}	C(3)···F(15)	388.0(6)	33.8(14)	1.0	29.2	
u_{22}	C(3)···H(8)	401.8(5)	11.7(fixed)	-2.8	11.7	
u_{23}	H(4)···F(16)	410.8(8)	43.7(fixed)	-1.1	43.7	
u_{24}	H(4)···H(8)	428.1(9)	22.5(fixed)	-3.0	22.5	
u_{25}	H(4)···H(13)	429.6(13)	22.3(fixed)	-3.0	22.3	
u_{26}	Si(1)···H(5)	440.5(5)	12.7(fixed)	-3.3	12.7	
u_{27}	C(3)···F(17)	474.5(4)	14.0(5)	-4.9	10.3	10.3(10)
u_{28}	H(4)···H(14)	487.5(9)	14.3(fixed)	-4.9	14.3	
u_{29}	H(5)···F(15)	488.9(6)	29.0(fixed)	-2.7	29.0	

u_{30}	H(4)···F(17)	496.9(8)	24.2(fixed)	-5.3	24.2
u_{31}	H(5)···F(17)	561.6(5)	13.7(fixed)	-7.3	13.7

[a] Distances are in pm. Estimated standard deviations, obtained in the least-squares refinement, are given in parentheses.

[b] Unrefined amplitudes of vibration were fixed at the values obtained using the HF/6-31G* force field.

Table A4.14 Refined and calculated (HF/6-31G*) amplitudes of vibration (u), associated r_a distances and corresponding correction values (k) for the r_{h1} refinement of 1,1,1-trichloro-2,2,2-trimethyldisilane.[a,b]

	Atom pair	r_a	u_{GED}	k	$u_{calc.}$	Restraint
u_1	C(3)–H(4)	107.4(3)	8.2(3)	0.4	7.5	
u_2	C(3)–H(5)	107.4(3)	8.2(Tied to u_1)	0.4	7.5	
u_3	H(4)···H(5)	173.2(6)	12.1(fixed)	-0.1	12.1	
u_4	H(4)···H(6)	173.2(6)	12.0(fixed)	-0.2	12.0	
u_5	Si(2)–C(3)	187.1(2)	6.1(2)	0.1	5.1	
u_6	Si(1)–Cl(15)	204.7(1)	5.3(1)	0.1	4.7	
u_7	Si(1)–Si(2)	233.3(2)	7.0(2)	0.1	5.5	
u_8	Si(2)···H(5)	246.3(4)	11.8(fixed)	-0.3	11.8	
u_9	Si(2)···H(4)	246.2(4)	11.7(fixed)	-0.3	11.7	
u_{10}	C(3)···C(7)	309.5(5)	10.1(fixed)	-0.2	10.1	
u_{11}	H(4)···H(10)	304.8(9)	33.4(fixed)	-3.9	33.4	
u_{12}	H(5)···H(9)	316.2(13)	33.1(fixed)	-3.4	33.1	
u_{13}	Cl(15)···Cl(16)	328.9(2)	9.5(1)	-0.2	8.8	
u_{14}	C(3)···H(10)	328.1(5)	22.9(fixed)	0.5	22.9	
u_{15}	C(3)···H(9)	333.1(8)	22.6(fixed)	0.4	22.6	
u_{16}	Si(1)···C(3)	338.5(4)	10.6(6)	-0.3	11.5	11.5(11)
u_{17}	Si(1)···H(4)	350.8(6)	24.8(fixed)	0.5	24.8	
u_{18}	H(4)···H(9)	357.7(8)	36.4(fixed)	-0.9	36.4	
u_{19}	Si(2)···Cl(15)	362.5(2)	11.8(2)	-0.3	11.6	
u_{20}	H(4)···Cl(15)	351.1(8)	41.7(fixed)	-6.8	41.7	
u_{21}	C(3)···H(8)	399.7(5)	11.8(fixed)	-2.9	11.8	
u_{22}	C(3)···Cl(15)	405.9(5)	35.5(10)	0.6	29.7	29.7(30)
u_{23}	H(4)···H(8)	422.6(7)	22.9(fixed)	-3.1	22.9	
u_{24}	H(4)···H(13)	428.6(9)	22.6(fixed)	-3.1	22.6	
u_{25}	H(4)···Cl(16)	428.0(6)	46.6(fixed)	-1.6	46.6	
u_{26}	Si(1)···H(5)	433.5(4)	12.7(fixed)	-3.4	12.7	
u_{27}	H(4)···H(14)	480.9(7)	14.5(fixed)	-5.1	14.5	
u_{28}	H(5)···Cl(15)	502.5(6)	30.3(fixed)	-3.5	30.3	
u_{29}	C(3)···Cl(17)	514.2(3)	13.1(4)	-4.0	10.6	

u_{30}	H(4)···Cl(17)	534.7(6)	23.3(fixed)	-4.4	23.3
u_{31}	H(5)···Cl(17)	596.9(4)	14.5(fixed)	-6.3	14.5

[a] Distances are in pm. Estimated standard deviations, obtained in the least-squares refinement, are given in parentheses.

[b] Unrefined amplitudes of vibration were fixed at the values obtained using the HF/6-31G* force field.

Table A4.15 Refined and calculated (HF/6-31G*) amplitudes of vibration (u), associated r_a distances and corresponding correction values (k) for the r_{h1} refinement of 1,1,1-tribromo-2,2,2-trimethyldisilane.[a,b]

	Atom pair	r_a	u_{GED}	k	$u_{calc.}$	Restraint
u_1	C(3)–H(4)	108.6(3)	7.6(4)	0.4	7.5	
u_2	C(3)–H(5)	108.6(3)	7.6(Tied to u_1)	0.4	7.5	
u_3	H(4)···H(5)	174.9(7)	12.1(fixed)	-0.1	12.1	
u_4	H(4)···H(6)	174.8(7)	12.0(fixed)	-0.2	12.0	
u_5	Si(2)–C(3)	189.2(1)	4.7(2)	0.1	5.2	
u_6	Si(1)–Br(15)	221.1(1)	6.0(1)	0.1	4.9	
u_7	Si(1)–Si(2)	234.8(2)	5.9(4)	0.1	5.5	5.5(5)
u_8	Si(2)···H(5)	249.1(5)	11.8(fixed)	-0.2	11.8	
u_9	Si(2)···H(4)	249.0(5)	11.8(fixed)	-0.3	11.8	
u_{10}	C(3)···C(7)	309.7(5)	10.5(fixed)	-0.2	10.5	
u_{11}	H(4)···H(10)	307.0(12)	33.3(fixed)	-4.3	33.3	
u_{12}	H(5)···H(9)	311.1(16)	34.2(fixed)	-3.1	34.2	
u_{13}	C(3)···H(10)	329.9(7)	22.9(fixed)	0.6	22.9	
u_{14}	C(3)···H(9)	331.1(9)	23.3(fixed)	0.3	23.3	
u_{15}	Si(1)···C(3)	344.9(4)	12.4(fixed)	-0.3	12.4	
u_{16}	Si(1)···H(4)	358.5(8)	26.4(fixed)	0.5	26.4	
u_{17}	Br(15)···Br(16)	356.4(1)	11.9(2)	-0.3	10.0	
u_{18}	H(4)···H(9)	357.2(10)	37.1(fixed)	-0.9	37.1	
u_{19}	H(4)···Br(15)	363.4(9)	46.8(fixed)	-6.0	46.8	
u_{20}	Si(2)···Br(15)	375.6(2)	12.5(4)	-0.5	13.0	
u_{21}	C(3)···H(8)	401.6(5)	12.0(fixed)	-3.1	12.0	
u_{22}	C(3)···Br(15)	420.1(5)	36.5(13)	0.3	31.6	31.6(30)
u_{23}	H(4)···H(8)	426.3(9)	22.9(fixed)	-3.1	22.9	
u_{24}	H(4)···H(13)	427.7(11)	23.0(fixed)	-3.4	23.0	
u_{25}	Si(1)···H(5)	440.1(5)	13.1(fixed)	-3.6	13.1	
u_{26}	H(4)···Br(16)	445.3(6)	43.9(fixed)	-1.6	43.9	
u_{27}	H(4)···H(14)	485.1(9)	14.7(fixed)	-5.2	14.7	
u_{28}	H(5)···Br(15)	516.5(6)	34.7(fixed)	-3.8	34.7	
u_{29}	C(3)···Br(17)	533.9(3)	12.8(5)	-4.0	11.2	

u_{30}	H(4)···Br(17)	557.0(7)	25.3(fixed)	-4.0	25.3
u_{31}	H(5)···Br(17)	614.2(5)	15.5(fixed)	-7.2	15.5

[a] Distances are in pm. Estimated standard deviations, obtained in the least-squares refinement, are given in parentheses.

[b] Unrefined amplitudes of vibration were fixed at the values obtained using the HF/6-31G* force field.

Table A4.16 Experimental GED coordinates from the refinement of 1,1,1-trimethyldisilane.[a]

Atom	*x*	*y*	*z*
Si(1)	0.0	0.0	0.0
Si(2)	233.5	0.0	0.0
C(3)	296.3	-88.7	-153.6
H(4)	261.5	-39.3	-243.5
H(5)	404.6	-89.9	-155.7
H(6)	261.5	-191.2	-155.8
C(7)	296.3	177.3	0.0
H(8)	261.5	230.5	87.7
H(9)	404.6	179.8	0.0
H(10)	261.5	230.5	-87.7
C(11)	296.3	-88.7	153.6
H(12)	261.5	-191.2	155.8
H(13)	404.6	-89.9	155.7
H(14)	261.5	-39.3	243.5
H(15)	-54.7	70.1	-121.3
H(16)	-54.7	-140.1	0.0
H(17)	-54.7	70.1	121.3

[a] Coordinates are given in pm.

Table A4.17 Experimental GED coordinates from the refinement of 1,1,1-trifluoro-2,2,2-trimethyldisilane.[a]

Atom	*x*	*y*	*z*
Si(1)	0.0	0.0	0.0
Si(2)	233.5	0.0	0.0
C(3)	294.3	177.9	0.0
H(4)	259.0	233.2	88.9
H(5)	404.6	183.4	0.0
H(6)	259.0	233.2	-88.9
C(7)	294.3	-88.9	154.0
H(8)	259.0	-193.6	157.5
H(9)	404.6	-91.7	158.9
H(10)	259.0	-39.6	246.4
C(11)	294.3	-88.9	-154.0
H(12)	259.0	-39.6	-246.4
H(13)	404.6	-91.7	-158.9
H(14)	259.0	-193.6	-157.5
F(15)	-59.3	73.3	126.9
F(16)	-59.3	73.3	-126.9
F(17)	-59.3	-146.6	0.0

[a] Coordinates are given in pm.

Table A4.18 Experimental GED coordinates from the refinement of 1,1,1-trichloro-2,2,2-trimethyldisilane.[a]

Atom	*x*	*y*	*z*
Si(1)	0.0	0.0	0.0
Si(2)	233.4	0.0	0.0
C(3)	288.1	179.0	0.0
H(4)	251.3	230.6	87.1
H(5)	395.5	186.5	0.0
H(6)	251.3	230.6	-87.1
C(7)	288.1	-89.5	155.0
H(8)	251.3	-190.7	156.1
H(9)	395.5	-93.2	161.5
H(10)	251.3	-39.9	243.2
C(11)	288.1	-89.5	-155.0
H(12)	251.3	-39.9	-243.2
H(13)	395.5	-93.2	-161.5
H(14)	251.3	-190.7	-156.1
Cl(15)	-76.1	95.1	164.7
Cl(16)	-76.1	95.1	-164.7
Cl(17)	-76.1	-190.1	-0.0

[a] Coordinates are given in pm.

Table A4.19 Experimental GED coordinates from the refinement of 1,1,1-tribromo-2,2,2-trimethyldisilane.[a]

Atom	*x*	*y*	*z*
Si(1)	0.0	0.0	0.0
Si(2)	234.8	0.0	0.0
C(3)	295.7	179.1	0.0
H(4)	260.2	232.5	87.9
H(5)	404.4	183.6	0.0
H(6)	260.2	232.5	-87.9
C(7)	295.7	-89.6	155.1
H(8)	260.2	-192.4	157.4
H(9)	404.4	-91.8	159.0
H(10)	260.2	-40.1	245.3
C(11)	295.7	-89.6	-155.1
H(12)	260.2	-40.1	-245.3
H(13)	404.4	-91.8	-159.0
H(14)	260.2	-192.4	-157.4
Br(15)	-80.1	103.1	178.5
Br(16)	-80.1	103.1	-178.5
Br(17)	-80.1	-206.2	0.0

[a] Coordinates are given in pm.

Table A4.20 Calculated coordinates at the MP2/6-311+G* level for 1,1,1-trimethyldisilane.[a]

Atom	*x*	*y*	*z*
Si(1)	0.0	0.0	194.9
Si(2)	0.0	0.0	-40.0
C(3)	0.0	177.5	-103.2
H(4)	88.3	232.6	-69.5
H(5)	0.0	179.4	-212.7
H(6)	-88.3	232.6	-69.5
C(7)	153.7	-88.8	-103.2
H(8)	157.3	-192.7	-69.5
H(9)	155.4	-89.7	-212.7
H(10)	245.6	-39.9	-69.5
C(11)	-153.7	-88.8	-103.2
H(12)	-245.6	-39.9	-69.5
H(13)	-155.4	-89.7	-212.7
H(14)	-157.3	-192.7	-69.5
H(15)	120.3	69.5	248.2
H(16)	-120.3	69.5	248.2
H(17)	0.0	-138.9	248.2

[a] Coordinates are given in pm.

Table A4.21 Calculated coordinates at the MP2/6-311+G* level for 1,1,1-trifluoro-2,2,2-trimethyldisilane.[a]

Atom	*x*	*y*	*z*
Si(1)	0.0	0.0	-116.7
Si(2)	0.0	0.0	117.4
C(3)	0.0	178.8	174.7
H(4)	-88.3	232.8	139.5
H(5)	0.0	183.6	284.1
H(6)	88.3	232.8	139.5
C(7)	-154.9	-89.4	174.7
H(8)	-157.5	-192.9	139.5
H(9)	-159.0	-91.8	284.1
H(10)	-245.8	-39.9	139.5
C(11)	154.9	-89.4	174.7
H(12)	245.8	-39.9	139.5
H(13)	159.0	-91.8	284.1
H(14)	157.5	-192.9	139.5
F(15)	-128.5	74.2	-179.4
F(16)	128.5	74.2	-179.4
F(17)	0.0	-148.4	-179.4

[a] Coordinates are given in pm.

Table A4.22 Calculated coordinates at the MP2/6-311+G* level for 1,1,1-trichloro-2,2,2-trimethyldisilane.[a]

Atom	*x*	*y*	*z*
Si(1)	0.0	0.0	-69.7
Si(2)	0.0	0.0	163.6
C(3)	154.9	89.5	220.2
H(4)	157.3	192.9	184.8
H(5)	159.3	92.0	329.6
H(6)	245.7	39.8	184.8
C(7)	-154.9	89.5	220.2
H(8)	-245.7	39.8	184.8
H(9)	-159.3	92.0	329.6
H(10)	-157.3	192.9	184.8
C(11)	0.0	-178.9	220.2
H(12)	88.4	-232.7	184.8
H(13)	0.0	-183.9	329.6
H(14)	-88.4	-232.7	184.8
Cl(15)	0.0	191.3	-144.6
Cl(16)	165.7	-95.6	-144.6
Cl(17)	-165.7	-95.6	-144.6

[a] Coordinates are given in pm.

Table A4.23 Calculated coordinates at the MP2/6-311+G* level for 1,1,1-tribromo-2,2,2-trimethyldisilane.[a]

Atom	*x*	*y*	*z*
Si(1)	0.0	0.0	-18.0
Si(2)	0.0	0.0	216.0
C(3)	155.0	89.5	272.1
H(4)	157.3	192.9	236.7
H(5)	159.3	92.0	381.5
H(6)	245.7	39.8	236.7
C(7)	-155.0	89.5	272.1
H(8)	-245.7	39.8	236.7
H(9)	-159.3	92.0	381.5
H(10)	-157.3	192.9	236.7
C(11)	0.0	-178.9	272.1
H(12)	88.4	-232.7	236.7
H(13)	0.0	-184.0	381.5
H(14)	-88.4	-232.7	236.7
Br(15)	0.0	208.7	-97.5
Br(16)	180.8	-104.4	-97.5
Br(17)	-180.8	-104.4	-97.5

[a] Coordinates are given in pm.

Table A4.24 Least-squares correlation matrix (x 100) for 1,1,1-trimethyldisilane.[a]

	u_9	u_{15}	k_2
p_1	74		
p_6		-80	
u_6			76
u_7	60		56

[a] Only elements with absolute values ≥50% are shown; k_2 is a scale factor.

Table A4.25 Least-squares correlation matrix (x 100) for 1,1,1-trifluoro-2,2,2-trimethyldisilane.[a]

	p_5	p_7	u_{10}	u_{14}	u_{17}	k_2
p_1	-58					
p_5		69				
p_6				-86	-69	
u_3						76
u_7			52			
u_{11}				70	54	
u_{14}					81	

[a] Only elements with absolute values ≥50% are shown; k_2 is a scale factor.

Table A4.26 Least-squares correlation matrix (x 100) for 1,1,1-trichloro-2,2,2-trimethyldisilane.[a]

	p_5	p_6	u_6	u_{13}	u_{16}	u_{19}	k_2
p_1	-54						-55
p_2			-52				-63
p_5		55			-69		
u_5			70				
u_6				55			89
u_{13}							61
u_{16}						67	

[a] Only elements with absolute values ≥50% are shown; k_2 is a scale factor.

Table A4.27 Least-squares correlation matrix (x 100) for 1,1,1-tribromo-2,2,2-trimethyldisilane.[a]

	p_5	u_7	u_{17}	u_{20}	k_2
p_3	51	60			
p_5			-60	-72	
u_6		69			73
u_{17}				85	56
k_1					53

[a] Only elements with absolute values ≥50% are shown; k_1 and k_2 are scale factors.

Figure A4.2 Experimental and final weighted difference (experimental – theoretical) MICs for 1,1,1-trimethyldisilane.

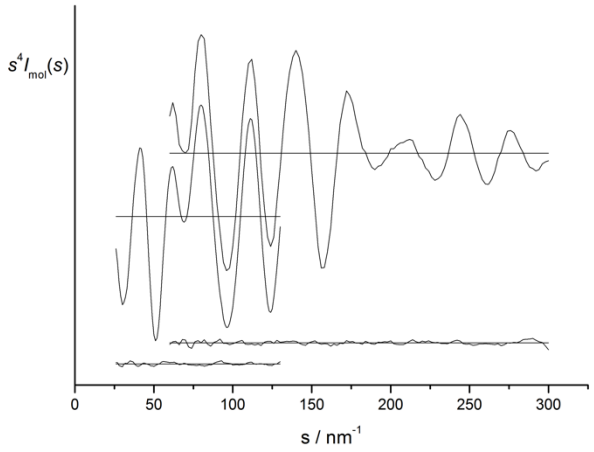

Figure A4.3 Experimental and final weighted difference (experimental – theoretical) MICs for 1,1,1-trifluoro-2,2,2-trimethyldisilane.

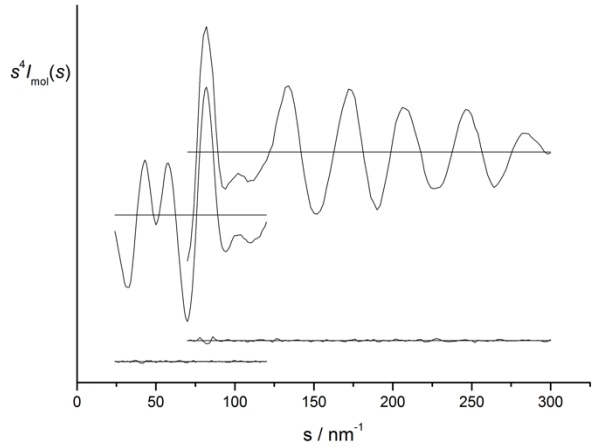

Figure A4.4 Experimental and final weighted difference (experimental – theoretical) MICs for 1,1,1-trichloro-2,2,2-trimethyldisilane.

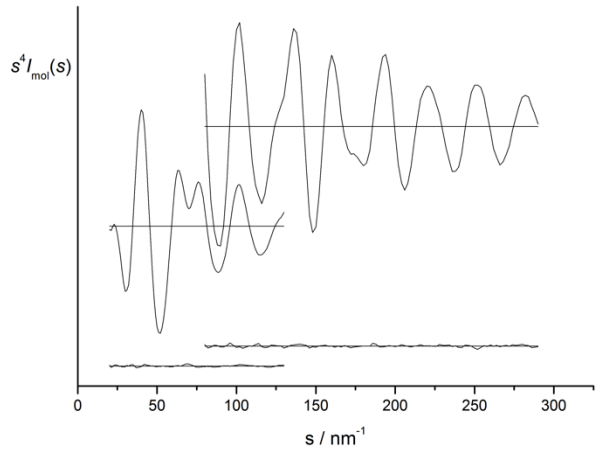

Figure A4.5 Experimental and final weighted difference (experimental – theoretical) MICs for 1,1,1-tribromo-2,2,2-trimethyldisilane.